



Smith, Rebecca Katherine Sherrard (2023) *Heparan sulphate mimetics as a therapeutic for central nervous system repair*. PhD thesis.

<https://theses.gla.ac.uk/83685/>

Copyright and moral rights for this work are retained by the author

A copy can be downloaded for personal non-commercial research or study, without prior permission or charge

This work cannot be reproduced or quoted extensively from without first obtaining permission from the author

The content must not be changed in any way or sold commercially in any format or medium without the formal permission of the author

When referring to this work, full bibliographic details including the author, title, awarding institution and date of the thesis must be given

Enlighten: Theses

<https://theses.gla.ac.uk/>
research-enlighten@glasgow.ac.uk

Heparan sulphate mimetics as a therapeutic for central nervous system repair

Rebecca Katherine Sherrard Smith BSc (Hons), MSc.

A thesis submitted in fulfilment of the requirements of the
University of Glasgow for the degree of Doctor of Philosophy



University
of Glasgow

Institute of Infection and Immunity
College of Medical, Veterinary and Life Sciences
University of Glasgow

February 2023

Abstract

The central nervous system (CNS) is composed of the brain, optic nerve and spinal cord and is responsible for most of the body's functions and processing external environmental information. Damage to the CNS can develop in different pathological conditions ranging from infection, traumatic injury of the spinal cord (SCI), traumatic brain injury (TBI), and degenerative disorders such as multiple sclerosis (MS). Neural degeneration and demyelination of axons are hallmarks of CNS injury. Demyelination in the CNS occurs due to a variety of pathophysiological conditions, therefore, any repair strategies for demyelination must consider multifactorial pathways including promotion of axonal outgrowth, and remyelination.

Previously, we have demonstrated that low sulphated modified heparin mimetics (LS-mHeps) enhance neurite outgrowth and myelination *in vitro*. Heparin mimetics (mHeps) are a class of glycomolecules with structural similarities to resident heparan sulphates (HS) and are made up of repeating disaccharide units with variable sulphation groups. They are thought to modulate cell signalling by both sequestering ligands and acting as a cofactor in the formation of ligand-receptor complexes. Thus, LS-mHeps have the capacity to represent novel candidates as therapeutics for CNS damage. However, a major hurdle for CNS therapeutics is for molecules and compounds to cross the blood brain barrier (BBB). Large molecular weight is known to prevent molecules crossing the BBB; therefore, we have developed a low molecular weight form of our lead compound LS-mHep7.

This thesis aimed to validate the ability of this low molecular weight form (LS-mHep7L) to maintain the ability to enhance repair in several CNS injury models including *in vitro* myelinating cultures, during both myelin development (MC-Dev) and demyelination (MC-DeMy), and astrocyte injury assays. Additionally, this thesis aimed to optimise an *ex vivo* slice culture model to further validate LS-mHeps and found that spinal cords from C57BL/6 P1 mice produced healthy myelinating axons for remyelination studies.

It was found that LS-mHep7L enhanced neurite outgrowth *in vitro* and remyelination both *in vitro* and *ex vivo*. LS-mHep7L was found to sequester CCL5 – a negative regulator of myelination both *in vitro* and *ex vivo*, and restored CCL5 induced hypomyelination in developing cultures. LS-mHeps also reduced signs of reactive astrocytes with a decrease in nestin expression and appeared to enhance gap closure in the injury model.

Finally, we investigated the use of recombinant heparin mimetics (rHS) as an alternative source for heparin derived therapeutics. Currently 80% of the world's heparin supply is sourced from China from porcine intestines and having such a reliance on a specific animal source for any new therapeutic comes with an elevated risk. Here we demonstrated that low sulphated recombinant heparan sulphate (rHS10) enhance remyelination in MC-DeMy and SC-DeMy, while rHS09 enhance neurite outgrowth in MC-Inj.

In summary, the results of this thesis demonstrated that low sulphated heparin mimetics have the potential to become novel therapeutics for remyelination and neurite outgrowth for diseases and injury of the CNS. Additionally, low molecular weight LS-mHeps show the same bioactivity as the high molecular weight form, by demonstrating neurite outgrowth *in vitro*, enhanced remyelination and sequestration of negative regulators of repair both *in vitro* and *ex vivo* cultures.

I dedicate this thesis to Penelope and Gillian Sherrard

Acknowledgements

I would like to start by thanking my supervisor Professor Susan Barnett, for giving me the opportunity to do this PhD, and for her continued support and guidance over the last 3.5 years, through a pandemic and Brexit! I know there were probably plenty of times that I was overly stressed when I didn't need to be and your time, patience, and encouragement was always valued.

Secondly, I'd like to thank Susan, who held my hand through many tears, gave me hugs when I didn't even know I needed them, and always picked me up on my lowest days. I think it's safe to say I wouldn't have finished this without you, and I will always be thankful for everything you have done for me. I was incredibly lucky to have such an amazing Postdoc and friend. Team Barnetto!

To all the Neuro-crew past and present. Chris K you are a newcomer, but I have appreciated all the time you have given to me, and the laughs we have had. To the Willisons, Jen, Rhona & Maddie for the jokes, lockdown laughs, Coro-no-she-betta-don't, outdoor lunches in the sun, and the competitive Christmas office decorations – honestly, one year our office WILL WIN! Clare Campbell ya slice a haem, you've got a sare sudder (honestly I did my best at spelling that), thank you for all the laughs and guidance even after you've gone off to be Dr Clare Campbell MacIver! Thank you Lina for always being on my side through every rant even when you secretly didn't agree with me because everyone knows, even when we are wrong, Scorpios and Geminis are always right. To Patrick, thank you for every à la Patrice, all the memes, singing to GaGa, and for letting my watch you discover Taylor Swift 12 years after everyone else. It was a magical journey for us both. Olivia, thank you for always being an overwhelming positive spirit in a room full of stressed PhD students. You always brought a smile to my face, and I take 'eat the frog' into all aspects of my life now! To Shazia, thank you for being so kind, and surrounding others around you with it. You made the hard days lighter. Jack J, you're a wee old man and I've loved moaning with you, it's been therapeutic. Alistair...OOPS jump scayyre! Thanks for the trauma bonding – we're going to be fine, but our fingers will not be. And finally, Katie-take-me-to-the-Chapple, thank you for so much guidance and advice, checking in on me when your spidey senses knew I was tired or down, and lifting me up with a hug, a smile or a cinnamon bun.

Colin Crawford, we all know you're getting your own section (I can hear everyone laughing and rolling their eyes). What a journey we have been on together, thank you for every moment. You have held my hand through all my challenges before, during, and (hopefully) after my PhD. The haters will say we were too attached, and the haters were probably...quite right. Thank you for every moment, all your guidance, sending emails I was too scared to send, singing defying gravity through the smoke of liquid nitrogen (for health and safety reasons that was a...joke), and every phone call. There is no way I would have finished this without you.

To my friends outside the lab, especially Fiona and Natu. Your support has dragged me from start to finish, and I think you both deserve a medal for getting me through. To my mum and dad- I swear I will have a grown-up job soon. Thank you for your endless support. You've always told me to shoot for the stars, and I did. It's been hard graft, but we got there!

And finally, Ruaridh. There is nothing I can write to thank you for your endless love and support. No one has believed in me the way you do. No one has lifted me up the way you do. And no one has loved me the way you have. Thank you for walking along side me on this journey and helping me cross the finish line. I could not have done this without you, and I would not have wanted to do this without you. (and before you say anything - Pepper, thanks for being the world's best dog!)

Declaration of authorship

I declare that, except where explicit reference is made to the contributions of others, this dissertation is the result of my own work and has not been submitted for any other degree at the University of Glasgow or any other institute.

Signed: Rebecca Katherine Sherrard Smith

Date: 27th February 2023

Publications

Lindsay, S.L.*; **Smith, R.S.***; Yates, E.A.; Cartwright, C.; Thacker, B.E.; Turnbull, J.E.; Glass, C.A.; Barnett, S.C. (2023) Validation of Recombinant Heparan Sulphate Reagents for CNS Repair. *Biology*, 12, 407. <https://doi.org/10.3390/biology12030407>

Lindsay, S.L., McCanney, G.A., Zhan, J., Scheld, M., **Smith, R.S.**, Goodyear, C.S., Yates, E.A., Kipp, M., Turnbull, J.E., Barnett, S.C (2023). Low sulfated heparan sulfate mimetic differentially affects repair in immune-mediated and toxin-induced experimental models of demyelination. *Glia*. 2023 Mar 21. doi: 10.1002/glia.24363. Epub ahead of print. PMID: 36945189.

Smith, R.S., Barnett, S.C., Lindsay, S.L. (2022). Generation of Rat Neural Stem Cells to Produce Different Astrocyte Phenotypes. In: Kannan, N., Beer, P. (eds) *Stem Cell Assays. Methods in Molecular Biology*, vol 2429. Humana, New York, NY.

Baldacchino, K., Peveler, W. J., Lemgruber, L., **Smith, R. S.**, Scharler, C., Hayden, L., ...Thümmeler, K. (2022). Myelinated axons are the primary target of hemin-mediated oxidative damage in a model of the central nervous system. *Experimental Neurology*, 354(May), 114113. <https://doi.org/10.1016/j.expneurol.2022.114113>

Edgar, J. M., **Smith, R. S.**, & Duncan, I. D. (2020). Transmission Electron Microscopy and Morphometry of the CNS White Matter Chapter. In: Elisabetta Babetto (eds), *Axon Degeneration: Methods and Protocols, Methods in Molecular Biology*, vol. 2143, 233–261 https://doi.org/10.1007/978-1-0716-0585-1_18

Abstracts

Smith, R.S., Lindsay, S.L., Turnbull, J.E., Goodyear, C.S., Barnett, S.C ‘Heparan Sulphate mimetics as a therapeutic for central nervous system repair’. MS Frontiers conference. Swansea, Wales, UK. July 8-9, 2022

Smith, R.S., Lindsay, S.L., Turnbull, J.E., Goodyear, C.S., Barnett, S.C ‘Heparan Sulphate mimetics as a therapeutic for central nervous system repair’. The 15th European Meeting on Glial Cells in Health and Disease (Virtual conference) July 2021

List of figures

Figure 1.1 |Cell types of the central nervous system

Figure 1.2 |Schematic of the myelin sheath

Figure 1.3 |Schematic of remyelination in the CNS

Figure 1.4 |Clinical sub-types of multiple sclerosis

Figure 1.5 | Heparan sulphate on the cell surface.

Figure 1.6 | Schematic of commercial heparin and LS-mHep7

Figure 2.1 |MC-DeMy schematic.

Figure 2.2 |MC-Dev schematic

Figure 2.3 |Representative images of myelin quantification

Figure 2.4 |Representative images of neurite outgrowth quantification

Figure 3.1 |P10 SD rat cerebellar slice cultures show signs of axonal degeneration and signs of oligodendrocyte dysfunction.

Figure 3.2 |Axon retraction bulbs and absence of myelin sheaths in P10 SD rat cerebellar slices

Figure 3.3 |High axon density with axonal degeneration in P7 mouse cerebellar slices.

Figure 3.4 |Myelin tracts without an associated axon observed in P7 mouse cerebellar slices.

Figure 3.5 |Non compact myelin observed in P7 mouse cerebellar slices.

Figure 3.6 |Improvement in axon appearance from slice cultures generated from P1 mouse cerebellar.

Figure 3.7 |Compact myelin and CASPR staining observed in slice cultures generated from P1 mouse cerebellum.

Figure 3.8 |Mouse P1 spinal cords show high axon density with no signs of axon degeneration.

Figure 3.9 |Mouse P1 spinal cord slice cultures show high levels of healthy myelination.

Figure 3.10 |Competent myelination confirmed with the presence of CASPR positive staining.

Figure 3.11 |Demyelination with lysolecithin successfully strips axons of myelin.

Figure 3.12 |Remyelination 9 days post demyelination and increases to 15 days post demyelination to restored levels.

Figure 3.13 |CASPR staining confirms compact re/myelination along axons after lysolecithin induced demyelination.

Figure 4.1 |LS-mHep7 and LS-mHep7L enhance remyelination in MC-DeMy.

Figure 4.2 |Axon density does not change across any treatment.

Figure 4.3 |Neither LS-mHep7 or LS-mHep7L affects axon width.

Figure 4.4 |Both LS-mHep7 and LS-mHep7L enhance neurite outgrowth in MC-Inj

Figure 4.5 |Repair is enhanced by early treatment in MC-Inj

Figure 4.6 |Effect of LS-mHeps on gap closure in MC-inj.

Figure 4.7 |LS-mHep7L and LS-mHep7 treatment reduced gap width in astrocytic injury model (scratch assay)

Figure 4.8 |LS-mHep7L and LS-mHep7 reduced gap width in astrocytic injury model (scratch assay).

Figure 4.9 |LS-mHeps restore CCL5 induced hypomyelination in MC-Dev

Figure 5.1 |LS-mHep7L enhances re/myelination after lysolecithin induced demyelination in *ex vivo* spinal cord slice cultures (SC-DeMy).

Figure 5.2 |LS-mHep7L/ LS-mHep7 have no effect on axon width in SC-DeMy during re/myelination.

Figure 5.3 |LS-mHep7L/LS-mHep7 treatment in SC-DEV has no effect on developmental myelination.

Figure 5.4 |CCL5 significantly reduces developmental myelination in SC-DEV, this effect is rescued by both LS-mHep7L and LS-mHep7.

Figure 5.5 | Changes in chemokine/cytokine secretion profile after demyelination in SC-DeMy

Figure 5.6 |CXCL5 has no negative effect on developmental myelination in SC-DEV

Figure 6.1 | Schematic of heparan sulphate mimetics and their sources

Figure 6.2 | Comparison of the predominant structure of rHS02, rHS09, rHS10 and LS-mHep7

Figure 6.3 |rHS10 and LS-mHep7 (H7) enhance re/myelination *in vitro* (MC-DeMy).

Figure 6.4 |Effect of LS-mHep7, rHS02, rHS09 and rHS10 on neurite outgrowth and myelination after injury (MC-Inj)

Figure 6.5 |rHS10 and LS-mHep7 enhances re/myelination after lysolecithin induced demyelination of *ex vivo* spinal cord slice cultures.

Figure 6.6 |Effect of LS-mHep7, rHS02, rHS09 and rHS10 on astrocyte reactivity after injury

Figure 6.7 |Effect of LS-mHep7, rHS02, rHS09 and rHS10 on astrocyte reactivity after injury (GFAP expression).

List of Tables

Table 1.1 |“Inside-out” and “Outside-in” disease model systems

Table 2.1 |Primary and secondary antibodies used in the immunostaining of in vitro cultures.

Table 2.2 |Primary and secondary antibodies used in the immunostaining for slice cultures.

Table 2.3 |Antibody table for Western blot

Table 2.4 |Secreted factors specific to the capture antibodies in the Proteome Profiler mouse Cytokine Array Kit XL

List of Abbreviations

A β amyloid beta

AD Alzheimer's disease

ALS amyotrophic lateral sclerosis

BBB blood-brain barrier

CCL5 C-C Motif Chemokine Ligand 5

CXCL5 (C-X-C Motif Chemokine Ligand 5)

CNS central nervous system

CSPG chondroitin sulphate proteoglycans

DAPI 4'-6'diamidino-2-phenylindole

DCM demyelination conditioned media

DIV days in vitro

DMEM Dulbecco's Modified Eagle Medium

DMTs disease-modifying treatments

DNA deoxyribonucleic acid

E15 embryonic day 15

EAE experimental autoimmune encephalomyelitis

ECM extracellular matrix

EGF epithelial growth factor

FBS foetal bovine serum

FGF fibroblast growth factor

GAG glycosaminoglycan

GFAP glial fibrillary acidic protein

GlcNAc N-acetylglucosamine

GlcNS N-sulphated glucosamine

HMW high molecular weight

HS heparan sulphate

HSPG heparan sulphate proteoglycan

IL interleukin

LMW low molecular weight

ULMW ultra low molecular weight

LPC Lysophosphatidyl choline (lysolecithin)

LS-mHep low sulphated heparin mimetics

LS-mHep7 low sulphated heparin mimetic 7

LS-mHep7L low molecular weight LS-mHep7

MBP myelin basic protein

MC myelinating cultures

MC-DeMy myelinating cultures-demyelination

MC-Dev myelinating cultures-development

MC-Inj myelinating cultures-injury

mHep modified heparin

MOG myelin oligodendrocyte glycoprotein

MRI magnetic resonance imaging

MS multiple sclerosis

MSCs mesenchymal stem/stromal cells

MW molecular weight

NS neurospheres

NSC neural stem cells

NsAs neurosphere-derived astrocytes

OECs olfactory ensheathing cells

ORNs the olfactory receptor neurons

ODS Osmotic demyelination syndrome

OPC oligodendrocyte precursor cell

P post-natal day

PDGF platelet-derived growth factor

PFA paraformaldehyde

PLL poly-L-lysine

PLP proteolipid protein

PM plating medium

PNS peripheral nervous system

PPMS primary progressive MS

rpm revolutions per minute

RRMS relapse-remitting MS

SC-DeMy slice cultures - demyelination

SC-DEV slice cultures- development

SCI spinal cord injury

SCM slice culture media

SCT stem cell therapy

SD Sprague Dawley

SEM standard error of mean

SPMS secondary progressive MS

TNF- α tumour necrosis factor α

TLRs Toll like receptors

TBI traumatic brain injury

Contents

Abstract	2
Dedication	3
Acknowledgements	5
Declaration of authorship	6
Publications	7
Abstracts	7
List of figures	8
List of Tables	10
List of Abbreviations	11
Chapter 1	18
Introduction	18
1.1 An introduction to the central nervous system	19
1.1.1 Astrocytes	19
1.1.2 Microglia	20
1.1.3 Oligodendrocytes	21
1.2 Damage to the central nervous system	23
1.2.1 Demyelination of the CNS	24
1.2.2 Failure to remyelinate.....	25
1.2.3 Multiple sclerosis.....	26
1.2.4 Spinal cord injury.....	29
1.2.5 Traumatic brain injury	30
1.3 Current strategies for CNS repair	31
1.3.1 Hurdles for CNS therapeutics	31
1.3.2 Current strategies for demyelinating diseases: multiple sclerosis	32
1.3.3 Current strategies for spinal cord injury.....	33
1.4 Heparan sulphate proteoglycans	35
1.4.1 Low sulphated heparan sulphates in CNS repair.....	37
1.4.2 The role of heparan sulphate in CNS development.....	39
1.4.3 Heparan sulphate mimetics as therapeutics in CNS.....	41
1.5 Experimental models of the mammalian CNS	42
1.5.1 <i>In vitro</i> models of the CNS.....	42
1.5.2 <i>In vivo</i> models of MS	44
1.5.3 <i>Ex vivo</i> slice cultures	48
1.6 Conclusion	49
1.7 Aims	49
Chapter 2	51
Methods and Materials	51
2.1 Compounds	52
2.1.1 Low sulphated modified heparin (LS-mHep7)	52
2.1.2 Low molecular weight LS-mHep7 (LS-mHep7L).....	52

2.1.3 Recombinant heparan sulphate compounds	52
2.2 Commonly used buffers and solutions	53
2.2.1 Phosphate buffered saline.....	53
2.2.2 Blocking buffer.....	53
2.3 Animals	53
2.3.1 Sprague Dawley rat	53
2.3.2 C57BL/6 mice.....	54
2.4 Cell culture	54
2.4.1 Commonly used materials.....	54
2.4.2 Stock solutions.....	54
2.4.3 Cell Culture Media	56
2.4.4 Primary Cell Culture.....	57
2.4.5 Cell culture assays	58
2.5 Immunocytochemistry	61
2.5.1 <i>In vitro</i> cell culture staining	61
2.5.2 <i>Ex vivo</i> slice culture staining.....	63
2.6 Microscopy and image analysis	63
2.6.1 Fluorescent microscopy.....	63
2.6.2 Confocal Imaging	63
2.6.3 Re/myelination quantification.....	64
2.6.4 Neurite diameter	66
2.7 Molecular Biology	67
2.7.1 Western blot.....	67
2.7.2 Cytokine array.....	68
2.8 Statistical analysis.....	70
Chapter 3.....	71
<i>Ex vivo slice cultures as a model for studying central nervous system repair</i>	71
3.1 Introduction	72
3.2 Aims	72
3.3 Cerebellar slice cultures from P10 SD rat did not maintain healthy myelinated axons	73
3.4 Cerebellar slice cultures from P7-10 C57BL/6 mouse pups did not maintain healthy myelinated axons	76
3.5 Mouse C57 P1-3 cerebellum contained healthy appearing axons but variable levels of myelination and expression of CASPR	82
3.6 Spinal cord slice cultures from P1 C57BL/6 mouse pups maintained healthy axons with consistent myelination	84
3.7 Lysolecithin induced demyelination is a successful tool without any detrimental effects on the properties of the cultures	88
3.8 Spontaneous remyelination is observed 9 days after demyelination in spinal cord slice cultures.....	90
3.9 Discussion	93
Chapter 4.....	98
<i>Low molecular weight mHeps modulate injury and repair in in vitro CNS models.</i>	98

4.1 Introduction	99
4.2 Aims	99
4.3 LS-mHep7L enhances remyelination in MC-Demy	100
4.4 Effect of LS-mHep7 and LS-mHep7L on neurite diameter	103
4.5 Neurite outgrowth was observed in MC-Inj following treatment with either LS-mHep7 or LS-mHep7L <i>in vitro</i>	104
4.6 LS-mHeps repair strategies are enhanced if present at earlier time points post-injury <i>in vitro</i>	107
4.7 LS-mHeps appear to reduce signs of astrocytosis <i>in vitro</i>	109
4.8 Both LS-mHep7 and LS-mHep7L appears to sequester CCL5 – a negative regulator of remyelination.....	112
4.9 Discussion.....	114
Chapter 5.....	120
<i>Low molecular weight LS-mHeps enhance repair in an ex vivo spinal cord injury model.</i>	120
5.1 Introduction	121
5.2 Aims	121
5.3 LS-mHep7L enhances re/myelination in demyelinated spinal cord slice cultures	122
5.4 LS-mHep7 and LS-mHep7L have no effect on axon width following re/myelination.....	124
5.5 LS-mHep7 and LS-mHep7L do not enhance developmental myelination levels in SC-DEV	125
5.6 LS-mHep7L and LS-mHep7 treatment rescues CCL5-induced inhibition of developmental myelination in SC-DEV	127
5.7 Changes in the secreted chemokine/ cytokine profile of spinal cord slice cultures after demyelination	129
5.8 CXCL5 does not significantly reduce developmental myelination in SC-DEV.....	131
5.9 Discussion	133
Chapter 6.....	137
<i>Validation of recombinant heparan sulphate panel for CNS repair</i>	137
6.1 Introduction	138
6.2 Aims	140
6.3 Effect of rHS02, rHS09 and rHS10 on <i>in vitro</i> re/myelination	141
6.4 Effect of rHS02, rHS09 and rHS10 and LS-mHep7 on neurite outgrowth and lesion width after injury in MC-Inj	143
6.5 Effect of rHS10 on <i>ex vivo</i> slice culture re/myelination.....	146
6.6 Effect of rHS02, rHS09 and rHS10 and LS-mHep7 on astrocytes – gap closure.....	148
6.6 Effect of rHS02, rHS09 and rHS10 and LS-mHep7 on astrocyte reactivity – GFAP expression	150

6.8 Discussion.....	152
Chapter 7.....	157
Discussion.....	157
7.0 General Discussion.....	158
7.1 Limitations of the study	158
7.1.1 Effective models of CNS injury?.....	159
7.2 Reparative compounds for CNS injury	160
7.2.1 Multiple sclerosis	160
7.2.2 Spinal cord injury	161
7.3 Low molecular weight heparin mimetics.....	162
7.4 Clinical use of heparin mimetics	162
7.5 Future work.....	163
7.6 Concluding remarks	166
References.....	167

Chapter 1

Introduction

1.1 An introduction to the central nervous system

The central nervous system (CNS) is composed of the brain, optic nerve and spinal cord and is responsible for most of the body's functions and processing external environmental information. The brain alone is responsible for many important functions such as movement, thinking, speech, and the 5 senses of seeing, hearing, feeling, tasting, and smelling. The CNS is a complex cellular environment made up of several cell types, and in humans it is estimated that the adult brain alone contains around 86 billion neurons (**Azevedo *et al.*, 2009**). Along with neuronal cells the CNS contains neuroglia cells – derived from the Greek 'glia' meaning glue – and consist of, astrocytes, microglia, ependymal cells, and oligodendrocytes.

1.1.1 Astrocytes

The word 'astrocyte' is derived from the Greek word 'astron' – meaning star – giving this cell its characteristic 'star' stellate shape with multiple processes. Astrocytes are the most abundant cell type in the CNS accounting for 19–40% of glial cells (**Pelvig *et al.*, 2008**) and have multiple homeostatic functions including regulating neuronal circuitry function (**Haim and Rowitch, 2017**), supporting myelination (**Traiffort *et al.*, 2020**) and secreting many factors important in energy metabolism (**Kiray *et al.*, 2016**). They are best known however for their role in the formation and maintenance of the blood brain barrier (BBB) (**Abbot *et al.*, 2006**), a tightly regulated interface in the CNS that regulates the exchange of molecules in and out of the brain. Some neurological disorders such as brain trauma, multiple sclerosis, Alzheimer's, and Parkinson's diseases, show a disruption of the BBB (**Bronsan & Raine, 2013; Al-Bachari *et al.*, 2020; Zlokovic, 2011**), with an increase in the permeability of the barrier and phenotypical changes in the astrocytes indicative of their activation. The activation of astrocytes is characterized by cellular hypertrophy, elevated expression of intermediate filament (glial fibrillary acidic protein (GFAP), vimentin, nestin) and hypertrophic morphology characterized by enlargement of the cell soma and cellular processes (**Pekny and Nilsson, 2005**). Following injury to the CNS astrocytes become activated and depending on the reactive phenotype induced can aid or impede repair (**Sofroniew and Vinters, 2010**).

After CNS injury, a series of stress responses induce astrocyte activation. Reactive astrocytes combined with extracellular matrix (ECM) components form a glial scar at the lesion site, which walls off the injured region from neighbouring healthy tissue. Mild to moderate astrogliosis is believed to protect CNS cells and tissue by uptake of potentially excitotoxic

glutamate, protects from oxidative stress, facilitates the blood–brain barrier repair and limits the spread of inflammatory cells or infectious agents from areas of damage or disease into healthy CNS tissue (Iglesias *et al.*, 2017). However, as a physical and molecular barrier, glial scar can impede functional recovery in the late period of CNS injury, by preventing neurite outgrowth. Following trauma to the CNS, axons begin to sprout and attempt to extend across the injury site in order to repair the damaged regions. However, the scar prevents axonal extensions via physical and chemical means (Bradbury *et al.*, 2002; McKeon *et al.*, 1991). Thus, inhibiting glial scar formation in the chronic stage after CNS injury may be a promising target to improve outcomes.

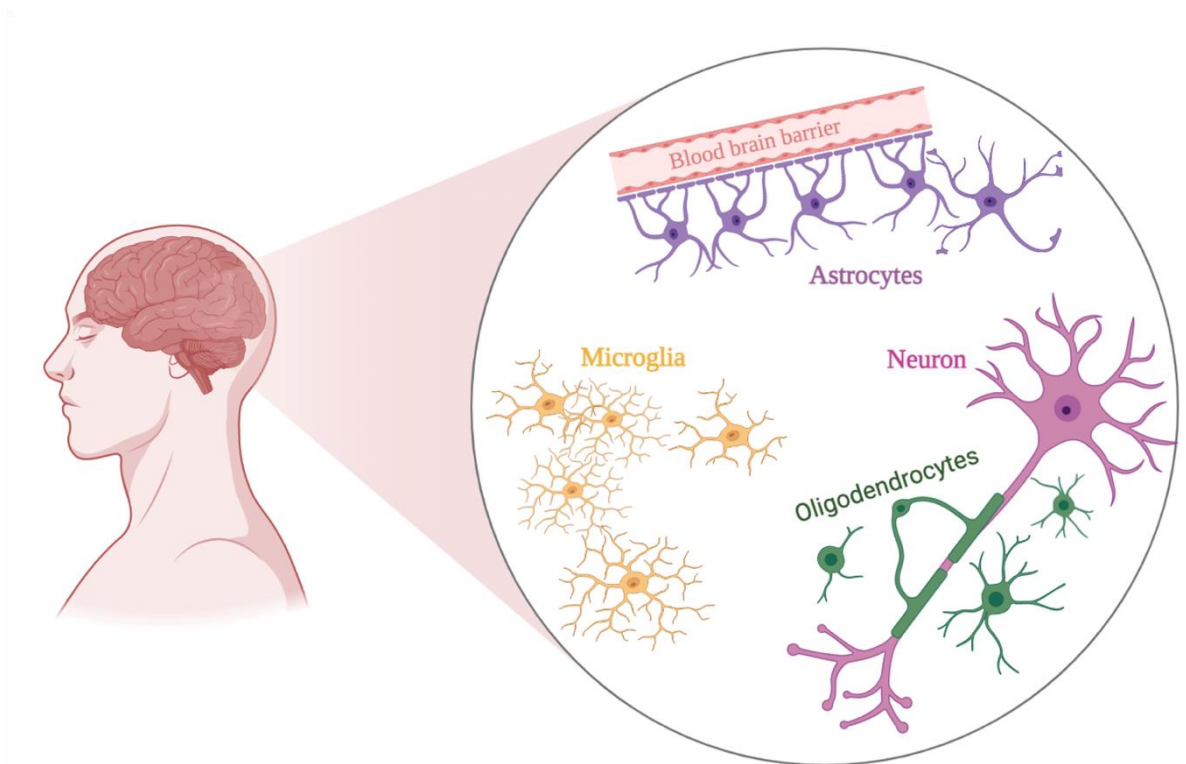


Figure 1.1 |Cell types of the central nervous system. The CNS predominantly contains astrocytes that maintain the blood brain barrier and secrete important trophic factors, microglia the immune cell of the CNS, and oligodendrocytes that produce and maintain myelin sheaths on myelinated axons.

1.1.2 Microglia

The resident immune cell of the CNS is the microglia, which under normal conditions actively survey the local environment in a ‘resting’ phenotype (Nimmerjahn *et al.*, 2005), continually patrolling the cerebral microenvironment for pathogens and damage. These

include damage-associated molecular patterns (DAMPs) (Edye *et al.*, 2013), pathogen-associated molecular patterns (PAMPs) (Esen and Kielian 2006), cytokines and chemokines. Derived from, erythromyeloid precursors in the extra-embryonic yolk sac, these tissue-resident macrophages occupy the brain in early embryonic development and remain there throughout adulthood (Kierdorf *et al.*, 2013; Ginhoux *et al.*, 2010). Microglia have been suggested to function in synaptic maturation and maintenance dictating neural progenitor fate decisions (Wake *et al.*, 2009), clearance of cellular debris (Hertzog *et al.*, 2019), synaptic pruning (Paolicelli *et al.*, 2011), and have shown to phagocytose excess myelin produced during myelination (Hughes and Appel, 2020). To perform these functions, microglia express Fc receptors, Toll-like receptors (TLRs), viral receptors, and antimicrobial peptides (Hickman *et al.*, 2013). Dysregulation of any of these microglia functions can result in an imbalance that initiates or propagates neurodegeneration including disorders such as multiple sclerosis (MS), amyotrophic lateral sclerosis (ALS) and spinal cord injury (SCI) (Frakes *et al.*, 2014; Kigerl *et al.*, 2009). Variants of the microglia gene *TREM2* increases the risk for late-onset Alzheimer's disease (AD) by two to three times in several European and North American populations (Jonsson *et al.*, 2013; Song *et al.*, 2017; Cuyvers *et al.*, 2014). *TREM2* variants associated with AD induce partial loss of function of the *TREM2* protein and alter the behaviour of microglial cells, including their response to amyloid plaques (Frank *et al.*, 2008). Microglia can also contribute positively to repair and regeneration of the CNS. Pro-repair microglia have been identified and secrete pro-repair factors after injury, such as activin-A expressed by 'M2' microglia. This secretion of pro-repair factors promoted Oligodendrocyte precursor cell (OPC) differentiation and remyelination (Miron *et al.*, 2013).

1.1.3 Oligodendrocytes

The cellular function of the oligodendrocyte is to form compact myelin sheaths around axons, thereby enabling fast saltatory conduction - pivotal to efficient neuronal function (Hartline and Colman, 2007). In the spinal cord, most oligodendrocytes derive from a specialized domain of the ventral portion of the neural tube, which first gives rise to motor neuron precursors and then undergo a gliogenic switch to oligodendrocyte precursor cells (OPCs) (Lu *et al.*, 2002). These cells migrate around the spinal cord as OPCs and then mature into myelin producing oligodendrocytes. Additionally, a population of OPCs arise from the dorsal spinal cord, contributing to 10-15% of the final oligodendrocyte population (Cai *et al.*, 2005). In the brain however, the rise of OPCs begins with a wave of cells from the medial

ganglionic eminence and anterior entopeduncular area of the ventral forebrain where they populate the embryonic telencephalon. A second distribution of OPCs begins with the population of cells derived from the lateral ganglionic eminences. Finally, a third wave of OPCs arises within the postnatal cortex (Kasseris *et al.*, 2006). OPCs proliferate and differentiate into mature oligodendrocytes depending on environmental cues (Emery, 2010). OPCs differentiate into oligodendrocytes not only during the development of the CNS but also in cases of pathological demyelination in the mature CNS (Boulanger *et al.*, 2010). Since oligodendrocytes play a crucial role in demyelinating diseases, such as multiple sclerosis, the study of oligodendrocytes and their differentiation mechanisms is essential for the development of novel therapies.

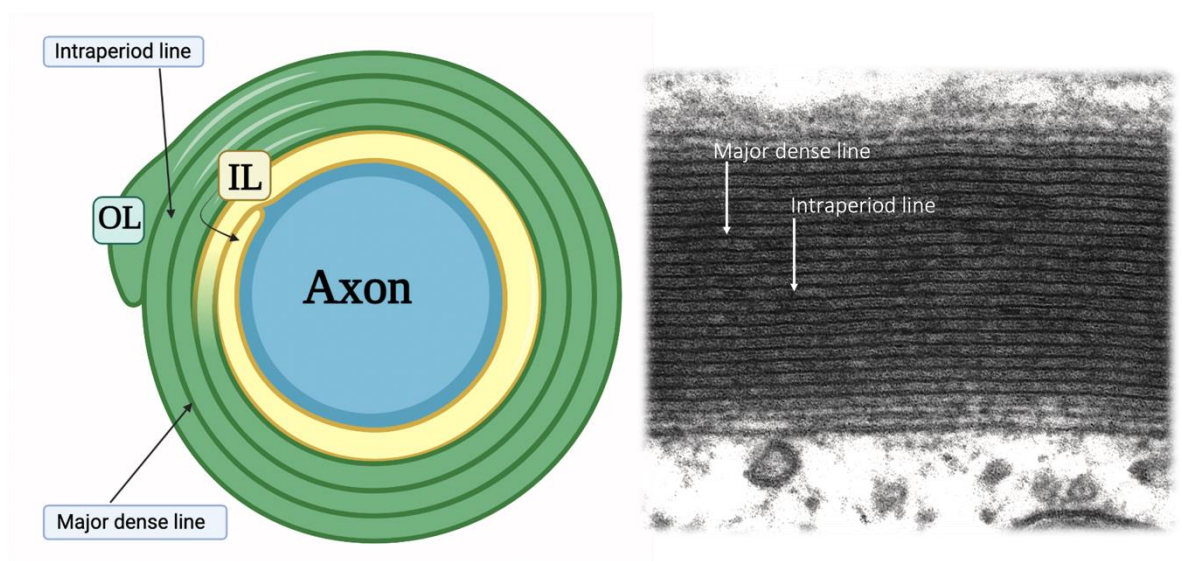


Figure 1.2 | Schematic of the myelin sheath. The myelin sheath forms from flattened cytoplasmic processes from the oligodendrocyte that are elaborated around the axon, which then compact their cytoplasmic content except for small pockets at the periphery of the membrane, which can appear as the inner loop (IL) immediately adjacent to the axon and the outer loop (OL) at the outer edge of the membrane. The major dense line represents the compacted cytoplasm. The intraperiod line is formed by close apposition of the membrane layers, microtubules (*), and neurofilaments (↑) *TEM image adapted from Edgar et al., 2020.*

As discussed previously the principal role of oligodendrocytes is to produce myelin which ensheath the axons of neurons. Oligodendrocytes deposit myelin in a spiralling pattern around the axon, which generates two morphological features of the myelin sheath, that is, alternating electron-dense and -light layers, termed the “major dense line” and the “intraperiod line,” respectively. The major dense line is formed when the cytoplasm within the myelin process is lost, and the opposing plasma membranes come together. While the

myelin is being further wrapped around, the outer faces of the plasma membrane oppose each other to form the intraperiod line. Myelin is a lipid-rich membrane that consists of approximately 70% lipid and 30% protein (**Norton and Cammer, 1984**). Myelin does not cover the axon fully, and instead there are intermittent gaps in the myelin where the axon is exposed to extracellular fluid – named the nodes of Ranvier (**Ranvier, 1871**). These gaps leave the axolemma exposed to extracellular fluid, including sodium ions which influx through voltage-gated sodium channels to potentiate action potentials (**Mueller, 1958**). Thus, myelin can reduce the energy load required and increase the speed of AP conduction. Myelination had a profound impact on vertebrate evolution with the myelin sheath allowing axons to function over much greater lengths, and in turn, allowing vertebrates to attain a larger size and diversity (**Zalc and Colman, 2000**). It has allowed rapid conduction of axon potentials without needing to increase axonal diameter, enabling the packing of larger numbers of axons necessary for the evolution of a complex central nervous system.

The importance of myelination in the vertebrate CNS is epitomised by dysmyelination disorders. Dysmyelination describes an inborn error of metabolism affecting myelinogenesis that causes it to be abnormal, arrested, or delayed. Such disorders include metachromatic leukodystrophy, Krabbe's disease, Zellweger disease and adrenoleukodystrophy (**Van Rappart et al., 2015; Mytake & Suzuki 1972; Klouwer et al., 2015; O'Neil and Moser, 1981**). Krabbe's disease for example, is caused by a deficiency of the acid hydrolase galactosylceramidase (GalC) which is responsible for the degradation of galactosylceramides and sphingolipids. Both galactosylceramides and sphingolipids are abundant in myelin membranes and the absence of GALC leads to the toxic accumulation of galactosylsphingosine in oligodendrocytes (**Mytake & Suzuki, 1972**). This ultimately leads to demyelination of the CNS. Children with an infantile onset generally appear normal at birth but begin to miss developmental milestones by six months of age and die by two to four years of age.

1.2 Damage to the central nervous system

Damage to the CNS can develop in different pathological conditions ranging from infection, traumatic injury of the spinal cord (SCI), traumatic brain injury (TBI), idiopathic degeneration, and degenerative disorders such as Alzheimer's disease (AD), multiple sclerosis (MS) and amyotrophic lateral sclerosis (ALS). Damage to the CNS is generally considered to be irreversible, mainly because the injured axons cannot be effectively regenerated. Regeneration of the adult mammalian CNS is weak, mostly attributed to the

poor regenerative microenvironment the injured neuronal axons inhabit (**Fawcett and Asher, 1999**).

1.2.1 Demyelination of the CNS

Demyelination is the destruction of formally healthy myelin sheaths opposed to dysmyelination, referring to the malformed and defective myelin sheath. Demyelinating diseases of the CNS can be classified according to their pathogenesis into several categories: demyelination due to inflammatory processes, viral demyelination, demyelination caused by acquired metabolic derangements, hypoxic–ischaemic forms of demyelination and demyelination caused by focal compression (**Love *et al.*, 2005**).

The principal viral demyelinating disease in humans is progressive multifocal leucoencephalopathy (PML) caused by the papovavirus, JC virus or John Cunningham virus. JC virus leads to demyelination by establishing a lytic infection of the oligodendrocytes. Approximately 50% of adolescents and 75% of adults have serological evidence of JC virus infection, but it is usually asymptomatic. The JC virus is harmless except in cases of weakened immune systems. In general, PML has a mortality rate of 30–50% in the first few months, and those who survive can be left with varying degrees of neurological disabilities (**Ferenczy *et al.*, 2012**).

Acquired metabolic demyelination includes osmotic demyelination syndrome (ODS), also known as central pontine myelinolysis (CPM), which is found to occur after the rapid correction of severe hyponatremia (**Kleinschmidt-DeMasters and Norenberg, 1981**). ODS occurs due to plasma osmotic changes and was first described in 1959 with “pontine myelinolysis” in alcoholic patients and is associated with chronic illness, alcoholism, and electrolyte derangements (**Adams *et al.*, 1959**). ODS is an uncommon neurological disorder characterized by damage of the myelin sheath due to rapid plasma osmotic shifts (**Singh *et al.*, 2014**). The pons is principally affected, but in severe cases demyelinated lesions have been found in the corpus striatum, in the thalamus, and at the junction of the grey and white matter in the cerebrum and the cerebellum (**Kallakatta *et al.*, 2011**). The intense osmotic stress sustained by brain cells is believed to be the major risk factor for demyelination resulting from astrocyte and oligodendrocyte loss, microglial activation, infiltration of myelin-degrading macrophages, BBB disruption and later myelin damage (**Gankam *et al.*, 2017**).

Hypoxic–ischaemic forms of demyelination occur in some circumstances where the oligodendrocytes bear the brunt of the damage after hypoxia or ischaemia in the brain. This however is rare but can occur with exposure to carbon monoxide which causes hypoxaemia

(Lv *et al.*, 2021), cardiac arrest (Alturkustani *et al.*, 2016), asphyxia or depression of cardiorespiratory function.

1.2.2 Failure to remyelinate

Remyelination in the CNS is the process in which entire myelin sheaths are restored to demyelinated axons (Smith *et al.*, 1979). It is mediated by OPCs, which are widely distributed throughout the adult CNS. There are two main phases of remyelination, the recruitment phase where OPCs are activated by pro-migratory factors and migrate into the demyelinated lesion (de Castro *et al.*, 2013), followed by the differentiation phase where OPCs differentiate into mature myelinating oligodendrocytes (Kotter *et al.*, 2011). However, despite its efficiency in experimental models and in some clinical diseases, remyelination is often inadequate in demyelinating diseases such as multiple sclerosis, producing thinner and shorter myelin (Ludwin, 1984) as identified in the post-mortems of MS patients (Perier and Gregoire, 1965; Albert *et al.*, 2007). This leads to the longstanding hypothesis that impaired differentiation of OPCs into mature myelinating cells results in this inefficient remyelination. However, recent studies have revealed a second mode of remyelination in which mature oligodendrocytes surviving within an area of demyelination are able to regenerate new myelin sheaths (Duncan *et al.*, 2018).

The absence or reduction of trophic factors essential for OPC survival, proliferation, and differentiation can compromise remyelination. Trophic factors, including insulin-like growth factor 1 (IGF-1) and brain-derived neurotrophic factor (BDNF), provide critical support for OPCs during remyelination (Van't Veer *et al.*, 2009; Kühl *et al.*, 2002). Insufficient levels or impaired signalling of these factors can hinder the regenerative process (Rajendran *et al.*, 2021).

The microenvironment following injury in the CNS may also contribute to inefficient remyelination; therefore, appropriate restoration of tissue homeostasis is also a critical component for remyelination to occur. Following injury of the myelin sheath, myelin debris can be found due to demyelination. Phagocytosis of myelin debris in the MS brain is essential for the initiation of neuro-repair as myelin debris inhibits OPC differentiation and therefore remyelination (Kotter *et al.*, 2006). Microglia play a key role in the clearance of myelin debris (Voet *et al.*, 2019). Their ability to detect and respond to demyelination cues, transition between phenotypic states (Miron *et al.*, 2013), and participate in phagocytosis (Fu *et al.*, 2014) and trophic factor release make them essential for promoting the regenerative potential of the CNS. It has been suggested that the initiation of remyelination

requires the establishment of microglia to move from a pro-inflammatory state (iNOS+ TNF α + CCL2+) to a pro-regenerative microglia state (Arg-1+ CD206+ IGF-1+) (Miron *et al.*, 2013). It is also proposed that dysregulation of microglia repopulation or the impairment of microglia death may contribute to the failure of the CNS to regenerate in demyelinating diseases (Lloyd *et al.*, 2019).

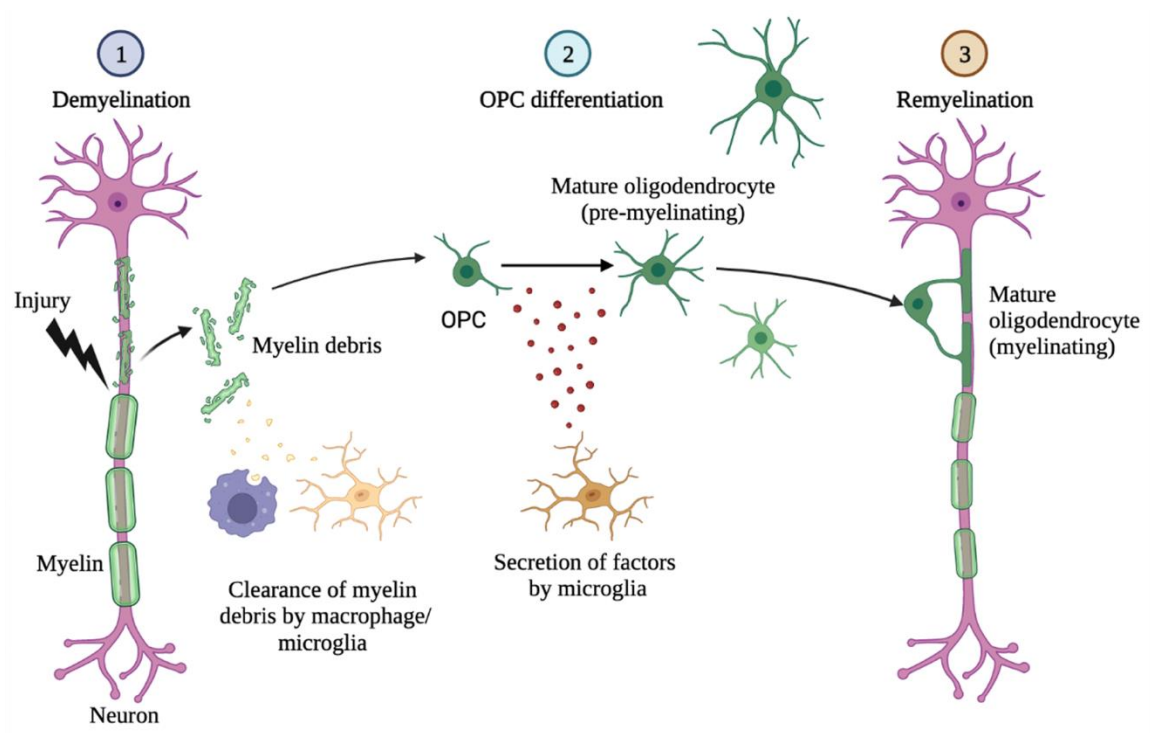


Figure 1.3 |Schematic of remyelination in the CNS. When the myelin sheath is damaged due to injury, clearance of myelin debris by microglia occurs. Secreted factors promote OPC differentiation and maturation into mature myelinating oligodendrocytes that remyelinate the axon.

1.2.3 Multiple sclerosis

The most common demyelinating disease is multiple sclerosis (MS). MS is an inflammatory demyelinating disease of the CNS whereby the myelin sheath is focally degraded leading to perturbed neuronal signalling, axonal degeneration, and neuronal cell death (Lassman *et al.*, 2007). The annual worldwide prevalence of MS is 30 per 100,000 people however, it is worth noting that this ranges greatly (5-80 per 100,000) between different regions (World Health Organization (WHO) and Multiple Sclerosis International Federation, 2008). It's estimated that 130,000 people in the UK have MS with around 130 more people a week being diagnosed. So far, it is still unclear about the precise nature of MS aetiology.

The traditional view is that MS is an autoimmune disorder of the CNS. This mechanism involves autoreactive immune cells that infiltrate the CNS, resulting in inflammatory demyelination episodes. The self-antigen or trigger is not known, although a variety of myelin self-antigens recognized by the immune system have been identified in MS patients. Viral infections have been implicated as potential triggers by breaking the self-tolerance for instance through mechanisms of molecular mimicry (**Fujinami and Oldstone, 1985**). Epstein Barr virus (EBV) has long been motioned to be linked to MS development with a recent study by **Bjornevik *et al.*, 2022**, considerably strengthening the theory. The study demonstrated that in a cohort of more than 10 million young adults on active duty in the U.S. military, those who were infected with EBV during their period of service had a 32-fold increased risk of developing MS. Although the exact mechanism behind ‘virus induced triggers’ is yet to be elucidated, the capacity of viral proteins to activate MOG-specific B-lymphocytes has been demonstrated (**Sanderson *et al.*, 2017**).

A genetic pre-disposition to MS has been proposed, however the consensus is that MS is considered as a complex polygenetic disease, which is not inherited, but one can inherit a greater susceptibility to develop MS. Siblings have an increased risk of 3%, and recurrence in identical twins is around 35% (**Compston & Coles, 2002**). Genome wide association studies have now identified numerous gene regions, associated with increased disease susceptibility, however, each of the individual genes have shown to have a minor impact (**IMSGC 2013, IMSGC 2018**). Environmental influences have also been identified as risk factors for MS. Vitamin D exposure has been identified as a risk factor, and in turn, as a protective factor, with high exposure levels being associated with a decreased risk of developing MS (**Salzer *et al.*, 2012**). In addition, smoking has been suggested as a contributor to the genetic susceptibility linked with high-risk HLA gene mutations (**Hedström *et al.*, 2011**). Overall, It is thought to be the result from interplay between yet unidentified environmental factors and susceptibility genes.

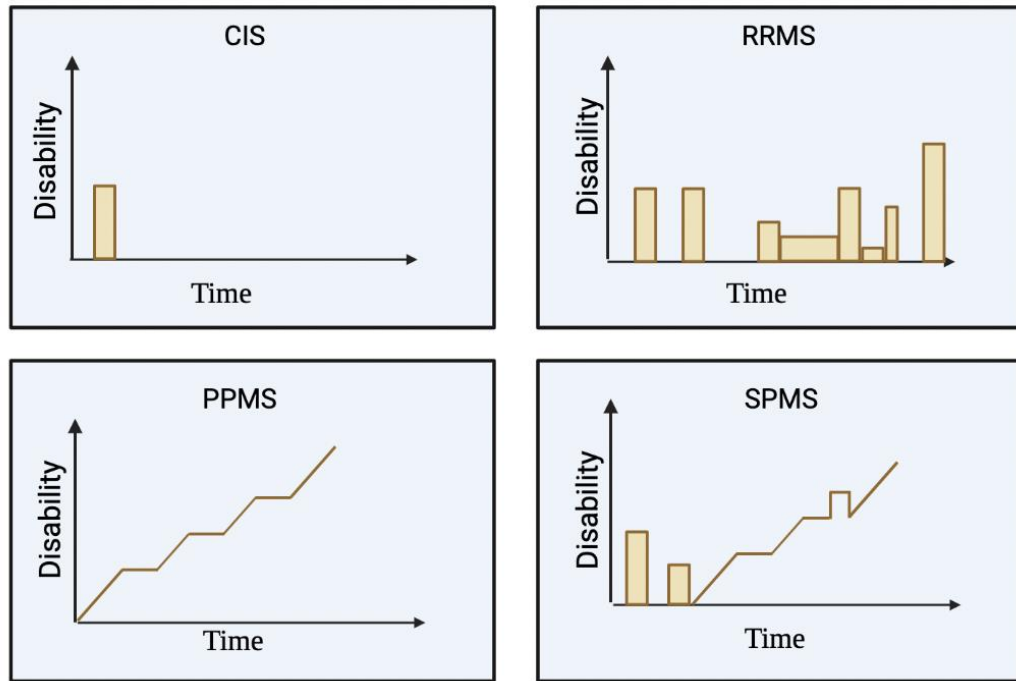


Figure 1.4 |Clinical sub-types of multiple sclerosis. Manifestations of MS include clinical isolated syndrome (CIS) now recognized as the first clinical presentation of a disease; relapse-remitting MS (RRMS) which accounts for 85% of MS patients; primary progressive MS (PPMS) accounting for 15% of MS patients present and secondary progressive MS (SPMS) begins with a series of relapses and remissions, prior to a gradual onset of disability.

There are different MS phenotypes including clinically isolated syndrome (CIS), primary progressive MS (PPMS), relapsing remitting MS (RRMS), and secondary progressive MS (SPMS) (Lublin *et al.*, 2014). PPMS is defined as gradual disease progression with unremitting characteristics (Miller and Leary, 2007), and affects about 10 -15% of people diagnosed with MS. The most common phenotype is RRMS, accounting for 85% of MS patients (Miller and Leary, 2007), where patients experience spontaneous episodes of demyelination called relapses. These episodes are then proceeded by periods of recovery, recognised as disease remission. The relapse rate varies from patient to patient, averaging one to two episodes per year; and the relapse remitting (RR) stage of MS can last for years or decades (Compston & Coles, 2002). Typical age of onset of RRMS is 20 – 40 years of age, with 60 – 70 % of patients converting to SPMS within 10 - 20 years of RRMS diagnosis (Confavreux and Vukusic, 2006). SPMS is defined as secondary phase of MS characterized by continuous, irreversible neurological decline associated with relapse. Prevention of conversion to SPMS is a major therapeutic goal of MS research.

MS pathogenetic theories have developed over time with the onset of the immune-mediated process favouring the ‘outside-in’ theory. The “outside-in” hypothesis constitutes a primary pathogenesis of autoimmune inflammation followed by a secondary pathogenesis of myelin degradation. The “inside-out” hypothesis has a primary pathogenesis of oligodendrocyte injury, myelin destruction and myelin destabilization. This then produces a secondary pathogenesis due to the activation of an inflammatory response. This reactive inflammation produces auto-reactive T cells that return to the PNS and recruit more proinflammatory lymphocytes (Titus *et al.*, 2020).

Table 1.1 “Inside-out” and “Outside-in” disease model systems

	“Inside-Out” models			“Outside-In” models			
	Epsilon Toxin Model	Diphtheria Toxin A (DTA) Model	Cuprizone autoimmune encephalitis (CAE) Model	Chronic Experimental Autoimmune Encephalomyelitis (C-EAE) Model	Relapsing Remitting Experimental Autoimmune Encephalomyelitis (R-EAE) Model	Theiler’s Virus-Induced Demyelinating Disease	Japanese Macaque Encephalomyelitis (JME) Model
Model species	Mouse	Mouse	Mouse	Mouse	Mouse	Mouse	Macaque
Induction of disease model (in Adults)	Epsilon toxin, produced by type B and D strains of <i>Clostridium perfringens</i> , a spore-forming gram-positive bacterium	Timed genetic expression of diphtheria toxin (tamoxifen induced <i>PLP^{CreERT}</i> for targeting OL)	Cuprizone diet for 2 weeks, then inject CFA (SubQ) and Pertussis Toxin (IP)	MOG _{35–55} + CFA (SubQ) and Pertussis Toxin (IP)	PLP _{139–151} + CFA (SubQ)	Theiler’s Murine Encephalomyelitis Virus (TMEV) intracerebral infection	Japanese Macaque Rhadinovirus (JMRV), spontaneous or injected
Disease model trigger	Epsilon Toxin induced cytotoxicity (OL)	DTA induced cell death (OL), secondary MOG peptide immune response	Cuprizone destabilizes myelin, Citrullinated MBP drives immune response	MOG _{35–55} peptide immune response	PLP _{139–151} peptide immune response	Response to TMEV and subsequent spreading to PLP and MBP epitopes	JMRV infection, MBP peptide immune response
Disease model pathogenesis	OL cytotoxicity, triggers demyelination	OL ablation, triggers demyelination/remyelination, secondary immune response (respond to MOG peptide)	Myelin breakdown, secondary immune response (respond to MBP epitope)	Immune infiltration (respond to MOG peptide), secondary CNS degeneration	Immune infiltration (initially respond to PLP peptide, later to MBP), secondary CNS degeneration	Immune response to virus, release of myelin epitopes inducing autoimmune pathology, secondary CNS degeneration	Immune response to virus and infiltration (respond to MBP peptide), secondary CNS degeneration

1.2.4 Spinal cord injury

The spinal cord is a thick bundle of nervous tissue situated in the vertebral column of vertebrates and when damaged causes major motor, sensory and autonomic dysfunctions. For the last 30 years the global prevalence of SCI has increased from 236 to 1298 cases per million populations, with the estimated global incidences of SCI falling between 250,000 and 500,000 individuals every year (Khorasanizadeh *et al.*, 2019). The CNS has limited regenerative and repair capacity when injured, and therefore any function lost due to SCI is generally permanent. SCI can be traumatic or non-traumatic and can be classified into three

types based on cause: mechanical forces, toxic, and ischemic (from lack of blood flow). Non-traumatic injuries or illnesses include bone cancers, osteoporosis, inflammation of the cord, with the most common causes being degenerative conditions of the spinal column and vascular problems resulting in infarction or haemorrhage (**New and Marshall, 2014; New et al., 2014**). These can have similar pathological outcomes as traumatic injury. Traumatic injuries, however, are caused by an abrupt traumatic hit to the spine which results in damage to one or more of the vertebrae, or a severing of the spinal cord. When the spinal cord is lacerated by a sharp penetrating force, contused, or compressed by a blunt force, or infarcted by a vascular insult, it referred to as the ‘primary injury’ (**Dumont et al., 2001**). Once the primary injury occurs it leads to ‘secondary injury’, characterised by an immunological cascade with the influx of immunological factors resulting in the death of neurons and glial cells, and focal inflammation. Most of the resulting cell death is caused by cell permeabilization, pro-apoptotic signalling and ischaemic injury due to the destruction of the microvascular supply of the spinal cord (**LaPlaca et al., 2007; Choo et al., 2007**). Additional contributors to SCI pathology are mechanisms via the excitatory process mediated by excessive glutamate release (**Liu et al., 1999**), generation of free oxygen radicals (**Ahmed et al., 2017; Jin et al., 2014**) and metabolic dysfunction. Glutamate receptors (GluRs) appear to contribute significantly to the pathology that develops in the spinal cord after traumatic injury. Early models of SCI showed that extracellular glutamate is transiently but significantly increased after trauma (**Panter et al., 1990; Liu et al., 1991; Liu et al., 1999**). This increase in GluRs activation and glutamate concentration creates toxic environment for both neurons and oligodendrocytes (**Xu et al., 2014**).

1.2.5 Traumatic brain injury

Traumatic brain injury causes substantial neurological disabilities, with annual TBI incidences reaching millions, making it a global health challenge. According to European Union statistics, there are 1.5 million hospital admissions due to TBI per year, with a mortality rate between 30% and 40% (**Maas et al., 2017**). TBI is categorised into severe, moderate, and mild by scores on the Glasgow coma scale (GCS) using evidence from standard brain imaging (CT) and based on clinical grounds. TBI is defined as alteration in brain function due to an external force with the presence of one of the following signs: loss/impaired consciousness, memory loss for events prior or after the injury, neurologic deficits, mental disturbances confusion, disorientation, and slow thinking (**Menon et al., 2010**). Like with SCI, TBI can be classified into primary and secondary injury, with secondary injury developing over minutes to months and with a cascade of metabolic,

cellular, and molecular events leading ultimately to brain cell death, tissue damage, and atrophy (**Bramlett *et al.*, 2015**). Secondary injury involves depolarization of the neurons with the release of excitatory neurotransmitters such as glutamate and aspartate that lead to increased intracellular calcium (**Guerrero *et al.*, 2015**, **Hinzman *et al.*, 2014**). Glutamate is the primary excitatory neurotransmitter in the brain, while γ -aminobutyric acid (GABA) is the principal inhibitory neurotransmitter. Intracellular calcium activates a series of mechanisms with the activation of enzymes caspases, calpain, and free radicals that results in degradation of cells either directly or indirectly through an apoptotic process. This degradation of neuronal cells is associated with an inflammatory response that further damages neuronal cells and incites a breach in the blood brain barrier (BBB) and further cerebral swelling.

1.3 Current strategies for CNS repair

1.3.1 Hurdles for CNS therapeutics

The development of therapeutics for diseases of the CNS is complicated by the presence of the BBB. The BBB is a highly selective semipermeable border of endothelial cells that prevents solutes in the circulating blood from crossing into the extracellular fluid of the CNS. This heavily restricting barrier capacity allows BBB endothelial cells to tightly regulate CNS homeostasis, which is critical for proper neuronal function, as well as protect the CNS from toxins, pathogens, inflammation, injury, and disease (**Risau and Wolburg, 1990**). However, as well as preventing harmful molecules into the CNS the BBB also prevents certain drugs and large-molecule therapeutics such as biopharmaceuticals from entering the CNS. In general, compounds must be small enough (<500 Daltons) to cross the BBB unless they are the subject of facilitated transport (**Fong *et al.*, 2015**). Intravenous immunoglobulins (IVIg) have been evaluated in clinical trials for the treatment of various disorders of the CNS, however, their poor brain bioavailability has limited their use for treating CNS diseases. Following parenteral administration of therapeutic IVIg's to mice, levels in the brain correspond to only 0.01–0.1% of those found in plasma, demonstrating the inability of IVIg's to cross the BBB (**St Amour *et al.*, 2013**). Drug development for Alzheimer's disease has proven to be difficult, with a 99.6% failure from 2002 to 2012, and the success rate continues to remain at this low level (**Cummings, 2017**). Essentially all large molecule pharmaceuticals (>500 Da), including peptides, recombinant proteins, monoclonal antibodies, RNA interference (RNAi) based drugs, and >98% of small-molecule drugs do not cross the BBB (**Pardridge, 2007**). Certain small molecule drugs can cross the BBB via

lipid-mediated free diffusion, providing the drug has a molecular weight <400 Da and forms <8 hydrogen bonds. Ultra-low molecular weight heparin for example, has demonstrated the capacity to cross the BBB (**Ma *et al.*, 2002**). BBB permeation decreases exponentially with the addition of each pair of hydrogen bonds added to the drug structure (**Pardridge *et al.*, 1979**; **van der Waterbeemd *et al.*, 1997**). These chemical properties are lacking in most small molecule drugs, and all large molecule drugs.

Due to the lack of effective BBB drug targeting technology, CNS drug developers are left with the traditional approaches to solving the brain drug delivery problem: small molecules, trans-cranial brain drug delivery, and BBB disruption. Specialized methods of drug delivery are required to maximize the therapeutic potential of fusion proteins, monoclonal antibodies, and other macromolecules for CNS indications. One of these methods is perispinal delivery. Perispinal administration involves delivery into the anatomic region posterior to the ligamentum flavum and the spinal canal and is therefore less complicated than epidural or intrathecal injection (**Tobinik, 2004**; **Tobinik *et al.*, 2014**). Other techniques that are currently in use for administration of CNS therapeutics include subcutaneous and intramuscular injections and intravenous infusion.

1.3.2 Current strategies for demyelinating diseases: multiple sclerosis

There is currently no cure for MS but there are several pharmaceuticals that have shown clinical efficacy in reducing disease progression, known as disease modifying therapies (DMTs). Nine classes of DMTs with varying mechanisms of action and routes of administration, are available for RRMS. These drugs include interferon β , glatiramer acetate, teriflunomide, sphingosine 1-phosphate receptor modulators, fumarates, cladribine, and 3 types of monoclonal antibodies. One additional DMT, ocrelizumab, is approved for PPMS.

Interferon β treatments are one of the most prescribed DMTs for MS and was first approved by the FDA in 1995. The effectiveness of β interferons is considered 'moderate' with a 33% reduction in relapses (**Johnson *et al.*, 1995**). The mechanisms of action, however, are still unknown with theories suggesting that beta interferons are involved with the downregulation of pro-inflammatory chemokines. This results in the reduction of immune cell trafficking - such as T cells and B cells - into the CNS (**Kieseier, 2011**).

Dimethyl fumarate (TecFidera™) is another popular DMT for RRMS, and like Interferon β , the mechanisms are relatively unknown. In 2012 a trial showed that a dimethyl fumarate-based drug called BG-12 used for psoriasis, also worked against MS, reducing the number of relapses individuals had (**Gold *et al.*, 2012**). The effectiveness of TecFidera™ is classified as ‘good’ by neurologists, with patients having a 53% reduction in relapses compared to placebo, with 73% of those patients receiving staying free of relapses for two years (**Gold *et al.*, 2014**).

Ocrelizumab (Ocrevus®) is a humanized anti-CD20 monoclonal antibody approved in 2017 for the treatment of adults with RRMS and is the first DMT approved for the treatment of PPMS. In RRMS, it reduces the number of relapses by 80% over a two-year period, giving it the classification of ‘high’ success by neurologists (**Hauser *et al.*, 2017, Sempere *et al.*, 2020**). In PPMS, however, disability was slowed down by 25% - a moderate success (**Montalban *et al.*, 2017**). The mechanism by which ocrelizumab produces its clinical benefits in MS is not fully understood but is thought to involve immunomodulation through a reduction in the number and function of CD20 expressing B cells. B cells play an important role in the pathogenesis of MS through autoantibody production, antigen presentation, pathogenic cytokine production and formation of meningeal ectopic lymphoid tissues (**Lehmann-Horn *et al.*, 2017**). Therefore, B cell depletion is an effective treatment strategy for MS by reducing B-cells reaching the CNS and eliciting their negative effects on myelinated axons.

Although there has been some success with DMT’s for MS, research continues to create more effective treatments. All DMT’s currently aim to reduce episodes of relapse for those with RRMS. Currently, there is only one approved treatment for PPMS, highlighting the need for continued efforts for drug discovery in the field.. An unmet and urgent need is for the development of myelin repair promoting therapies for MS, especially for remyelination after relapses, and during PPMS.

1.3.3 Current strategies for spinal cord injury

The prognosis for neurological recovery in SCI patients is variable, however any such recovery, even to a limited degree, is expected mostly within the first 6 months following injury, with more limited further improvements observed within 5 years (**Kirshblum *et al.*, 2004**). Any treatment for SCI should target cell survival, axonal growth, remyelination and synapse formation. As previously discussed, SCI injury involves the initial primary injury followed by an immunological cascade, termed secondary injury. Currently, strategies for

SCI involve reducing this secondary immunological response. To date, the administration of systemic immunosuppressive medications, in particular methylprednisolone sodium succinate (MPSS), a steroid, has been the primary pharmacological treatment. MPSS has been shown to be an anti-inflammatory agent reducing TNF- α and NF- κ B synthesis (**Oudega *et al.*, 1999**), and clinical trials have shown that patients receiving MPSS within 48 hours of initial injury have improved motor function outcome (**Bracken *et al.*, 1990; Bracken *et al.*, 1997**). However, in these trials it was also reported that there was a higher rate of sepsis and pulmonary complications particularly with a 48-hour infusion of MPSS (**Bracken *et al.*, 1998**). These adverse effects have left many clinicians divided with some continuing to employ MPSS feeling that the risks are justified in the context of the severe deficits that accompany SCI (**Fehlings 2001**). Current guidelines recommend against MPSS administration as the risk for harm is considered higher than potential benefits (**Hurlbert *et al.*, 2015**). This subject remains under debate (**Fehlings *et al.*, 2014; Hurlbert, 2014**).

Riluzole is a glutamatergic modulator that has recently shown potential for neuroprotection after SCI. Riluzole blocks voltage-activated sodium and calcium ion channels, inhibits glutamate release, and activates potassium ion channels (**Duprat *et al.*, 2000**). The blockage of sodium channels causes neuroprotective activity in primary and early acute injury phase of SCI, and this effect could inhibit accumulation of intracellular sodium ions, which is toxic to neurons. While the effects of riluzole are extensively documented in animal models of SCI (**Lang-Lazdunski *et al.*, 2000**), the effect in humans is not completely understood. In a clinical trial conducted at the Tabriz University of Medical Sciences, 60 patients with acute SCI were referred. For all of them, surgery was performed and Riluzole was prescribed for half of them. In the 6-week and 3-month follow-ups, no sensory and motor improvement was observed, but in 6 months, a significant improvement was detected in the case group compared to the control group (**Meshkini, 2000**).

More recently, stem cell therapy (SCT) has come to the forefront of SCI repair. Studies have shown that stem cells can protect and regenerate the injured spinal cord through neuroprotection, immunomodulation, axon sprouting and/or regeneration, neuronal relay formation, and myelin regeneration, among other mechanisms (**Ashammakhi *et al.*, 2019**). However, due to the complex nature of SCI, vast majority of preclinical trials have been conducted in rodents, and there are fewer than 20 studies in large animal models, accounting for < 2% of all preclinical research (**Gabel *et al.*, 2017**). Although the progress made for SCT is exciting for future SCI repair, currently there are many adverse effects that need to be managed first as SCT can lead to tumour formation, inappropriate migration, secondary

injury, infection, and other adverse effects (**Matsuda *et al.*, 2009**). A recent single-arm meta-analysis based on 62 clinical trials of SCT for SCI found that although the efficacy of SCT is encouraging, the subsequent adverse effects remain concerning, and that current evidence is not sufficiently strong to support the clinical translation of stem cell therapy for spinal cord injury. Cell types that are currently being reviewed and investigated for SCI include mesenchymal stem/stromal cells (MSCs) (**Lindsay and Barnett 2021**), and olfactory ensheathing cells (OECs) (**Chen *et al.*, 2019; Lindsay *et al.*, 2020**).

In summary, there are many challenges for developing novel therapeutics for CNS injury. Continued research is needed for developing novel therapeutics that focus on neurite outgrowth, and remyelination. Screening for molecules that can encompass several areas of repair is essential for successful treatment of CNS injury. One such molecules with the potential to do so are heparan sulphate proteoglycans and are discussed below.

1.4 Heparan sulphate proteoglycans

Heparan sulphates (HS) are part of the glycosaminoglycan (GAG) family, consisting of a *N*-acetylglucosamine (GlcNAc)-uronic acid (UA) repeating disaccharide. Heparan sulphates are conjugated to a core protein (proteoglycans) to form heparan sulphate proteoglycans (HSPGs) (**Lindahl *et al.*, 1989**). HSPGs are ubiquitously expressed on cell surfaces and in the extracellular matrix of most animal tissues, having essential functions in development and homeostasis, as well as playing various roles in disease processes. They interact with basic amino acid residues in the binding grooves of numerous extracellular proteins, to function as regulators of cell signalling (**Turnbull *et al.*, 2001**). Heparin is a highly sulphated sub-class of HS, and is widely known for its anticoagulant properties, hence its use as a prophylaxis pharmaceutical (**Choay *et al.*, 1980**). The current distinction between heparin and HS is not based primarily on carbohydrate structure but rather on proteoglycan (PG) type and cellular distribution. Generally, it is that heparin is exclusively produced by mast cells, whereas HS are produced by all cells of the body. HS are thought to operate through numerous mechanisms of action including 1) acting as a cofactor in the formation of ligand-receptor complexes (**Yayon *et al.*, 1991**) 2) the sequestering of ligands in the extracellular matrix (**Vlodavsky *et al.*, 1991; Elkin *et al.*, 2001; Massena *et al.*, 2010**) and 3) acting as an endocytic receptor, enabling the cellular internalisation of ligands (**Colin *et al.*, 1991; Belting, 2003**). For example, the gene *N*-acetylglucosamine *N*-deacetylase-*N*-sulfotransferase 1 (Ndst1) is a HS biosynthetic enzyme. When selectively knocked out of

macrophages an increased responsiveness was shown to IFN- β stimulation and elevated production of pro-inflammatory cytokines and chemokines, suggesting that the role of HSPGs in IFN- β signalling is to sequester it away from its receptor and thus maintain macrophages in acquiescent state (**Gordts *et al.*, 2014**). Additionally, a rodent bioavailability study demonstrated that the level of exogenous ¹⁴C-labeled FGF-2 was controlled by HSPGs (**Colin *et al.*, 1999**). This deduction was made following the incubation of tissue sections in 2M NaCl, which resulted in the elution of all ¹⁴C-labeled FGF-2, indicating that the cellular uptake was HSPG-mediated most likely by functioning as an endocytic receptor, aiding in the cellular internalisation of ligands. In summary, HS is a polyanionic molecule located on the cell surface and in the ECM, it modulates cell signalling through specific protein interactions.

The highly sulphated chain of HS binds to proteins mainly through electrostatic interactions between its sulphate groups and positively charged groups of the protein, typically lysine/arginine residues (**Cardin and Weintraub, 1989**). Therefore, changes in sulphate groups modifies the electrostatic interactions between the HSPG and proteins such as chemokines and cytokines. The specificity and the affinity of a protein for HS chains depends largely on the sulphation profile and chain length of HS (**Lindahl and Li, 2009**). The sulphation profile and backbone modifications of HS allows for the diversity of HS to interact with a multitude of chemokines and proteins. Modifications occur during HS biosynthesis through *N*-acetylglucosamine residues being *N*-sulphated, via *N*-deacetylase/*N*-sulphotransferase (**Aikawa *et al.*, 2001**), and the glucuronic acid residues being subjected to C5 epimerisation, results in a multitude of HS variations (**Feyerabend *et al.*, 2006**). Even when biosynthesis is complete, and HSPGs are secreted or presented on the cell surface, the modification of the fine structure continues. This is due to the activity of the previously sulf-1 and sulf-2 - endosulphatases that remove sulphate groups (**Morimoto-Tomita *et al.*, 2001**). As a result, HSPGs can interact with a multitude of chemokines and proteins.

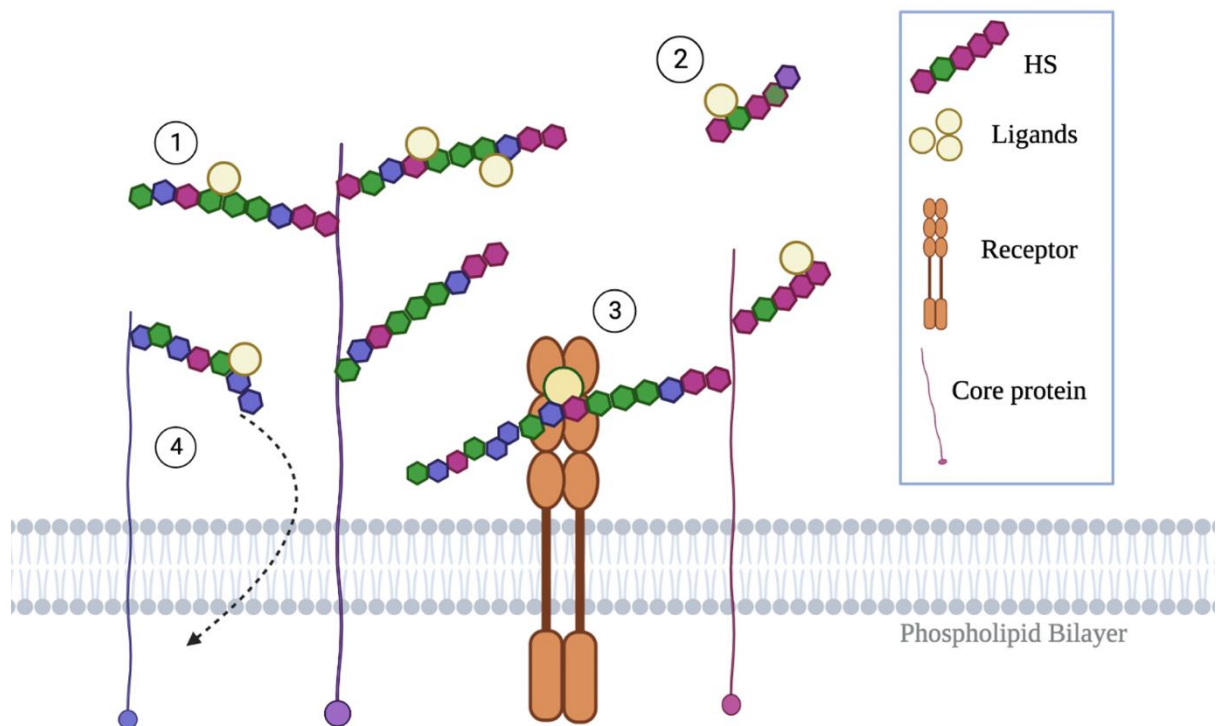


Figure 1.5 |Heparan sulphate on the cell surface. Heparan Sulphate chains are conjugated to core proteins on the plasma membrane. The HS functions as a regulator of cell signalling, this can occur via the sequestering of ligands in the extracellular matrix (1), heparinase can then cleave the HS, releasing the bound factor with the adjoined oligosaccharide (2). Furthermore, HS can act as a cofactor, facilitating the formation of functional ligand-receptor complexes (3), HS has also been shown to act as an endocytic receptor, enabling the cellular internalisation of ligands (4)

1.4.1 Low sulphated heparan sulphates in CNS repair

Olfactory ensheathing cells are a class of mature functionally differentiated glial cells that function between Schwann cells (SCs) (the myelinating cells of the peripheral nervous system) and oligodendrocytes. OECs ensheath and guide the olfactory receptor neurons (ORNs) from the olfactory mucosa epithelium that lines the upper aspect of the nasal cavity to the outer layer of the olfactory bulb, which resides in the CNS (**Barber *et al.*, 1982**). After injury, the ORNs die back, and new nerves are generated from basal stem cells in the epithelium. OECs are thought to encourage the peripheral ORNs to enter and re-synapse in the glomerulus layer of the olfactory bulb. OECs have been found to secrete low sulphated

heparan sulphates (**Higginson et al., 2012**), that have been shown to modulate their reparative mechanisms, and are discussed below.

OECs and SCs have the capacity to remyelinate axons in the CNS, during cell translation (**Blakemore, 1977; Franklin et al., 1996**). Since this discovery it has been important to understand the mechanisms behind the cell interactions between glial cells and OECs/SCs, for CNS integration. An *in vitro* confrontation assay was developed to assess the interactions of astrocytes and OECs/SCs. This confrontation assay revealed that SCs could not freely mingle with astrocytes, and formed a distinct non-overlapping boundary, separating the two cell types. Additionally, these astrocytes became hypertrophic and increased their expression of glial fibrillary acidic protein (GFAP) and chondroitin sulphate proteoglycan (CSPG). What was interesting however, was that OECs could freely intermingle with these astrocytes (**Lakatos et al., 2000**). This astrocyte inducing effect was later confirmed *in vivo* with the injection of SCs directly injected into the spinal cord of adult rats (**Santos-Silva et al., 2007**). Additionally, Schwann cell-conditioned media (SCM) was added to monocultures of astrocytes where there was induced proliferation and increased CSPG expression in a fibroblast growth factor receptor 1 (FGFR1)-independent manner. However, when SCM was added to OECs/astrocyte co-cultures this also induced reactive astrocytosis and boundary formation. This finding suggested that it was a SC-secreted factor that produce this boundary formation and reactive astrocytes (**Santos- Silva et al., 2007**). It was shown that highly sulphated HSs and FGF 1 and 9 were the possible determinants of boundary formation induced by SCs. Disaccharide analysis of HS in SC-conditioned and rat OEC-conditioned media showed that SCs secreted more highly sulphated HS than OECs (**Higginson et al., 2012**). Furthermore, extracellular HS 6-*O*-endosulfatase enzymes, sulf-1, and sulf-2 (which remove sulphate groups) were expressed at a significantly lower level by SCs compared with OECs. This lower expression of extracellular sulfs would lead to the production of a higher sulphated heparan sulphate content exhibited by SCs (**Higginson et al., 2012**) Additionally, sulf-1 and sulf-2 display a strict specificity for 6-*O*-sulphate moieties (**Frese et al., 2009**). As such, the decrease in sulf expression by SCs, leads to the production of 6-*O*-sulphate rich HS. This data provides evidence that HSs are important mediators of cell integration, and cell communication within the CNS, making them attractive candidates for novel therapeutics of the CNS. A panel of modified heparins (mHeps- which lack anti-coagulation activity), were introduced to models of CNS injury, and their activity was observed (**McCanney et al., 2019**). The panel of mHeps had varying sulphation levels and it was found that low sulphated mHeps (LS-mHeps) enhanced neurite outgrowth and myelination, whereas highly sulphated mHeps (HS-mHeps) had attenuating effects. One hypothesised

mechanism as to how these LS-mHeps were eliciting repair was through the sequestration of negative regulators of myelination. One such regulator is the chemokine CCL5 (RANTES) which is upregulated after demyelination *in vitro* (McCanney *et al.*, 2019) and has shown to cause significant inhibition of developmental myelination, *in vitro* (Schultz *et al.*, 2021). CCL5 is produced by many cell types including monocytes/macrophages, microglia, astrocytes, and neurons (Rock *et al.*, 2004), and CCL5 gene polymorphisms are associated with clinical course severity in patients with MS – specifically an increased risk of severe axonal loss (Van veen *et al.*, 2007). By sequestering CCL5 it was hypothesised that LS-mHeps negated the hypomyelination caused by CCL5. It was proposed that LS-mHeps exerted multiple beneficial effects on mechanisms supporting enhanced repair and represented novel candidates as therapeutics for CNS damage.

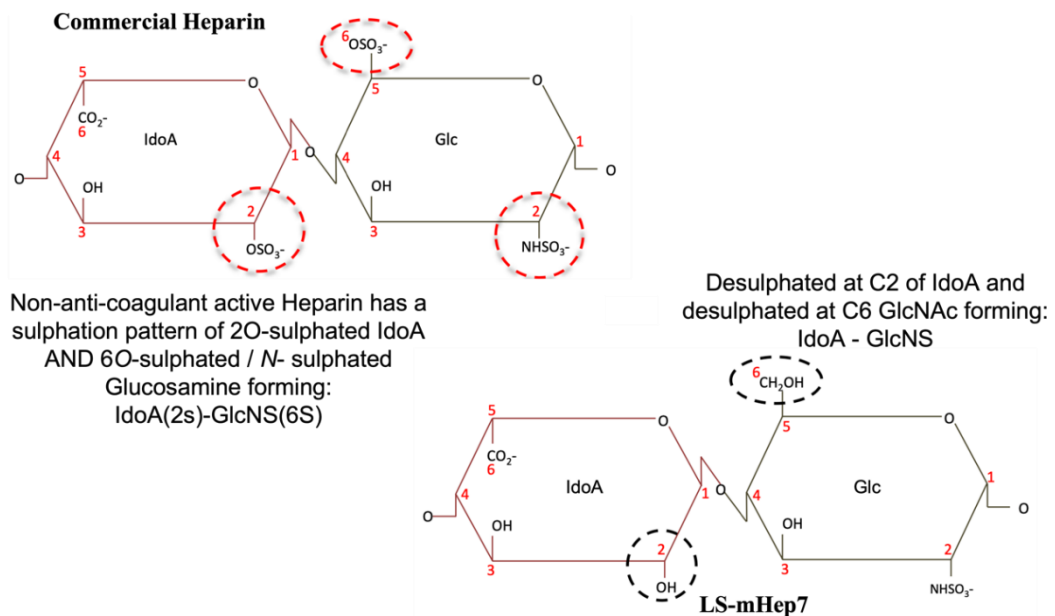


Figure 1.6 |Schematic of commercial heparin and LS-mHep7. Heparan sulphate chains are made up of a *N*-acetylglucosamine (GlcNAc)–uronic acid (UA) disaccharide repeats, which is conjugated to a core protein via a tetrasaccharide linker sequence. Commercial heparin (left) is a highly sulphated heparan sulphate. Low sulphated heparin mimetic 7 (LS-mHep7) has been selectively desulphated at C2 of IdoA and C6 GlcNAc (right).

1.4.2 The role of heparan sulphate in CNS development

Development of the mammalian nervous system can be roughly divided into three stages 1) neurogenesis 2) axon guidance and 3) synaptogenesis. Neurogenesis is the process of generation and differentiation of neurons from neural stem cells (NSCs) that reside in the ventricular zone of the embryonic cerebral cortex. Neurogenesis occurs predominantly during embryonic stages and completes before birth in most parts of the mammalian CNS.

Neurogenesis is regulated by several growth factors and morphogens. Fibroblast growth factor-2 (FGF2) is an established neurogenic factor for proliferation and differentiation of multipotent neural stem cells both during development and in the adult mouse brain (**Tao *et al.*, 1996; Rai *et al.*, 2007; Werner *et al.*, 2011**). FGF2 also regulates the fate of progenies generated from these neural stem cells: in low FGF2 concentrations, stem cells generate predominantly neurons, whereas at higher FGF2 concentrations, they generate glial cells (**Quian *et al.*, 1997**). It is well established that that HSPGs play a key role in the modulation of FGF2 activity (**Burgess and Maciag 1989; Ornitz, 2000**) as FGF2 binds heparan sulphate chains (**Nugent and Edelman 1992; Pellegrini 2001**). Some HSPGs play crucial roles in FGF2 signalling by acting as coreceptors for FGF2 (**Aviezer *et al.*, 1994**), while others may act as reservoirs of FGF2 in the extracellular spaces.

Neuronal cells generated from NSCs in the ventricular zone migrate outwardly toward specific locations in the developing brain and extends axons and dendrites to form stereotypic neuronal connections. Axonal guidance is incredibly important during this process to ensure the correct formation of neuronal networks. The role of heparan sulphate on axon guidance has been demonstrated using the developing *Xenopus* retinotectal pathway (**Walz *et al.*, 1997**). In *Xenopus*, adding HS to the developing retinotectal pathway or removing HS with heparinase severely disrupt target recognition causing axons from the retina to bypass their primary target, the optic tectum, in the brain. Additional morphogens such as Wnt, FGF, BMP, or Shh, whose role as guidance molecules has been identified, also bind to HS with a high affinity. Research has identified that Wnt signalling is regulated by HSPGs, with heparin activating Wnt-mediated neuronal morphogenesis in rodent primary cultures (**Colombres *et al.*, 2008**). Wnt signalling regulates different aspects of neuronal behaviour, from neural patterning to synapse formation and function (**Ciani and Salinas 2005; Cerpa *et al.*, 2008**).

The synapse is the fundamental functional element of the nervous system, where neurotransmitters are released from presynaptic nerve termini and bind to their receptors on the postsynaptic membranes. HSPGs, such as syndecans, have been considered as the regulators of synapse formation (**Condomitti *et al.*, 2018**).

Recent findings from vertebrate and invertebrate studies have raised the importance of glycosylphosphatidylinositol-anchored HSPGs, glypicans, as central players in the development and functions of synapses. Glypicans constitute one of the two major families of HSPGs, with the other major family being syndecans. It has shown that astrocyte-secreted factors powerfully induce the formation of functional excitatory synapses between CNS

neurons (Ullian *et al.*, 2001). Upon further investigation it was found that these secreted factors were glypican 4 (Gpc4) and 6 (Gpc6) and were sufficient to induce functional synapses between purified retinal ganglion cells (RGC). It was also demonstrated that Gpc4-deficient mice have defective synapse formation, with decreased amplitude of excitatory synaptic currents in the developing hippocampus and reduced recruitment of AMPARs to synapses (Allen *et al.*, 2012). Syndecans are known to regulate cellular and axonal migration in the brain (Condomitti and de Wit, 2018; Yuzaki, 2018), but are also enriched at synapses. Until recently their role in synaptic function remained elusive. Zhou *et al.*, 2021 has demonstrated that syndecans SDN-1 is a core organizer of cholinergic synapses and stands at the core of the cholinergic synapse organization by bridging the extracellular synaptic determinants to the intracellular synaptic scaffold that controls the postsynaptic receptor content.

Thus, HSPGs are required for CNS development, including neurogenesis, axon guidance and synaptogenesis, and their importance in mammalian development is known.

1.4.3 Heparan sulphate mimetics as therapeutics in CNS

Based on the knowledge that HSs are regulators of cell signalling within the CNS, it is not surprising that they are already being investigated as therapeutics in CNS disease and injury. Enoxaparin is a common low-molecular-weight heparin (LMWH) used in the prevention and management of various thromboembolic disorders. Previously enoxaparin has been shown to reduce cerebral edema and improve neurologic recovery in TBI, through blunting of cerebral leukocyte recruitment. High mobility group box 1 (HMGB1) is a structural DNA-binding protein secreted by various cell lines including glial cells. HMGB1 has been implicated in the pathogenesis of various CNS diseases including TBI (Gao *et al.*, 2012) subarachnoid haemorrhage (Sun *et al.*, 2014) autoimmune encephalomyelitis (Uzawa *et al.*, 2013), transient Ischemia (Liu *et al.*, 2007), and seizures (Maroso *et al.*, 2010). It is thought that HMGB1 induces inflammation by recruiting leukocytes to areas of CNS damage, and enoxaparin has shown to interfere with this HMGB1 signalling – potentially through sequestration (Li *et al.*, 2016). Further investigations have demonstrated that enoxaparin ameliorates TBI edema and neurologic recovery, via the reduction of cerebral leukocyte endothelial interactions and vessel permeability (Li *et al.*, 2015). Recently, a pilot study determining the effects of early enoxaparin administration to patients suffering TBI was investigated. The two groups were compared for the occurrence of intracranial hematoma (ICH) and for clinical neurological outcome, assessed by the Glasgow Outcome Scale. The

treatment group displayed improved clinical outcomes compared to the placebo, reaffirming the potential of heparin mimetics as a TBI therapeutic (**Baharvahdat et al., 2019**).

Tauopathies are progressive neurodegenerative diseases characterized by intracellular accumulation of tau fibrils in defined brain regions – such as Alzheimer’s disease. Tau is the major microtubule associated protein (MAP) of a normal mature neuron, and in the case of AD is abnormally hyperphosphorylated and aggregated into bundles of filaments (**Grundke-Iqbal et al., 1986**). It has been observed that heparin competitively inhibits cellular tau uptake (**Holmes et al., 2013**) and binds to toxic tau species. The binding significantly reduces the cellular uptake of toxic tau oligomers and protects cells from tau oligomer induced cytotoxicity (**Wang et al., 2018**). Other LMW heparins such as neuroparin have demonstrated neuro-protective effects in mouse models of AD (**Dudas et al., 2002; Bergamaschini et al., 2004; Timmer et al., 2010**). Recently a synthetic heparin mimetic, SN7-13, was produced as a potential AD therapeutic, and was found to successfully blocks tau aggregate cell uptake (**Stopschinski et al., 2020**).

HSPGs have been investigated in SCI therapeutic studies. The receptor-type protein tyrosine phosphatase sigma (PTPR σ) regulates axonal regeneration/sprouting as a molecular switch in response to glycan ligands. Targeting the CS-PTPR σ pathway could prove as a beneficial target in the treatment of axonal injury observed in SCI. HSPGs have been found to interact with PTPR σ and promotes growth of axons (**Aricesu et al., 2002; Coles et al., 2011**). Recently, systemic administration of enoxaparin was found to promote anatomical recovery after both optic nerve and spinal cord injuries in rats at clinically tolerated doses. Moreover, enoxaparin promoted recovery of motor function without obvious haemorrhage (**Ito et al., 2021**). This data shows a promising future for HSPGs in SCI novel therapeutics.

1.5 Experimental models of the mammalian CNS

1.5.1 *In vitro* models of the CNS

Cell culture models are important for studying injury in the CNS. Although there are some limitations, overall *in vitro* models allow experimentation that would otherwise be very challenging or impossible *in vivo*. *In vitro* culture systems are desirable as they reduce or replace animal use and can often be adapted for high-throughput screening (**Bijland et al., 2019; Aldewachi et al., 2021**).

1.5.1.1 Neurite outgrowth assays

A variety of *in vitro* models have been developed to understand the mechanisms underlying the regenerative failure of the CNS, and to guide pre-clinical development of regeneration-promoting therapeutics. Typically, cell preparations are obtained by mechanical dissection, enzymatic dissociation, and centrifugation. Filtration or affinity separation techniques may be utilized to produce relatively homogenous cultures from mixed cell preparations. Neurite outgrowth assays are among the most utilized phenotypic screens relevant to axon regeneration. They have been successfully used to identify genetic regulators of axon regeneration (**Moore *et al.*, 2009; Blackmore *et al.*, 2019**), perform mechanistic studies of the involved pathways (**Buchser *et al.*, 2010; Loh *et al.*, 2008**), and identify small molecules that can promote regeneration (**McCanney *et al.*, 2019**). In most methods of neurite outgrowth assays neuronal cells are grown on an adherent substrate coated with a nonspecific attachment factor to additionally help promote cell adhesion to solid substrates. Often cells are plated on cover slips coated in poly-L-lysine. Neurons plated directly on poly-L-lysine will adhere and extend neurites. From here neurite outgrowth cultures provides an easy way to determine the effects of a particular substrate or exogenous factor on neuron behaviour – important for studying injury in the CNS such as TBI and SCI.

Variations of the neurite outgrowth assays can develop including neurite retraction assays. In the case of retraction assays, neurons are cultured for a given amount of time and allowed to extend neurites. Then, neurons are challenged with a substance (e.g., lysophatidic acid) that causes growth cone collapse and neurite retraction (**Fukushima, 2004**). The neurites are allowed time to respond, after which the cultures are analysed. Retraction assays allow the investigation of mechanisms that lead to the neurite collapse and retraction by inducing the process in an entire cell culture (**Burgos-Bravo *et al.*, 2020; Konaka *et al.*, 2020; Roloff *et al.*, 2015**).

1.5.1.2 Myelinating cultures

Studying the growth and myelination of CNS axons is pertinent to research into both myelination and spinal cord repair. Myelination cell culture systems are useful tools for studying myelin biology and myelin-related disorders. Established methods have produced these cultures in mice (**Thomson *et al.*, 2006**) and rats (**Sorensen, 2008**). In both cases cultures are generated from embryonic spinal cords and developed until they produce mature, compact myelin.

Myelinating cultures can be manipulated to represent SCI by creating a cell free area down the centre of the cover slip using a scalpel (**Boomkamp *et al.*, 2014**), which recounts many

features of SCI in vivo (**Boomkamp *et al.*, 2012**). After time, neurite outgrowth can be studied across the cell free area, with the addition of repair enhancing molecules (**McCanney *et al.*, 2019**). Myelination at the side of the cut can also be studied, as myelination levels at the side of SCI lesions is a large area of interested in the development of SCI and MS therapeutics.

For demyelination studies, such of those required for MS research, these cultures can be demyelinated using an antibody mediated process (**Elliot *et al.*, 2012**). At developmental day 24, cultures can be demyelinated by overnight incubation with compliment and Z2 antibody, which identifies MOG. This successfully demyelinated the cultures without any negative impact on Axons and other glial cells. This assay enables the identification of remyelination enhancing molecules, which is an important area for MS novel therapeutics.

1.5.2 *In vivo* models of MS

While *in vitro* models have advantages to further study injury of the CNS, they are unable to allow the study of complex systems with multi-cell communications that are seen *in vivo*. Since MS is a complex disease, there is no single animal model that can capture the entire spectrum of heterogeneity of human MS and its variety in clinical and radiological presentation. However, there are a few models of MS that have enabled the study of the immune response observed in human MS.

1.5.2.1 Experimental autoimmune encephalomyelitis

The most-studied animal model of MS is experimental autoimmune encephalomyelitis (EAE), in which autoimmunity to CNS components is induced in susceptible mice through immunization with self-antigens derived from basic myelin protein. EAE is induced by passive or active immunization with a variety of myelin compounds and the pathological picture depends on strain of animal and antigen used. Sensitization to myelin antigens in EAE typically occurs using an adjuvant, usually containing bacterial components highly capable of activating the innate immune system via pattern recognition receptors (**Libbey and Fujinami, 2010**). In this model autoreactive T-cell are induced where they collect in the spleen (**Flugelet *et al.*, 2001**) before migrating to the ‘target compartment’ where they recognize their cognate antigen, e.g., myelin oligodendrocyte glycoprotein (MOG), on local APCs. Here they are activated and start an inflammatory cascade which eventually leads to demyelination of CNS axonal tracts (**Miller *et al.*, 2007**). EAE in mice is characterized by an ascending paralysis beginning at the tail (**Batoulis *et al.*, 2011**), followed by limb and forelimb paralysis, assessed by using a 5-points scale (**McRae *et al.*, 1992; Rangachari *et***

al., 2012). From the pathogenesis point of view, EAE is a good model for studying MS mechanisms, even more so than for testing or developing drugs. For example, the most convincing correlations between EAE for studying MS for novel therapeutics are those that lead to the currently licensed and used DMT's, including IFN-beta (**Abreu *et al.*, 1982**), glatiramer acetate (**Teitelbaum *et al.*, 1971**) and anti-VLA-4 antibody (Natalizumab) (**Yednock *et al.*, 1992**).

However, in EAE, the processes of demyelination and remyelination occur simultaneously. Therefore, remyelination cannot be well studied. This lack of temporal separation makes it difficult to distinguish between an effect that is enhancing remyelination and one that is ameliorating the inflammatory response to EAE (**Buckley *et al.*, 2008**). One of its major shortcomings is the short-term nature of EAE experiments, lasting several weeks in the acute phase, without a 'chronic phase'. Current therapy for MS must be considered chronic, extending over years and decades, like what is seen in humans.

1.5.2.2 Toxic demyelination – Cuprizone

While EAE is the most used model to reflect the autoimmune origin of MS, toxic demyelination is more suitable to study the de- and re-myelination processes (**Blakemore and Franklin, 2008**). One of the most common agents used to induce demyelination is cuprizone (bis-cyclohexanone-oxaldihydrazone) a copper chelating reagent which when supplemented to normal rodent chow causes oligodendrocyte cell death. Along with death of oligodendrocytes there is subsequent demyelination and observed is profound activation of astrocytes and microglia (**Matsushima and Morell, 2001**). Once demyelination is complete, new oligodendrocytes, generated from the pool of OPCs begin to form new myelin sheaths soon after the removal of cuprizone from the diet. It is not known why administration of cuprizone only leads to a specific cell death in the oligodendrocytes, but cuprizone is a copper chelator, which in turn leads to inhibition of the copper-dependent mitochondrial enzymes cytochrome oxidase and monoamine oxidase. Thus, a plausible hypothesis is that disturbance in energy metabolism leads to apoptosis in the oligodendrocytes. Although not appropriate to study autoimmune mediated demyelination, the cuprizone model is a suitable tool to study basic mechanisms during de- and re-myelination in absence of primarily immune-mediated phenomena (**Matsushima and Morell, 2001**). Unlike with EAE, the cuprizone model does not rely on an adaptive immune response to see demyelination, and thus reflects several important characteristics seen in PPMS and the 'inside out' theory of MS pathogenesis.

1.5.2.3 Mechanical spinal cord transections

The simplest method of modelling SCI is the transection model, involving a partial or complete surgical incision in the cord that severs axonal connections. This model is well established in rats, mice, and cats (**Jeffrey-Gauthier *et al.*, 2021; Tan *et al.*, 2014; Lukovic *et al.*, 2015**). In this model an incision is made in the spinal cord using a blade while the animal is under anaesthetic, and exercise training is usually observed the weeks following to study locomotive recovery. The convenience of this model, requiring relatively simple surgical procedures, makes it an attractive prospect for SCI studies. However, complete spinal cord transections represent a very small portion of SCI seen in humans, with one of the leading causes of SCI in humans being vehicle collisions followed closely by falls (**National SCI Statistical Centre, 2020**) These types of SCI involve compression rather than laceration.

1.5.2.4 Compression and contusion models of SCI

To replicate spinal cord compression that mimics injuries seen with osteoarthritis, spinal tumours and infection, compression injuries are performed in animal models. Compression injuries are usually carried out using clips, forceps or gradually inflating balloons inserted into the spinal canal (**Zhang *et al.*, 2021; Vanick`y *et al.*, 2001; Tang *et al.*, 2020**). The most common method used is clip compression, making up over 50% of all compression models (**Sharif-Alhoseini *et al.*, 2017**). This is followed by balloon compression models and then several less utilized methods such as screw compression, solid spacer compression, weight drop compression, remote compression, expanding polymers, and spinal cord strapping. These models can be used to investigate specific aspects of spinal cord compression but may not entirely cover the broad range of compressive SCI seen clinically. A significant clinically relevant finding from compression studies is the reduction in the severity of secondary injury pathophysiology by decompression of the cord, leading to the development of surgical interventions in the immediate aftermath of SCI to decompress injured cord tissue (**Dimar *et al.*, 1999; Fehlings and Perrin, 2005**).

Additionally, to cover the wide range of injuries seen with SCI, contusion models are also used. Spinal cord contusion injury is one of the most serious injuries, characterized by high morbidity and disability. Spinal cord contusion (SCC) is an injury caused by crushing of the cord with part of its tissue spared, particularly the ventral nerve fibres connecting the spinal cord rostral and caudal to the injury remain physically intact (**Beattie and Bresnahan, 2000**). The spinal contusion injury may be complete or incomplete. A complete spinal contusion injury is associated with complete loss of motor and sensory function below the level of the injury, whereas an incomplete contusion injury may produce partial loss of

function below the injury level. To mimic the spinal cord contusion of humans in animals, various animal models have been developed including 1) bilateral contusion injury models (Anderson *et al.*, 2009; Gaudet *et al.*, 2017; Dunham *et al.*, 2010) and 2) unilateral contusion injury models (Nicaise *et al.*, 2012; Geremia *et al.*, 2017). One of the most common contusion models is the ‘The Multicentre Animal Spinal Cord Injury’ or MASCIS weight drop model. MASCIS impactors use a rod of specific weight, usually 10g, to be dropped from a precise height above the surface of the cord to induce SCI of defined severity. Key parameters such as height, time, velocity upon impact and cord compression are recorded digitally that enable experiments to be analysed and discarded if out of desired range (Cheriyana *et al.*, 2014). The MASCIS impactor is widely used and produces a validated and reproducible contusion injury in rat models.

1.5.2.5 limitations of *in vivo* studies

In vivo studies in biology offer invaluable insights into complex biological processes. However, acknowledging and addressing the limitations associated with these experiments is essential for accurate interpretation, reliable reproducibility, and effective translation of findings into clinical practice. The ethical implications surrounding the use of animals in *in vivo* studies cannot be overstated. Animal welfare concerns and the moral dimensions of manipulating or harming living organisms for scientific purposes have prompted increased scrutiny and regulatory measures. Certain *in vivo* experiments necessitate invasive procedures, such as surgeries or tissue samplings, to investigate specific physiological processes or study organ systems directly. These interventions introduce additional variables, potential complications, and physiological perturbations that can confound the interpretation of experimental outcomes. Furthermore, invasive procedures may trigger stress responses or alter the natural physiological state of the organism, thereby influencing the very processes under investigation. Careful consideration should be given to the selection and optimization of invasive techniques to minimize any unintended effects and ensure the validity and reliability of the obtained data. While *in vivo* studies provide crucial insights into biological phenomena, the generalizability of findings to other species or even different individuals within the same species is not guaranteed. Genetic variations, diverse environmental factors, and distinct physiological characteristics across organisms can significantly influence the observed outcomes and limit the applicability of results beyond the specific experimental context.

One of the main limitations however is the resource intensive nature of *in vivo* work. *In vivo* studies often demand substantial resources in terms of infrastructure, equipment, and skilled personnel. The maintenance of animal colonies, provision of appropriate housing and care,

and the execution of comprehensive experimental protocols contribute to the financial and logistical burden associated with these studies. Additionally, the extended duration required to observe long-term effects and establish robust conclusions further amplifies the resource-intensive nature of *in vivo* research. These constraints can limit the scale and scope of experiments.

1.5.3 *Ex vivo* slice cultures

Both *in vitro* and *in vivo* models are incredibly important in CNS research. However, they both have their limitations that can make it difficult to produce high output sound data. Monocultures of neurons for example do not model the complex interactions between them and other glial cells e.g., oligodendrocytes which is a crucial area of investigation for CNS regeneration. Progressing to co-cultures helps circumnavigate this issue such as neurons grown on a monolayer of astrocytes, but again the limitation of interactions with other glial cells can be seen. Co-cultures also do not represent the three-dimensional multicellular structures seen *in vivo*. *In vivo* on the other hand does demonstrate the complex nature of the CNS as a whole system, however, data output can be slow and costly due to the nature of the procedures. *Ex vivo* slice cultures offer an excellent alternative to *in vivo* work and bridges a gap between *in vitro* and *in vivo*. Slice cultures provides at least partly maintained original tissue architecture with some intact functional neural networks. To generate these cultures systems, tissue from the brain or spinal cord is dissected from rats (**Church and Gold, 2021**) and mice (**Ruiz-Perera, 2021**) and cut into sections using a tissue chopper – usually around 300 µm – and carefully placed on specialised membranes. These cultures can be robustly maintained for up to 4 weeks, with some protocols demonstrating the successful maintained for 2-3 months (**Sekizar and Williams, 2019**). In these cultures, mature myelin can be observed along axons within 14 days. Slice cultures are easily manipulated for studying injury of the CNS, with the addition of the chemical demyelinating agent Lysophosphatidyl choline (LPC, Lysolecithin) (**Miron *et al.*, 2013**) to induce demyelination. Cells such as microglia/OPCs/other immune cells of such as T/B lymphocytes can also be added to study they cellular interactions (**Sekizar and Williams, 2019**).

To summarise there are many models of CNS injury both *in vivo* and *in vitro* that have their benefits and limitations. *In vivo* work allows the study of complex systems with the presence of all glial cells and tissue. It also allows the study of behaviour work and can hugely benefit in the search for new therapeutics. However, *in vivo* work is often incredibly time consuming, expensive, and often has low research output. These limitation can be helped with the use of

in vitro work, which hugely reduces the use of animals, and can have a much higher data output that is easier to produce at a much lower expense. However, it is difficult to include all glial cells that are found in the CNS and doesn't represent the three-dimensional multicellular structures found *in vivo*. Here, *ex vivo* slice cultures bridge a gap between these two methods and provides a more complex system that what is seen *in vitro*, but at a much-reduced cost – both economic and time.

1.6 Conclusion

There is a clear unmet need for novel therapeutics for CNS injury, spanning a variety of issues including injury and diseases such as MS. It is evident that the CNS is a complex system, with its isolation from the PNS through the BBB creating hurdles for therapeutic access. Keystone features to a successful therapeutic that can repair the CNS should include the capacity to enhance remyelination and neurite repair through regeneration and cross the BBB into the CNS. Heparan sulphates are anionic polysaccharides that function as regulators of cell signalling that have proven themselves essential in the development and maintenance of the CNS. They have already demonstrated the capacity to become novel therapeutics for diseases such as Alzheimer's disease and show promising results as a novel therapeutic for CNS remyelination. Thus, low molecular weight heparin mimetics present a potential novel therapeutic for CNS repair.

1.7 Aims

The aim of this thesis was to compare the ability of a low molecular weight form of LS-mHep7 (LS-mHep7L), to enhance remyelination and neurite outgrowth in CNS injury models to its high molecular weight form (LS-mHep7). This was achieved using *in vitro* CNS models of demyelination and injury. Additionally, the validation of LS-mHep7L to sequester CCL5, a known negative regulator of developmental myelination *in vitro* was investigated. LS-mHep7 is known to sequester CCL5 and negates the hypomyelination caused by CCL5 in *in vitro*.

Once validated, we aimed to develop and optimize a method for organotypic slice cultures to study the remyelinating capacity of both LS-mHep7 and LS-mHep7L *ex vivo*. This was achieved by investigating published methods to ascertain the most suitable animal, tissue, and postnatal age to generate robust remyelination data. Once an established method was

identified these cultures were demyelinated and treated with LS-mHep7 or LS-mHep7L, and remyelination levels were be investigated.

Finally, we aimed to validate the use of next generation recombinant heparan sulphate mimics derived from cultured cells, as an alternative to animal derived heparin. TEGA Therapeutics have modified the mammalian heparan sulphate biosynthetic pathway to produce recombinant heparin. We aimed to validate a panel of recombinant mimetics with varying sulphation levels and molecular weights in our CNS injury models to ascertain their abilities to enhance repair. Recombinant heparan sulphates provide a stable production of heparin mimetics in terms of supply and pharmaceutical production for a safer more reliable product.

Chapter 2

Methods and Materials

2.1 Compounds

2.1.1 Low sulphated modified heparin (LS-mHep7)

LS-mHep7 was produced and gifted by Dr. E. A Yates and Prof. J.E Turnbull (University of Liverpool). Low sulphated modified heparin 7 (LS-mHep7) was produced semi-synthetically by chemical selective desulphation of porcine mucosal heparin, as described (Yates *et al.*, 1996). The compound had the predominant disaccharide repeating structure IdoA-GlcNS and corresponding chemical desulphation at both the 2-*O* and 6-*O* positions.

2.1.2 Low molecular weight LS-mHep7 (LS-mHep7L)

LS-mHep7L was produced and kindly gifted by Dr. E. A Yates and Prof. J.E Turnbull (University of Liverpool). LS-mHep7L was produced semi-synthetically by chemical selective desulphation of low molecular weight heparin (the commercial pharmaceutical, Enoxaparin) derived from porcine mucosal heparin, and was prepared essentially as described (Yates *et al.*, 1996) but, replacing the final dialysis step with purification using a gel filtration column (Sephadex G-25, 3 x 15 cm). The compound had the predominant disaccharide repeating structure IdoA-GlcNS and corresponding chemical desulphation at both the 2-*O* and 6-*O* positions.

2.1.3 Recombinant heparan sulphate compounds

Recombinant HS was manufactured using methods published previously (Thacker *et al.*, 2022), and a kind gift from TEGA Therapeutics Inc. Briefly, CHO or MST cells were grown in suspension in shaker flasks at 0.2×10^6 cells/mL in 30 mL at 37 °C, 5% CO₂/95% air for seven days. Cells and medium were separated by centrifugation and the cell pellet resuspended in 25 mM sodium acetate, pH 6.0, 0.25 M NaCl, 0.1% Triton X100 (wt/vol) and 0.5 mg/mL Pronase and incubated shaking overnight at 37 °C. Conditioned medium and protease digested cells were filtered through a 0.45 µm PES filter and applied to 0.5 mL DEAE-Sephacel columns, equilibrated and washed with DE-AE wash buffer (25 mM sodium acetate, pH 6.0, 0.25 M NaCl) and eluted with the same buffer containing 2M NaCl. The eluate was desalted on PD10 columns or by dialysis for large volumes and then dried by lyophilisation. The dried product was reconstituted in water, then digested with micrococcal nuclease overnight at 37 °C followed by Pronase digestion for 3 h at 37 °C. Beta-elimination was performed to liberate the HS from core protein by addition of NaOH to 0.4 M with overnight incubation at 4 °C. After neutralisation with acetic acid, samples were diluted with water and reapplied to DE-AE-Sephacel, then washed and eluted as

described above. The eluate was desalted and lyophilised. Protein and DNA content were measured using BCA assay and UV absorbance. The nuclease and Pronase digests were repeated as needed to eliminate residual nucleic acid or protein contamination.

2.2 Commonly used buffers and solutions

Commonly used materials such as buffers and solutions are referenced throughout this chapter. The basic composition of these are detailed in the following subsections.

2.2.1 Phosphate buffered saline.

A 10x stock solution of phosphate buffered saline (PBS), was prepared as follows: 1400 mM NaCl, 18 mM KH₂PO₄, 27 mM KCl, 100 mM Na₂HPO₄ made up to 400ml in distilled water (dH₂O). 10x PBS was used at a 1 in 10 dilution to give 1x PBS working buffer. Buffer was prepared and used at a pH 7.3.

2.2.2 Blocking buffer

Blocking buffer was made using 2% gelatine (G2500, Sigma) dissolved in 1x PBS (see 2.2.1). Aliquots were stored at -20°C.

2.3 Animals

All animals were maintained in the University of Glasgow's central research facility and methods of sacrifice were deemed ethical and humane in accordance with the Animals Scientific Procedures Act 1986 and the University of Glasgow's ethical guidelines. Animals were housed under 12-hour light-dark cycles with food and water available *ad libitum*.

2.3.1 Sprague Dawley rat

Sprague Dawley (SD) rats (Envigo, UK) were used to generate primary cell cultures. Neurospheres were generated from SD rat pups culled on postnatal (P) day 1, using pentobarbitone administered via intraperitoneal injection. Myelinating cultures were generated from embryos taken from time-mated females, which were culled by a rising concentration of CO₂ followed by confirmation of permanent cessation of the circulation via cutting of the femoral artery.

2.3.2 C57BL/6 mice

C57BL/6 mice (Charles River, UK) were used for the generation of organotypic spinal cord slice cultures. C57BL/6 mouse pups were culled on P1, using pentobarbitone administered via intraperitoneal injection followed by confirmation of permanent cessation of the circulation via cutting of the femoral artery.

2.4 Cell culture

All cultured cells were maintained in an incubator at 37 °C under a humidified 5% CO₂ atmosphere. Aseptic technique was employed throughout all cell culture procedures and only cell culture grade materials and reagents were used.

2.4.1 Commonly used materials

- 35mm Petri dish (430165 VWR-734-1698, Corning)
- 140mm Petri Dish (PDS140080T, Thermo Fisher)
- TC 24 well plate (3524, Corning)
- TC 6 well plate (3516, Corning)
- 15ml centrifuge tubes (734-1862, Corning)
- 50ml centrifuge tubes (734-1827, Corning)
- Leibovitz's L-15 medium (11415049, Invitrogen)
- Penicillin-streptomycin (Pen/Strep) 100x stock (P0781, Sigma Aldrich)
- Gentamicin solution (G1397, Sigma Aldrich)
- Heat inactivated horse serum (HS) (26050088, Thermo Fisher)
- Minimum essential medium (31095029, Thermo Fisher)
- Earle's Balanced Salt Solution (14155063, Thermo Fisher)
- Dulbecco's Modified Eagle Medium (41965-039, Invitrogen)
- Dulbecco's Modified Eagle Medium, Glutamax (21885-025, Invitrogen)

2.4.2 Stock solutions

2.4.2.1 Biotin

Biotin (B4501, Sigma) was diluted in 1M filter sterilised NaOH to 1mg/ml. A 10µg mL⁻¹ working stock was then made by diluting 1:100 in cell culture grade water. Aliquots were stored at -20°C.

2.4.2.2 Hydrocortisone

Hydrocortisone (H0396, Sigma-Aldrich) dissolved in cell culture grade water to 10 mM, and stored in aliquots at -20°C. A working stock was then made by diluting to 10 µM and 250 µl aliquots were stored at -20°C.

2.4.2.3 Epithelial growth factor

Recombinant murine epithelial growth factor (EGF) (315-09, Peprotech) was made up to a stock concentration of 100 µg/ml by reconstituting in ddH₂O containing 0.1% bovine serum albumin (A2153, Sigma). Aliquots were stored at -20°C.

2.4.2.4 Poly-L-lysine

Poly- L- lysine (P1274, Sigma) was dissolved in cell culture grade water to a final concentration of 13 µg/ml. Aliquots were stored at -20°C.

2.4.2.5 30%/45% Glucose

Glucose (G7021, Sigma) was slowly dissolved in ddH₂O with constant stirring before being filter sterilised. The weight of glucose used was appropriate to make a mg/vol percentage solution. Aliquots were stored at 4°C.

2.4.2.6 7.5% NaHCO₃

NaHCO₃ (S-5761, Sigma) was weighed out at 7.5g and added slowly to 100ml of ddH₂O. Solution was then filter sterilised and aliquots were stored at 4°C.

2.4.2.7 HEPES

HEPES (H-4034, Sigma) was weighed out at 23.8g and slowly added to 80ml ddH₂O. Once dissolved the final volume was brought to 100ml. Solution was filter sterilised and stored at -20°C.

2.4.2.8 Insulin

Human recombinant insulin (I2643, Sigma-Aldrich) dissolved in filter sterilised 0.01 M HCl to a final concentration of 2.5 mg mL⁻¹. Aliquots were stored at -20°C.

2.4.2.9 SBTI-DNase

SBTI-DNase was made up in L-15 media. To 25ml of L-15, the following was added; 0.52 mg/ml soybean trypsin inhibitor (Sigma T-9003), 0.04 mg/ml bovine pancreas DNase (D-4263), 3.0 mg/ml BSA fraction V (bovine serum albumin, Sigma A2153).

2.4.2.10 Collagenase

Collagenase type I power (10114532, Gibco™) dissolved in Leibovitz's L-15 media to 1.33%. Aliquots were stored at -20 °C.

2.4.2.11 Paraformaldehyde (4%)

Paraformaldehyde (PFA) powder (P6148, Sigma) was dissolved in PBS to make a 4% solution and pH was adjusted to 7.4. Solution was then filter sterilised and aliquots were stored at 4°C.

2.4.3 Cell Culture Media

2.4.3.1 Plating media (PM)

Mixture of 50% DMEM (31885-023, Gibco), 25% HBSS with 25% horse serum (26050-088, Gibco), and 2 mM L-glutamine. Filter sterilised with a 0.22 µm filtration unit and stored at 4°C.

2.4.3.2 Differentiation media (DM-)

Differentiation media is DMEM (41965-039, Gibco) with 10 ng/ml biotin, 50 nM hydrocortisone, and 1% N1 supplement (N6530, Sigma). Filter sterilised with a 0.22 µm filtration unit and stored at 4°C.

2.4.3.3 Differentiation media with insulin (DM+)

Differentiation media is made up in DMEM (41965-039, Gibco) with 10 ng/ml biotin, 50 nM hydrocortisone, 1% N1 supplement (N6530, Sigma) and 0.5 mg/ml insulin. Filter sterilised with a 0.22 µm filtration unit and stored at 4°C.

2.4.3.4 Astrocyte media

Astrocyte media is made up in DMEM (21885-025, Gibco) with 10% foetal bovine serum (Sigma, UK) and 2 mM L- glutamine (Sigma, UK). Filter sterilised with a 0.22 µm filtration unit and stored at 4°C.

2.4.3.5 Neurosphere media

Neurosphere media was made up in Dulbecco's Modified Eagle Medium/F12 (11320033 Life Technologies), enriched with 0.105% NaHCO₃, 5 µg/ml streptomycin, 5 mM HEPES 100 µg/ml apotransferrin, 25 µg/ml insulin, 30 µM sodium selenite, 60 µM putrescine and 20 µM progesterone (all from Sigma, UK). Filter sterilised with a 0.22 µm filtration unit and stored at 4°C.

2.4.3.6 Slice Culture Media

Slice culture media was made by combining 50% MEM (31095029, Gibco), 25% EBSS (14155063, Gibco), 2.6 mg/ml of 45% glucose (see 2.4.2.5), 1% Pen/Strep, 1% GlutaMAX™ Supplement (35050061, Thermofisher), and 50% horse serum. Filter sterilised with a 0.22 µm filtration unit and stored at 4°C.

2.4.3.7 Slice culture blocking buffer

Slice culture blocking buffer was made up in HBSS, enriched with 1mM HEPES (see 2.4.2.7), 2% heat inactivated horse serum, 10% heat inactivated goat serum (G9023, Sigma), 1% bovine serum albumin (A2153, Sigma), 0.25% Triton-X (T9284, Sigma). Filter sterilised with a 0.22 µm filtration unit and stored at 4°C.

2.4.4 Primary Cell Culture

2.4.4.1 Neurosphere-derived astrocytes

Neurospheres (NS) were generated from the striata of P1 SD rat pups using a modified published method (Reynolds & Weiss., 1996). The dissected striata was mechanically dissociated, homogenised, and centrifuged for 3 minutes at 120 revolutions per minute (rpm). The pellet was resuspended in 20 ml of neurosphere media (see 2.4.3.5), supplemented with 20 ng/ml EGF (see 2.4.2.3) in an uncoated T75 vented flask (Greiner, UK).

Cellular neurospheres formed over 7 days and were differentiated into astrocytes (Sorenson *et al.*, 2008). Briefly, neurospheres were triturated and seeded down onto 13 mm PLL coated

coverslips (see 2.4.2.4) divided up into 24 well plates, with the volume of media brought up to 0.5 ml per well. Astrocytes were incubated for a further 5-7 DIV, maintained at 37°C in an atmosphere of 7% CO₂. A confluent monolayer is normally formed at around 5 DIV. Astrocytes were maintained in astrocyte media and fed ever 3-4 days by removing half the media and replacing with fresh (see 2.4.3.4).

2.4.4.2 Rat myelinating cultures

Generation of rat myelinating cultures was based on previously described methods (Sorensen *et al.*, 2008). Pregnant females were sacrificed at E15.5 by rising concentration of CO₂ and death confirmed by severing the femoral artery. Embryos were excised and embryonic spinal cords extracted. Spinal cord tissue was enzymatically dissociated by incubation with 100 µl collagenase (see 2.4.2.10) and 100 µl 1x trypsin (9002-07-7, Sigma) for 15 minutes at 37°C. The digestion was quenched using 0.52 mg/ml soybean trypsin inhibitor (10109886001, Sigma), 3.0 µg/ml bovine serum albumin (A2153, Sigma), and 0.04 mg/ml DNase (see 2.4.2.9). Coverslips with a confluent monolayer of Neurosphere-derived astrocytes (see 2.4.4.1) were placed into 35-mm Petri dishes (three per dish) and the cell suspension was seeded on top at 150,000 cells per coverslip in plating medium (PM) (see 2.4.3.1). Cells adhered to the cover slips for 2 hours at 37°C, then supplemented with 300 µl PM and 500 µl DM+ (see 2.3.3.3). Cultures were maintained at 37°C in an atmosphere of 7% CO₂ and every 2-3 days with DM+ for the first 12 DIV, and then with DM- (see 2.4.3.2) until DIV 30.

2.4.5 Cell culture assays

2.4.5.1 Myelinating cultures modified to study CNS injury (MC-Inj)

Myelinating cultures were set up and maintained as described above (see 2.4.4.2). At 24 DIV, myelinating cultures were cut using a 11 mm single edge razor blade down the middle of each cover slip, creating a cell free area (approx. 650 µm wide). Cultures were then treated with either LS-mHep7 or LS-mHep7L at a concentration of 1 ng/ml. Cultures were allowed to recover to 30 DIV then, fixed for 20 minutes at RT with 4% PFA, then immunolabelled.

2.4.5.2 Myelinating cultures experimentally demyelinated (MC-DeMy)

Myelinating cultures were set up and maintained as described above (see 2.4.4.2). At 24 DIV, myelinating cultures were demyelinated by overnight incubation at 37°C with 100 ng/ml

anti-myelin oligodendrocyte glycoprotein (MOG) antibody (Z2 clone from hybridoma, kindly gifted by Prof. Christopher Linington) and 100 µg/ml, rabbit complement (234400, Millipore). Cultures were then treated with LS-mHep7 or LS-mHep7L at 1ng/ml. Cultures were allowed to recover until DIV 30 then, fixed for 20 minutes at RT with 4% PFA, then immunolabelled

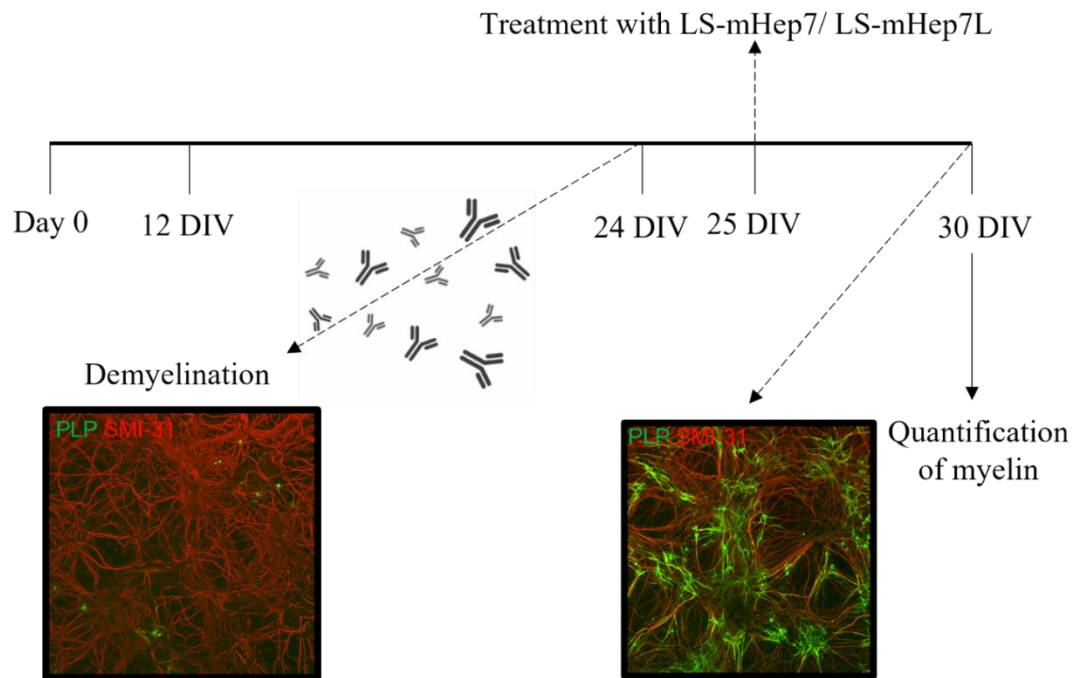


Figure 2.1 |MC-DeMy schematic. Myelinating cultures were set up and allowed to mature until DIV 24, at which point they were demyelinated, via overnight incubation with the MOG-specific antibody Z2 (100 ng/ml) and rabbit complement (100 µg/ml). Treatment occurred at DIV 25 with LS-mHep7 (1ng/ml) or LS-mHep7L (1ng/ml). Cultures were maintained until DIV 30 where they were fixed with 4% PFA and fluorescently marked for PLP (green, myelin) and SMI-31 (red, axons).

2.4.5.3 Myelinating spinal cord cultures to study the development of myelination (MC-Dev) with the addition of CCL5

Myelinating cultures were set up and maintained as described above (see 2.4.4.2). At 16 DIV approximately when myelin first forms along axons, cultures were treated with 100 ng/ml CCL5 (250-07, peprotech) at 16 DIV. Treatment was repeated at 19 DIV and 21 DIV. Some cultures received co-treatment with LS-mHep7 or LS-mHep7L at 1ng/ml. At 24 DIV cultures were fixed for 20 minutes at RT with 4% PFA, then immunolabelled

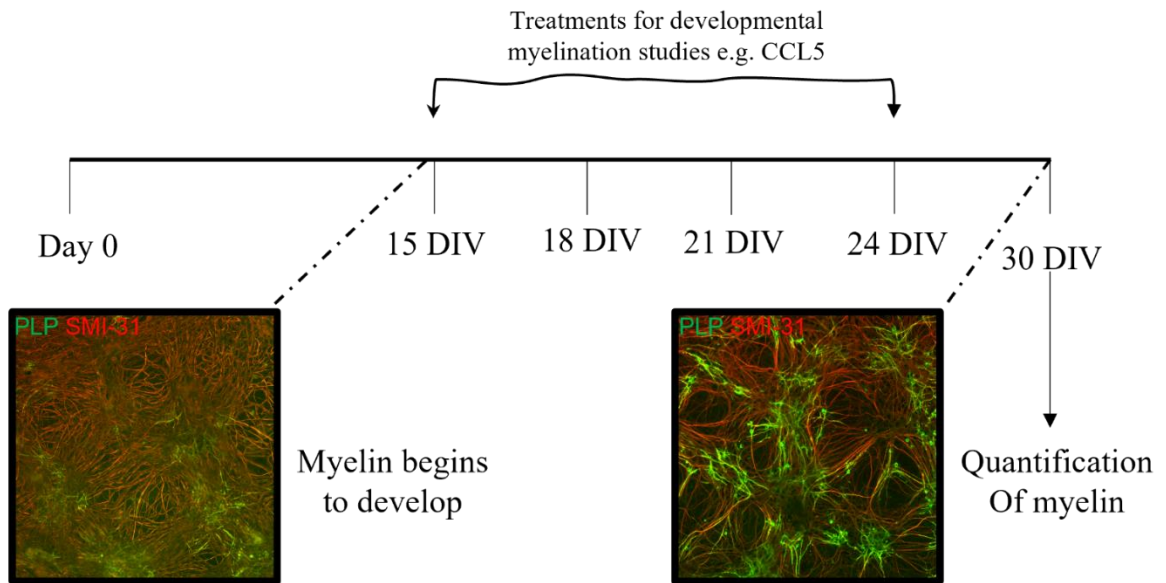


Figure 2-1 |MC-Dev schematic. Myelinating cultures were set up and allowed to mature until DIV 15, at which point they were treated with either (i) CCL5 alone (100 ng/ml) or in combination with (ii) LS-mHep7 (1ng/ml) or LS-mHep7L (1ng/ml). Treatments occurred at DIV 15, DIV 18, DIV 21, and maintained until DIV 24 where they were fixed with 4% PFA and fluorescently marked for PLP (green, myelin) and SMI-31 (red, axons).

2.4.5.4 Spinal cord slice cultures (SC-DeMy and SC-DEV)

C57BL/6 mouse pups were culled on postnatal day 1. Pups were decapitated and their spinal cords dissected into Leibovitz's L-15 medium. Sagittal slices of spinal cord 200– 300 μm thickness were cut using a McIlwain tissue chopper, and carefully placed onto Millicell Cell Culture Insert (PICM0RG50, Merck Millipore). Each insert was placed into a 6 well plate, and 1ml of slice culture media (SCM) added underneath the insert. Cultures were maintained at 37°C in an atmosphere of 7% CO₂ and every 2-3 days media was replaced with fresh SCM. For the study of de/remyelination (SC-DeMy) at DIV 14, demyelination was induced by addition of 0.5 mg/ml lysophosphatidylcholine (L1381-25MG, Sigma) to the medium for 18–24 h, after which slices were transferred back into normal medium or treated with 100ng/ml LS-mHep7 or LS-mHep7L. At 28 DIV, cultures were fixed in 4% PFA for 1 hour RT then immunolabelled (See Table 2-2). For the study of developmental myelination (SC-DEV), cultures were maintained until DIV14, fixed in 4% PFA for 1 hour RT then immunolabelled (See Table 2-2).

2.4.5.4 Astrocyte monolayers modified to study signs of astrocytosis (Scratch assay)

Astrocyte monolayers were set up and maintained as described in **2.4.4.1**. Once a confluent monolayer was observed, astrocytes were either treated with 10ng/ml HEP7 or HEPL in astrocyte media. Once treatments were added, each coverslip was ‘scratched’ down the centre of the cover slip using the end of a P200 pipette tip. This created a cell free area down the middle of the cover slip. Scratches were live imaged using a Etaluma Lumascope 560 Inverted Microscope at 0h, 1h, 2h, 4h, 24h. At each time interval coverslips were fixed with 4% PFA. Gap width change of each cover slip was analysed using ImageJ. Cell lysates were also produced to tie with each time point. Cell lysates were produced by scratching each cover slip three times. At each appropriate time point 50 µl CelLytic™ (C3228-50ML, Sigma) containing protease inhibitor (1/1000) was added to each cover slip. Lysate solution was left on each coverslip for 15 mins, at which point it was then transferred into PCR tubes and kept on ice. These protein lysates were then analysed using western blot analysis (see 2.7.1).

2.5 Immunocytochemistry

2.5.1 *In vitro* cell culture staining

For staining of cultures with intracellular antibodies, cultures were fixed with 4% paraformaldehyde (see 2.4.2.11) for 20 minutes at room temperature and permeabilised with 0.2% Triton X-100 (T9284, Sigma) in PBS at room temperature for 15 minutes. Once washed with PBS, cultures were blocked using blocking buffer (see **2.2.2**) for 1 hour at room temperature. The primary antibodies were diluted in blocking buffer, and the cells incubated for 1 hour at room temperature (Table 2-1). After washing, the cultures were incubated with the appropriate secondary antibodies for 45 minutes at room temperature (Table 2-1) and mounted in Vectashield (H-1200-10, Vector laboratories).

Table 2-1 | Primary and secondary antibodies used in the immunostaining of *in vitro* cultures.

Primary Antibody	Isotype	Dilution	Source
MBP	Rat IgG2a	1:500	BioRad
SMI-31	Mouse IgG1	1:1000	Biologand
AA3 (PLP)	Rat IgG	1:100	Hybridoma
Secondary Antibody	Conjugate	Dilution	Source
Goat anti-mouse IgG1	Alexa Flour ® 568	1:500	Life Technologies
Goat anti-rat IgG	Alexa Flour® 488	1:500	Life Technologies

Table 2-2 | Primary and secondary antibodies used in the immunostaining for slice cultures.

Primary Antibody	Isotype	Dilution	Source
MBP	IgG2a	1:500	BioRad
SMI-31	IgG1	1:1000	Biologend
CASPR	IgG	1:500	Abcam
Secondary Antibody	Conjugate	Dilution	Source
Goat anti-mouse IgG1	Alexa Flour®: 568	1:500	Life Technologies
Goat anti-rat IgG	Alexa Flour®: 488	1:500	Life Technologies
Goat anti-rabbit IgG	Alexa Flour®: 647	1:500	Life Technologies

2.5.2 *Ex vivo* slice culture staining

Individual slices were then cut out of the plastic insert while keeping the membrane intact, being careful to avoid touching or damaging the tissue. Tissue sections were then transferred to a 24-well plate, one slice per well. Slices were washed three times in PBS on a rocker for 5 mins before permeabilization using pre-cooled (-20°C) absolute ethanol for 30 mins at -20°C. The ethanol is removed, and slices are washed three times with PBS, on a rocker for 5 mins. Slices were blocked using slice culture buffer (see 2.4.3.7) for 1 hour at room temperature on a rocker. The primary antibodies were diluted in slice culture blocking buffer, and the cells incubated for 48 hours at 4°C on a rocker (Table 2-1 | Primary and secondary antibodies used in the immunostaining of *in vitro* . After washing, the cultures were incubated with the appropriate secondary antibodies for 2 hours at room temperature on a rocker (Table 2-2) and mounted in Vectashield (H-1200-10, Vector laboratories).

2.6 Microscopy and image analysis

2.6.1 Fluorescent microscopy

Images of myelinating cultures were obtained using an Olympus BX51 fluorescence microscope with a 10x objective. Conditions were blinded by colleague before 10 randomised images were captured from each coverslip (totalling 30 images per treatment condition). Images were saved as tiff files.

2.6.2 Confocal Imaging

Images of slice cultures were obtained using a Zeiss LSM 880 upright confocal multiphoton microscope with a 63x objective. SMI-31 (axons), MBP (myelin), and CASPR (internodes) immunofluorescence were imaged. Conditions were blinded by a colleague before 30 images were taken for each treatment condition. Images were taken across each slice at an optimal depth, spanning the entire portion of spinal cord. Images were saved as tiff files.

2.6.3 Re/myelination quantification

2.6.3.1 Myelinating cultures

Quantification of re/myelination was carried out using the CellProfiler Image Analysis software (Carpenter *et al.*, 2006). Axonal density was measured using the immunofluorescence pixel value for SMI-31 obtained from each image, set at a threshold level. This pixel number was then divided by the total number of pixels of the entire image to produce an axon density percentage. The percentage of myelinated axons was obtained by the amount of PLP or MBP fluorescent pixels obtained from each image and standardising the value to the neurite density value as a percentage. The CellProfiler pipeline used for this analysis utilises pattern recognition software to distinguish linear myelinated internodes from oligodendrocyte cell bodies. This enables the isolation of ‘myelin pixels’ stained by the PLP/MBP and ignores other fluorescent pixels from oligodendrocyte labelling which can occur when using PLP/MBP. Due to the variability of myelination between culture sets, the myelination percentage was standardised to each experimental control. An example of the CellProfiler analysis of analysis can be seen in see **Figure 2.2**. The CellProfiler pipeline used in this thesis is available at <https://github.com/muecs/cp>.

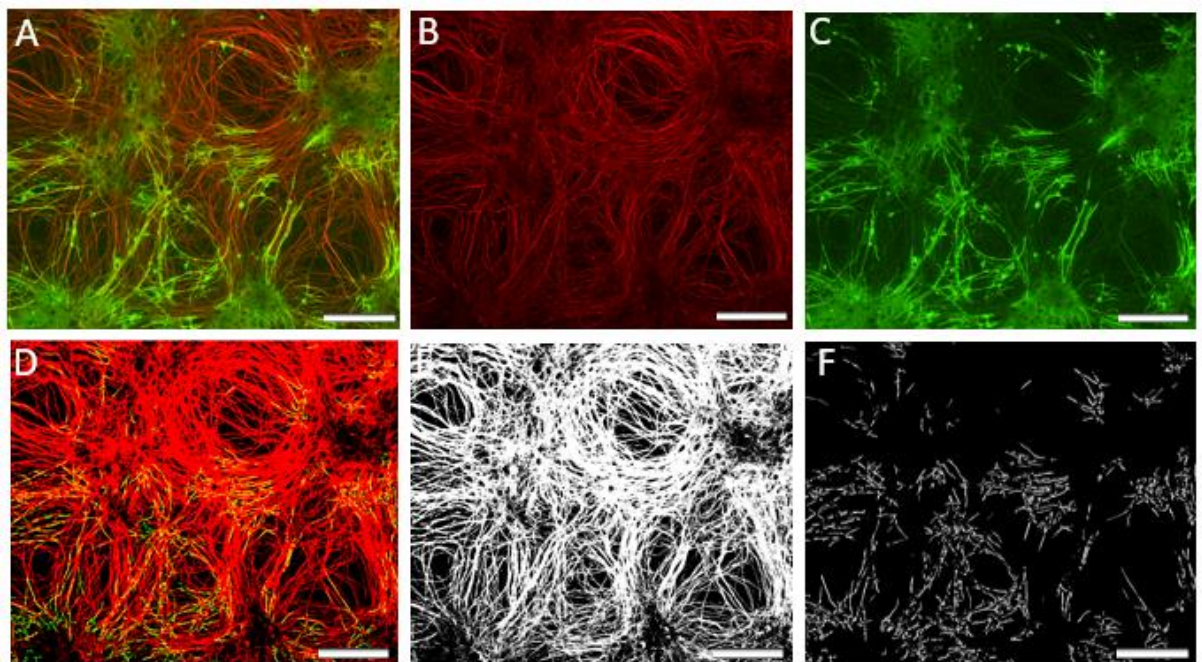


Figure 2.2 |Representative images of myelin quantification | A) Representative image of a myelinating culture at DIV30, immunolabelled for SMI-31 (red, axons) and PLP (green, myelin). B-C) shows the unmodified split colours of (A). D) Shows the colour split of (A) emphasised for the macro used, and (E-F) depicts the analysis of (D). Linear myelinated internodes are used to quantify myelination. The neurite density of the culture is quantified by SMI-31 immunoreactivity. Scale bars 100 μ m

2.6.3.2 Slice culture re/myelination quantification

As with the myelinating cultures quantification of re/myelination was carried out using the CellProfiler Image Analysis software (**Carpenter *et al.*, 2006**). This pipeline was adapted to have a higher threshold for both axons and myelin to adapt to the images being acquired at a higher magnification. Like in section **2.6.2.1** axonal density was established using the immunofluorescence pixel value for SMI-31 obtained from each image, set at the new threshold level. This pixel number was then divided by the total number of pixels of the entire image to produce an axon density percentage. The percentage of myelinated axons was obtained by the amount of MBP fluorescent pixels obtained from each image and standardising the value to the neurite density value as a percentage.

2.6.3.3 MC-Inj neurite outgrowth quantification

Neurite outgrowth was represented as a percentage of SMI-31 immunofluorescence per field of view. Image analysis was carried out using ImageJ. For each image, the area of injury was cropped, clearing all pixels on each side of the injured area, leaving pixels pertaining only to the injury site. The cropped image was then reverted to black and white to reduce background fluorescence within the cropped field. Neurite outgrowth was measured by calculating the immunofluorescence pixel value for SMI-31(white pixels) obtained from each image. This pixel number was then divided by the total number of pixels of the entire cropped injury (black pixels) site to produce a neurite outgrowth percentage per field of view. See **Figure 2.3**.

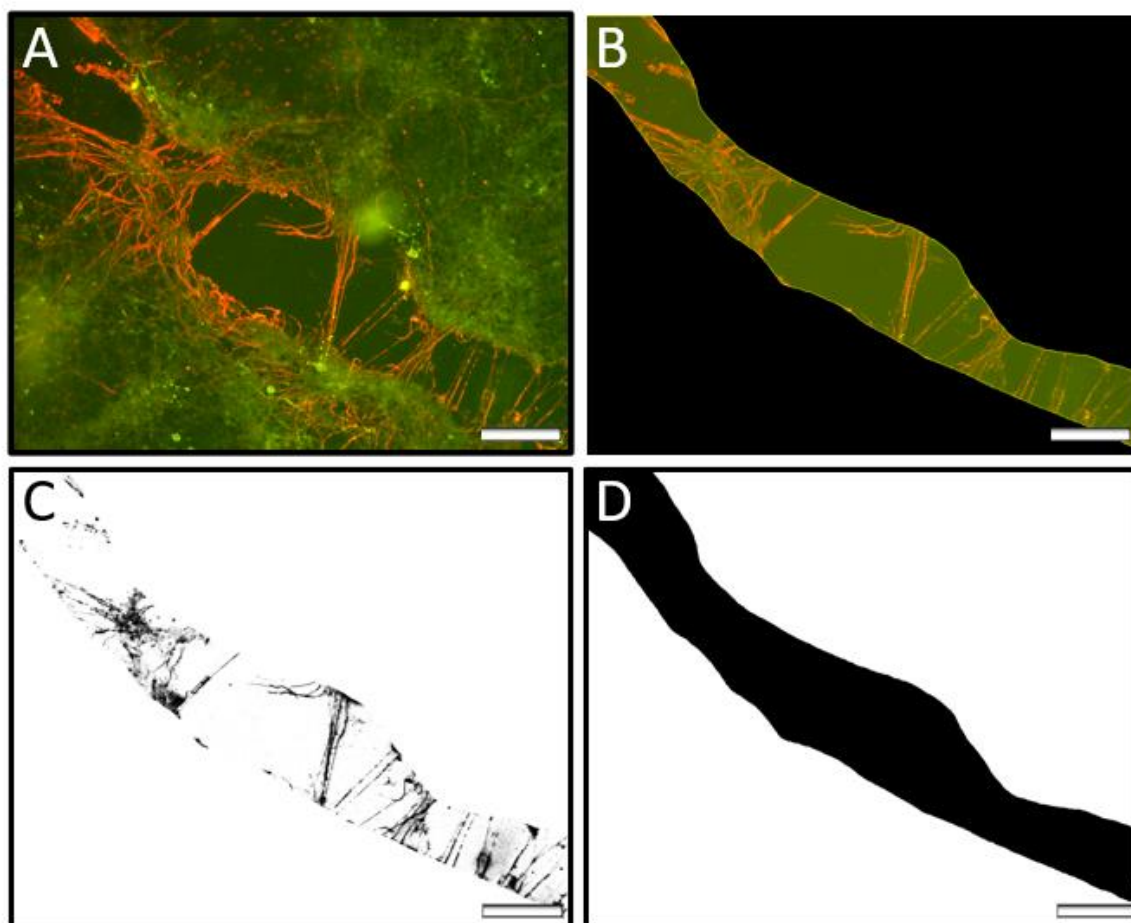


Figure 2.3 | Representative images of neurite outgrowth quantification. A) Representative image of a MC-Inj, immunolabelled for SMI-31 (red, axons) and PLP (green, myelin). B) shows cropped area of injury site seen in (A) which was then converted to black and white pixels (C-D). The neurite outgrowth was then calculated via the pixel density of the neurite outgrowth (white, C) and the entire cropped injury site (Black, D). Scale bars 100 μm .

2.6.4 Neurite diameter

Neurite diameter was analysed using Image J. MC-DeMy cultures were set up and maintained as described above. Cultures were fixed and immunolabelled with antibody clone SMI-31 at the appropriate time point (DIV 30). 10 images of each condition were taken at 10x magnification. Each image was opened in Image J and a representative area was zoomed into 6 times (6 clicks). Using the straight-line selection, a line was drawn across the diameter of the SMI-31 positive neurite and these measurements recorded. Within the area, 10 axons were chosen randomly, per image. The arbitrary measurements were converted to μm using the scale bar in the image. Experiments were done in triplicate.

2.7 Molecular Biology

2.7.1 Western blot

2.7.1.1 Protein lysates

Protein lysates were collected from astrocyte monolayers that were set up as described previously (2.4.5.4). Monolayers were washed 3x in PBS and lysed by incubation in 50 µl CellLytic™ (C3228-50ML, Sigma) for 15 min at RT. The reagent was removed from each well and transferred to Eppendorf tubes on ice. A Pierce BCA assay (23225, ThermoFisher) was performed to quantify protein concentration, according to manufacturer's instructions. Briefly, reagent A and reagent B were mixed at a ratio of 1:50, protein lysate was added at a ratio of 1:20. The resulting solution was incubated at 37 °C for 30 min. Protein concentration was quantified using the BCA assay programme on a Nanodrop 1000 (Thermo Fisher). Bovine serum albumin (BSA) was used for known protein concentrations to generate a standard curve from which the protein concentrations of samples were deciphered.

2.7.1.2 Sample preparation & gel electrophoresis

10µl protein samples were prepared for electrophoresis, containing 1 µl 10x reducing agent (Invitrogen), 2.5 µl 4x sample buffer (Invitrogen), 10 µg protein and ddH₂O (as required). The samples were heated on a heat block at 70 °C for 10 min, immediately transferred to ice. Pre-cast 4-12% Bis-Tris gels (NP0322BOX, Invitrogen) were placed in a mini-cell gel tank and Invitrogen NuPAGE running buffer was added. Gel combs were removed and 10 µl protein samples were transferred to wells, alongside 5 µl See Blue™ protein ladder (LC5925, Invitrogen). Gels ran at a constant 200V for 45-60 min.

2.7.1.3 Protein transfer & detection

The iblot Blotting System (ThermoFisher) was used to transfer proteins onto a nitrocellulose membrane using Invitrogen gel transfer stacks according to manufacturer's instructions. The anode was placed at the bottom of the iblot, and gels were placed atop the nitrocellulose membrane. Filter paper soaked in ddH₂O was placed over the gel and any bubbles were removed using a roller. This was covered by the cathode and sponge before running the iblot for 7 min on the P3 setting. The nitrocellulose membrane was blocked with 5% milk in PBS-Tween (0.1%, ThermoFisher) for 1 hr at RT. This was followed by incubation with primary anti- body diluted in PBS-Tween for 1 hr at RT or overnight at 4°C. Blots were washed 3x for 5 mins each in PBS-Tween (P1379, Sigma) and incubated in horse radish peroxidase (HRP)-linked secondary antibody (32230, Invitrogen) for 1 hr at RT. Blots were washed extensively 3x for 5 mins each and then incubated in 2 ml enhanced chemiluminescence (ECL) solution (R-03025-) for 3 min. Excess ECL was removed, and the bound antibodies

were visualised using Konica Minolta SRX101A imaging system, and exposure to Amersham hyperfilm™ (28-9068-38, VWR).

Densitometry was carried out on the bands using Image J. See Table 2-3 for antibodies.

Table 2-3 | Antibody table for western blot

Antibody	Manufacturer	Host species	Concentration
β-actin	Sigma	Mouse	1:1000
GFAP	Dako	Rabbit	1:100000
NESTIN	Merck Millipore	Mouse	1:5000

2.7.2 Cytokine array

Conditioned media was collected from P1 mouse spinal cord slice cultures (see 2.4.5.4) at DIV 14 before chemical demyelination with lysolecithin, and 24 hours after demyelination. A 400 µl sample of each conditioned media was analysed using a Proteome Profiler Rat XL Cytokine Array (R&D Systems, ARY030) following the manufacturer's protocol. The cytokines, chemokines, growth factors and other soluble proteins detected in the Mouse XL Cytokine Array are detailed in Table 2-4. Visualisation of captured protein was achieved by chemiluminescence of the biotinylated detection antibodies, and exposure to Amersham hyperfilm™ (28-9068-38, VWR). Densitometry was carried out on the bands using Image J and the relative expression levels of each protein were assessed.

Table 2-4| Secreted factors specific to the capture antibodies in the Proteome Profiler mouse Cytokine Array Kit XL

Proteome Profiler Mouse XL Cytokine Array					
Adiponectin/Acrp30	CD40/TNFRSF5	EGF	IL-1 alpha/IL1F1	IL-33	Proprotein Convertase 9/PCSK9
Amphiregulin	CD160	Endoglin/CD105	IL-1 beta/IL-1F2	LDL R	RAGE
Angiopoietin-1	Chemerin	Endostatin	IL-1ra/IL-1F3	Leptin	RBP4
Angiopoietin-2	Chitinase 3-like 1	Fetuin A/AHSG	IL-2	LIF	Reg3G
Angiopoietin-like 3	Coagulation Factor III/Tissue Factor	FGF acidic	IL-3	Lipocalin-2/NGAL, LIX	Resistin
BAFF/BLyS/TNFSF13B	Complement Component C5/C5a	FGF-21	IL-4	M-CSF	E-Selectin/CD62E
C1q R1/CD93	Complement Factor D	Fit-3 Ligand	IL-5	MMP-2	P-Selectin/CD62P
CCL2/IE/MCP-1	C-Reactive Protein/CRP	Gas6	IL-6	MMP-3	Serpin E1/PAI-1
CCL3/CCL4 MIP-1 alpha/beta	CX3CL1/Fractalkine	G-CSF	IL-7	MMP-9	Serpin F1/PEDF
CCL5/RANTES	CXCL1/KC	GDF-15	IL-10	Myeloperoxidase	Thrombopoietin
CCL6/C10	CXCL2/MIP-2	GM-CSF	IL-11	Osteopontin (OPN)	TIM-1/KIM-1/HAVCR
CCL11/Eotaxin	CXCL9/MIG	HGF	IL-12p40	Osteoprotegerin/TNFRSF11B	TNF-alpha
CCL12/MCP-5	CXCL10/IP-10	ICAM-1/CD54	IL-13	PD-ECGF/Thymidine phosphorylase	VCAM-1/CD106
CCL17/TARC	CXCL11/I-TAC	IFN-gamma	IL-15	PDGF-BB	VEGF
CCL19/MIP-3 beta	CXCL13/BLC/BCA-1	IGFBP-1	IL-17A	Pentraxin 2/SAP	WISP-1/CCN4
CCL20/MIP-3 alpha	CXCL16	IGFBP-2	IL-22	Pentraxin 3/ TSG-14	
CCL21/6Ckine	Cystatin C	IGFBP-3	IL-23	Periostin/OSF-2	
CCL22/MDC	Dkk-1	IGFBP-5	IL-27	Pref-1/DLK-1/FA1	
CD14	DPPIV/CD26	IGFBP-6	IL-28	Proliferin	

2.8 Statistical analysis

For data presentation and statistical testing, Prism software version 6.0 (GraphPad Software) was used. For simple comparison, a paired-student t-test was utilised to determine statistical significance. For multiple condition comparisons a One-way ANOVA repeated measures was employed to data sets, followed by Dunnett's multi-comparison test. For western blots, a paired 2 sample t-test was used on the densitometry arbitrary values, comparing band intensity of treatment group to control group for both test protein and β -actin. Data is presented as mean \pm standard errors of the mean (SEM). Asterisks within graphed data to represent significance (less than * $p < 0.05$, ** $p < 0.01$, *** $p < 0.001$). Information detailing the number of technical and biological repeats for every experiment throughout the thesis is provided in the corresponding figure legends.

Chapter 3

Ex vivo slice cultures as a model for studying
central nervous system repair

3.1 Introduction

The success rate of novel therapeutics for CNS repair are incredibly low, specifically for disease modifying treatments. The reason for this consists of many obstacles that are hard to overcome including incomplete understanding of disease-relevant biology and physical barriers to the CNS such as the BBB. Therefore, methods that allow the screening of potentially bioactive molecules for therapeutic effect in a quantitative, cost effective and timely manner, are invaluable in the search for new drugs. To facilitate screening, *in vitro* models are often employed in semi-high to high-throughput systems as they permit the study of intrinsic properties of oligodendrocytes and cell–cell interactions between the glia present in the system. However, these do not replicate the three-dimensional structure and architecture of cells in tissue. Organotypic cultures which are slices of the brain or spinal cord maintained on a semi-permeable membrane that preserves the structural and synaptic organization of the original tissue. *Ex vivo* cultures allow the study of the CNS in a variety of ways, including the study of hypoxic insult (Cui *et al.*, 2020), remyelination of Purkinje axons (Thetiot *et al.*, 2019), and oligodendrocyte proliferation (Sherafat *et al.*, 2017). Additionally, organotypic cultures allow a high output of information in a cost-effective manner making them an excellent model for preliminary screening of molecules for therapeutic effect.

To determine the therapeutic potential of our novel LS-mHep compounds in promoting repair, we first aimed to establish a reproducible *ex vivo* model of the CNS. We required a model that had robust and consistent myelination of axons which was also amenable to experimental demyelination. To do this we trialled *ex vivo* slice cultures generated from SD rats and or C57BL/6 mice, and from various regions of the brain harvested at different postnatal ages.

3.2 Aims

The overall aim of this chapter was to optimise an *ex vivo* slice culture protocol that enabled the study of remyelination and repair of the CNS using LS-mHep7 and LS-mHep7L. The specific aims were to:

- i) Determine the suitability of SD rat or C57BL/6 mouse tissue to generate *ex vivo* slice cultures.
- ii) Ascertain the best age of postnatal animal to obtain tissue slices from for a successful culture of myelinating cells.

- iii) Compare cerebellum and spinal cord-derived *ex vivo* slice cultures for axon health and myelination.
- iv) Establish a successful *ex vivo* slice culture model amenable to demyelination and determine the appropriate experimental protocol for studying remyelination following LS-mHep7 and LS-mHep7L treatment.

3.3 Cerebellar slice cultures from P10 SD rat did not maintain healthy myelinated axons

Cerebellar slice cultures generated from P10 SD rats are a commonly used *ex vivo* model of the CNS (Birgbauer *et al.*, 2004). The cerebellum is well-myelinated at P10 and therefore provides an ideal tissue to maintain *ex vivo* for the study of demyelination/remyelination. We generated slice cultures from P10 SD rats, which were maintained until DIV 12, before fixation in 4% PFA. Axons were visualised with antibody clone SMI-31 and anti-MBP. **Figure 3.1** shows axon degeneration within the slice, with white arrows indicating sections of fragmented axons. Green fluorescence that is observed in **Figure 3.1 (a)** can be deduced as a bleed through artefact due to it being thinner than the red fluorescence when overlapped in **Figure 3.1 (a)**. If this green fluorescence was true myelin, it would be thicker in width than the red axons observed. Also observed throughout the slices are additional signs of degeneration including axonal swelling as indicated in **Figure 3.1 (b)** with white arrow heads. Abnormal MBP staining is indicated by yellow arrowheads in **Figure 3.1 (b)**. Typically anti-MBP stains mature myelin sheaths along axons and is not located within the cell body. However, identified here is the staining of a large spherical object – potentially a degenerating oligodendrocyte. Morphologically, these cultures had an unexpected ‘wavy’ appearance as opposed to the expected lateral fibres. These ‘wavy’ axons are not phenotypical of healthy appearing axons, which run in organised bundles.

Additional signs of degeneration in the slice cultures are observed in **Figure 3.2** with features that indicate oligodendrocyte dysfunction (indicated by asterisk). In addition there appears to be spherical structures surrounded by myelin debris and might indicate the breakdown of oligodendrocytes.

To summarise we were unable to produce slice cultures generated from P10 SD rats that could produce and maintain healthy myelinated axons. Signs of axon degeneration could be observed throughout the slices with low axonal density. This allowed us to conclude that P10 SD cultures were not an appropriate culture system to enable the study of remyelination and repair of the CNS using LS-mHeps.

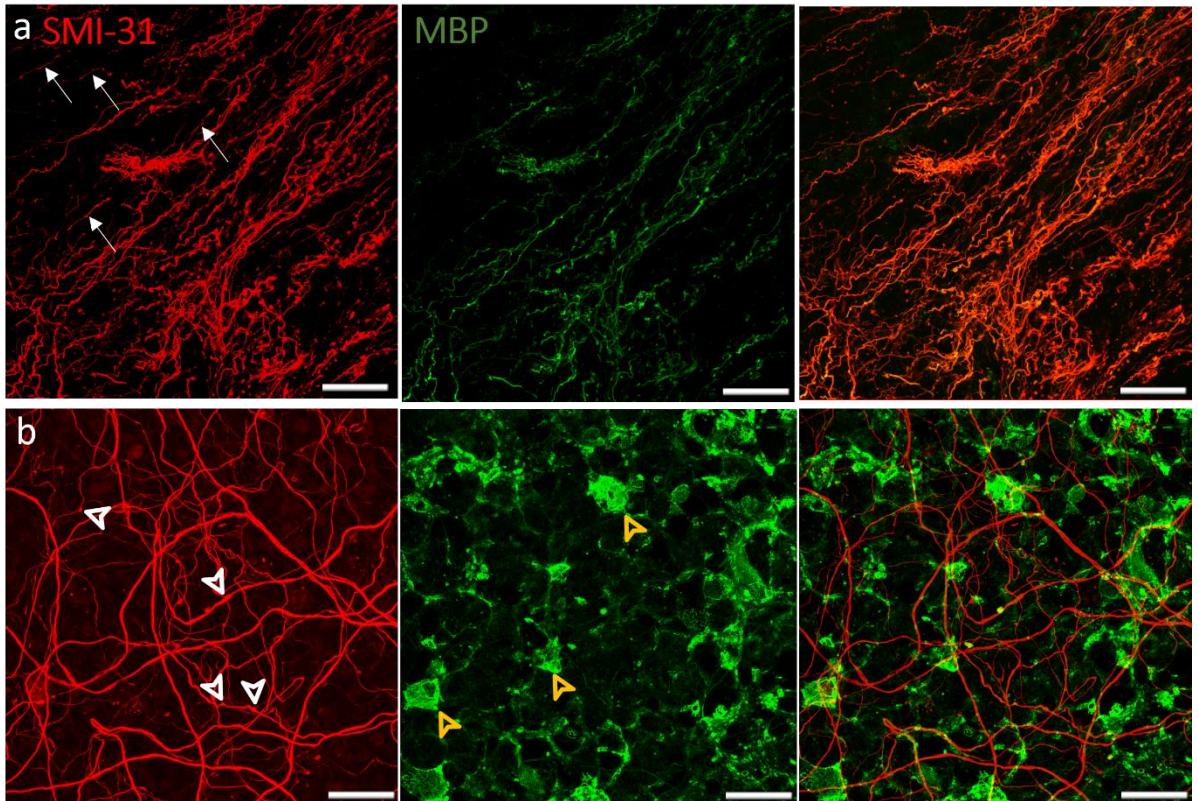


Figure 3.1 | P10 SD rat cerebellar slice cultures show signs of axon degeneration and signs of oligodendrocyte dysfunction. Confocal images of cerebellar slices generated from P10 SD rats maintained to DIV 12. (a) Axonal degeneration is observed with axonal fragmentation (SMI-31, red) (indicated by white arrows). Abnormal MBP staining (green, myelin) was observed throughout. (b) Axonal swellings (indicated by white arrowheads) were also observed alongside MBP positive spherical structures, likely indicative of abnormal oligodendrocyte cell body labelling (yellow arrowheads). Scale bars = 20 μm
Representative images from five independent cultures

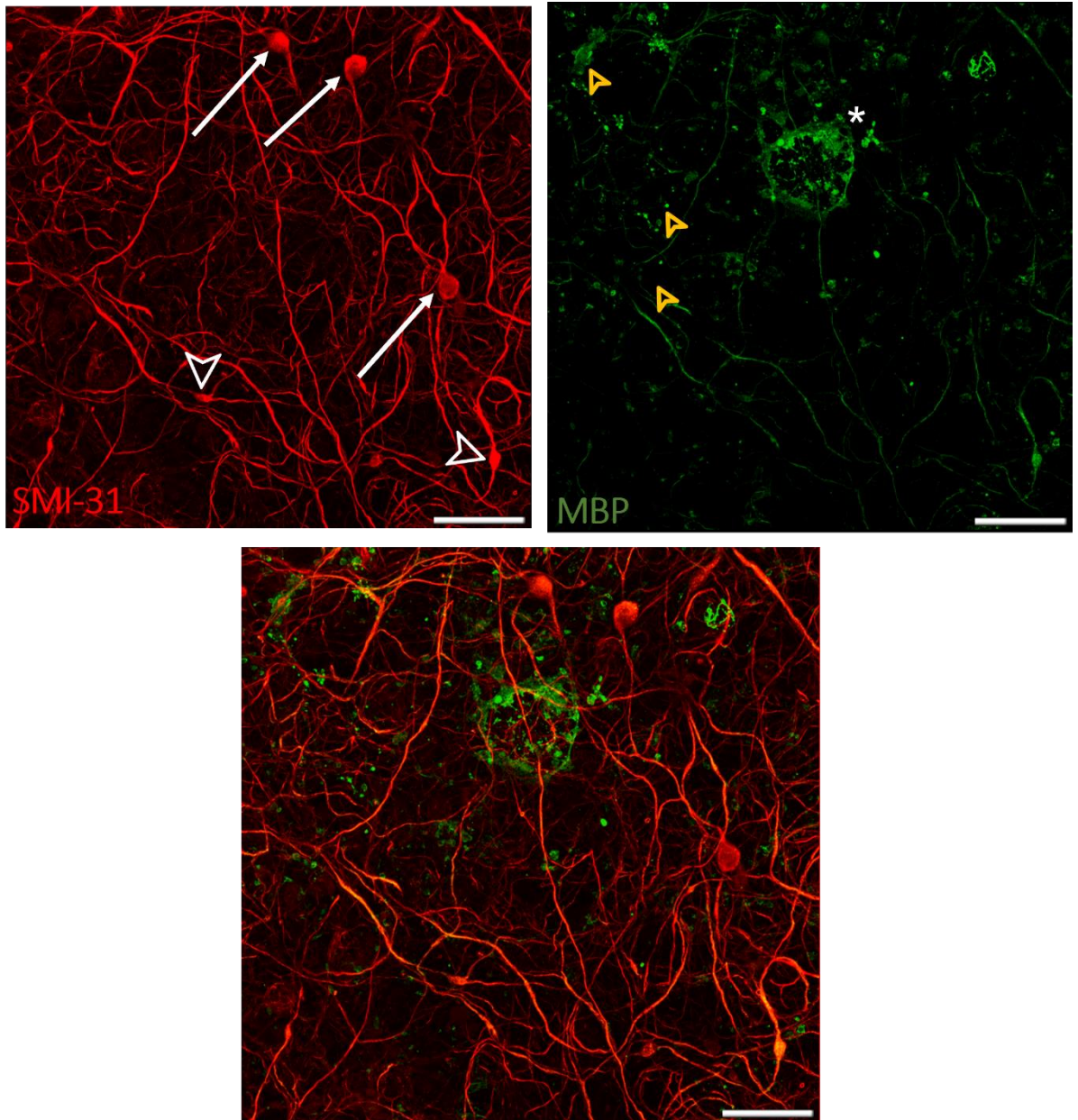


Figure 3.2 |Axon retraction bulbs and absence of myelin sheaths in P10 SD rat cerebellar slices. Confocal images of cerebellar slices maintained to DIV 12. Signs of axonal degeneration is seen with the presence of terminal bulbs (SMI-31, red; indicated by white arrows) and axonal swellings (indicated by white arrowhead). Abnormal MBP staining (green, myelin) was observed throughout with signs of myelin debris (indicated with yellow arrow heads) alongside abnormal MBP positive spherical structures (indicated with an asterisk). Scale bars = 20 μm *Representative images from five independent cultures*

3.4 Cerebellar slice cultures from P7-10 C57BL/6 mouse pups did not maintain healthy myelinated axons

Cerebellum from C57BL/6 P10 mice have been used previously to produce myelinating organotypic slice cultures (**Thetiot *et al.*, 2019**). As in rat cerebellar cultures, P10 is a time corresponding to the onset of Purkinje cell myelination, providing ideal tissue for subsequent remyelination studies. Therefore, we generated cerebellar slice cultures from P10 C57BL/6 mice and maintained them to DIV 12, fixed with 4% PFA, and immunolabelled with antibody clone SMI-3 and anti-MBP. **Figure 3.3 (a-c)** visualises abnormal ‘wavy’ axonal morphology indicative of axonal degeneration. Additionally, axonal swellings were present through the slices (indicated by white arrowheads). However, axonal density appeared greater compared to slices cultures generated from P10 SD rats shown previously (**Figure 3.1 and 3.2**). Hallmark features of Wallerian degeneration are observed in **Figure 3.4** with axonal fragmentation presenting with clear breaks in the SMI-31 staining (indicated with white arrowheads). Furthermore, we observed MBP positive tracts without an associated SMI-31 stained axon suggesting axonal degeneration with the myelinated tract which is yet to degenerate (**Figure 3.4**, white arrows). Additionally, a large quantity of myelin debris (indicated by yellow arrowheads) is observed around these MBP positive tracts (**Figure 3.4**) indicative of myelin degeneration. Also, of note - the myelin debris appears to present in long lateral tracts, that could suggest previous establishment of myelinated tracts that are undergoing degeneration, leaving myelin debris in this formation.

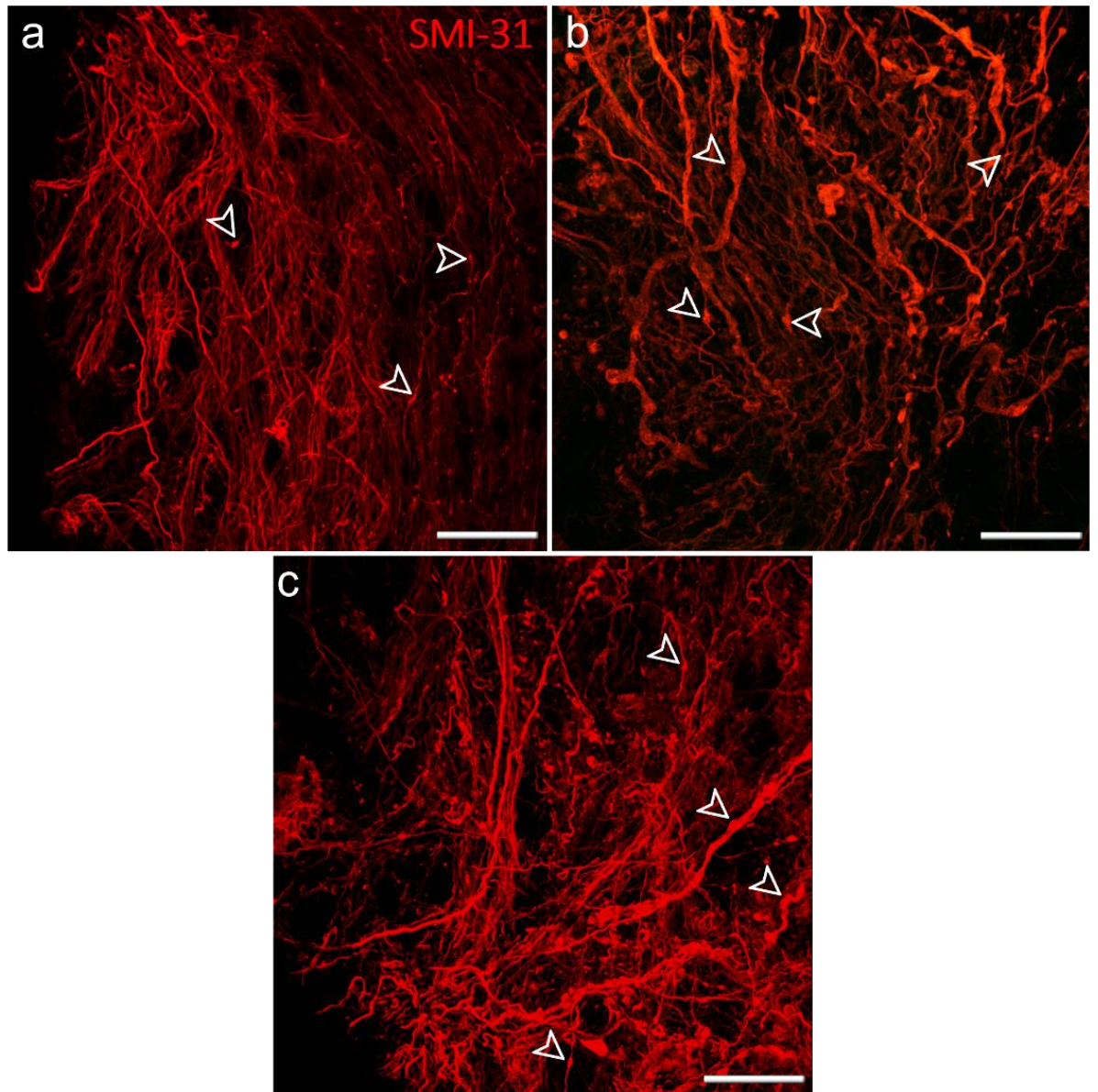


Figure 3.3 | Reasonable axon density with appearance of degeneration in P10 mouse cerebellar slices. Confocal images of cerebellar slices from P7 C57BL/6 mice. Cultures were allowed to recover until DIV 12, following which they were fixed with 4% PFA, and immunolabelled with antibody clone SMI-31 (red, neurites) and anti-MBP (green, myelin). (a-c) Axonal degeneration can still be identified with prominent swelling of the axons (indicated by white arrow heads). Scale bars = 20 μm *Representative images from 4 independent cultures*

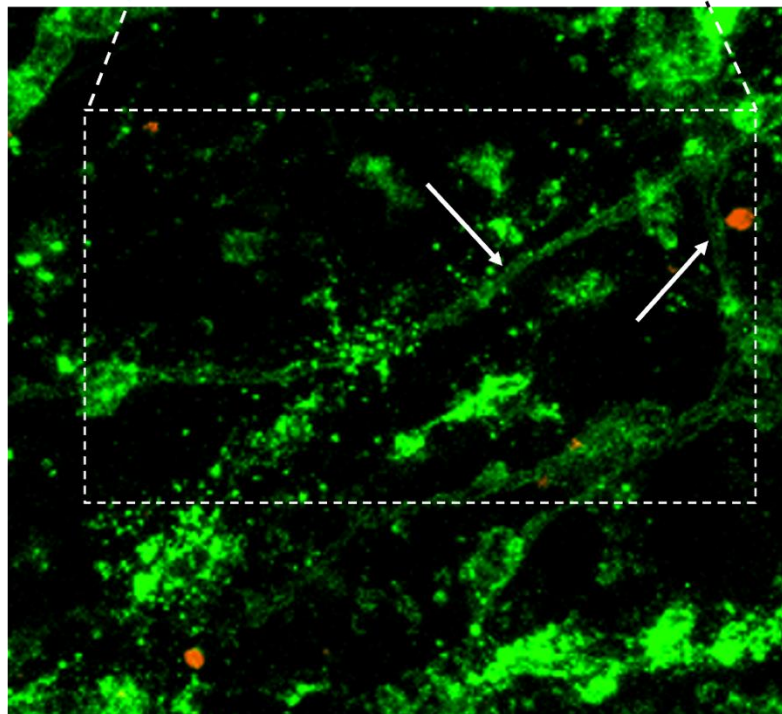
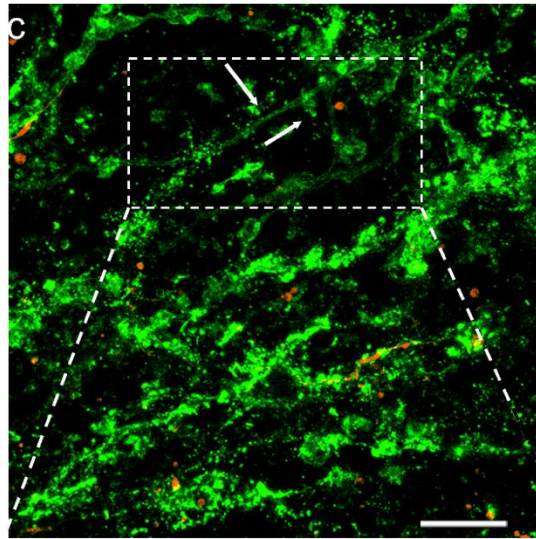
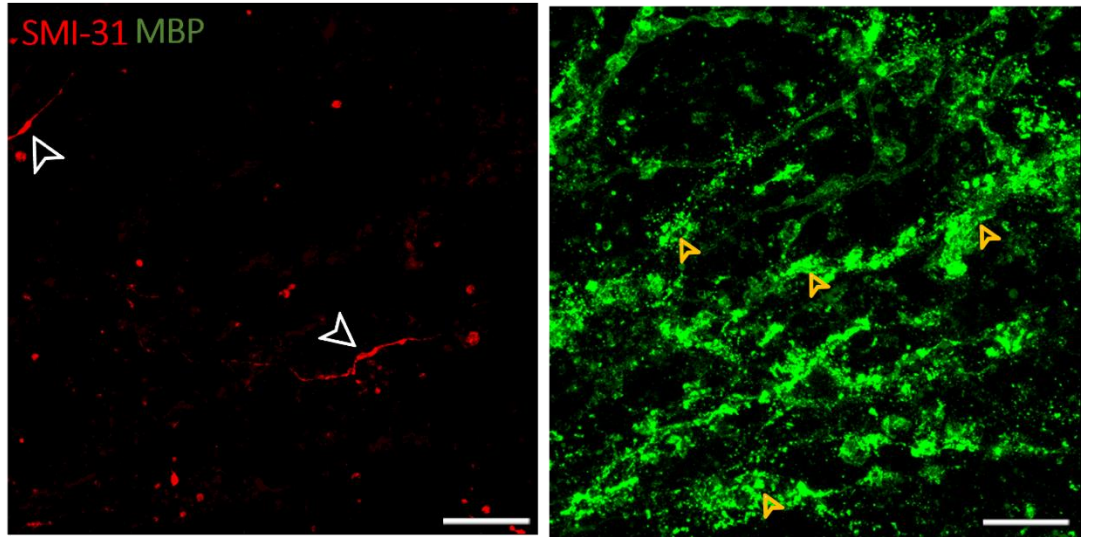


Figure 3.4 [Myelin tracts without an associated axon observed in P7 mouse cerebellar slices. Confocal images of cerebellar slices from P7 mice. Cultures were allowed to recover until DIV 12, following which they were fixed with 4% PFA, and immunolabelled with antibody clone SMI-31 (red, neurites) and anti-MBP (green, myelin). Images shows signs of Wallerian degeneration including swollen axons (indicated by white arrowheads), myelin debris (indicated by yellow arrowheads) and MBP stained tracts with no associated axon (indicated by white arrows). Magnification insert section showing detail of tracts with no associated SMI-31 (axon) staining. MBP staining suggest the axon has degenerated leaving the white matter tract, which ultimately degenerate leaving myelin debris. Scale bars = 20 μ m, *Representative images from a single culture*

A necessary feature of a successful *ex vivo* slice culture method to study re/myelination is the production and maintenance of compact myelin around the axons. **Figure 3.5** shows the appearance of MBP positive tracts within the slice. These tracts do appear to have associated SMI-31-stained axons however their morphology does not appear typical of compact myelin, as it does not wrap closely along the axons, and instead appears non-compact, potentially degenerating. **Figure 3.5** demonstrates no staining for CASPR (paranodes), suggesting that this is not compact myelin. Another feature observed that suggests that this myelin is degenerating and no longer compact is the myelin debris (indicated by yellow arrow heads) seen in **Figure 3.5**, surrounding these myelin tracts. Axonal swellings can be seen along the axons – indicative of axon degeneration (indicated by white arrowheads).

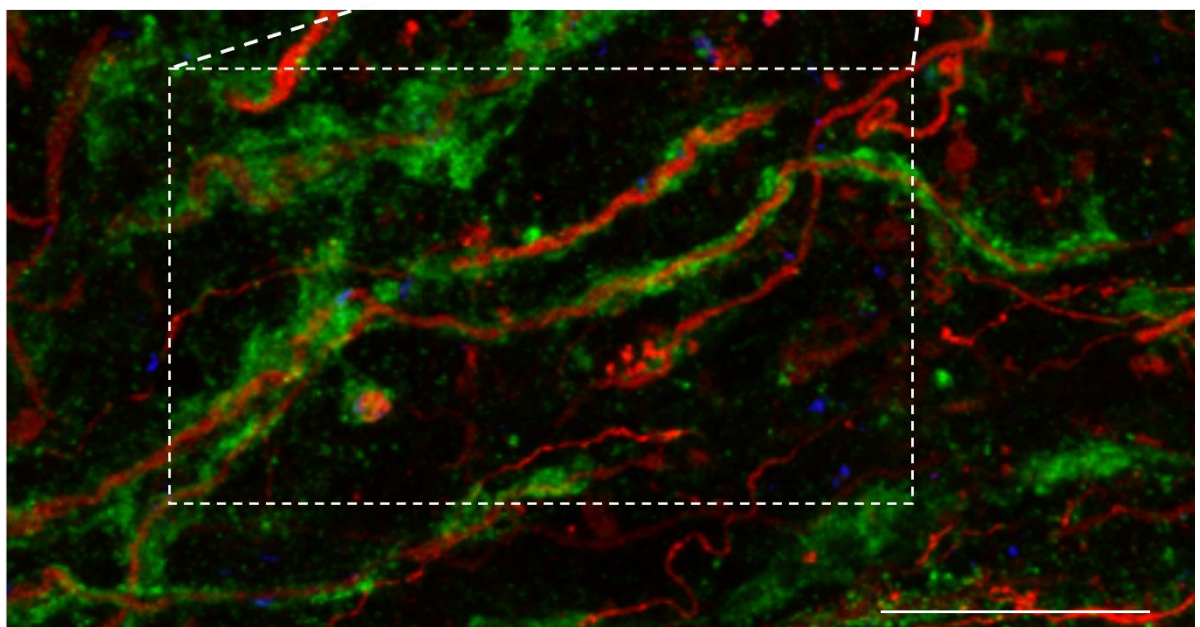
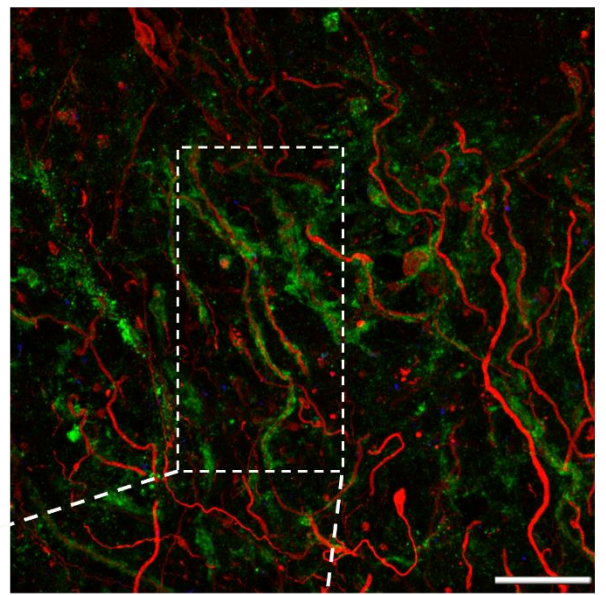
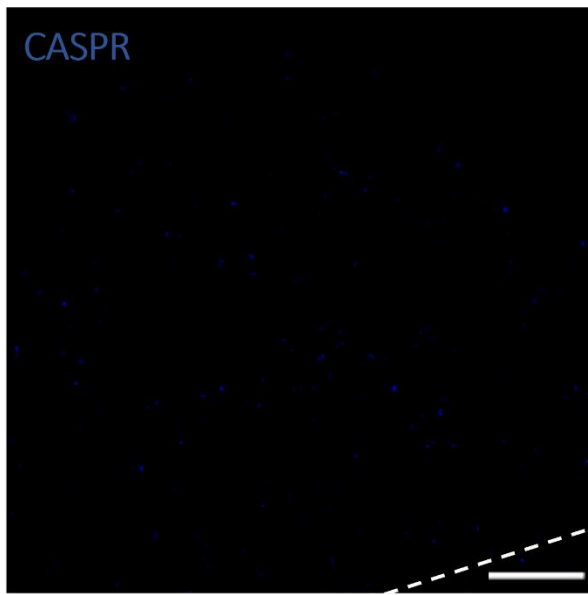
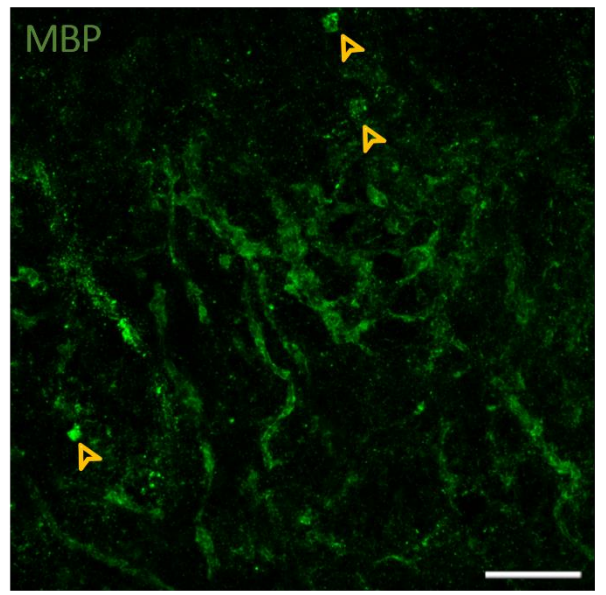
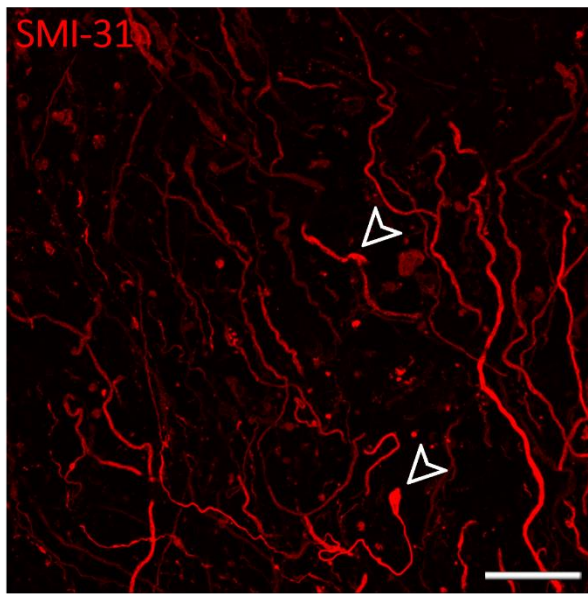


Figure 3.5 | Non compact myelin observed in P7 mouse cerebellar slices. Confocal images of P7 mouse cerebellar cultures at DIV 12, fixed with 4% PFA, and immunolabelled with SMI-31 (red, neurites), anti-MBP (green, myelin) CASPR (blue, internodes). MBP staining suggests production of myelin around axons, however morphologically, myelin appears unhealthy and non-compact. No CASPR staining was noted, further suggesting no presence of compact myelin around the axons, with a lack of internodes. Swelling of axons (indicated by white arrowheads) can be observed along the axons, a further suggestion of axon degeneration. Myelin debris can be observed (indicated by yellow arrowheads) Scale bars = 20 μ m *Representative images from four independent cultures*

To summarise we were unable produce slice cultures from P7-10 C57BL/6 mouse cerebellum that could produce and maintain healthy myelinated axons. Despite the culture appearing dense with axons, and containing myelinating oligodendrocytes, they showed signs of degeneration making them unsuitable to employ as an *ex vivo* model of the CNS.

3.5 Mouse C57 P1-3 cerebellum contained healthy appearing axons but variable levels of myelination and expression of CASPR

Cerebellar slice cultures from rat and mouse at P7-10 did not produce useful *ex vivo* models to study the CNS myelination. Others have shown viable cultures when generated from early postnatal tissue from P1-2 mouse brains (Zhang *et al.*, 2011). Here we dissected brains from P1-3 mice that were allowed to recover until DIV 12, following which they were fixed with 4% PFA, and immunolabelled with SMI-31. **Figure 3.6 (a-c)** demonstrates healthier appearing axons compared to those seen in previous figures. The axons are orientated parallel in organised bundles to each other suggestive of healthy axons as reported in other studies.

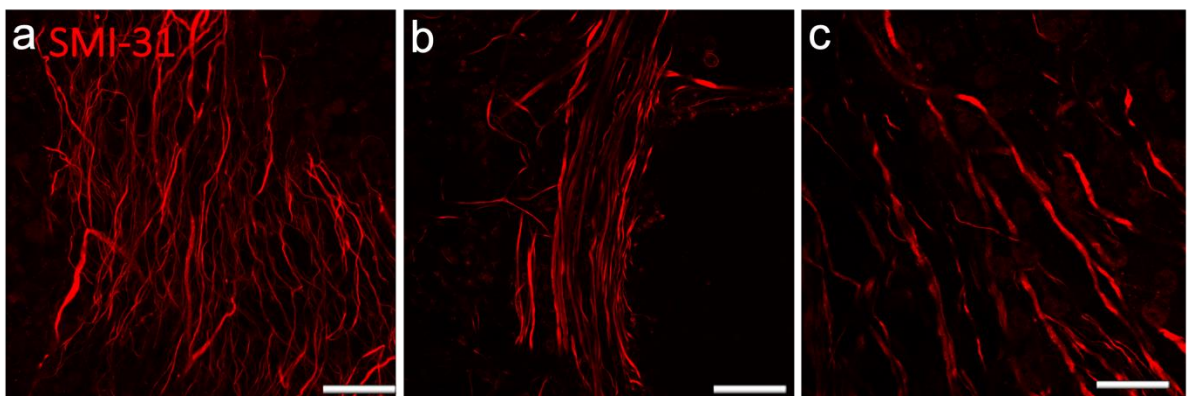


Figure 3.6 /Improvement in axon appearance from slice cultures generated from P1 mouse cerebellar. Confocal images of cerebellar slices from P1 C57BL/6 mice. Cultures were allowed to recover until DIV 12, following which they were fixed with 4% PFA, and immunolabelled with SMI-31 (red, neurites). (a-b) SMI-31 staining shows healthy appearing axons, however, axon density appears to vary amongst slices, which can be seen in (c) compared to (a). Scale bars = 20 μ m. *Representative images from 3 cultures*

Additionally, there were MBP- stained myelin sheaths that appeared healthy and thicker than SMI-31-stained axons (**Figure 3.7**). Myelin integrity was confirmed using CASPR staining, which indicated the presence of paranodes within the slices and therefore highly suggested compact myelin along the axons (although very few). Where two myelin segments approach each other to form a node, CASPR staining appears as a dimer. Of note, the CASPR staining is found within the gap of MBP staining but does not extend into the node itself. Two representative nodes are indicated by the white arrowheads in **Figure 3.5** and at higher power view of the node is shown in the inset.

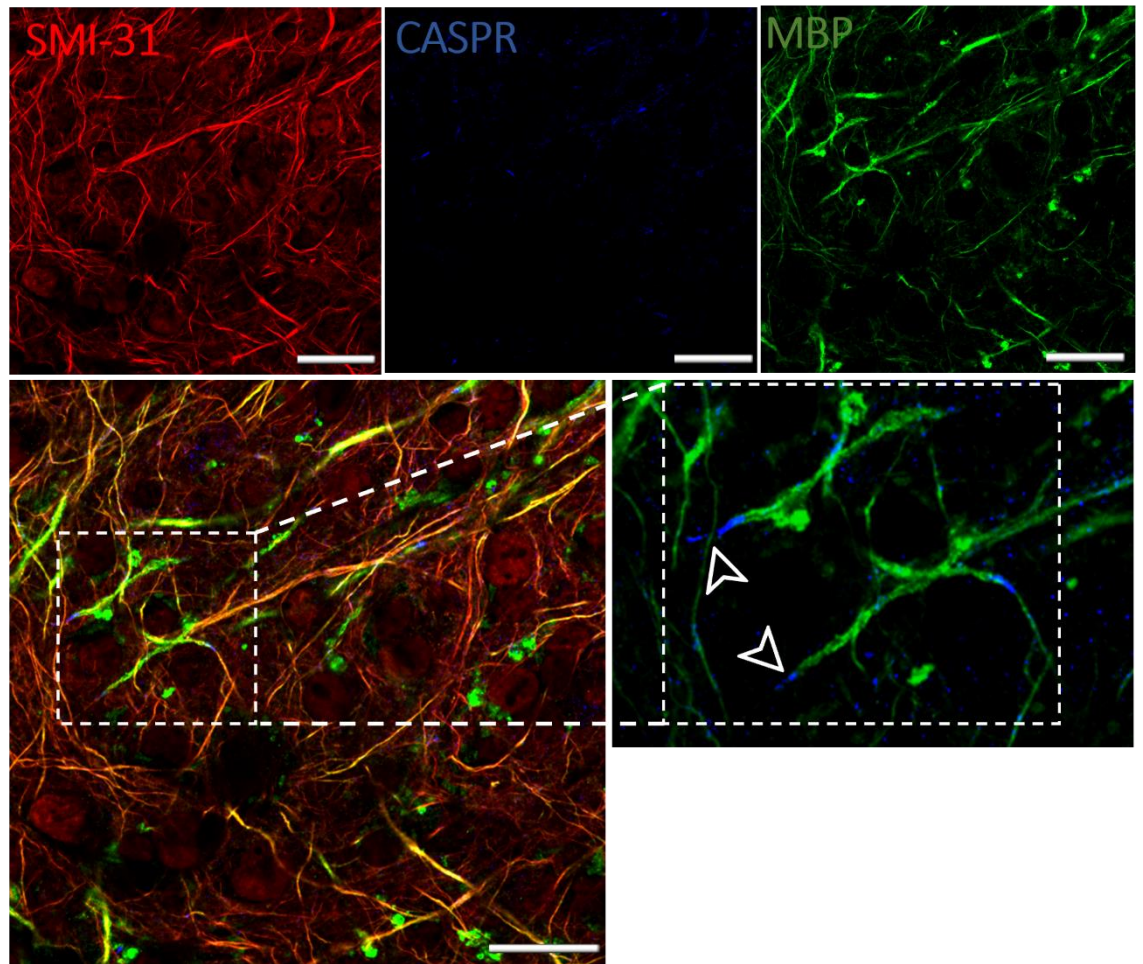


Figure 3.7 /Compact myelin and CASPR staining observed in slice cultures generated from P1 mouse cerebellum. Confocal images of cerebellar slices from P1 C57BL/6 mice. Cultures were allowed to recover until DIV 12, following which they were fixed with 4% PFA, and immunolabelled with antibody clone SMI-31 (red, neurites), anti-MBP (green, myelin), CASPR (blue, internodes). First indication of CASPR staining can be visualised and can be seen labelling paranodes between MBP staining (indicated by white arrow heads) running along axons. CASPR staining suggests compact myelin is being produced along axons and axons appear healthy with reasonable density. Scale bars = 20 μ m. *Representative images from 4 independent cultures*

To summarise we were able produce slice cultures from P1 C57BL/6 mouse cerebellum that could produce and maintain healthy myelinated axons. However, myelination levels were very low, and signs of degeneration could still be seen in the slices. Despite myelin being observed the low levels of myelination this still leaves this method for slice cultures unsuitable to employ as an *ex vivo* model for study of repair of the CNS myelination.

3.6 Spinal cord slice cultures from P1 C57BL/6 mouse pups maintained healthy axons with consistent myelination

Slice cultures generated from cerebellum did not produce viable organotypic slice cultures, suggesting (to our surprise) that this tissue is unsuitable for culture. **Sekizar and Williams, 2019** suggested that spinal cord slice cultures can be successfully generated and maintained for the study of the CNS; therefore, we generate spinal cord slice cultures from P0-2 mice.

We dissected spinal cords from P1 C57BL/6 mice and cultured them for 14 DIV before visualising with SMI-31, CASPR, and MBP. As we observed in **Figure 3.8 (a-d)** healthy axons were observed traversing throughout the slices. The axons are long and flow together in organised bundles. There were no visible signs of axon degeneration in the form of axon swelling, axonal fragmentation or retraction end bulbs.

Figure 3.9 (a-c) shows high levels of compact myelin on the axons through the slice. The myelin can be observed as being thicker than the SMI-31 axonal staining, due to the external wrapping which occurs. To note, it is important that the staining for MBP is thicker than what is seen for SMI-31, as any SMI-31 visualised within the staining of MBP must be taken as bleed through and not real myelin (this is dealt with in analysis via our macro that eliminates this issue). Myelin will always be identified as external to the axon, and never internal.

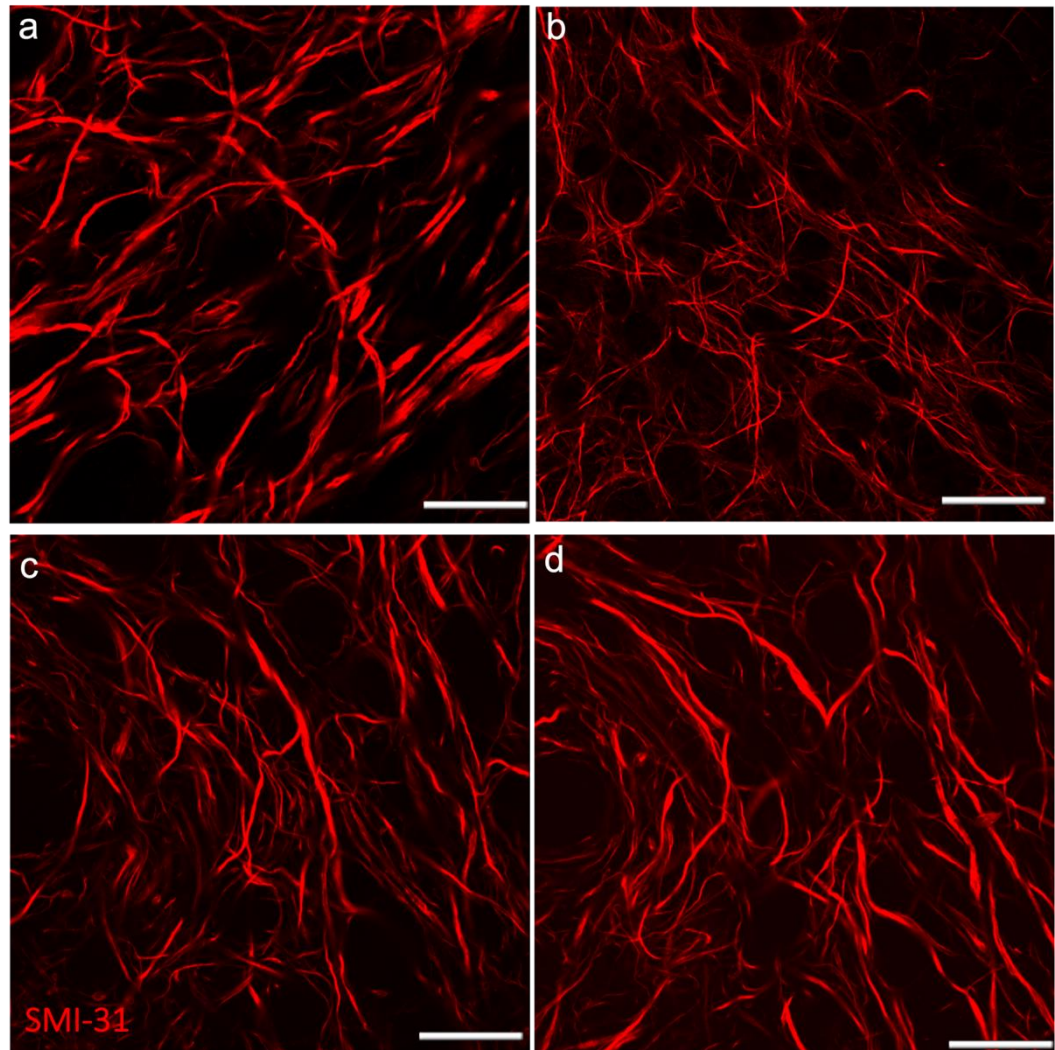


Figure 3.8 [Mouse P1 spinal cords show high axon density with no signs of axon degeneration. Confocal images of spinal cord slices from P1 C57BL/6 mice. Cultures were allowed to recover until DIV 14 following which they were fixed with 4% PFA, and immunolabelled with antibody clone SMI-31 (red, neurites). (a-d) SMI-31 staining shows healthy appearing axons. Axon density appears to be high amongst all slices and throughout each slice. Scale bars = 20 μ m *Representative images from three independent cultures*

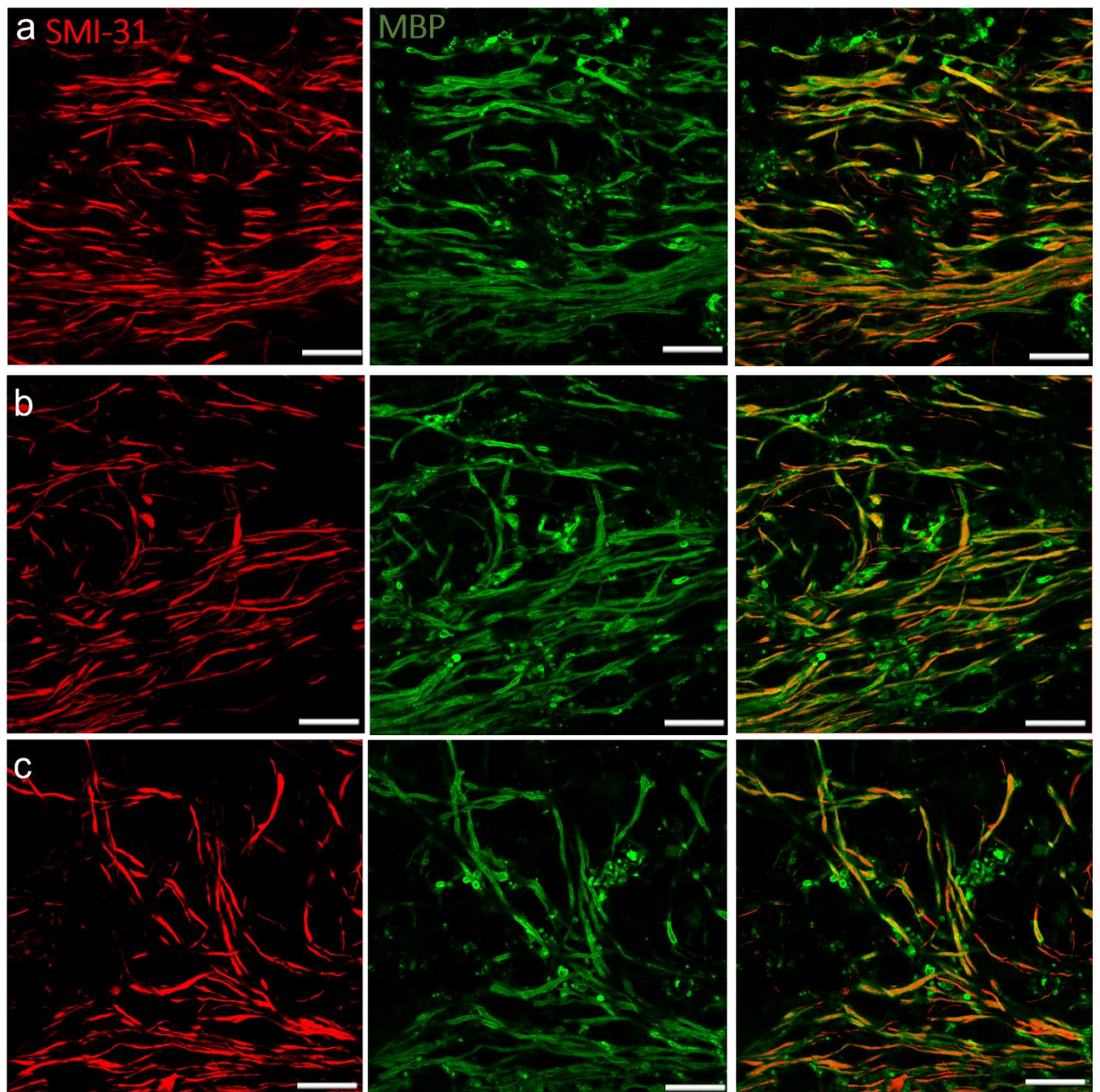


Figure 3.9 | **Mouse P1 spinal cord slice cultures show high levels of healthy myelination.** Confocal images of spinal cord slices from P1 C57BL/6 mice. Cultures were allowed to recover until DIV 14 after which they were fixed with 4% PFA, and immunolabelled with SMI-31 (red, neurites) and MBP (green, myelin). (a-c) Axon density remains high throughout the slices with no appearance of degenerating axons. MBP staining shows a high density of compact myelin wrapping around the axons. Overlay of SMI-31 and MBP shows thicker myelin wrapping along the axons. Scale bars = 20 μ m *Representative images from three independent cultures*

To further confirm that the MBP observed in these slices was real, additional staining of CASPR at the Nodes of Ranvier was performed. **Figure 3.10** indicates successful identification of CASPR dimers, suggesting myelination of the axon. Of note, the MBP staining does not continue between the two dimers as myelin is not present here. This non myelinated region represents the paranode of the axon. A large amount of MBP staining can be observed in **Figure 3.10**, again confirming that these cultures are able to produce a higher percentage of myelinated axons compared to our previous cultures. Abnormal MBP staining is observed in **Figure 3.10** with circular staining (indicated by yellow arrowheads), most likely the soma of the oligodendrocyte cell, which should not occur. MBP staining should be localised exclusively to the myelin sheath.

Overall **Figure 3.10** confirms that the myelin observed in our slices is real and not bleed through observed during the imaging process.

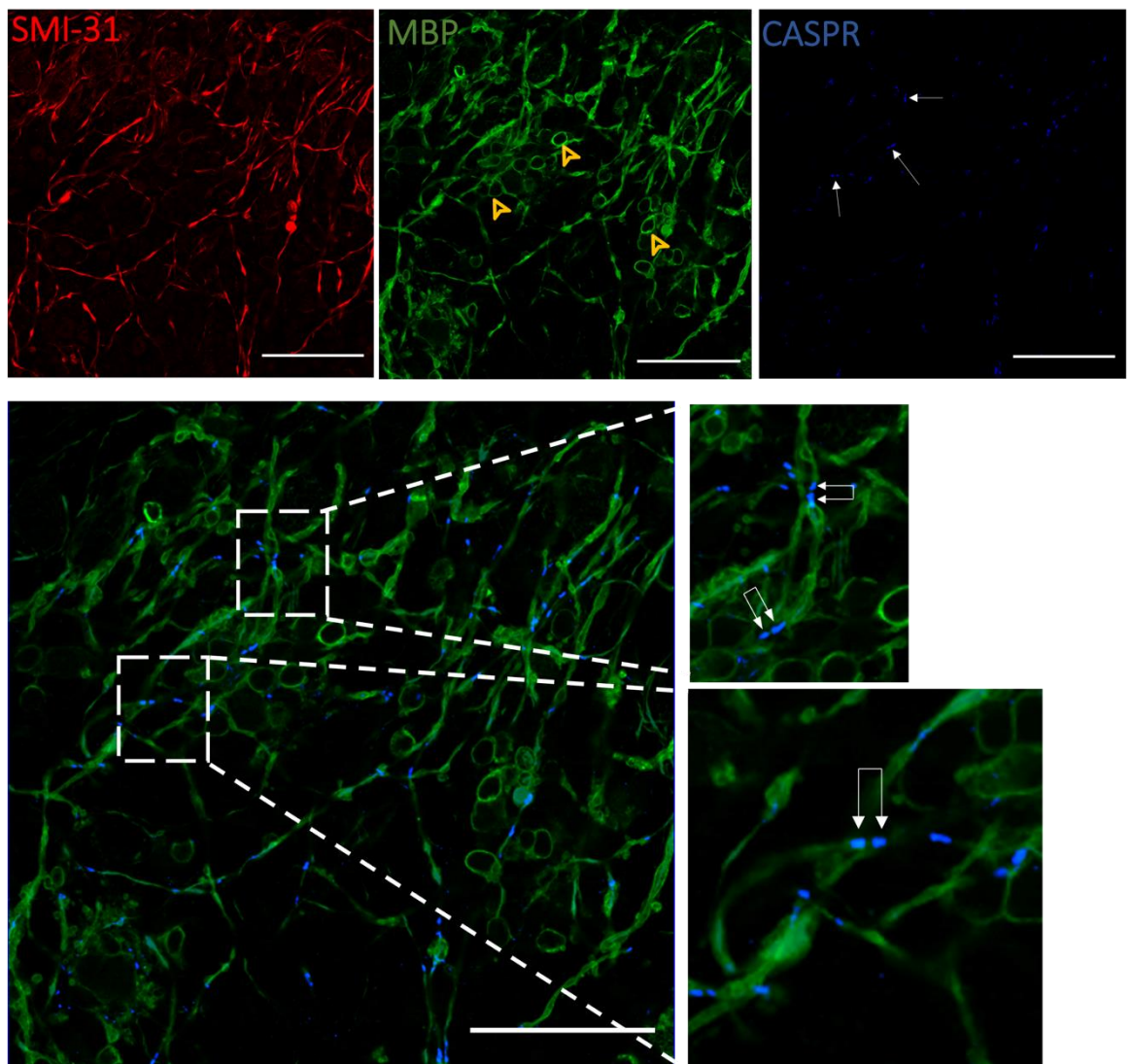


Figure 3.10 /Competent myelination confirmed with the presence of CASPR positive staining. Confocal images of P1 C57BL/6 mice spinal cord slices maintained until DIV 14 where they were fixed with 4% PFA and immunolabelled with SMI-31 (red, neurites) and MBP (green, myelin), and CASPR (blue, paranodes). CASPR staining appears as dimers (indicated by white arrows) as they identify the end and beginning of the myelin sheath. To note MBP staining does not appear between the CASPR dimers. Abnormal staining of MBP can be observed with circular staining and is indicated with yellow arrowheads. Scale bars = 20 μ m. *Representative images from 3 independent cultures.*

In summary, we found that P1 mouse spinal cord slice cultures produce healthy axons that are well myelinated throughout the slice at DIV 14, providing a suitable model for the *ex vivo* study of re/myelination and repair of the CNS.

3.7 Lysolecithin induced demyelination is a successful tool without any detrimental effects on the properties of the cultures

After establishing and characterising spinal cord slice cultures from P1 C56BL/6 mice as an *ex vivo* model of the CNS, the next step was to determine a successful demyelination protocol to study the pro-remyelination properties of LS-mHeps (see *Chapter 5*). It was critical to employ a method that strips axons of myelin without damaging axons. The bioactive lipid lysolecithin (lysophosphatidylcholine) is a well-established reagent for demyelination in slice cultures (**Birgbauer *et al.*, 2004; Miron *et al.*, 2010; Sekizar and Williams, 2019**). In many of these methods lysolecithin is added to cultures at 0.5 mg/ml for 24 hr. Therefore, we used this to initiate demyelination in our slices.

Figure 3.11 (b-c) shows successful demyelination throughout the spinal cord slices without any apparent toxic effect on the axons (**Figure 3.11 a**). Axon density remained relatively the same at DIV 14 before lysolecithin exposure, 24 hours after demyelination (DeMy 24hr), and two weeks after demyelination (DeMy DIV 28). Representative images from slices 24 hr after lysolecithin exposure shows no compact myelin around axons (**Figure 3.11 b, c**), and myelin debris is observed (indicated by yellow arrowheads) 24 hr after demyelination. Literature reports that it can take 2-3 days for partial myelin debris clearance by microglia (**Sekizar and Williams, 2019**).

In summary, lysolecithin appears to be a suitable reagent for demyelinating spinal cord slice cultures without any apparently toxic effect on axons.

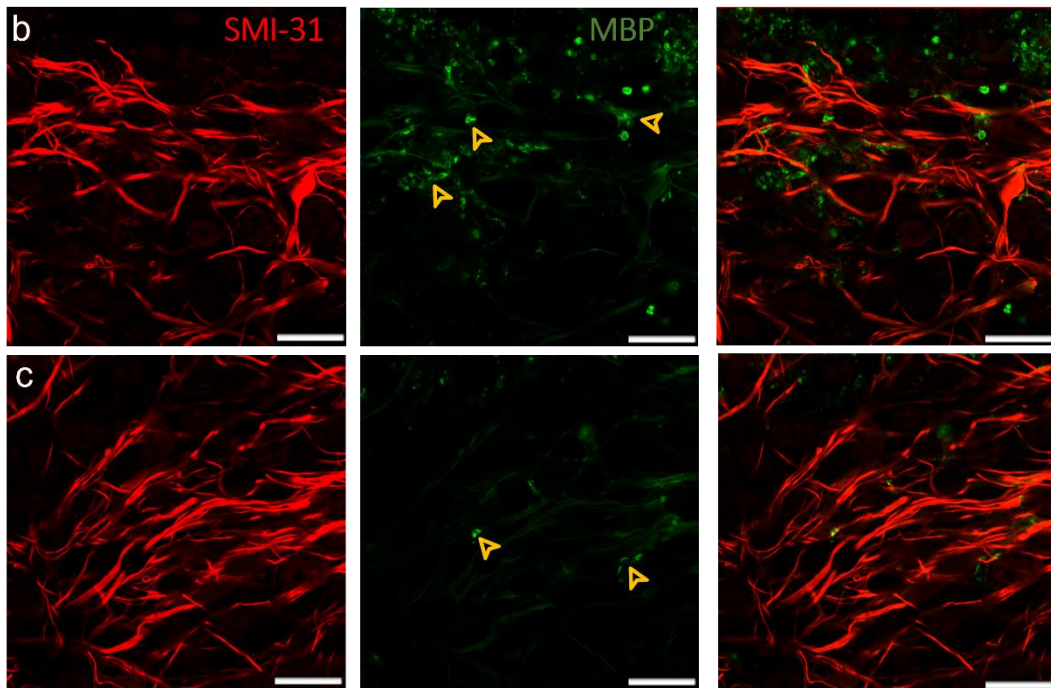
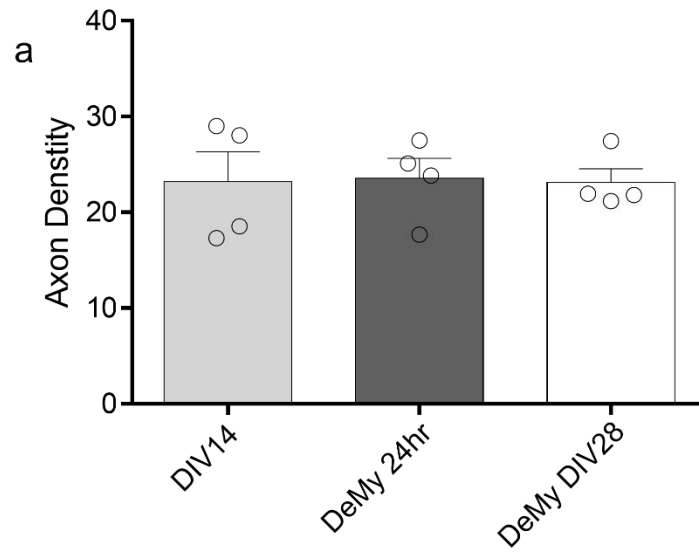


Figure 3.11 |Demyelination with lysolecithin successfully strips axons of myelin. Confocal images of P1 C57BL/6 mice spinal cord slices 24 hours after lysolecithin exposure. Cultures were maintained until DIV 14 where they were chemically demyelinated with lysolecithin (from bovine) (0.5 mg/mL) for 24 hr and immunolabelled with antibody clone SMI-31 (red, naxons) and MBP (green, myelin). (a) No significant axon loss is observed with % density remaining high throughout the demyelination process. Myelin debris (indicated with yellow arrowheads) is observed around axons (red), often related to demyelination, with no compact myelin observed (b,c). Scale bars = 20 μ m, Data were obtained from 4 biological repeats (n=4)

3.8 Spontaneous remyelination is observed 9 days after demyelination in spinal cord slice cultures.

In models of CNS demyelination, spontaneous remyelination occurs when resident oligodendrocytes remyelinate axons. It is important to determine when spontaneous remyelination occurs, to differentiate natural remyelination levels within the culture system and the effects of out LS-mHeps after demyelination.

To determine when spontaneous remyelination begins within this culture system P1 mouse spinal cords were demyelinated at DIV 14 using 0.5 mg/ ml lysolecithin treatment. They were then fixed 3-, 6-, 9-, 12-, and 15-days post demyelination, and immunolabelled with SMI-31, and MBP. **Figure 3.12** highlights representative images indicating the presence of MBP staining. These images demonstrate that there is no MBP staining present along the axons in the cultures 3 and 6 -days post demyelination, with some potential appearance of myelin debris that has been indicated previously (**Figure 3.11**). Nine days after demyelination, MBP staining is observed, with myelin wrapping around axons. However, the amount of myelin present is low with thin strips of myelin being observed (indicated by white arrowheads), possibly indicating early remyelination along the axons. Also noted at 9 days post demyelination is the presence of potential MBP positive cells (indicated with a yellow arrowheads). Although MBP positive spherical cells cannot be confirmed as myelinating oligodendrocytes, we can theorise that this could be the case. By day 12 post demyelination, qualitative assessments suggest an increase in the percentage of myelinated axons present pre field of view, and this increase continues to 15 days post demyelination, where remyelination appears to be fully established within the slice.

Additionally, **Figure 3.13** shows CASPR staining appearing on slices fixed and immunolabelled 12 days post demyelination. SMI-31-stained axons framed by a CASPR dimer are observed. Once more, MBP does not appear between the CASPR dimers as paranodes are non-myelinated areas along the axon. However, this CASPR staining confirms successful remyelination in our slices after lysolecithin induced demyelination.

To summarise, we found that spontaneous remyelination in mouse spinal cord begins approximately at 9 days post demyelination and continues to increase up to 15 days post demyelination where myelination levels appear to be fully restored.

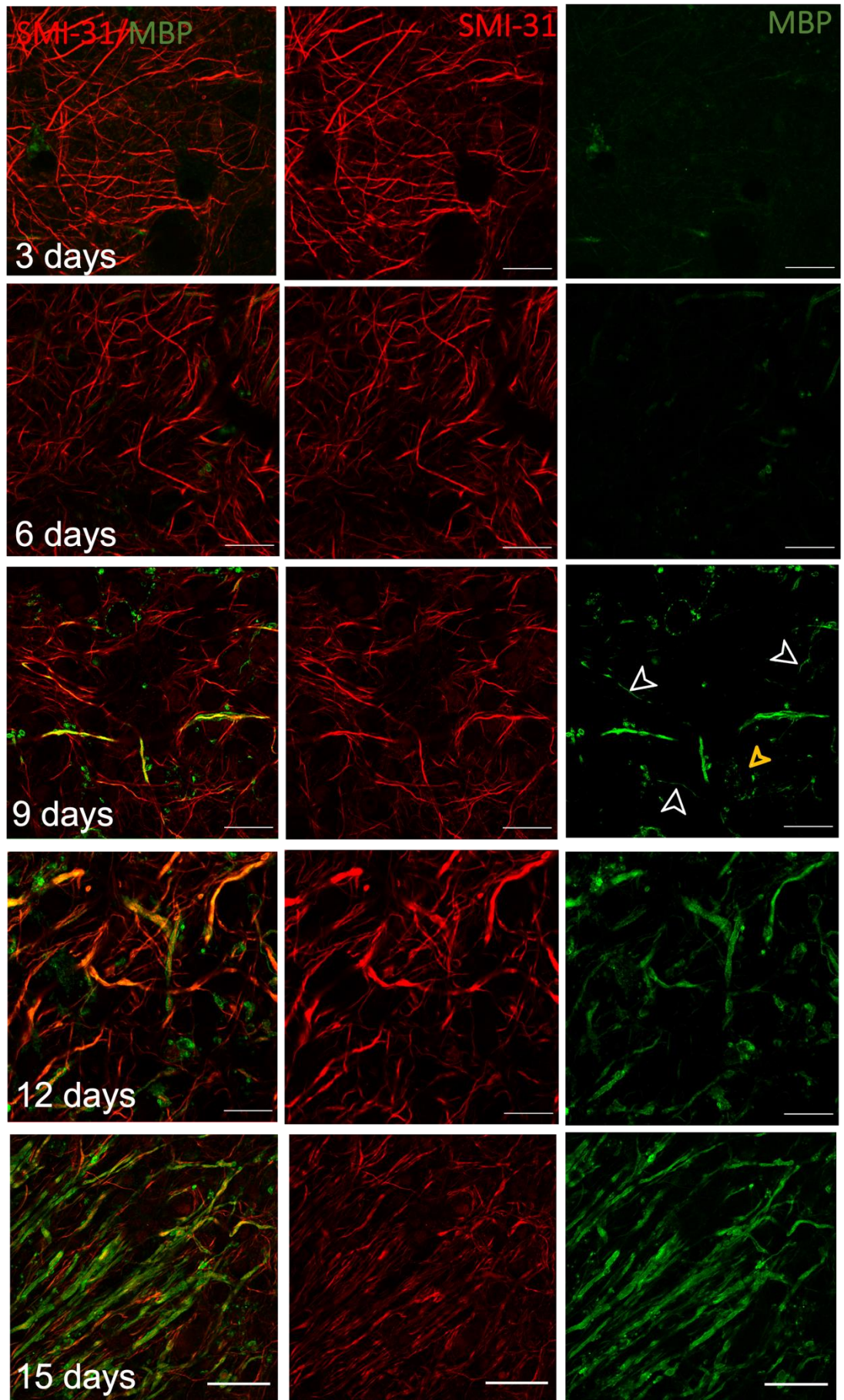


Figure 3.12 | Remyelination 9 days post demyelination and increases to 15 days post demyelination to restored levels. Confocal images of P1 C57BL/6 mice spinal cord slices after demyelination via lysolecithin exposure. Cultures were maintained until DIV 14 then chemically demyelinated with lysolecithin (0.5 mg/mL) for 24 hr. Cultures were then fixed with 4% PFA at day -3, -6, -9, -12, and -15 post demyelination. Cultures were immunolabelled with SMI-31 (red, axons) and MBP (green, myelin). First indications of MBP staining begins at 9 days post demyelination with signs of very thin myelin (indicated with white arrows) and some thicker myelinated axons. Also identified is what appears to be MBP stained cells (indicated with yellow arrows). Remyelination continues until day 15 where a high percentage of axons appear well myelinated. Scale bars = 20 μ m. *Images representative of two independent cultures.*

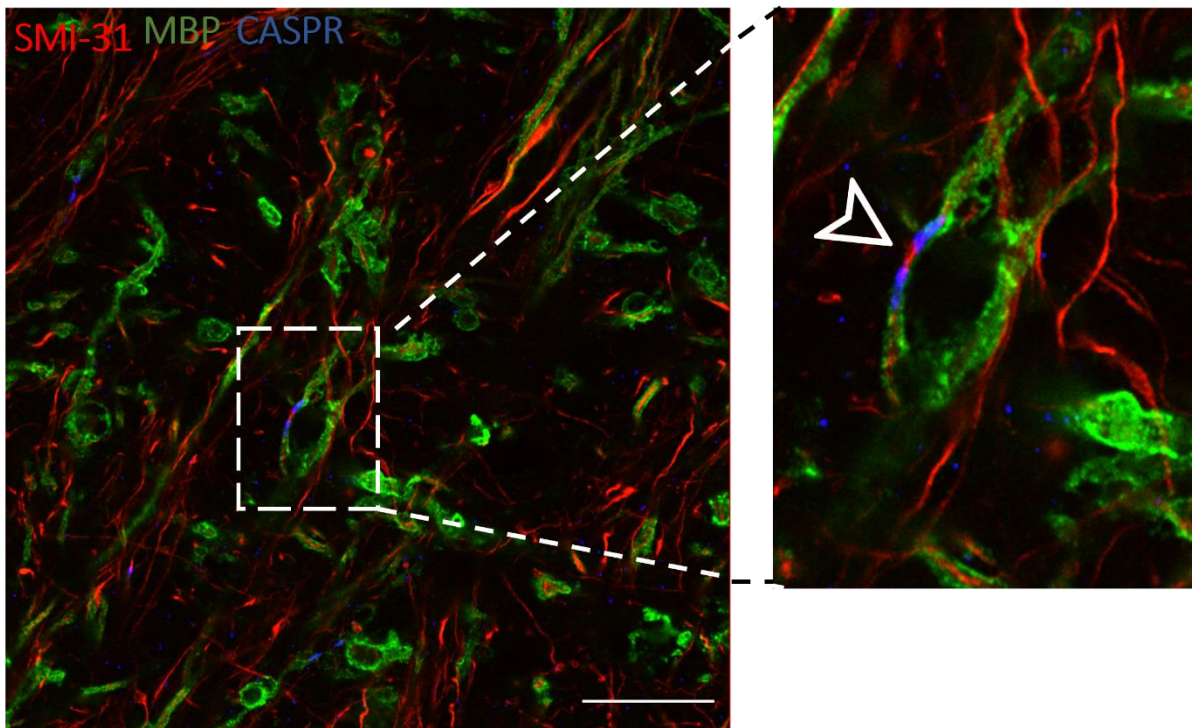


Figure 3.13 | CASPR staining confirms compact re/myelination along axons after lysolecithin induced demyelination. Confocal images of remyelinated P1 C57BL/6 mice spinal cord slices 12 days after demyelination via lysolecithin exposure. Cultures were maintained until DIV 14 then chemically demyelinated with lysolecithin (0.5 mg/mL) for 24hr. Cultures were then fixed with 4% PFA 12 days post demyelination. Cultures were immunolabelled with SMI-31 (red, neurites), MBP (green, myelin), and CASPR (blue, internodes). CASPR staining can be identified as remyelination progressed to produce mature compact myelin. Scale bars = 20 μ m

3.9 Discussion

The development of novel treatments that promote CNS repair relies on preliminary screening of molecules for therapeutic effect in a cost effective and timely manner. In this chapter, we aimed to optimise a method for organotypic slice cultures that allowed the reproducible study of re/myelination. Here we demonstrated that early postnatal spinal cord tissue from C57BL/6 mice produced healthy organotypic slice cultures that could be maintained for several weeks and allowed for the chemical demyelination with lysolecithin. Additionally, these slices were able to re/myelinate to produce high levels of myelinated axons. This was in large contrast to organotypic slice cultures that were produced from late postnatal rat and mouse cerebellum.

Previously our lab has used SD rats as a source for tissue while investigation remyelination and neurite outgrowth (**McCanney et al., 2019**), and therefore we decided to continue with this for scientific comparison between remyelination in the *ex vivo* cultures and the *in vitro* system.

Axonal swellings are an observed feature of axonal degeneration in the CNS (**Wang et al., 2012; Cui et al., 2020**) and were noted in the cerebellar slice cultures from P7-10 SD rats. These swollen axons accumulate abnormal amounts of microtubule-associated proteins, molecular motor proteins, vesicles and organelles including smooth endoplasmic reticulum (**Chretien et al., 1980**) and mitochondria (**Ferreirinha et al., 2004**). This build up ultimately leads to the disruption of further axonal transport and in the case of mitochondria this can be detrimental to cell survival. Mitochondria are transported to specific sites in axons where high energy is in demand, such as in growth cones and axonal branches (**Morris and Hollenbeck, 1993**) Impairment of axonal mitochondria transport ultimately induces local energy depletion and further axon degeneration (**Sheng and Cai, 2012**). It is thought that these accumulations are due transport deficits during early axonal degeneration and has been identified in early pathogenesis in animal models of Alzheimer's disease **Stokin et al., 2005**, and is documented in many neurodegenerative disease (**Millecamps et al., 2013**).

Furthermore, accumulation of molecules along axons can result in retraction bulbs, observed in these rat cerebellum slices. These swollen bulb structures form at the terminal ends of a broken axon (through transection or degeneration) due to an accumulation of molecules from anterograde and retrograde transport (**Griffin et al., 1995**). One of these accumulation molecules that has been documented as a marker for axonal degeneration is amyloid precursor protein (APP), which is normally transported through healthy axons but

accumulates in axonal spheroids or varicosities in degenerating axons (**Liu *et al.*, 2018**; **Craner *et al.*, 2004**; **Sherrif *et al.*, 1994**). APP accumulation has been found in axons that have been damaged during TBI (**Gentleman *et al.*, 1997**), and MS (**Ferguson *et al.*, 1997**). Eventually, the block of axonal transport is of sufficient magnitude to trigger Wallerian degeneration of the distal axon and end bulb remains on the proximal axon stump (**Coleman *et al.*, 2005**). Overall, retraction bulbs signify destabilisation and disorganisation of the microtubules network which results in unhealthy axons and ultimately, degeneration (**Eturk *et al.*, 2007**).

Abnormal staining of MBP, in the form of large spherical ‘cell like’ structures, was observed in rat cerebellum slice cultures, which we speculate are degenerating oligodendrocytes. Of course, we are unable to confirm this without any additional investigations. This MBP staining resembles that noted in **Creeley *et al.*, 2014**, with oligodendrocyte apoptosis identified via co-staining of MBP and activated caspase-3 (AC3), a marker for cellular apoptosis. Pathology studies have shown the presence of apoptotic cells, mainly oligodendrocytes and neurons (**Peterson *et al.*, 2001**), at the site of MS lesions (**Barnett & Prineas, 2004**), making oligodendrocyte apoptosis one of the earliest pathological changes observed in new white matter lesions. Oligodendrocyte apoptosis is also observed in EAE C57 BL/6 mice, with apoptotic cells being observed in the spinal cord as early as three days postimmunization (**Feng *et al.*, 2014**). The presence of these dying cells is suggesting degenerating cerebellum slice cultures which further.

In mouse cerebellar slices we noted an abnormal axonal morphology with a ‘wavy’ appearance being observed. Healthy axons run along in organised bundles of fibres, which was not the case here. ‘Wavy’ morphologies have been noted by **Waly *et al.*, 2020** and was observed prior to Wallerian degeneration and suggested that these ‘spring-like wavy’ axons were occurring due to mechanical constraints on otherwise linear healthy axons sheaths - 14.5% of axons presented neuronal swelling apparently resulting from presumed lipidic constrictions.

Wallerian degeneration itself was observed in the mouse cerebellar slice cultures, in the form of axon fragmentation. Axonal fragmentation is well documented as a key indicator of Wallerian degeneration (**Beirowski *et al.*, 2004**; **Jung *et al.*, 2014**; **Canty *et al.*, 2020**; **Cui *et al.*, 2020**). Although the mechanism that initiate Wallerian degeneration are not fully understood, the process of how axon fragmentation occurs is generally known. After cutting of the axon (axotomy) the axonal skeleton disintegrates distal to the injury site, and the axonal membrane breaks apart, leading retrograde degeneration (**Coleman and Freeman,**

2010). Wallerian degeneration is a major component of axonal pathology in the periplaque white matter in early MS (**Dziedzic *et al.*, 2010**), is observed in magnetic resonance imaging (MRI) of SCI patients (**Mittal *et al.*, 2016**) and is being investigated as a potential therapeutic target in TBI (**Koliatsos and Alexandris, 2019**).

MBP positive tracks that had no associated axons was observed in mouse cerebellum slice cultures. The MBP positive tracts suggest that the axon has degenerated leaving its myelin behind that will soon degenerate and loose form. However, we cannot confirm this without a further investigation – mostly with a more appropriate marker for axon degeneration. Immunolabelling for non-phosphorylated neurofilaments, an established marker for axonal damage (**Wallis *et al.*, 2012; Chan *et al.*, 2011**), would be a useful in future experiments to assess the levels of axonal degeneration in a more direct approach. Although we observed axonal degeneration, we have not examined the health of neurons per se. It has been observed previously in culture models that axonal degeneration can occur without neuronal cell body loss (**Crawford *et al.*, 2022**); therefore, it is possible that neuronal soma was unaffected in our model. However, this would require further investigation.

We observed ‘abnormal myelin’ within these same slices with MBP positive proteins indicated surrounding SMI-31 positive axons. However, this myelin appeared to be degenerating with a lack of compaction around the axon, and an appearance of caving in within its own structure. This morphology suggested that the myelin was disassembling/de-compacting, which was further suggested by the lack of CASPR staining. Individual components of CNS myelin is found to degrade at different rates during Wallerian degeneration (**Buss and Schwab, 2003**), with myelin-associated glycoprotein (MAG) - located in the peri-axonal oligodendroglia membranes of myelin sheaths - more rapidly than either MBP or Nogo-A. This could explain this abnormal morphology with the myelin proteins disbanding within the myelin sheath structure.

Tissue from younger postnatal animals (P1) provided the first glimpse of compact myelin in the mouse cerebellar slice cultures with CASPR immunofluorescence. Qualitatively these axons looked healthier with a higher axon density. Early postnatal ages are better suited for culturing because the essentials of the cytoarchitecture are already established in most brain areas, and the nerve cells survive explantation more readily. In general, the older the animal, the less tissue survives and the greater the cell death is (**Humpel, 2015**). We can speculate this is because neurogenesis begins at E11.5 in mice until P4, when the brain regions have assumed their final morphology, mature neural cell types are present, and synaptic

connections are beginning to form (**Chen *et al.*, 2017**). After P4, mouse brain tissue may struggle to replace the loss of mature neural cell types compared to younger <P4 tissue, and ultimately these cultures die.

Slice cultures obtained from P0-2 C57BL/6 mouse spinal cords, produced well myelinated axons. Additionally, we observed large amount of CASPR immunofluorescence strongly suggesting the formation of compact myelin. This contrasts with previous cultures generated from cerebellum and likely highlights intrinsic differences in the tissues used, particularly the glial populations. In recent years it has become apparent that homogeneity of oligodendrocytes does not exist (**Foerster *et al.*, 2019**), and differing areas of the CNS appear to be populated by a varying sub population of oligodendroglia. **Khandker *et al.*, 2022**, demonstrated that brain and spinal cord oligodendroglia precursors are transcriptionally distinct, defined predominantly by cholesterol biosynthesis. A difference in OPC populations is also known to exist between white matter and grey matter, with the former proliferating more rapidly and having a shorter cell cycle time (**Dawson *et al.*, 2003**). This has been replicated *in vitro* (**Hill *et al.*, 2013**). Recently, **Floriddia *et al.*, 2020** demonstrated that mature oligodendrocyte (MOLs) populations have spatial preference in the mammalian CNS, with MOL type 2 (MOL2) being enriched in the spinal cord when compared to the brain. Alongside providing new oligodendrocytes for myelination during development and adulthood, OPCs have a central role in oligodendrocyte regeneration (**Franklin and Ffrench-Constant, 2017**). In response to oligodendrocyte local OPCs migrate to the site of CNS damage (such as demyelination), proliferate, and differentiate into oligodendrocytes. **Crawford *et al.*, 2016** demonstrated that dorsal OPCs respond more vigorously than ventral OPCs to focal acute demyelination in the spinal cord. If differences do lie in OPC populations of spinal cord and cerebellum, this could explain the regenerative differences between the two forms of slice culture.

Abnormal MBP immunofluorescence was observed in spinal cord slices of P1 C57BL/6 mice with circular staining, most likely a cell soma, which should not occur. MBP is a major structural protein that plays a crucial role in the formation and maintenance of myelin. The synthesis of MBP occurs within the endoplasmic reticulum of oligodendrocytes, where it undergoes post-translational modifications and is subsequently transported to the myelin membrane (**Boggs *et al.*, 2006**). Therefore, MBP is a component of the myelin sheath and is localized within the compacted regions of the myelin membrane, providing structural stability, and facilitating the compaction of myelin layers. Therefore, MBP should not be expressed and visualised on an oligodendrocyte soma. Similar staining was observed by

Redmond *et al.*, 2006 while investigating the role of a protein called JAM2 (Junctional Adhesion Molecule 2) in the process of myelination. In wildtype mice, JAM2 in the soma of a neuron inhibits an oligodendrocyte process from wrapping the somato-dendritic compartment of the neuron during myelination. However, when JAM2 is absent or blocked, the oligodendrocyte process is not inhibited, and continues to wrap myelin membranes on the neuron cell body. We could hypothesise that what is observed in our spinal cord slice cultures is the result in a gene mutation, where JAM2 is absent in the soma of neurons, and wrapping of the soma is occurring, resulting in circular staining of MBP. Without further investigation we cannot confirm this.

The toxin lysolecithin has been used to successfully demyelination slice cultures for decades (**Miron *et al.*, 2010; Miron *et al.*, 2013, Birgbauer *et al.*, 2004**) although the mechanisms to how this is achieved is not fully understood. Here we showed the successful demyelination of spinal cord slice cultures from P1 C57BL/6 mice, using lysolecithin, that were then capable of re/myelinating with MBP observations approximately 9 days post treatment. This spontaneous re/myelination time correlates with remyelination studies in literature (**Birgbauer, 2004**). Toxin induced demyelination models do not attempt to mimic demyelinating diseases such as MS but are mainly established as systems to study the process of focal demyelination and re/myelination.

In summary, here we have determined and optimised an appropriate *ex vivo* slice culture method from P1 C57 BL/6 mouse spinal cord for the study of CNS remyelination following lysolecithin demyelination. This *ex vivo* model system enables us to study the capabilities of our LS-mHep7/L to enhance repair in **Chapters 5 and 6** of this thesis.

Chapter 4

Low molecular weight mHeps modulate injury and repair in *in vitro* CNS models.

4.1 Introduction

Previously published data (McCanney *et al.*, 2019) demonstrated that LS-mHeps promotes both remyelination and neurite outgrowth in *in vitro* models of CNS injury. These heparin mimetics are a class of glycomolecules with structural similarities to resident heparan sulphates (HS) and are made up of repeating disaccharide units with variable sulphation groups (Yates *et al.*, 1996). They are thought to modulate cell signalling by both sequestering ligands (chemokine/cytokines in the ECM) (Vlodavsky *et al.*, 1991; Elkin *et al.*, 2001; Massena *et al.*, 2010) and acting as a cofactor in the formation of ligand-receptor complexes (Yayon *et al.*, 1991). For these to translate to the clinic it has been suggested that low molecular weight reagents have better bioavailability (Baharvahdat *et al.*, 2019; Veber *et al.*, 2002; Gordon *et al.*, 1990; Rhones and Bond, 2008) and have a higher chance of crossing the BBB (Carecho *et al.*, 2020). Failure of the last is a well-recognised hurdle for CNS therapeutics. Therefore, we generated a low molecular weight form of our lead compound LS-mHep7 termed 'LS-mHep7L'. This chapter aimed to validate the biological properties of LS-mHep7L in comparison to LS-mHep7. For this reason, the ability of LS-mHep7L to enhance myelination and neurite outgrowth in several *in vitro* models was assessed. This chapter compared the properties and abilities of both forms to enhance myelination and neurite outgrowth *in vitro*, and to sequester a known negative regulator of remyelination (CCL5) (Schultz *et al.*, 2021). CCL5 is known to be upregulated in MC-DeMy and MC-Inj and is likely being sequestered by LS-mHep7 *in vitro* (McCanney *et al.*, 2019).

4.2 Aims

The overall aim of this chapter was to validate the abilities of LS-mHep7L to enhance repair using several *in vitro* CNS injury models and compare its efficacy to the well-established higher molecular weight form, LS-mHep7. This was achieved by assessing the following:

- i) The ability of LS-mHep7L to enhance remyelination after complement induced demyelination in MC-DeMy
- ii) The ability of LS-mHep7L to enhance neurite outgrowth in the CNS injury model (MC-Inj)
- iii) The ability of LS-mHep7L to sequester a known negative regulator of myelination (CCL5) to restore myelin levels in MC-Dev
- iv) The effect of LS-mHep7L to modulate on astrocytic responses after injury.

4.3 LS-mHep7L enhances remyelination in MC-DeMy

LS-mHep7 enhances remyelination in MC-DeMy (McCanney *et al.*, 2019), by a mechanism that is hypothesised to involve sequestration of negative regulators of remyelination. Here we tested if LS-mHep7L retained the ability to achieve a similar outcome by comparing LS-mHep7L alongside LS-mHep7. To validate LS-mHep7L, cultures were treated with either LS-mHep7 or LS-mHep7L at 1ng/ml, 10 ng/ml, or 100 ng/ml on DIV 25, 24 hr after demyelination (DeMy) and maintained until DIV 30. At this point they were immunolabelled with anti-PLP (proteolipid protein, myelin) and antibody clone SMI-31 (neurofilament; axons). Quantification of re/myelination demonstrated that both LS-mHep7 and LS-mHep7L significantly enhanced re/myelination compared to the non-treated control (**Figure 4.1**).

Since the myelination is calculated by standardising the myelinated fibre pixel value by the pixel value for SMI density as a percentage, the impact of treatments on axon density alone was investigated. Axon density was quantified using the pixel value for SMI-31 immunoreactivity divided by the total number of pixels within each image. **Figure 4.2** shows that there were no significant differences in axon density between any of the treatments or compared to the untreated control. This suggests that LS-mHep7 and LS-mHep7L have no effect on axons and verifies that demyelination using complement and anti-MOG nor LS-mHep7/ LS-mHep7L have detrimental effects on culture viability and/or are cytotoxic at any of the concentrations tested.

A

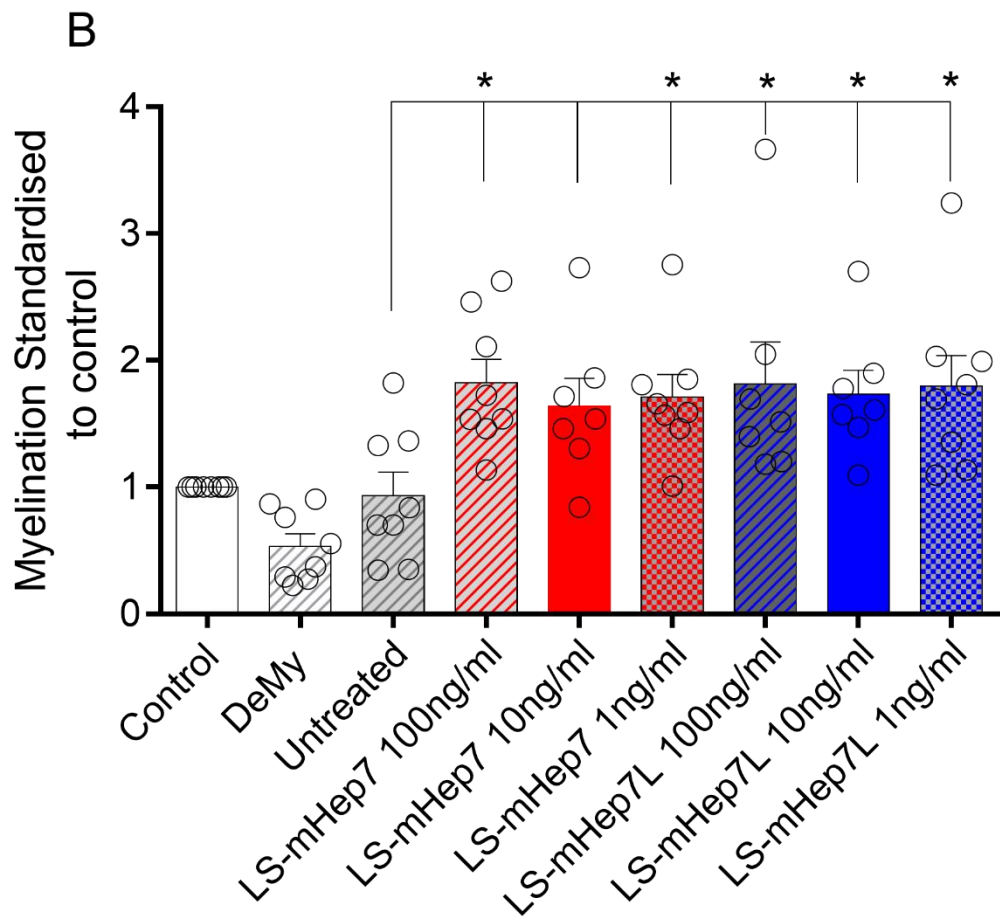
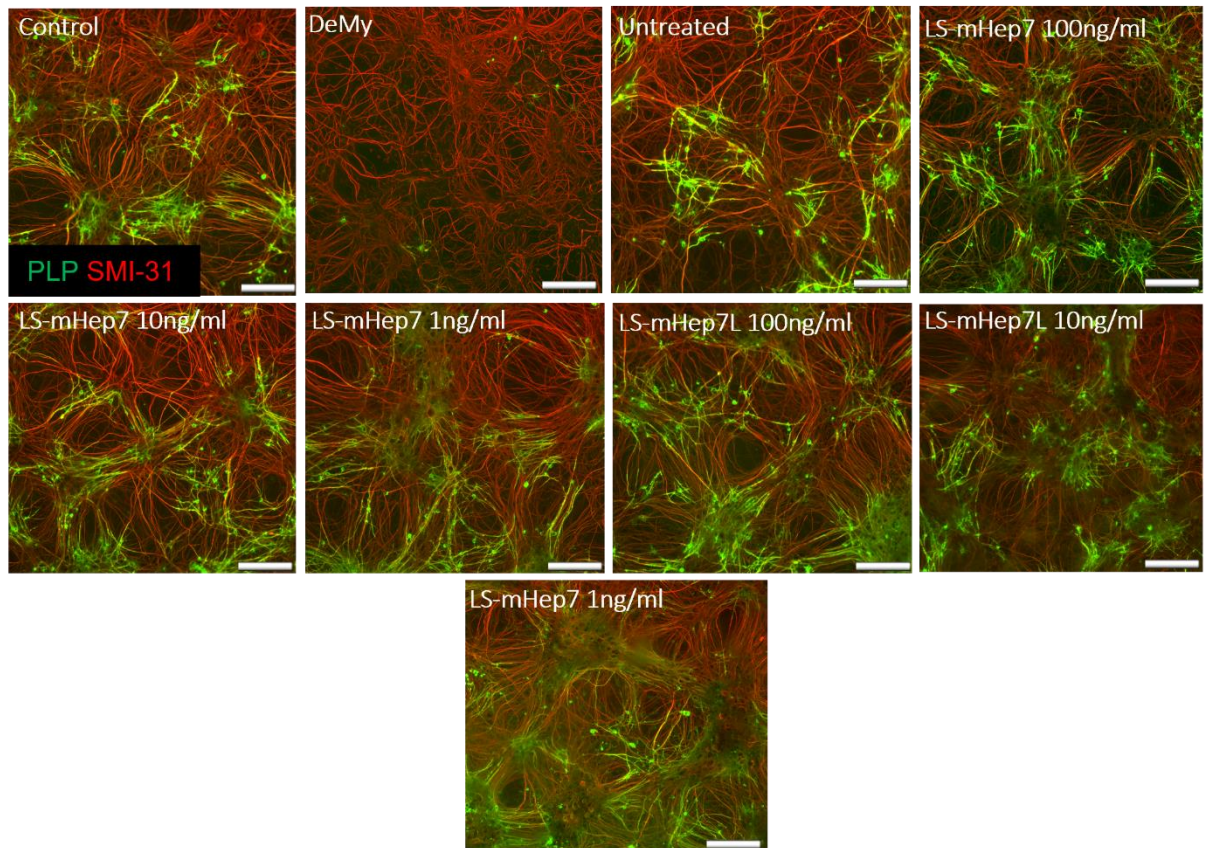


Figure 4.1 |LS-mHep7 and LS-mHep7L enhance remyelination in MC-DeMy. Myelinating cultures were allowed to mature until 24 DIV at which point, they were demyelinated with MOG specific antibody Z2 (100 ng/ml) and rabbit complement (100ng/ml). Cultures were treated with LS-mHep7 or LS-mHep7L at either 100 ng/ml, 10 ng/ml, or 1 ng/ml at DIV 25. Cultures were allowed to recover until 30 DIV, then fixed with 4%PFA, and immunolabelled with antibody clone SMI-31 (red, neurites) and anti-PLP (green, myelin). (A) Representative images of MC-DeMy treated with LS-mHep7 at 100 ng/ml, 10 ng/ml, 1 ng/ml, or LS-mHep7L at 100 ng/ml, 10 ng/ml, 1 ng/ml. (B) Quantification of remyelination shows enhanced remyelination with both LS-mHep7 and LS-mHep7L at various concentrations, when compared to untreated demyelinated control cultures at 30 DIV. (one-way ANOVA with Dunnett's multiple comparison, * = $P \leq 0.05$), Scale bars 100 μm , error bars SEM (n = 8; technical replicates = 3)

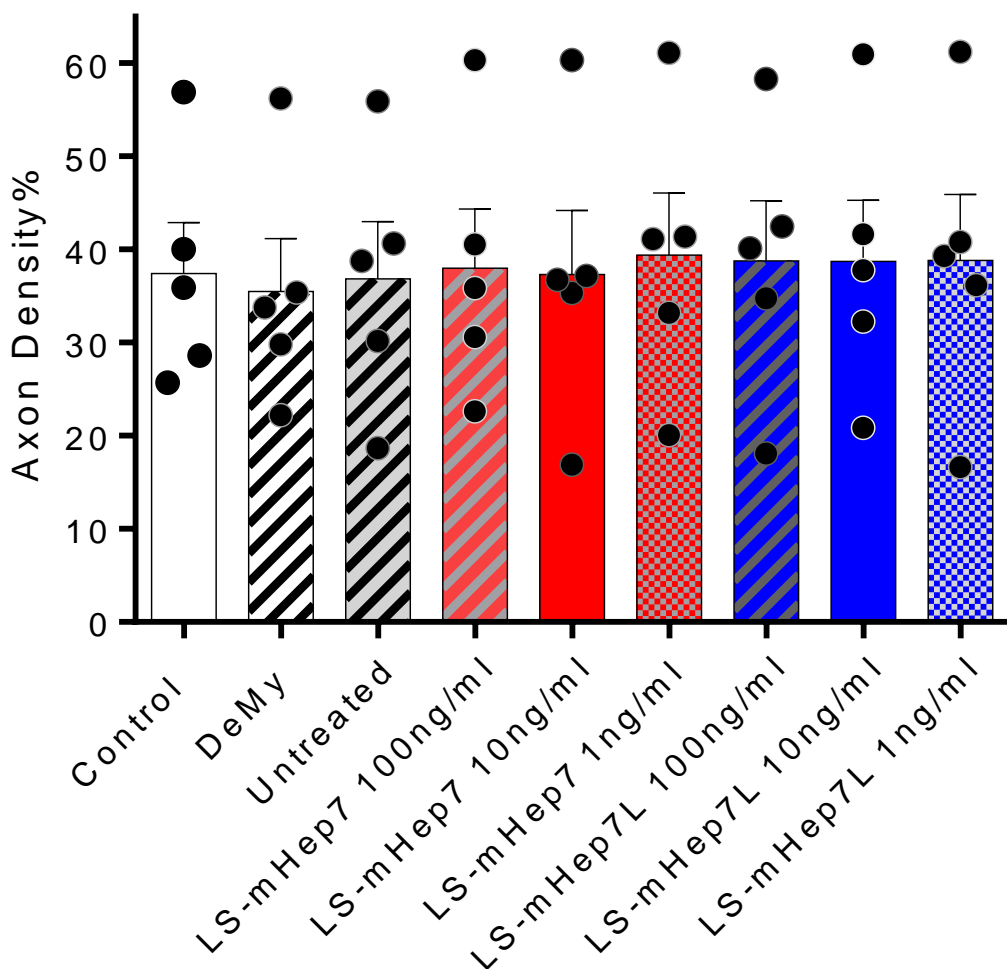


Figure 4.2 |Axon density does not change across any treatment. Myelinating cultures were allowed to mature until 24 DIV at which point, they were demyelinated with MOG specific antibody Z2 (100 ng/ml) and rabbit complement (100ng/ml). Cultures were treated with LS-mHep7 or LS-mHep7L at 1 ng/ml at DIV 25. Cultures were allowed to recover until 30 DIV, then fixed with 4%PFA, and immunolabelled with SMI-31 (red, neurites). Quantification of axon density shows no significant difference between treatments. (one-way ANOVA with Dunnett's multiple comparison), error bars SEM (n = 5; technical replicates = 3)

4.4 Effect of LS-mHep7 and LS-mHep7L on neurite diameter

Typically, the axon diameters of myelinated axons are significantly larger than those of non-myelinated axons (Basu *et al.*, 2022). To determine if LS-mHep7 and LS-mHep7L affected neurite diameter we analysed SMI-31- stained images of cultures treated at 1 ng/ml using Image J. **Figure 4.3 (D)** indicates that there were no significant differences between the axon diameter of treated and non-treated cultures. This indicates that enhanced myelination seen in **Figure 4.1 (B)** was not associated with an increase in axon diameter.

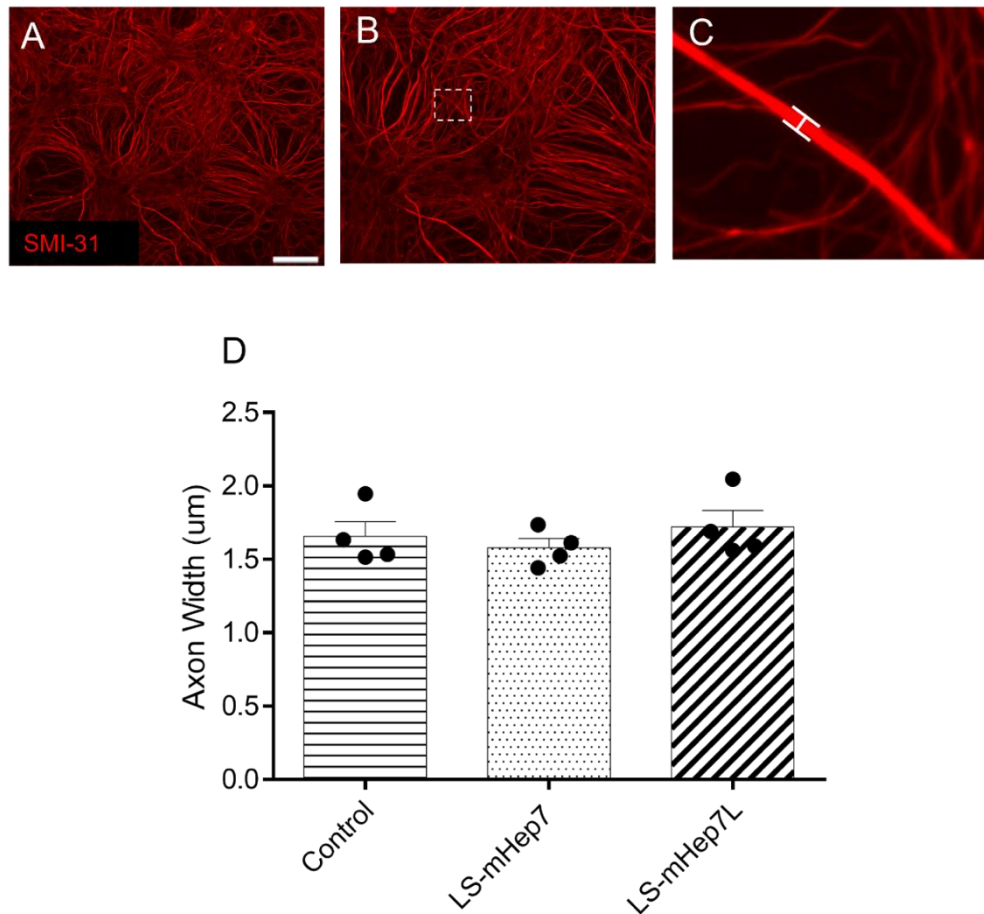


Figure 4.3 |Neither LS-mHep7 or LS-mHep7L affects axon diameter. Myelinating cultures were allowed to mature until 24 DIV at which point, they were demyelinated with MOG specific antibody Z2 (100 ng/ml) and rabbit complement (100 ng/ml). Cultures were treated with LS-mHep7 and LS-mHep7L at 1 ng/ml at DIV 25. Cultures were allowed to recover until 30 DIV, following which they were fixed with 4%PFA, and immunolabelled with SMI-31 (A) (red, neurites). Ten images were randomly selected per treatment and for each, 10 neurites were selected at random per image. Width was measured in μm using ImageJ and averaged (C). Quantification of axon width (D) shows no significant difference between treatments. (one-way ANOVA with Dunnett's multiple comparison), error bars SEM (n = 4; technical replicates = 3)

4.5 Neurite outgrowth was observed in MC-Inj following treatment with either LS-mHep7 or LS-mHep7L *in vitro*

LS-mHep7 promotes neurite outgrowth in MC-Inj compared to the untreated control (McCanney *et al.*, 2019). To assess if LS-mHep7L similarly enhances neurite outgrowth in our CNS injury model, myelinating cultures were cut using a 11mm single edge on DIV 24. LS-mHeps (1ng/ml) were added immediately after creating the injury site. The injured cultures recapitulate features of SCI observed *in vivo*, including focal demyelination, astrogliosis, neurite density depletion and the absence of spontaneous neurite outgrowth (Boomkamp *et al.*, 2012).

Ten images of each injury site per cover slip was taken down the length of the entire injury site. Neurite outgrowth was defined as a SMI 31 positive projection which enters and crosses the lesion site. The lesion site was cropped, and the percentage of SMI-31 immunofluorescence was calculated against the total injury site pixel number. This enabled the neurite outgrowth percentage per individual injury site. Any area around the lesion that appeared uninjured was excluded from analysis.

Both LS-mHep7 and LS-mHep7L significantly enhanced neurite outgrowth into the injury site compared to untreated injured control cultures (**Figure 4.4**), LS-mHep7 showed significantly higher levels of neurite outgrowth compared to LS-mHep7L, suggesting the higher molecular weight form is more efficacious at enhancing neurite outgrowth.

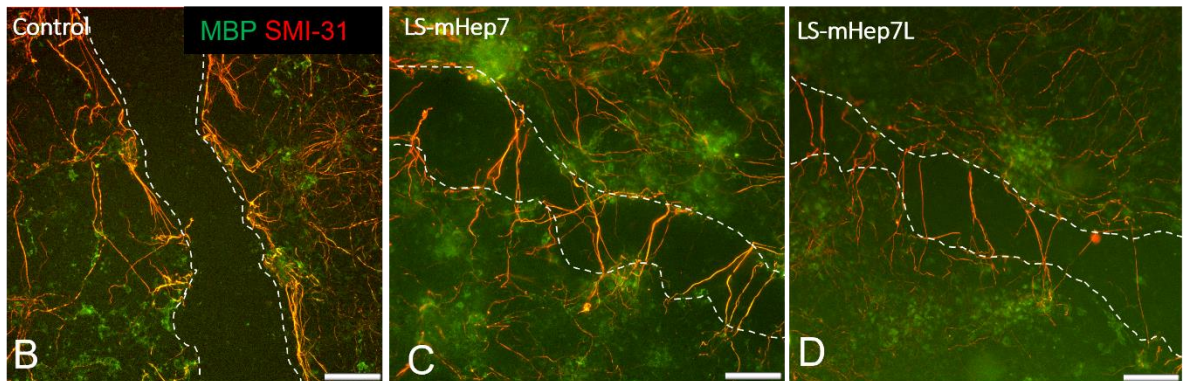
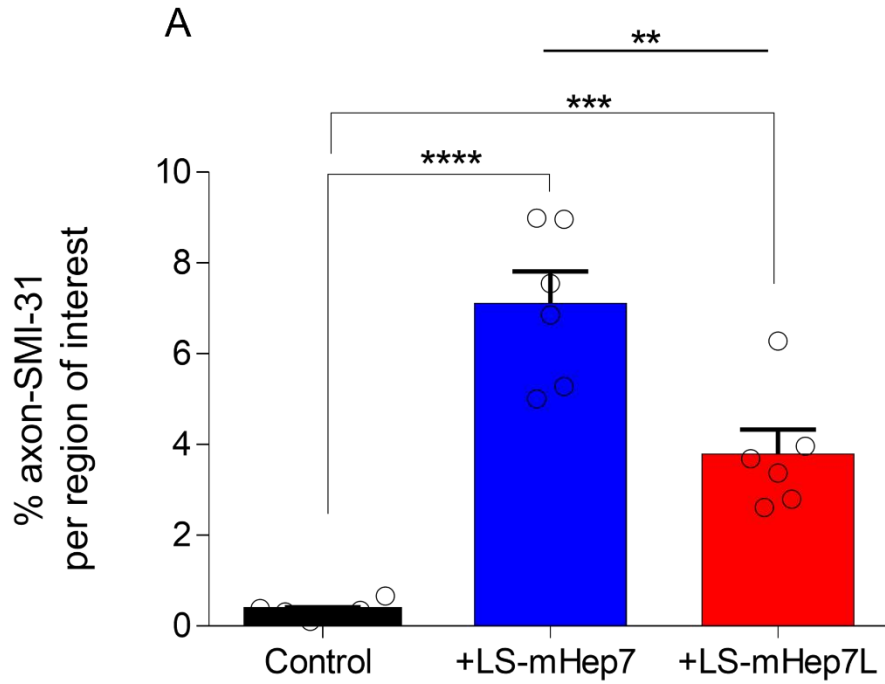


Figure 4.4 |Both LS-mHep7 and LS-mHep7L enhance neurite outgrowth in MC-Inj. Myelinating cultures were allowed to mature until 24 DIV at which point cultures were cut using an 11 mm single edge razor blade (MC-Inj). Cultures were treated with LS-mHep7 or LS-mHep7L (1 ng/ml) immediately after the cutting process. Cultures were allowed to recover until 30 DIV, following which they were fixed with 4%PFA, and immunolabelled with antibody clone SMI-31 (red, neurites) and anti-MBP (green, myelin). Quantification of neurite outgrowth is represented as % SMI-31 fluorescence per injury region of interest. (A) Control cultures showed minimal neurite outgrowth. Both LS-mHep7 and LS-mHep7L enhanced neurite outgrowth compared to untreated cut controls. LS-mHep7 was more efficacious than LS-mHep7L in promoting neurite outgrowth. Representative images of MC-Inj control cultures (B) or treated with or LS-mHep7(C) or LS-mHep7L(D) all at 1 ng/ml. (one-way ANOVA with Dunnett's multiple comparison, ** = $P \leq 0.01$, *** = $P \leq 0.001$, **** = $P \leq 0.0001$, Scale bars 100 μm , error bars SEM (n = 6, technical replicates = 3))

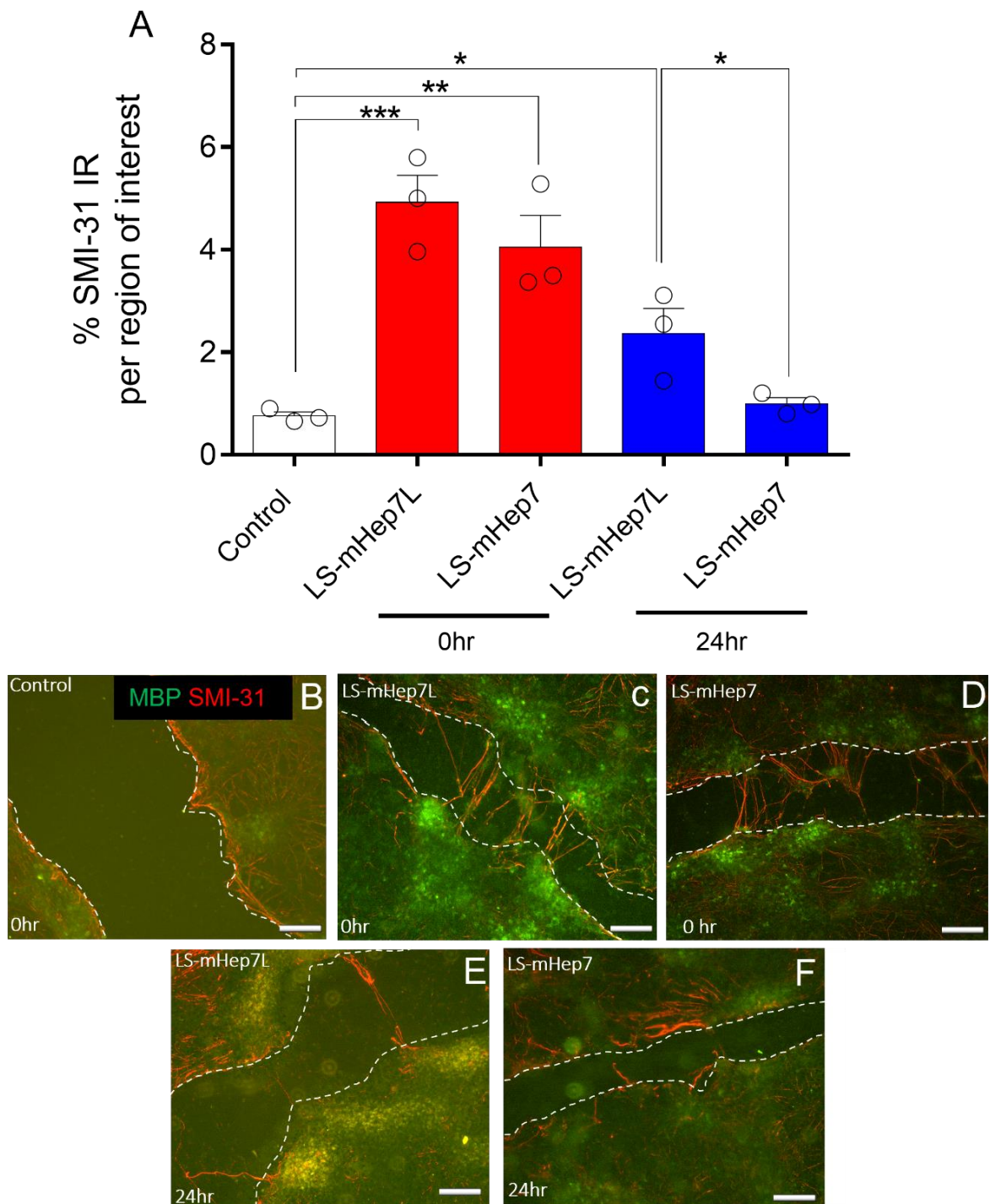


Figure 4.5 | Repair is enhanced by immediate treatment after injury with LS-mHep7 or LS-mHep7L in MC-Inj. Myelinating cultures were allowed to mature until 24 DIV at which point cultures were cut using an 11 mm single edge razor blade (MC-Inj). Cultures were treated with LS-mHep7 or LS-mHep7L (1 ng/ml) immediately after (0hrs) or on 25 DIV (24hr) after the cutting process. Cultures were allowed to recover until 30 DIV, then fixed with 4%PFA, and immunolabelled with antibody clone SMI-31 (red, neurites) and anti-MBP (green, myelin). (A) Quantification of neurite outgrowth is represented as % SMI-31 fluorescence per region of interest. Control treatments showed minimal neurite outgrowth. LS-mHep7 and LS-mHep7L treated cultures showed significant neurite outgrowth when treated at 0 hr. Treating at 24 hr post-injury reduced the amount of neurite outgrowth. (B-D) Representative images of MC-Inj control cultures (B) or treated at 0 hr with LS-mHep7L (C) or LS-mHep7L (D). Representative images of MC-Inj cultures treated at 24 hr with LS-mHep7L (E) or LS-mHep7 (F). (one-way ANOVA with Dunnett's multiple comparison, * = $P \leq 0.1$, *** = $P \leq 0.001$, **** = $P \leq 0.0001$, Scale bars 100 μm , error bars SEM (n = 3; technical replicates = 3))

4.6 LS-mHeps repair strategies are enhanced if present at earlier time points post-injury *in vitro*

Previously, LS-mHep7 was observed to enhance neurite outgrowth in MC-Inj (McCanney *et al.*, 2019) when added at DIV 25, 24 hr after the initial injury. Here, we tested the hypothesis that LS-mHeps sequester negative regulators that are present or upregulated immediately after injury. Therefore, MC-Inj cultures were treated either immediately (0 hr) or 24 hr after injury to determine the effect of treatment timing on the ability to enhance neurite outgrowth. MC-Inj cultures were treated with LS-mHep7 or LS-mHep7L at 1 ng/ml, either 0 hr (DIV 24), or 24 hr (DIV 25) after injury.

When treatment commenced immediately after injury, both LS-mHep7 and LS-mHep7L had a more beneficial effect compared to those cultures treated 24 hr after the initial insult (**Figure 4.5 A**). Further, cultures that were exposed to an earlier treatment appeared to have ‘bridging’ of the injury gap (**Figure 4.5 C, D**), unlike those treated 24 hr after injury (**Figure 4.5 E,F**), where individual neurites could be counted.

To establish if this bridging was influenced by an increase in the rate of gap closure, we imaged injury gaps at 0, 1, 2, 3 and 24 hr, following treatment with either LS-mHep7 or LS-mHep7L (1 ng/ml). The percentage gap closure was calculated as a % of the initial injury site measured at the 0-hr time point. After injury in control cultures, there was an increase in gap width over the first 2 hr. This was not observed in LS-mHep7L treatment which had a significant reduction in gap size compared to control. We observed a significant reduction in gap size after injury in both LS-mHep7 and LS-mHep7L treated cultures after 24 hr, compared to control (**Figure 4.6, A**). Further, an influx of cells into the cell free area was observed after 24hr treatment with either LS-mHep7 and LS-mHep7L (**Figure 4.6, B**).

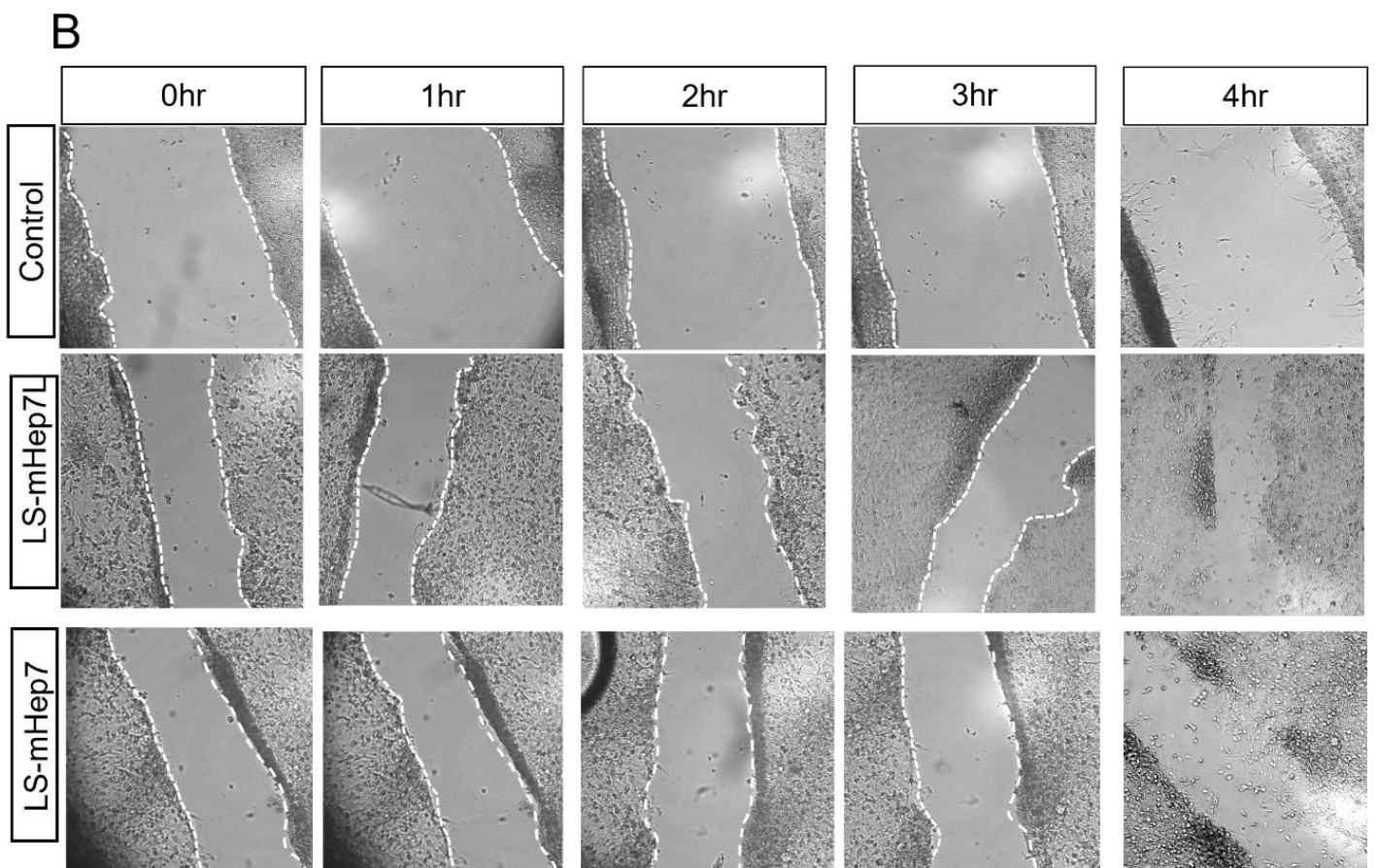
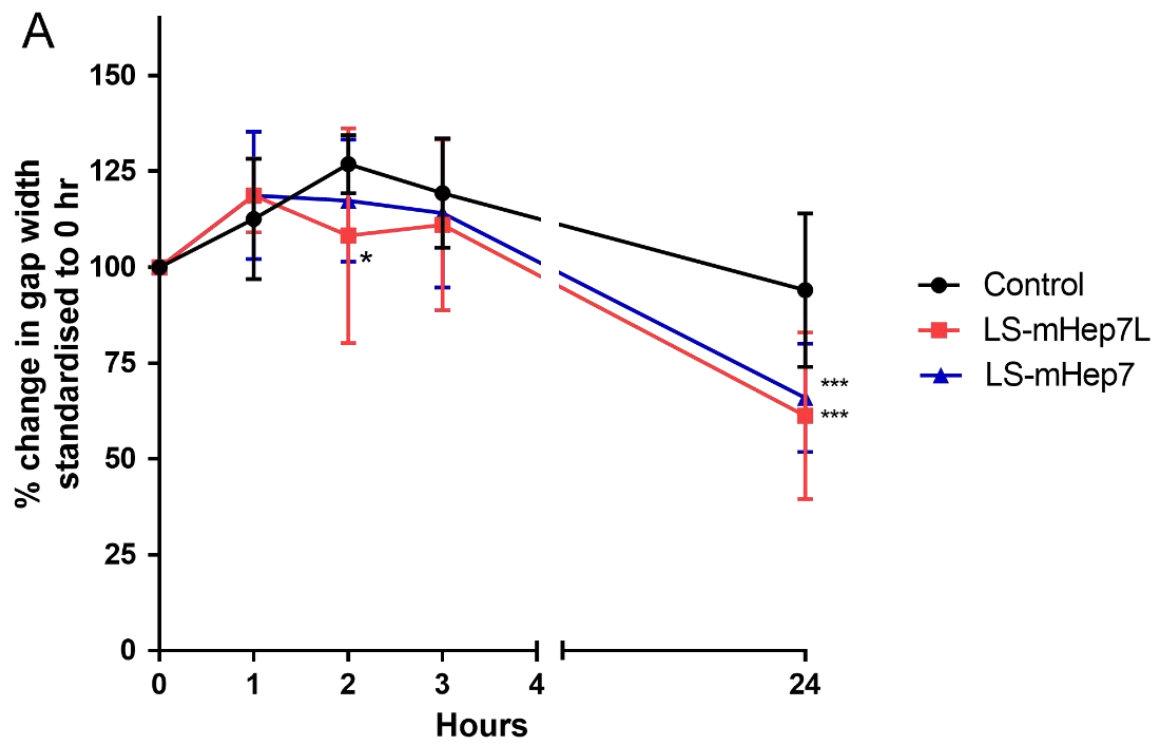


Figure 4.6 |Effect of LS-mHep7 and LS-mHep7L treatment on gap injury in MC-Inj. Myelinating cultures were allowed to mature until 24 DIV at which point cultures were cut using an 11 mm single edge razor blade (MC-Inj) to create a cell free area within each coverslip. Cultures were treated with LS-mHep7 or LS-mHep7L (1 ng/ml). Cultures were imaged at 0, 1, 2, 3 and 24hrs. Percentage change of gap width was measured using ImageJ. Gap width of each coverslip was standardised to its own 0 hr injury width (A) Quantification of % gap width revealed that both LS-mHep7 and LS-mHep7L increased gap closure significantly compared to control untreated cultures at 24 hr. LS-mHep7L also significantly promoted gap closure at 2 hr compared to control. (B) Representative images of treatments at each time point (two-way ANOVA with Dunnett's multiple comparison, * = $P \leq 0.1$, *** = $P \leq 0.001$, (n = 5; technical replicates = 3)

4.7 LS-mHeps appear to reduce signs of astrocytosis *in vitro*

It is not known if the LS-mHeps are exerting multiple benefits to multiple cellular targets which in turn can mediate several different cellular processes. One of the cell types of interest within our cultures are astrocytes. Reactive astrocytes lose their supportive role and gain toxic function in the progression of neurodegenerative diseases (**Liddelow *et al.*, 2017**).

The poor regenerative capability of CNS axons is thought to be related to the limited ability of astrocytes to migrate and repopulate the injury site. Indeed, the slow repopulation of the injury site by astrocytes correlates with the failure of injured axons to cross the injury site (**Rhodes *et al.*, 2003; Silver and Miller 2004**). Therefore, determining the effect of potential therapeutics on the ability of astrocyte migration and reactivity may help overcome this failure and contribute to CNS regeneration.

To investigate if LS-mHeps have any effect on astrocytes migrating to injury sites and extending their processes, we investigated gap closure in an astrocyte injury model. Neurosphere-derived astrocytes were treated with LS-mHep7 or LS-mHep7L (10 ng/ml), and a cell free area was created by scratching the centre of each cover slip with a pipette tip. Cultures were imaged at 0, 1, 2, 3 and 24 hr post-injury. Both LS-mHep7 and LS-mHep7L demonstrated a significant increase in gap closure over the 24hr compared to control untreated cultures, with significant gap closure already occurring at the 2hr time point, where instead the control cultures reached their peak gap size (**Figure 4.7 A**). 24 hr after the initial injury there was a significant difference between the size of the gap in LS-mHep7 and LS-mHep7L treated cultures compared to the control, with LS-mHep7L showing the most

significant differences, LS-mHep7. This data suggests that both LS-mHep7 and LS-mHep7L are modulating astrocyte migration and facilitating gap closure.

Additionally, we examined nestin expression, a useful marker of astrocytosis, within these cultures using western blotting. We observed a significant reduction in nestin levels at 2 hr, in cultures treated with LS-mHep7, and after 24 hr, compared to control cultures (**Figure 4.8**). What is interesting is that we seem to see our most significant differences at the 2 hr time point, both in gap change and nestin levels (**Figure 4.7** and **Figure 4.8**).

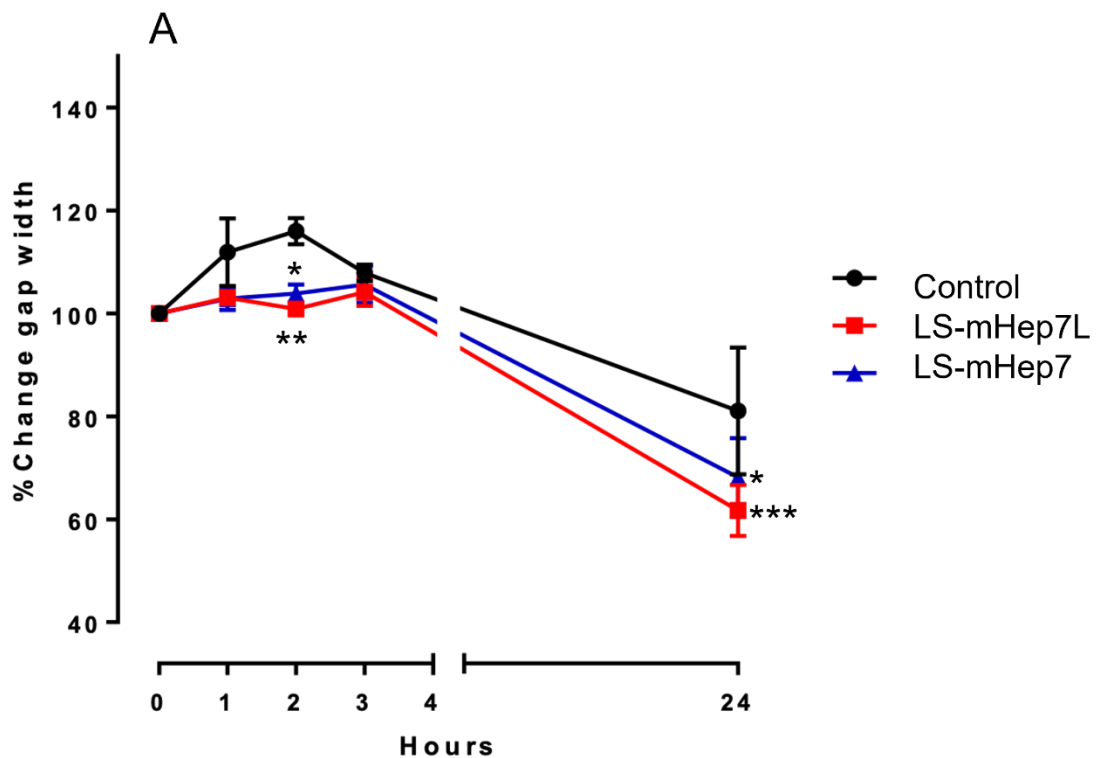


Figure 4.7 |LS-mHep7L and LS-mHep7 treatment reduced gap width in astrocytic injury model (scratch assay). Neurosphere derived astrocytes were allowed to mature until a confluent monolayer was achieved. Astrocytes were either treated with LS-mHep7 or LS-mHep7L (10ng/ml), and a cell free area was created by scratching the centre of each cover slip. Cultures were imaged at 0, 1, 2, 3 and 24hrs. Percentage gap width change was analysed using ImageJ by taking an average width at each time point, and expressing it as a percentage change from 0 hr. Both LS-mHep7 and LS-mHep7L treatment show an increase in gap closure at 2 hr and 24 hr post injury compared to control. (two-way ANOVA with Dunnett's multiple comparison, * = $P \leq 0.1$, ** = $P \leq 0.01$ *** = $P \leq 0.001$ (n = 4; technical replicates = 3)

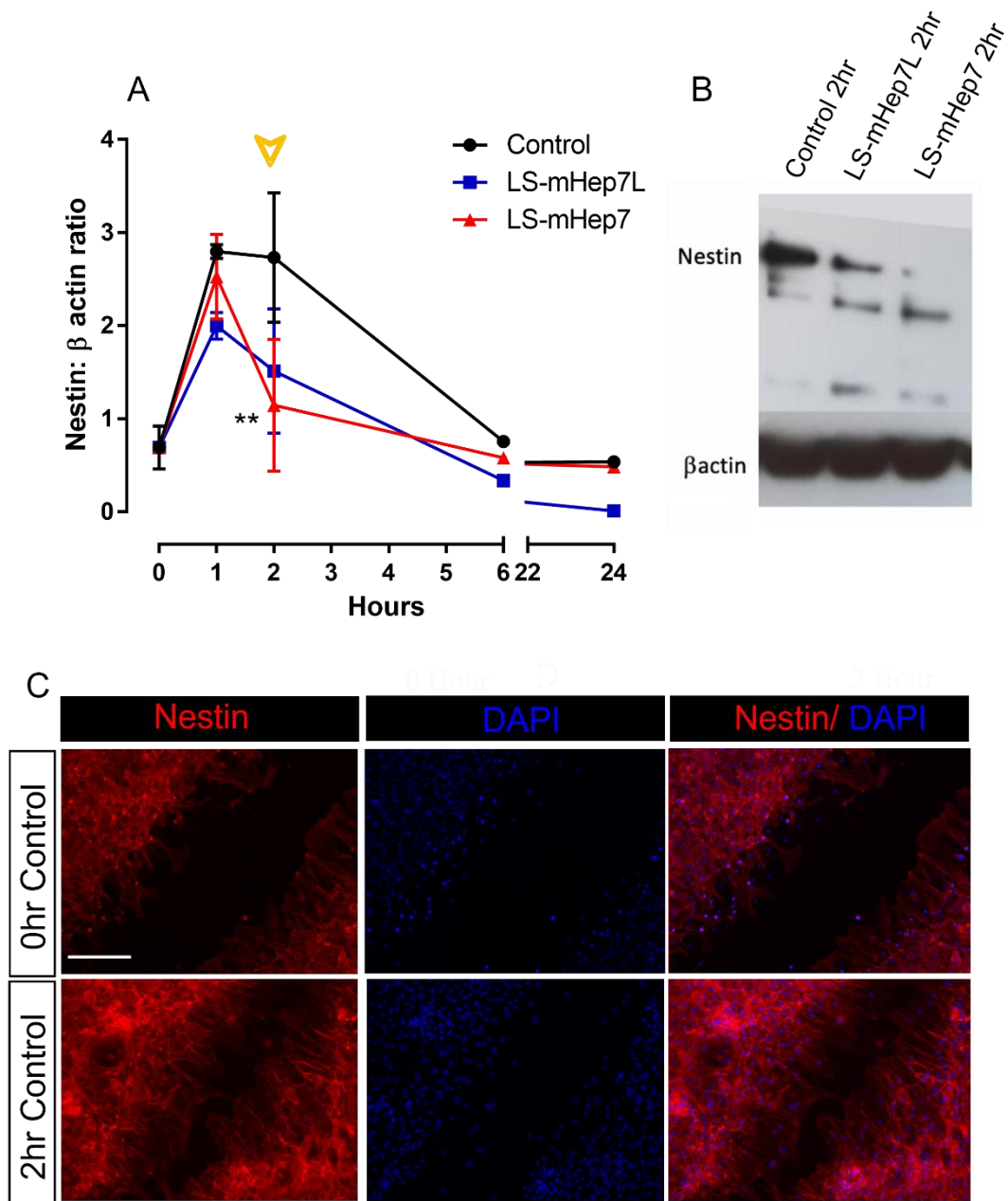


Figure 4.8 |LS-mHep7L and LS-mHep7 reduced gap width in astrocytic injury model (scratch assay). Neurosphere-derived astrocytes were allowed to mature over 7 DIV until a confluent monolayer was achieved. Astrocytes were treated with LS-mHep7 or LS-mHep7L (10 ng/ml), and then a cell free injury area was created by scratching each cover slip 3 times. Lysates were collected at 0, 1, 2, 3 and 24 hr and were analysed for levels of nestin via western blot analysis. (A) Quantification of western blot analysis showed that LS-mHep7 and LS-mHep7L significantly reduced nestin expression 2 hr post-injury (yellow arrow). (B) Representative western blot image of nestin expression at 2 hr post-injury. Nestin levels were standardised to β -actin which was used as loading control. (C) Representative images of control (untreated) cut astrocyte monolayers immunolabelled with DAPI (blue) and nestin (red) at 0 and 2 hr post injury (two-way ANOVA with Dunnett's multiple comparison, $** = P \leq 0.01$ ($n = 4$; technical replicates = 3) scale bar represents 50 μ m

4.8 Both LS-mHep7 and LS-mHep7L appears to sequester CCL5 – a negative regulator of remyelination

Chemokine (C-C motif) ligand 5 (CCL5), is a negative regulator of myelination *in vitro* (Schultz *et al.*, 2021). Furthermore, CCL5 has been shown to play a role in neurodegenerative diseases including multiple sclerosis and Parkinson's Disease (Reale *et al.*, 2008; Szczucinski *et al.*, 2006). Unpublished data from the lab has demonstrated that LS-mHep7 treated MC-Dev cultures rescued CCL5 induced hypomyelination. Here we investigated the effects of CCL5 in MC-Dev cultures, and the effect of co-treatment with either LS-mHep7 or LS-mHep7L, to investigate whether LS-mHep7L had the ability to do the same. MC-Dev cultures were allowed to mature until 16 DIV, the point at which myelin just begins to form along the axons. Cultures were treated with CCL5 alone (100 ng/ml) or with LS-mHep7L or LS-mHep7 (10 ng/ml) at 16, 19 and 21 DIV. Quantification of myelination at 24 DIV demonstrated a significant reduction in myelination after CCL5 treatment compared to the non-treated control. This affect is rescued with the additional co-treatment of CCL5 with LS-mHep7 or LS-mHep7L. This raises the hypothesis that both LS-mHep7 and LS-mHep7L can sequester negative regulators of repair, including chemokines such as CCL5 (Figure 4.9).

Together this data validates LS-mHep7L to have similar bioactivity in sequestering negative regulators of repair as that observed by LS-mHep7.

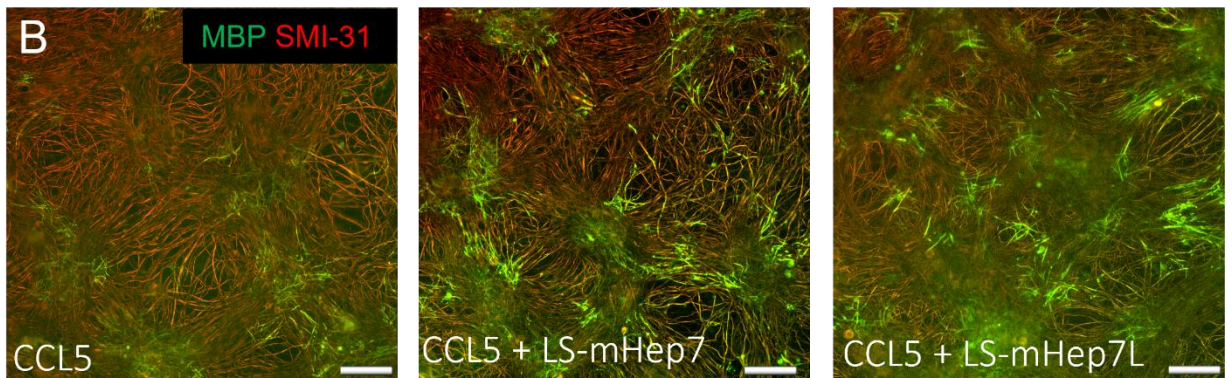
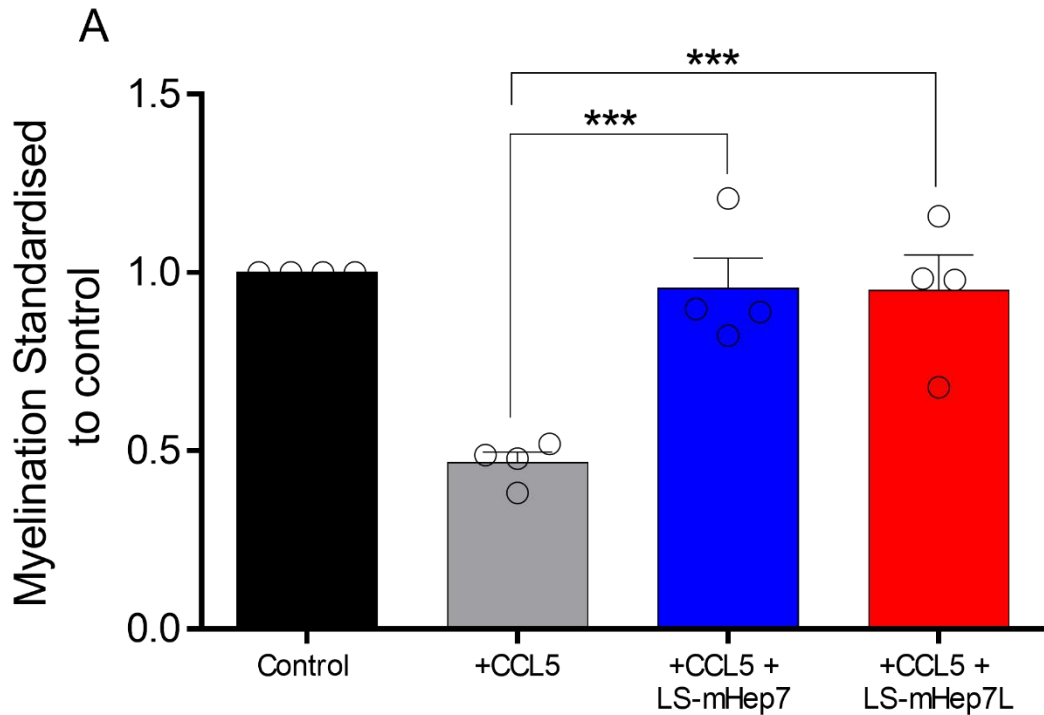


Figure 4.9 |LS-mHep7 and LS-mHep7L treatment overcomes CCL5 induced hypomyelination in MC-Dev. Myelinating cultures were allowed to mature until 16 DIV. Cultures were treated with CCL5 (100 ng/ml) at 16, 19, 21 DIV. In addition, cultures were either co-treated with CCL5+ LS-mHep7 or CCL5+LS-mHep7L (LS-mHep7 & LS-mHep7L, 10 ng/ml). At 24 DIV cultures were fixed with 4%PFA, and immunolabelled with antibody clone SMI-31 (red, neurites) and anti-MBP (green, myelin) (A) Quantification of myelination at 24 DIV shows a significant decrease in developmental myelination after CCL5 treatment. However, co-treatment with either LS-mHep7 or LS-mHep7L significantly overcomes CCL5 induced hypomyelination. (B) Representative images of cultures treated with CCL5, CCL5 + LS-mHep7 or CCL5 + LS-mHep7L. *** = $P \leq 0.001$ (values are the mean \pm SEM, One-way ANOVA with Dunnett multiple comparison). Scale bars 100 μ m

4.9 Discussion

The aim of this chapter was to validate the ability of a low molecular weight version of our low sulphated heparin mimetic – LS-mHep7. Previously our lab showed that low sulphated heparin mimetics have the ability to enhance repair in our *in vitro* CNS injury models. However, a hurdle of CNS therapeutics, is the ability for molecules to cross the BBB. The BBB prevents most pharmaceutical drugs from entering the brain via the blood and generally only lipid soluble (lipophilic) molecules with a low molecular weight (under 400–600 Da) and of positive charge can cross the BBB. However, studies have shown that ultralow molecular weight (ULMW) heparin fragment C3 has the ability to cross the BBB (**Ma et al., 2002**). Therefore, to increase the bioavailability of our heparin mimetics, the use of a low molecular weight LS-mHep7 (LS-mHep7L) is essential.

Our first validation of LS-mHep7L was in our *in vitro* demyelination cultures (MC-DeMy). Cultures were set up and maintained until DIV 25 and then demyelinated using anti-MOG with compliment. Cultures were then left to recover until DIV 30 and fixed before being immunolabelled. Both LS-mHep7 and LS-mHep7L treatment enhanced remyelination compared to our untreated control. Currently, we can only hypothesise how the LS-mHeps are able to enhance re/myelination in these cultures, as HSPGs regulate cellular communication in a variety of manners. Oligodendrocytes are known to secrete CSPGs and keratan sulphate proteoglycans but have only HSPGs associated with their surface. Secreted proteoglycans are temporally modulated but adhesion-independent, whereas surface-associated proteoglycans are adhesion-induced. **Szuchet et al., 2000** reported a significant fraction of the surface-associated HSPGs are assembled into a cell-associated matrix, which implicates HSPGs in the establishment of oligodendrocyte differentiated phenotypes. This could suggest that LS-mHep7 or LS-mHep7L are directly interacting with oligodendrocytes to initiate their myelinogenic phenotype, and therefore enhancing myelination. Additionally, other members of the HSPGs family - syndecan, perlecan, and glypican, have been suggested to regulate oligodendrocyte progenitor proliferation, migration, and adhesion phenomena. The appearance of these HSPGs occur to be upregulated during difference stages of oligodendrocyte development. Syndecan-3 is synthesized by oligodendrocyte progenitors, perlecan synthesis increases as oligodendrocytes undergo terminal differentiation and glypican-1 is expressed by both progenitors and differentiated oligodendrocyte (**Winkler et al., 2002**). All three of these HSPGs are shed from the oligodendrocyte cell surface and bind to specific substrates – suggesting they maintain and regulate a developmentally specific

environment around these oligodendrocyte cells – potentially involving growth factor receptors in the ECM.

Although it is unknown how LS-mHep7 and LS-mHep7L are enhancing remyelination, it is clear that HSPGs interact with oligodendrocyte cells throughout their differentiation and could suggest our mHeps are able to enhance OPC proliferation, or the differentiation of OPCs into mature myelin producing cells.

We next validated the LS-mHep7L in our MC-Inj cultures, which are designed to model aspects of CNS injury by cutting mature cultures with a scalpel blade, generating a cell-free area characterized by a persistent lack of neurite outgrowth (**Boomkamp *et al.*, 2012**). Unpublished data from the lab observed that the cell-free area becomes infiltrated with reactive astrocytes, and microglia, as seen in animal models of CNS injury. Here we demonstrated that both LS-mHep7 and our LS-mHep7L enhanced neurite outgrowth across the cell free area. Heparan sulphates have previously been reported in modulating the proteins that drive CNS regenerative axonal growth and sprouting through binding to co-receptors. One example of this is the role heparan sulphate has with Neuropilin-1 and Semaphorin 3A. Semaphorin 3A (Sema3A) is a protein secreted by neurons and surrounding tissue to guide migrating cells and axons in the developing nervous system. Sema3A acts as a repulsive axon guidance molecule, inhibiting CNS regenerative axonal growth and sprouting, therefore, interfering with Sema3A increases neuron regeneration. Heparin has been shown to interfere with the co-localisation of secreted Sema3A with its receptor proteins, Neuropilin-1 and Plexin. Studies have shown that heparin binds to Sema3A's co-receptor neuropilin-1 – negatively regulating its activity (**Perez *et al.*, 2021**). Also of note, the overexpression of Plexin-A1, is found to be upregulated in MS patients (**Williams *et al.*, 2007**). This is just one example of how HSPGs can modulate repair through binding to, and regulating factors important in neurite regeneration, but could be how the LS-mHeps are working.

What is interesting however, is that whatever interactions are at play between our LS-mHeps and neurite outgrowth, it seems to occur immediately after injury. Previously the lab published data showing that LS-mHep7 enhanced neurite outgrowth in MC-Inj (**McCanney *et al.*, 2019**), however, the treatment with LS-mHep7 occurred 24 hours after the initial cut. We have since validated both LS-mHep7 and LS-mHep7L in the same injury model, however, we treated the cultures immediately after the injury. This was based on the hypothesis that our LS-mHeps are sequestering injury secreted molecules that negatively regulate repair. Therefore, if these injury factors are being released, then the faster our LS-

mHeps can interact and sequester these molecules, the better it will be for repair. The results from this showed that the earlier treated cultured had a significantly higher neurite outgrowth across the cell free area compared to cultures that were treated 24 hours later. These results from this experiment contributed to our hypothesis that our heparan sulphate mimetics are interacting with these molecules, binding to them, and sequestering them away. Additionally, HSPGs are well known to have many effects on axon growth and guidance, especially in the involvement of the Wnt pathway. Wnt signalling regulates different aspects of neuronal behaviour, from neural patterning to synapse formation and function. For instance, activation of Wnt signalling induces neurite outgrowth in dorsal root ganglia neuron cultures (**Lu *et al.*, 2004**) and dendritogenesis in hippocampal neuron cultures (**Rosso *et al.*, 2005**). Research has also identified that Wnt signalling is regulated by HSPGs, with heparin activating Wnt-mediated neuronal morphogenesis in rodent primary cultures (**Colombres *et al.*, 2008**). Therefore, one hypothesis of how the heparin mimetics are enhancing neurite outgrowth is through this signalling pathway. However, it is not known if our mHeps are exerting multiple benefits to multiple cellular targets which in turn can mediate several different cellular processes. One of these cell types of interest within our cultures are astrocytes. After CNS injury, astrocytes become reactive and secrete inflammatory molecules that modify the environment around the injury or disease (**Barnett & Linington, 2003**).

An important factor to consider is the functionality of these neurite outgrowth. We are unable to say at this point whether these neurites are functional across the cell free area. Electrophysiological techniques such as patch clamp recording could be used to measure the electrical properties of these neurite outgrowths, such as membrane potential, action potential firing, and synaptic activity (**Kornreich, 2007**). This information can provide insights into the functional connectivity and excitability of the developing neurites. Concurrently, live imaging techniques like time-lapse microscopy can be utilized to visualize the dynamic changes in neurite morphology and growth patterns over time, as well as organelle transport (**Li *et al.*, 2010**). Fluorescent markers can be employed to label specific neuronal structures, allowing for the tracking of neurite extension and branching (**Manzella-Lapeira *et al.*, 2021**). By combining electrophysiological measurements with live imaging in future experiments, we could determine the functionality of these neurite outgrowths.

Reactive astrocytes are well known to have a negative impact in remyelination studies, and the glial scar is a major feature of both MS and SCI pathology. Astrocytosis occurs following injury which is characterised by an alteration in astrocyte phenotype to a more reactive state – notably with an increased production of the intermediate filaments nestin.

Nestin is a type VI intermediate filament protein that is typically expressed in neural stem cells during development (**Lendahl *et al.*, 1990**). It is also present in reactive astrocytes, in response to injury, inflammation, or other pathological conditions in the CNS (**Clarke *et al.*, 1994**). During astrogliosis, astrocytes become hypertrophic, proliferate, and migrate to the site of injury. This response is characterized by an upregulation of various proteins, including nestin (**Lin *et al.*, 1995; Brook *et al.*, 1990**). Nestin expression in astrocytes is considered a marker of astrogliosis because its upregulation is associated with the activation and remodelling of astrocytes.

The poor regenerative capability of CNS axons is thought to be related to the limited ability of astrocytes to migrate and repopulate the injury site. Indeed, the slow repopulation of the injury site by astrocytes correlates with the failure of injured axons to cross the injury site (**Rhodes *et al.*, 2003; Silver and Miller, 2004**). Therefore, we investigated the effects of both LS-mHep7 and LS-mHep7L in an astrocytic injury model where monocultures of astrocytes were ‘scratched’ down the centre of the cover slip and nestin production was investigated over time. Additionally, the gap width of these scratches was also investigated. Here we observed an increase in nestin expression in our control cultures- an expected result in an astrocyte injury model. However, compared to control cultures, nestin expression was decreased with the treatment of LS-mHep. This suggests that LS-mHep7 can potentially influence the phenotypic change of an inactive astrocyte into a reactive state. Interestingly, gap closure was also reduced in the astrocyte scratch assays treated with LS-mHep7/LS-mHep7 compared to control cultures. This could be a contributing factor to the increased neurite outgrowth seen in MC-Inj treated with LS-mHep7 or LS-mHep7L, where the astrocyte monolayer underneath the myelinating cultures are keeping the cut closed enough for more successful neurite outgrowth to occur. We could hypothesise that there is a maximum injury distance that can occur that prevents or allows neurite outgrowth and if the injury site is too wide, then successful outgrowth does not occur. Overall, this contributes to our assumption that our heparan sulphates are exerting multiple benefits to multiple cellular targets.

Finally, we aimed to validate LS-mHep7L’s ability to sequester CCL5. Newly published data from our lab (**Lindsay *et al.*, 2023**) demonstrated that CCL5 was found to significantly reduce developmental myelination in MC-Dev, and the co-treatment of LS-mHep7 was able to overcome this CCL5-induced hypomyelination. To validate the ability of LS—mHep7L to also rescue this induced hypomyelination, myelinating cultures were set up and maintained until DIV 16, the point at which myelination begins in our model. Cultures were

then treated with CCL5 alone or co-treated with the addition of LS-mHep7 or LS-mHep7L. Here we saw that both LS-mHep7 and LS-mHep7L were able to overcome CCL5's hypomyelination. The hypothesis is that our mHeps can bind to – and sequester the CCL5 molecules, preventing them from downstream communications that are involved in the negative regulation of myelination. Heparan sulphates can sequester cytokines and chemokines such as CCL5 by interacting with basic amino acid residues in the binding grooves of these proteins (**Turnbull *et al.*, 2001**). The HS chains contain specific binding sites that can interact with complementary regions on the chemokine or cytokine molecules, allowing for strong binding. Additionally binding can occur through electrostatic interactions as HS chains carry negative charges due to the presence of sulphate groups (**Crikns *et al.*, 2020**). Chemokines and cytokines, on the other hand, often contain positively charged regions. This electrostatic interaction facilitates the binding of chemokines and cytokines to HSPGs and could contribute to the interactions between LS-mHep7 and CCL5. The implications of CCL5 have been well documented in cases of neurodegenerative diseases. While investigating brain tissue of people who had MS, CCL5 was amongst one of the CC chemokines that was significantly elevated – mainly localized in reactive astrocytes (**Boven *et al.*, 2000**). Additionally, cerebrospinal fluid of patients with relapse remitting MS had significantly higher levels of CCL5 compared to control patients (**Szczuciński, 2011**). **Van Veen *et al.*, 2007** has hypothesised that a functional polymorphism in CCL5 influences perivascular leukocyte infiltration, inflammation, axonal loss, remyelination, and disease course, in patients with MS. CCL5 appears to have implications in other neurodegenerative disease other than MS. Parkinson disease (PD) is second only to Alzheimer disease as the most common human neurodegenerative disorder. Neutralization of CCL5 in a mouse model of PD, prevented the loss of dopaminergic neurons. It was observed by this attenuation of CCL5 reduced the infiltration of CD4+ and CD8+ T cells into the nigra pars compacta, attenuated nigral expression of proinflammatory molecules, and suppressed nigral activation of glial cells (**Chandra *et al.*, 2016**). However, it is still unclear if T cell infiltration is primary or secondary to nigrostriatal degeneration, but CCL5 is well known to induce the migration and homing of classical lymphoid cells. Although T-cells are not necessarily relevant in our MC-DEV cultures – being that they are made of glial cells alone – this suggests that the attenuation of CCL5 via LS-mHep7/ LS-mHep7L could be a potential therapeutic for a variety of degenerative disease including PD. CCR5 is a seven-transmembrane G protein-coupled receptor that binds to CCL5 and mediates a signal transduction cascades in response to CCL5-ligand binding. The CCR5 receptor is primarily found on the surface of certain immune cells, such as T cells and

macrophages. It plays a crucial role in the immune response by enabling these cells to migrate to sites of inflammation and infection (**Zeng *et al.*, 2022**). The $\Delta 32$ mutation refers to a specific mutation in the CCR5 gene. This mutation is characterized by the deletion of 32 base pairs in the CCR5 gene, resulting in a non-functional or defective CCR5 receptor (**Hütter *et al.*, 2011**). It has been suggested that the $\Delta 32$ polymorphism is associated with a slower rate of disease progression in RR-MS (**D'Angelo *et al.*, 2011**). However, this has also been contradicted with other population studies where no link to disease progression was found (**Arababadi *et al.*, 2010**).

In summary, this chapter was able to validate the ability of LS-mHep7L to enhance repair in our *in vitro* CNS models. Although it is difficult to establish how LS-mHep7L can achieve this, it is clear that it is most likely by regulating many different factors that can have a plethora of effects on cellular targets which in turn can mediate several different cellular processes.

Chapter 5

Low molecular weight LS-mHeps enhance repair in an *ex vivo* spinal cord injury model.

5.1 Introduction

To continue validating the effects of LS-mHep7 and LS-mHep7L as a potential therapeutic for CNS repair, we needed to introduce them to a more complex cellular environment more typical of the *in vivo* environment of the CNS. Our co-cultures used in **Chapter 4** have limitations as they do not represent the three-dimensional multicellular structures and cellular environment found *in vivo*. *Ex vivo* slice cultures provide a partly maintained original tissue architecture with some intact functional neural networks and allow us to validate the LS-mHeps in a more complex cellular model (**Croft *et al.*, 2019**). After optimising the slice culture method in **Chapter 3**, we used this *ex vivo* culture system to investigate LS-mHeps ability to enhance repair. Like we have done in previous chapters, we used both LS-mHep7 and LS-mHep7L to compare their ability to enhance repair after injury in CNS cultures. This was achieved through the chemical demyelination of the spinal cord slices with lysolecithin, and re/myelination levels were calculated across the treatments. Additionally, we determined the ability of LS-mHep7L to sequester CCL5 and negate the hypomyelination as seen *in vitro*.

5.2 Aims

The overall aim of this chapter was to validate the abilities of LS-mHep7 and LS-mHep7L to enhance repair in an *ex vivo* spinal cord slice culture model. This was carried out as follows:

- i) Assessing the ability of LS-mHep7/ LS-mHep7L to enhance re/myelination after chemically induced demyelination using lysolecithin (SC-DeMy)
- ii) Assessing the ability of LS-mHep7/ LS-mHep7L to sequester CCL5 and negate CCL5 induced hypomyelination (SC-DEV)
- iii) Identify key chemokine/ cytokine candidates that are released after injury that could interact with LS-mHep7/ LS-mHep7L.

5.3 LS-mHep7L enhances re/myelination in demyelinated spinal cord slice cultures

In *Chapter 4* we demonstrated that both LS-mHep7 and LS-mHep7L enhance re/myelination in our *in vitro* MC-DeMy. However, demyelination in the spinal cord slice cultures was chemically induced, via lysolecithin exposure, unlike in MC-DeMy where demyelination was antibody and complement mediated. Cellular interactions and signalling events may therefore differ between these two demyelination models. Additionally, these slice cultures are cellularly more complex than the *in vitro* cultures, and LS-mHeps may no longer be effective in sequestering chemokines/cytokines due to rapid and more dramatic changes in the secretome. To investigate these differences, slice cultures were set up and maintained for 14 days at which point they were demyelinated with lysolecithin (see **section 2.4.5.4**). Cultures were treated with either 100ng/ml LS-mHep7L or LS-mHep7.

LS-mHep7L significantly enhanced re/myelination when compared to untreated controls (**Figure 5.1 A**). Although LS-mHep7 did not significantly enhance re/myelination there does appear to be a trend towards this. Both LS-mHep7L and LS-mHep7 treated slices enhanced myelination past control levels (naïve) at DIV 14 (pre-DeMy) and DIV 28. Additionally, cultures from DIV 14 (pre-DeMy) and naïve DIV 28 demonstrated similar myelination levels (~ 20%) suggesting a balanced maintenance level of myelination is achieved in control cultures. This is also seen in the untreated DeMy slices where myelination levels were restored to a similar level (~ 20%), suggesting that once demyelinated, slices spontaneously remyelinate to pre-lysolecithin myelin levels. Axon density was not significantly changed across the treatments (**Figure 5.1 B**), suggesting that the increase in myelination was not due to a change in axon density, and further confirms that neither treatment with lysolecithin or LS-mHeps have any toxic effect in the cultures.

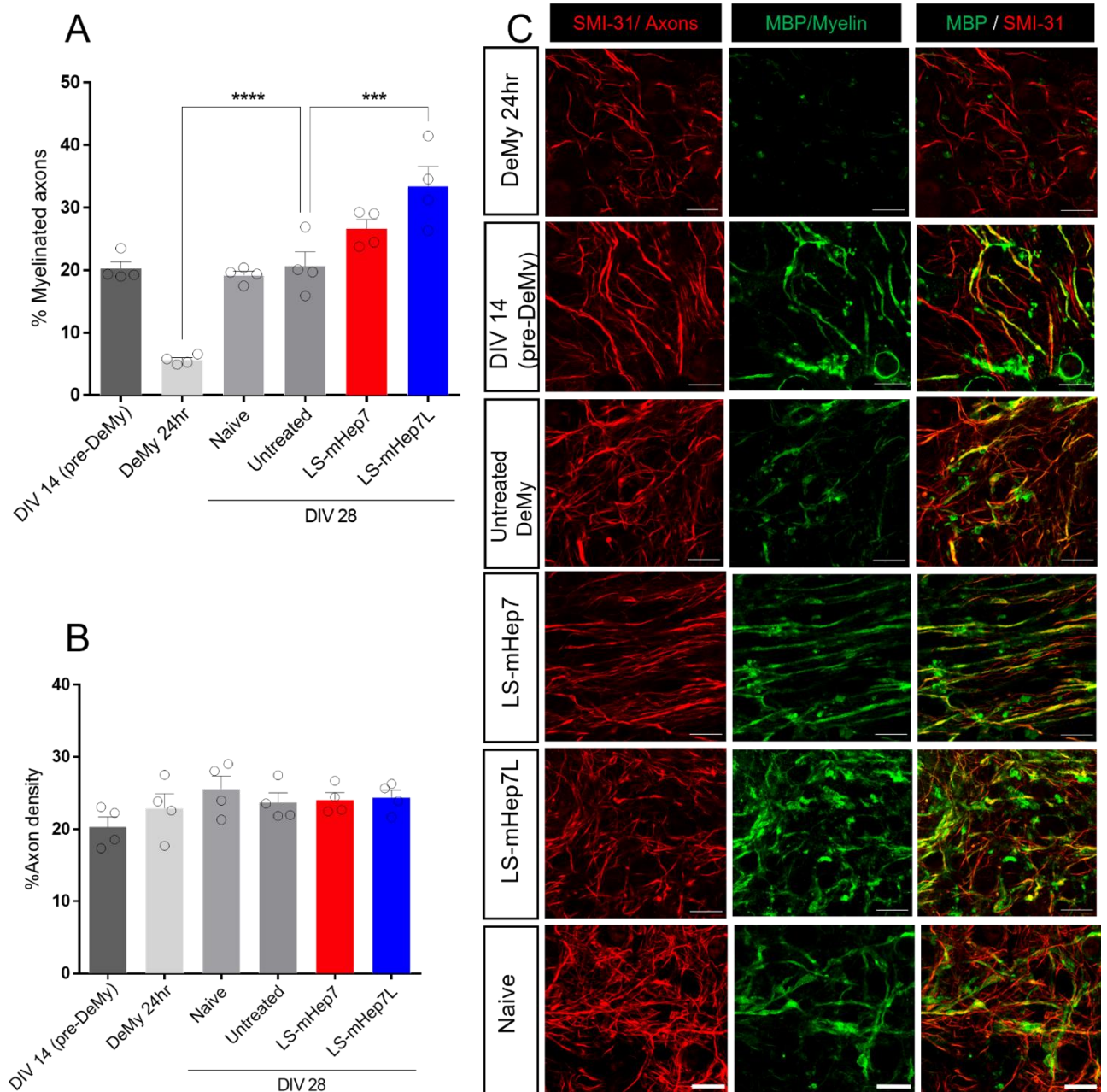


Figure 5.1 |LS-mHep7L enhances re/myelination after lysolecithin induced demyelination in *ex vivo* spinal cord slice cultures (SC-DeMy). (A) Quantification of myelination and axonal density in slice cultures maintained for 14 DIV, then chemically demyelinated with 0.5 mg/ml lysolecithin for 24 hours. Slices were treated with 100 ng/ml LS-mHep7 or LS-mHep7L for 14 days then fixed with 4% PFA. (A) Quantification of myelinated axons showed LS-mHep7L significantly enhanced re/myelination. (B) Quantification of axons did not reveal significant differences between the treatments. Data were compared to the untreated demyelinated control using an unpaired one-way ANOVA with Dunnett's multiple comparison test. *** = $P \leq 0.001$, **** = $P \leq 0.0001$. $n=4$, error bars are SEM. (C) Illustrative images of cultures immunolabelled with anti-MBP (green, myelin), antibody clone SMI-31 (red, axons). Scale bars 200 μm .

5.4 LS-mHep7 and LS-mHep7L have no effect on axon width following re/myelination

Axon calibre is directly linked to myelination status, with smaller axon remaining unmyelinated. To determine if LS-mHeps were directly affecting axon width and enhancing re/myelination in the cultures we quantified axon width across treatments. Slice cultures were set up and maintained for 14 days at which point they were demyelinated with lyssolecithin (see section 2.4.5.4). Cultures were treated with either 100ng/ml LS-mHep7L or LS-mHep7 for 14 days, and then fixed and immunolabelled with antibody clone SMI-31 and axon calibre was quantified. Compared to control cultures there is no significant change in axon width with either LS-mHep7 or LS-mHep7L treatment **Figure 5.2 (B)** (one-way ANOVA with Dunnett's multiple comparison, error bars SEM, $n=3$). This suggests that the LS-mHeps do not influence axon width and therefore the enhanced re/myelination seen in these cultures post demyelination, is likely due to the interactions of another glial cell in the CNS.

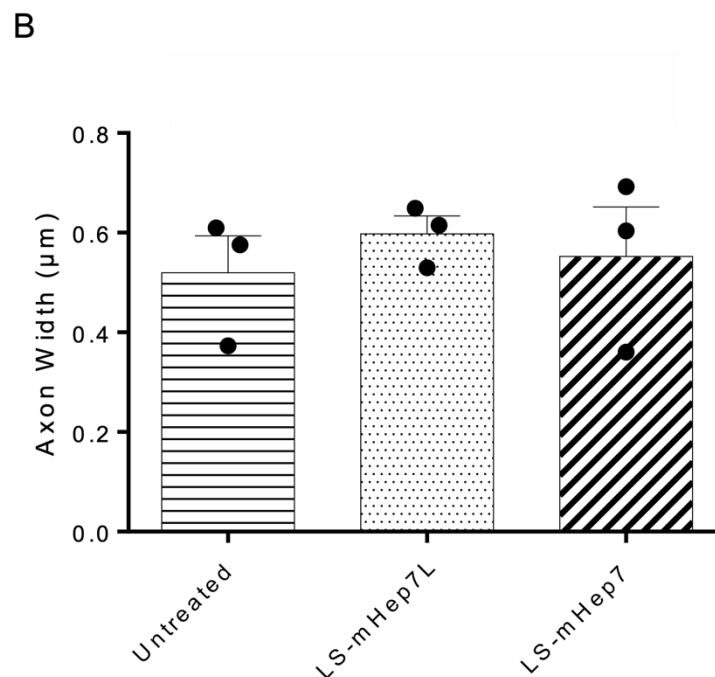
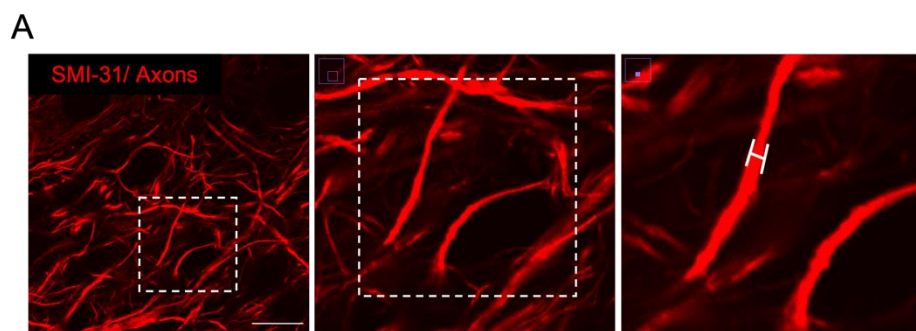


Figure 5.2 |LS-mHep7L/ LS-mHep7 have no effect on axon width in SC-DeMy during re/myelination. Slice cultures were maintained for 14 DIV, then chemically demyelinated with 0.5 mg/ml lysolecithin for 24 hours. Slices were treated with 100ng/ml LS-mHep7 or LS-mHep7L for 14 days and fixed with 4% PFA. Cultures were immunolabelled with antibody clone SMI-31 (red, axons). Axon width was unchanged across treatments (B) (one-way ANOVA with Dunnett's multiple comparison, error bars SEM n=3).

5.5 LS-mHep7 and LS-mHep7L do not enhance developmental myelination levels in SC-DEV

In *Chapter 4* we demonstrated that LS-mHeps have no effect on developmental myelination *in vitro*, suggesting that LS-mHeps exert their effects via interactions with factors released after injury/demyelination (McCanney *et al.*, 2019). To validate the heparin mimetics efficacy in a more translational relevant model we used *ex vivo* slice cultures to study developmental myelination. These cultures are cellularly more complex than the *in vitro* models used in *Chapter 4* with more intercellular communications between glial cells that better replicate *in vivo*, suggesting that interactions involved in the developmental process may interact differently with LS-mHeps. Additionally, compared to *in vitro* cell cultures, *ex vivo* slices are likely to sustain comparatively more damage during explanation of the tissue. The release of damage-induced factors during the preparation of slice cultures may inhibit myelination in our *ex vivo* model system, which we hypothesised could be enhanced by treatment with LS-mHep7 or LS-mHep7L. Spinal cord slices were set up (see section 2.4.5.4) and maintained for 14 days and treated with 100 ng/ml of LS-mHep7 or LS-mHep7L. Myelination levels were quantified after fluorescent labelling with anti-MBP and antibody clone SMI-31.

Developmental myelination levels were unchanged by the treatment of LS-mHep7 or LS-mHep7L (Figure 5.3 A) corroborating with previous data in *Chapter 4* (MC-Dev). Axon density was also unchanged across the treatments during developmental phases (Figure 5.3 B).

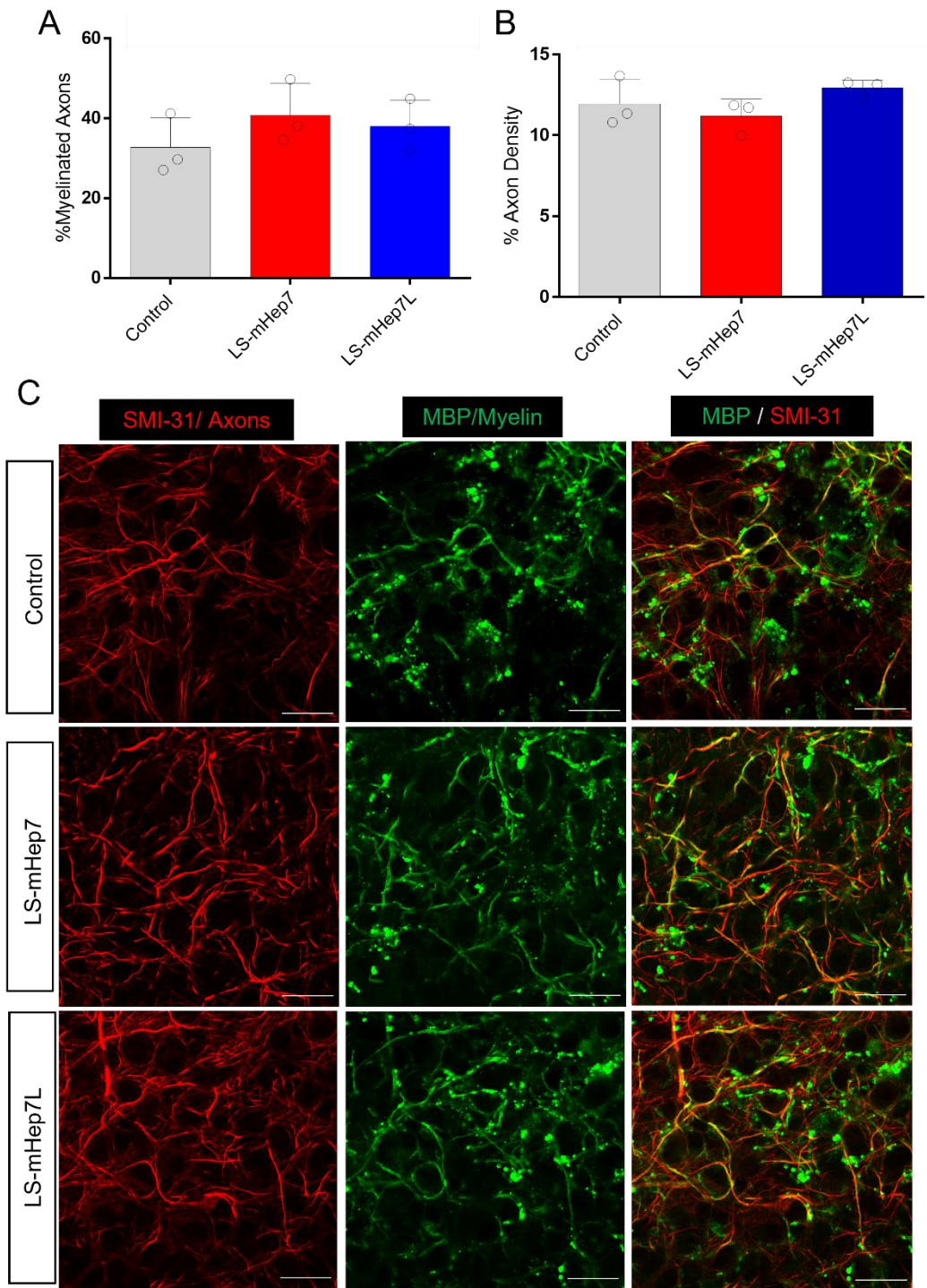


Figure 5.3 |LS-mHep7L/LS-mHep7 treatment in SC-DEV has no effect on developmental myelination. Slice cultures were set up and treated with 100ng/ml LS-mHep7 or LS-mHep7L until DIV14. Cultures were fixed with 4% PFA and immunolabelled with anti-MBP (green, myelin) and antibody clone SMI-31 (red, axons). (A) Myelin levels did not significantly differ between treatments and (B) axon density was not significantly different between treatments. (C) Illustrative images of cultures immunolabelled with anti-MBP (green, myelin), antibody clone SMI-31 (red, axons) (one-way ANOVA with Dunnett's multiple comparison, error bars SEM n=3). Scale bars 200 μ m

5.6 | LS-mHep7L and LS-mHep7 treatment rescues CCL5-induced inhibition of developmental myelination in SC-DEV

Previously in *Chapter 4* we have shown that CCL5 is a negative regulator of developmental myelination. However, the co-treatment with LS-mHep7 and LS-mHep7L rescued this CCL5 induced hypomyelination. We hypothesised that LS-mHeps sequester CCL5, preventing downstream cellular communications that inhibit myelination. Here, we applied the same experimental paradigm in a more complex *ex vivo* slice culture system to determine if LS-mHeps co-treatment can rescue CCL5-induced hypomyelination. Spinal cord slices were set up and maintained for 14 days and treated with 100 ng/ml CCL5 alone, or co-treatment with 100 ng/ml LS-mHep7 or LS-mHep7L from DIV 0. At DIV 14 cultures were fixed and immunolabelled with anti-MBP and antibody clone SMI-31, followed by quantification of myelin. (**Figure 5.4 (A)**) Treatment with CCL5 resulted in significant decrease in the percentage of myelinated axons per field of view ($n = 4, p \leq 0.05$). However, when co-treated with LS-mHep7 or LS-mHep7L, CCL5 induced hypomyelination was rescued, with the significant restoration of myelination levels ($n = 4, p < 0.001$).

This further supports our hypothesis that LS-mHep7 and LS-mHep7L sequesters CCL5, producing a reparative effect in the CNS. This also validates that LS-mHep7 and LS-mHep7L have similar biological properties despite differences in molecular weight and supports their use as future therapeutics for CNS repair.

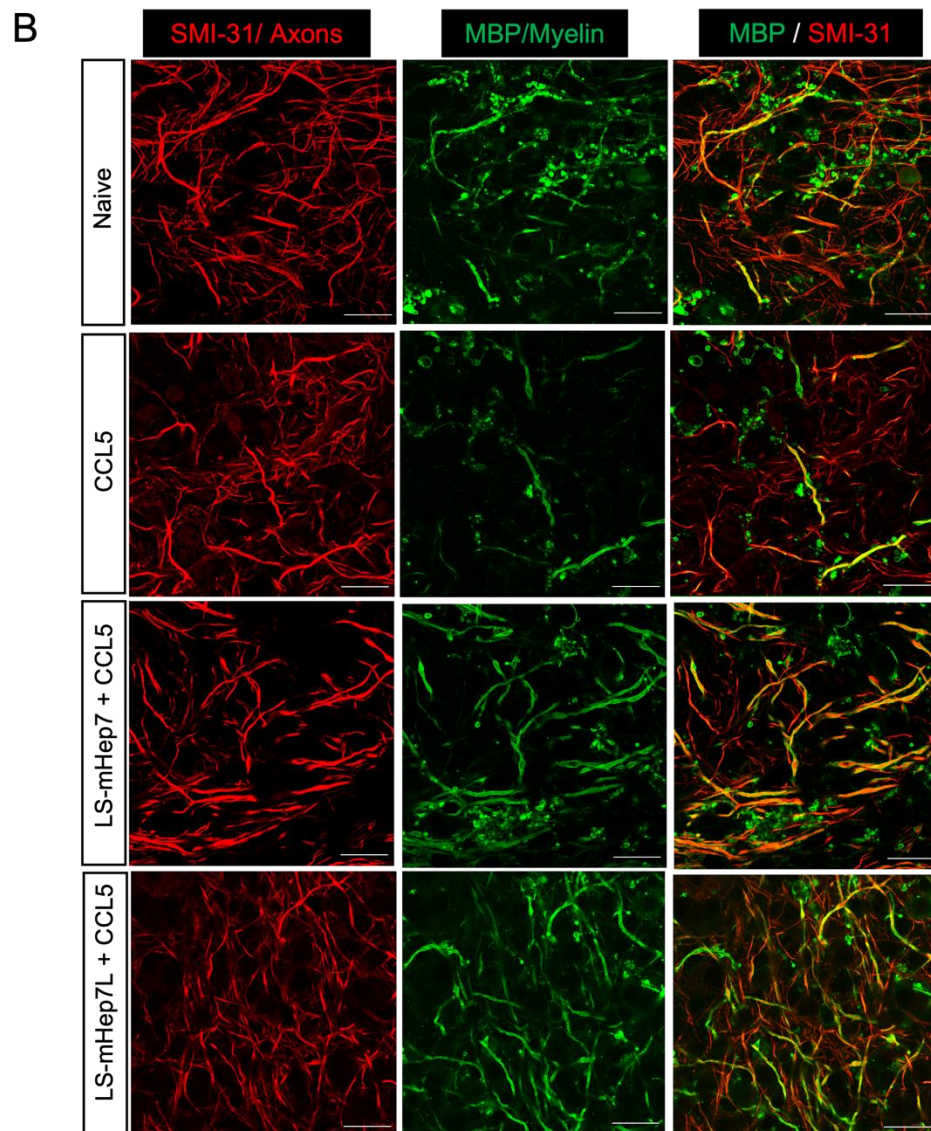
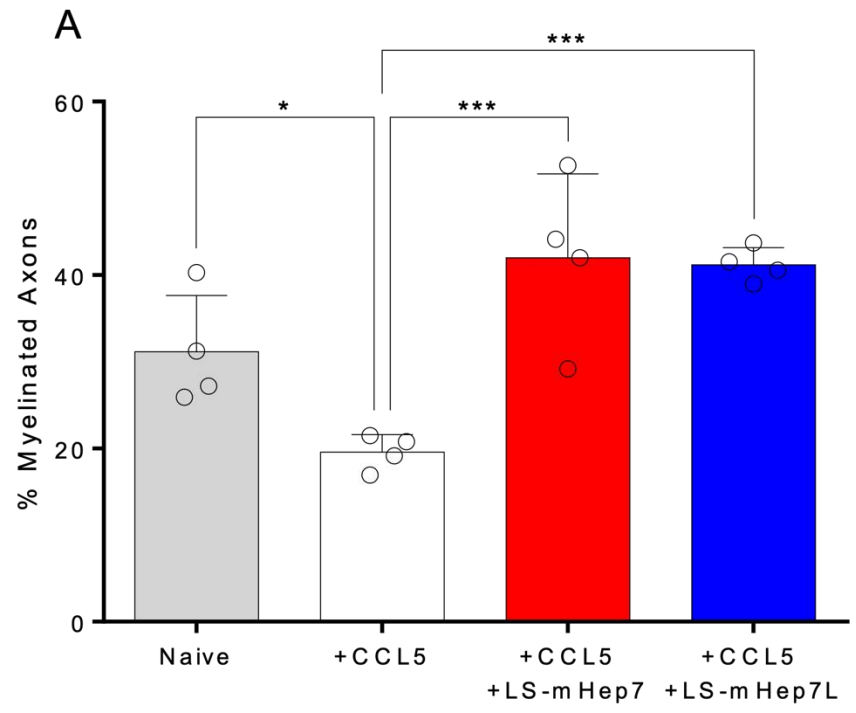


Figure 5.4 |CCL5 significantly reduces developmental myelination in SC-DEV, this effect is rescued by both LS-mHep7L and LS-mHep7. Slice cultures were treated with 100 ng/ml CCL5 alone or co-treated with either 100 ng/ml LS-mHep7/ LS-mHep7L and maintained for 14 DIV. Cultures were fixed with 4% PFA immunolabelled with anti-MBP (green, myelin), antibody clone SMI-31 (red, axons). (A) Quantification of myelination showed CCL5 treatment significantly reduces developmental myelination levels at DIV 14 (One-way ANOVA with Dunnett multiple comparison * = $P \leq 0.1$). However, co-treatment with both LS-mHep7 (*** = $P \leq 0.001$) and LS-mHep7L (****= $P \leq 0.001$) overcomes this CCL5 induced hypomyelination (A). (B) Representative images of slices at DIV 14 treated with; untreated, CCL5 alone, CCL5 + LS-mHep7, CCL5 + LS-mHep7L (one-way ANOVA with Dunnett's multiple comparison, error bars SEM n=4) Scale bars 200 μm ,

5.7 Changes in the secreted chemokine/ cytokine profile of spinal cord slice cultures after demyelination

To help identify other negative regulators of myelination released following injury that could be sequestered by LS-mHeps we determined the relative expression of chemokines and cytokines in our slice cultures after demyelination. This was achieved using a mouse proteome profiler array, and conditioned media from the spinal cord slice cultures. It is important to note that due to the inter-experiment variability, none of the specific protein expression changes are statistically significant, hence findings should be interpreted with caution. The aim of this array was to identify a shift rather than to make inferences on specific factors. Some of the chemokines/cytokines that were upregulated in the demyelination culture are most likely upregulated due to the demyelination **process** and have no negative effect on remyelination or repair. However, this is a useful tool to identify candidates for further investigation. To allow a fair comparison between the shift observed *in vitro* (**Lindsay et al., 2023**) and that observed *ex vivo* the same array profiler (R&D systems) was selected. Media was collected on DIV 14 before demyelination (UCM – uninjured conditioned media) and collected from the same slices 20 hours after demyelination (DCM – demyelinated conditioned media). Analysis demonstrated significant differences in the chemokine/cytokine expression profiles of DCM and UCM (**Figure 5.5 A&B**). Comparison of the dot plots identifies a large increase in many chemokines and cytokines that are expressed following demyelination, producing a distinct chemokine/cytokine profile compared to healthy control conditions. Average pixel intensity of dots visualised in both UCM and DCM, enabled the comparison of both chemokine secretion profiles. 110 chemokines/cytokines were analysed between control and demyelinated media with 95 of those being upregulated in the demyelinated media, and only 15 that were downregulated. Factors that were upregulated included CCL5, CXCL5, CCL2, CCL3, FGF-

21, and IL-1 alpha (**Figure 5.5C**). Downregulated factors include adiponectin, CD160 and PDGF-BB.

CCL5 has already been identified as a negative regulator of re/myelination as previously described in *Chapter 4* and here in *Chapter 5*. LS-mHeps are thought to sequester these molecules, preventing them from exerting their negative effects on myelination. However, heparan sulphates are involved in many cellular communications, suggesting that another chemokine/cytokine could be interacting with LS-mHep7 or LS-mHep7L to produce these positive repair effects *in vitro* and *ex vivo*.

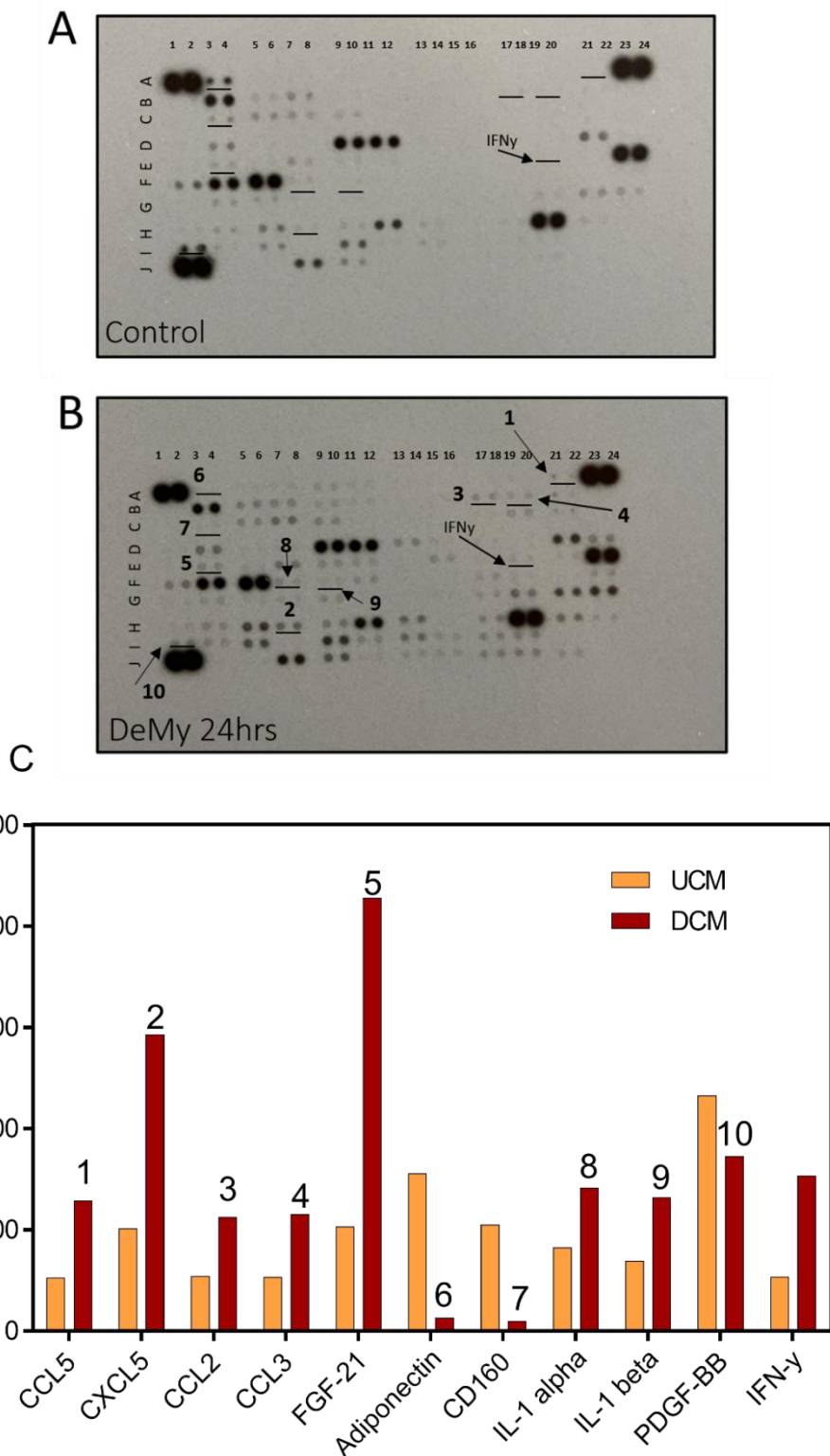


Figure 5.5 | Changes in chemokine/cytokine secretion profile after demyelination in SC-DeMy. Pre-demyelination conditioned medium (UCM) and demyelinated conditioned medium (DCM) were collected from slice cultures. The cytokine profile was assessed using a mouse proteome profiler array. The dot blots of the cytokine arrays for both UCM (A) and DCM (B). Comparisons between the UCM and DCM can be visualised with the side-by-side comparison of the average pixel density of the dots from the candidates with the largest changes (C). Changes in cytokine secretions can be identified, suggesting a shift in the secretome following injury.

5.8 | CXCL5 does not significantly reduce developmental myelination in SC-DEV

To identify a candidate from the cytokine array to further investigate in relation to LS-mHep7 interactions, we referred to unpublished data collected from the Barnett lab. Previously the lab used an LS-mHep7 affinity pull-down column using conditioned media from demyelinated *in vitro* cultures (MC-DeMy) and control conditioned media from cultures pre-demyelination. The affinity pulldown experiment identified secreted factors that were able to bind specifically to LS-mHep7. Analysis of the array identified several LS-mHep7-binding factors including, CCL5, CCL20, CXCL1, CXCL5, CXCL10 and vascular endothelial growth factor (VEGF). Here we can see that CXCL5 is identified in both the LS-mHep7 affinity pull down and is also identified as up regulated in the slice culture cytokine/chemokine array (**Figure 5.5**), making it an attractive candidate for further study.

Here we investigated the effects of CXCL5 in the SC-DEV model. Spinal cord slices were set up and maintained for 14 days (**as described in 2.4.5.4**) and treated with 100 ng/ml of CXCL5 alone or co-treated with 100 ng/ml LS-mHep7 or LS-mHep7L until DIV 14.

CXCL5 alone does not appear to reduce developmental myelination when compared to the untreated control after 14 days (**Figure 5.6**). However, co-treatment with LS-mHep7/LS-mHep7L saw a significant increase in developmental myelination compared to CXCL5 alone.

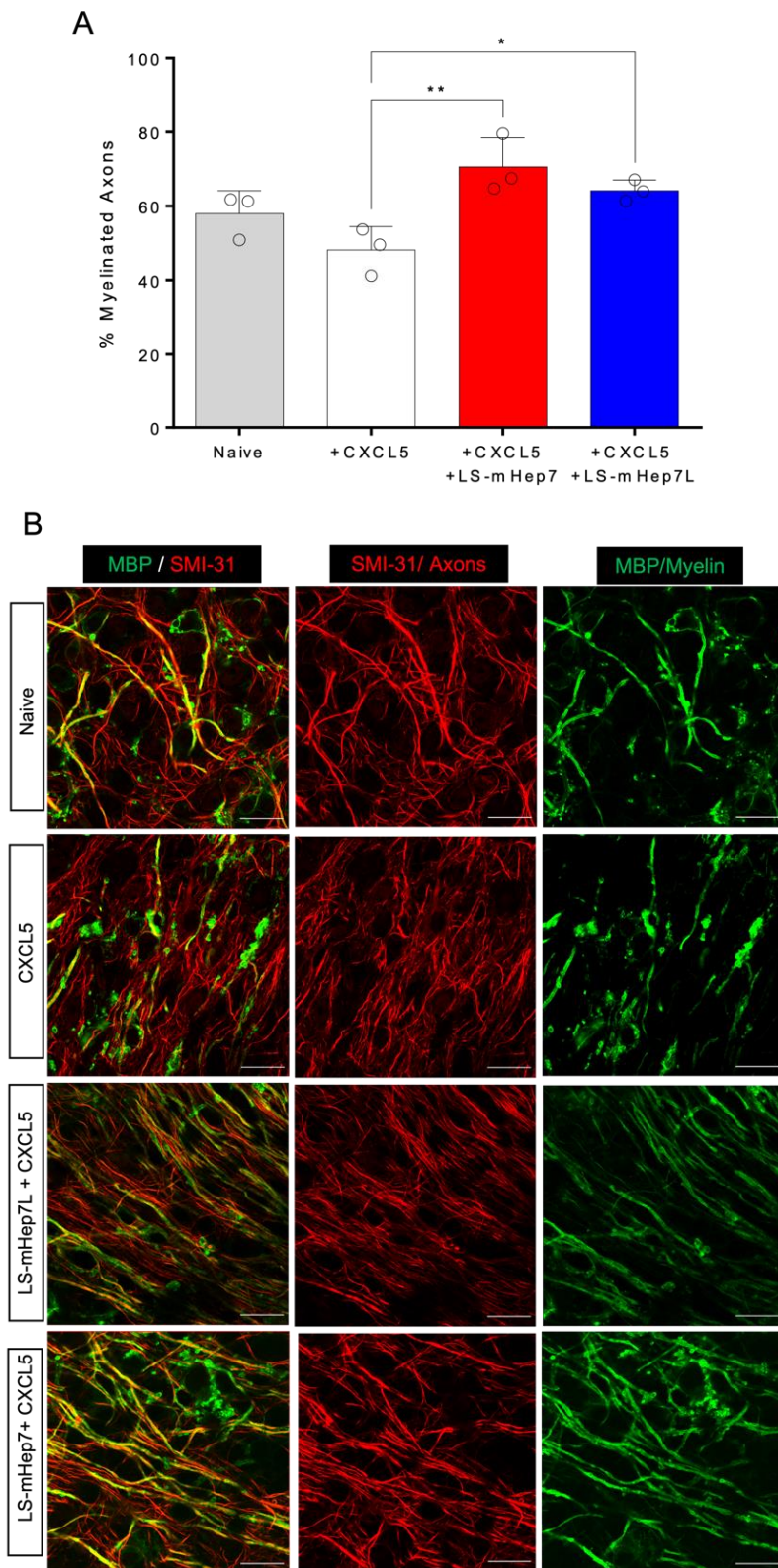


Figure 5.6 | CXCL5 has no negative effect on developmental myelination in SC-DEV. Slice cultures were treated with 100 ng/ml CXCL5 alone or co-treated with either 100 ng/ml LS-mHep7 or LS-mHep7L and maintained for 14 days. Cultures were fixed with 4% PFA immunolabelled with anti-MBP (green, myelin), antibody clone SMI-31 (red, axons). (A) Quantification of myelination showed CXCL5 treatment did not significantly reduce developmental myelination levels at DIV 14. However, co-treatment with both LS-mHep7 (** = $P \leq 0.01$) and LS-mHep7L (* = $P \leq 0.5$) with CXCL5 significantly increased myelination levels compared to CXCL5 treated cultures. (B) Representative images of slices at DIV 14 treated with; untreated, CXCL5 alone, CXCL5 + LS-mHep7, CCL5 + LS-mHep7L (one-way ANOVA with Dunnett's multiple comparison, Scale bars 200 μm , error bars SEM $n=3$)

5.9 | Discussion

Previously in **Chapter 4**, we investigated how both LS-mHep7 and LS-mHep7L can enhance repair in our *in vitro* models of the CNS. In this chapter, however, we have explored how the LS- mHeps can enhance repair in a more complex cellular model of the CNS, that maintains the three-dimensional multicellular structures seen *in vivo*. To do this we used our established method of *ex vivo* spinal cord slice cultures that were described in **Chapter 3** – bridging the gap between our *in vitro* work, and future *in vivo* work.

In SC-DeMy we observed enhanced re/myelination with the treatment of LS-mHep7 which corroborated previous data collected in **Chapter 4**, and published work (**McCanney et al., 2019**). We can only speculate how LS-mHeps are eliciting their effect in our cultures as HSs have numerous mechanisms-of-action to regulate cell signalling including acting as a co-factor in the formation of functional ligand-receptor complexes (**Yayon et al., 1991**), functioning as an endocytic receptor, aiding in the cellular internalisation of ligands (**Belting, 2003**) and sequestering of ligands in the ECM (**Vlodavsky et al., 1991**). One mechanism involved could be the relationship between HSPGs and FGF signalling. One major function of HSPGs is to interact with FGFs and their receptors (FGFRs) to form signalling complexes – making them essential for FGF signalling (**Wu et al., 2003; Venero et al., 2015; Yayon et al., 1991**). FGFs have a critical role in myelination in the CNS. For example, myelin growth, and myelin sheath thickness is controlled by FGF signalling (**Furusho et al., 2012**), and FGFs are also involved in OPC proliferation (**Bögler et al., 1990; Butt 2005**). Additionally, LS-mHep7 could be interacting with a multitude of molecules at the same time to elicit these effects. The chemokine CXCL10 is known to bind to HSPGs (**Luster et al., 1995**) and has shown to be a negative regulator of myelination *in vitro* (**Nash et al., 2011**). CXCL10 signalling has also been shown to promote OPC apoptosis through a caspase-dependent mechanism (**Tirotta et al., 2011**). LS-mHep7/L could be sequestering CXCL10 in SC-DeMy, reducing OPC apoptosis, and indirectly re/myelination. Due to the high prevalence of HS binding myelination-associated factors, it is unlikely that there is a single protein target through which the low-sulphated HS mimetics exert their pro-remyelination effect (**Zong et al., 2017**)

The relationship between axon calibre and myelination is well documented, with larger axon width being associated with myelination status and low axon width often being unmyelinated (**Friede, 19752; Goebbels et al., 2017; Mayoral et al., 2018**). In SC-DeMy, it was found that neither treatment with LS-mHep7 or LS-mHep7L increased the calibre of axons during

the remyelination period. This leads to the assumption that enhanced remyelination in these cultures is not linked to the direct effect of LS-mHeps on neurons and their axons – increasing their size.

Investigations into LS-mHeps effect in SC-DEV, showed that neither compound enhanced developmental myelination. The absence of any effect from LS-mHep7/L on developmental myelination leads us to hypothesise that any endogenous HS in the cultures that may contribute to developing myelin during this time are sufficiently present. Previously, **McCanney *et al.*, 2019** investigated LS-mHep7's effect on OPC proliferation *in vitro* and found that there was no increase in OPC proliferation with mHep treatment during development. This implies that the promotion of remyelination reported in the SC-DeMy cultures, is not the result of a direct effect by mHeps on oligodendrocytes, which would be consistent across both cultures (SC-DeMy and SC-DEV). Any effect LS-mHep7/L has on myelination in the developing slice cultures is most likely due to the interactions of LS-mHeps with injury secreted factors, and not developmental factors.

Known negative regulators of developmental myelination were investigated in the slice cultures. Previously in **Chapter 4** we observed the CCL5 induced hypomyelination in developmental myelination cultures. Here, observed that the addition of CCL5 alone in SC-DEV lead to hypomyelination which could be rescued with the addition of either LS-mHep7/LS-mHep7L. This corroborates with our previous results in **Chapter 4**, further validating the ability of LS-mHeps to sequester this negative regulator of myelination.

After validating LS-mHep7/LS-mHep7Ls ability to enhance repair in our spinal cord slice cultures we assessed if there were any changes in the secretion profile of cytokines following CNS injury. There are many known chemokines and cytokines that are HS binding, so identifying potential candidates is essential in understand the mechanisms behind the positive repair observed. This was achieved by assessment of conditioned media from the spinal cord slice cultures on a Proteome Profiler XL array. Again, it is important to note that due to the inter-experiment variability, none of the specific protein expression changes are statistically significant, hence findings should be interpreted with caution. The aim of this array was to identify a shift rather than to make inferences on specific factors. Some of the chemokines/cytokines that were upregulated in the demyelination culture are most likely upregulated due to the demyelination **process** and have no negative effect on remyelination or repair. However, this is a useful tool to identify candidates for further investigation. Analysis of the full data set demonstrated differences in the chemokine/cytokine expression profiles of DCM compared to the UCM, suggesting that demyelination in the CNS induces

a chemokine secretion profile distinct from the normal CNS. 110 chemokines/cytokines were analysed between control and demyelinated media with 95 of those being upregulated in the demyelinated media, and only 15 that were downregulated. Factors that were upregulated included CCL5, CXCL5, CCL2, CCL3, FGF-21, IFN- γ and IL-1 alpha. The upregulation of CCL5 in SC-DeMy further confirms this chemokine as an important regulator in CNS injury and repair and is a likely candidate for how the LS-mHeps are enhancing re/myelination.

The pro-inflammatory cytokine IFN- γ is chronically elevated in patients with MS (**Beck *et al.*, 1988**) and has recently been associated with inducing quiescence in human OPCs (**Saraswat *et al.*, 2020**). HSPGs have been found to modulate IFN- γ signalling following demyelination, directly antagonize IFN- γ to rescue human OPC proliferation and differentiation *in vitro* and blocked the IFN- γ -mediated inhibitory effects on OPC recruitment *in vivo* (**Saraswat *et al.*, 2021**). Additionally, **Saraswat *et al.*, 2020** found that HSPGs acts via inhibition of OPC-expressed sulfatases (Sulf1/2) to enhance remyelination, and IFN- γ signalling in OPCs resulted in activation of Wnt and Bmp target genes, suggesting a possible mechanism by which oligodendrocyte differentiation was delayed. The mechanisms in which these HSPGs act upon, could be a similar molecular pathway that LS-mHeps use to enhance remyelination.

CCL5 was upregulated in the cytokine array which further confirms this chemokine as an important regulator in CNS injury and repair and is a likely candidate for how the LS-mHeps are enhancing myelination.

A candidate for further interest was CXCL5. This chemokine was upregulated after demyelination in the array but was also found to be a LS-mHep7 binding chemokine. Previously the lab has shown that CXCL5 is an LS-mHep7 binding protein after performing an affinity pull-down and the resultant eluate was assessed on a Proteome Profiler array. CXCL5 may play a central role in the inflammatory cascade of TBI and has recently been suggested as a potential inflammatory biomarker in patients with TBI (**Dyhrfort *et al.*, 2019**). Additionally, CXCL5 has been found to be overexpressed in patients with multiple sclerosis, where CXCL5 serum levels were shown to correlate with blood–brain barrier dysfunction (**Rumbles *et al.*, 2015; Haarman *et al.*, 2019**).

CXCL5 was assessed in SC-DEV to investigate if CXCL5 treatment, or co-treatment with LS-mHep7/LS-mHep7L had any effect on myelin development. CXCL5 alone had no significant effect on myelin levels in SC-DEV. However, co-treatment of CXCL5 and LS-

mHeps had a significant increase in myelination levels, that increased past a control level. Previously we have shown that our LS-mHeps alone do not influence developmental myelination, which has been shown numerous times including in our *in vitro* cultures. This suggests that our LS-mHeps could be acting as a co-factor for CXCL5 to induce enhanced myelination. Although CXCL5 has previously been associated with BBB dysfunction and is associated with MS inflammatory lesions, it is also reported to have reparative effects in optic nerve regeneration (**Liu et al., 2021**). CXCL5/CXCR2 promoted retinal ganglion cell (RGC) survival, neurite outgrowth and microglia activation *in vivo*.

In summary, this chapter validated the ability of LS-mHep7 and LS-mHep7L to enhance and repair the CNS in our *ex vivo* spinal cord slice cultures. Here we observed repeated outcomes where results from our *in vitro* models were re-observed here in our more complex *ex vivo* models. This continues to establish LS-mHeps as potential therapeutics for CNS repair.

Chapter 6

Validation of recombinant heparan sulphate panel for CNS repair

6.1 Introduction

In previous chapters we have validated both LS-mHep7 and LS-mHep7L as a potential therapeutic for CNS injury repair. We have discussed that these mHeps are modified from the blood-thinning drug heparin whose structure resembles heparan sulphate. However, the heparin is manufactured and obtained from pig intestines, the supply of which can risk contamination (such as viral, bacterial, and previously, over-sulphated chondroitin sulphate) or suffer shortages. Currently 80% of the world's heparin supply is sourced from China from porcine intestines (**McCarthy *et al.*, 2020**). Having such a huge reliance on a specific animal source for any new therapeutic comes with an elevated risk. This includes the threat of outbreaks of disease within the pig population (in 2007, an outbreak of a respiratory disease called blue-ear pig disease in Asia resulted in considerable shortages of heparin), leading to mass culls and therefore shortages of a source to generate heparin. Furthermore, animal derived heparin products have previously been contaminated with over-sulphated chondroitin sulphate, resulting in anaphylactic like re-actions and deaths in the USA and other countries (**Kishimoto *et al.*, 2008**). Recently, the modification of the mammalian heparan sulphate biosynthetic pathway has produced recombinant heparin in cultured mammalian cells as an alternative to animal derived heparin (**Thacker *et al.*, 2022, TEGA Therapeutics, Inc.**). These recombinant heparan sulphates (rHS) represent an attractive source of heparin for patient use and for therapeutics derived from heparin. **Thacker *et al.*, 2022** employed CRISPR-Cas9 technology to edit the genome of Chinese hamster ovary (CHO) cells, to target 26 genes involved in heparin biosynthesis to enhance the production of heparin precursors, specifically the heparan sulfate chains. Each cell line had altered expression of key enzymes involved in heparin biosynthesis, such as over expression of heparan sulfate 2-O-sulfotransferase (HS2ST) or heparan sulfate 6-O-sulfotransferase (HS6ST), which contributes to the production of a rHS with varying sulfate groups. Through the combination of either under or over production of these enzymes, a panel of rHS was produced with high purity, and specific sulphation levels on the HS chains. We were provided with 3 rHSs from this panel of rHS compounds by TEGA Therapeutics, - rHS02, rHS09 and rHS10, all with varying levels of sulphation and molecular weight. To assess these heparin mimetics to enhance repair in our CNS injury models, we compared their capacity to remyelinate and repair, and compared the results to our 'gold standard' mimetic, LS-mHep7. This side-by-side comparison will enable us to determine if rHSs are a suitable cell-derived alternative for heparin-based therapeutics.

All experiments completed in this chapter were done in collaboration with Dr Susan Lindsay at the University of Glasgow, compounds were provided by TEGA Therapeutics, Inc. (San Diego, California, U.S.A).

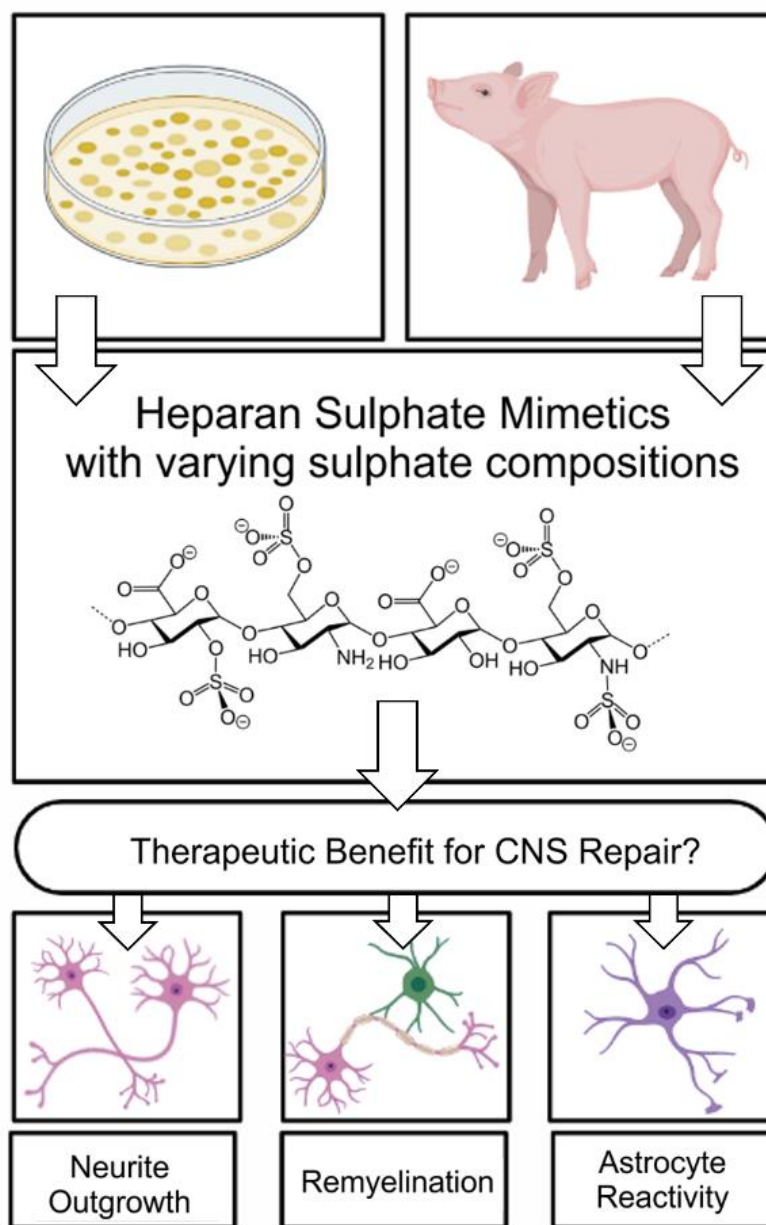


Figure 6.1 |Schematic of heparan sulphate mimetics and their sources. The heparan sulphate mimetics discussed in this thesis are produced semi-synthetically by chemical selective desulphation of porcine mucosal heparin. Currently 80% of the world’s heparin supply is sourced from China from porcine intestines. Heparan sulphate mimetics have recently been produced via the modification of the mammalian heparan sulfate biosynthetic pathway to produce recombinant heparin in cultured mammalian cell. These mimetics can easily be added to models of CNS injury to ascertain their reparative abilities in neurite outgrowth, re/myelination, and astrocyte reactivity.

6.2 Aims

The overall aim of this chapter was to validate the ability of recombinant heparan sulphates to enhance repair in our models of CNS injury *in vitro* and *ex vivo*. This was achieved by assessing the following:

- i) the abilities of rHS02, rHS09 and rHS10 to enhance re/myelination after compliment induced demyelination in MC-DeMy
- ii) the abilities of rHS02, rHS09 and rHS10 to enhance neurite outgrowth in our CNS injury model (MC-Inj)
- iii) the effects of rHS02, rHS09 and rHS10 on astrocyte reactivity after injury

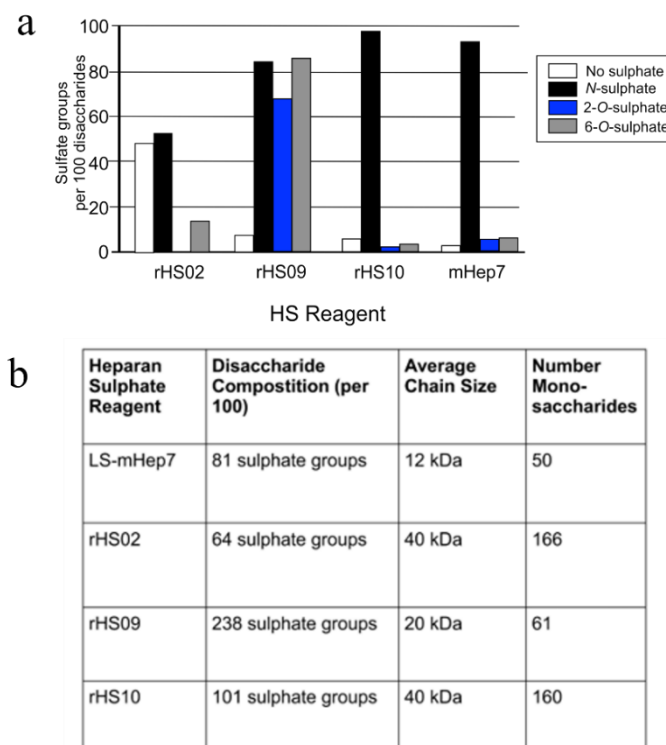


Figure 6.2 | Comparison of the predominant structure of rHS02, rHS09, rHS10 and LS-mHep7. Heparan sulphates are purified from cultured cells from porcine tissue. (a) The number of sulphate groups per 100 disaccharides present in recombinant HS mimetics and LS-mHep7. rHS10 and LS-mHep7 are both predominantly N-sulphated. rHS09 is highly sulphated containing N-, 2-O-, and 6-O groups. rHS02 has a predominant mixture of no sulphate and N-sulphate. (b) The predominant reagent structure detailing information on approximate disaccharide composition, average chain length and approximate number of monosaccharides. *Data for rHS provided by TEGA therapeutics Inc and for LS-mHep7 by Dr Edwin Yates (University of Liverpool).*

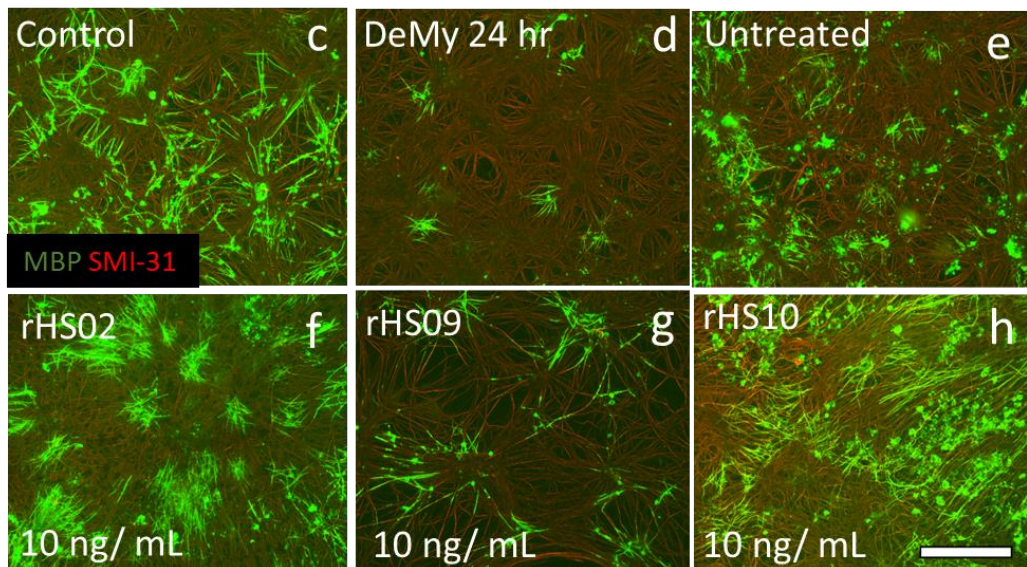
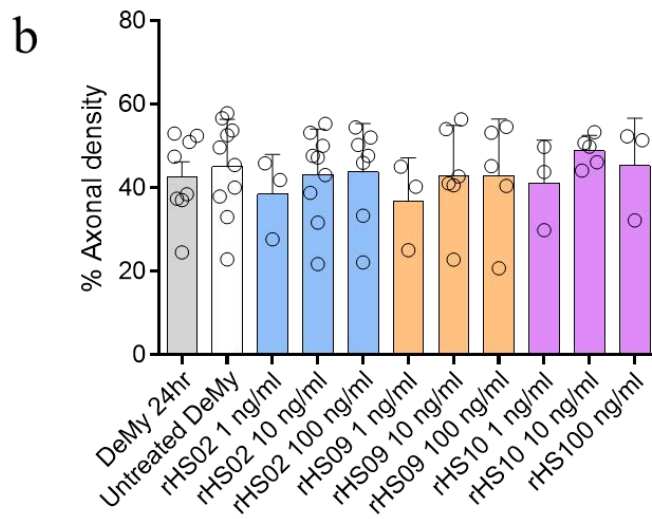
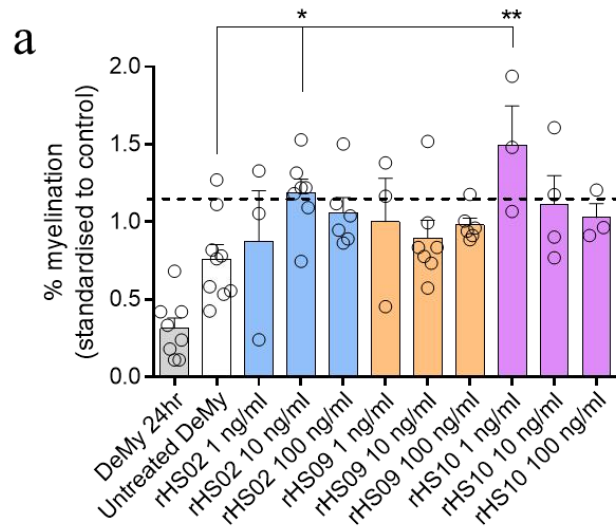
6.3 Effect of rHS02, rHS09 and rHS10 on *in vitro* re/myelination

Three recombinant HS mimetics were used to treat MC-DeMy cultures - rHS02, rHS09 and rHS10, following anti-MOG induced demyelination with compliment. These rHSs have varying levels of sulphation (Figure 6.1) which has been shown by **McCanney *et al.*, 2019** to influence whether HS mimetic positively or negatively influence repair in CNS injury models. Therefore, it was likely that our recombinant panel would regulate repair in varying capacities.

Myelinating cultures were established and demyelinated by overnight treatment with MOG antibody and complement as previously described (see 2.4.5.2). The following day, cultures were treated with rHS02, rHS09 or rHS10 at 1, 10 or 100 ng/ml followed by an assessment of the level of re/myelination 5 days post-treatment (Figure 6.2). Treatment with rHS02 at 10 ng/ml and rHS10 at 1 ng/ml both significantly promoted re/myelination to similar levels to that published previously for LS-mHep7 at 1 ng/ml (Figure 6.3 (a)), represented by dashed line). rHS09 had no effect on re/myelination compared to controls. Fold change (FC) increase of re/myelination levels indicates rHS10 at 1 ng/ml promoted re/myelination by 2.76-fold. This was comparable to the 2.68-fold increase exerted by LS-mHep7 at 1 ng/ml (Figure 6.3 (i)). Additionally, rHS02 promoted a 1.74-fold and rHS09 promoted a 1.61-fold suggesting that very low sulphated compounds are more efficacious.

Treatment with rHS02, rHS09 or rHS10 indicated no significant difference in axon density between treatments (Figure 6.3 (b)). This suggests that both demyelination using compliment/anti-MOG and treatment with rHSs has no toxic effect on neurites in cultures.

This data suggests that low sulphated rHS compounds have a positive effect on re/myelination whilst high sulphated rHS compounds (rHS09) have no effect. This corresponds to previous observations from **McCanney *et al.*, 2019**, as well as repeated observations throughout this thesis that low sulphated HS (LS-mHep7/LS-mHep7L) promotes CNS repair.



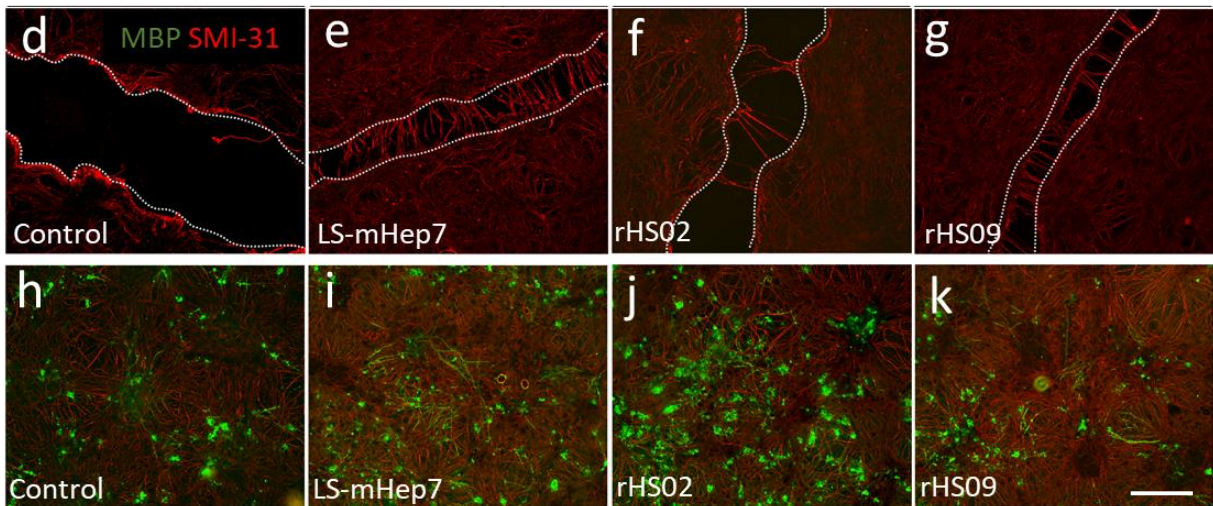
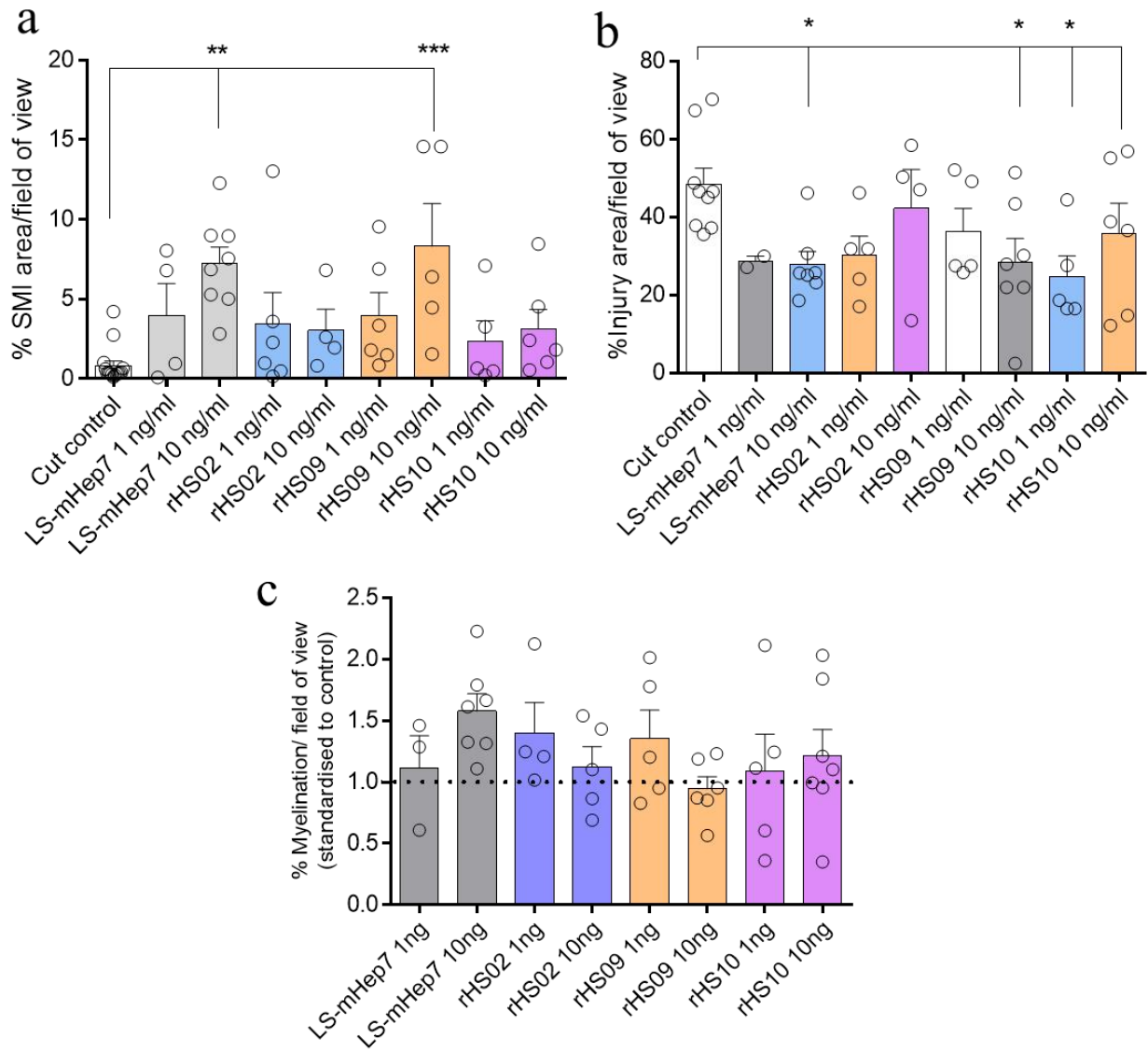
i

Compound	H7	rHS02	rHS09	rHS10
FC	2.68	1.74	1.61	2.76
Concentration	1 ng/ml	10 ng/ml	1 ng/ml	1 ng/ml

Figure 6.3 | rHS10 and LS-mHep7(H7) enhance re/myelination *in vitro* (MC-DeMy). Myelinating cultures were allowed to mature until DIV 24 then demyelinated with MOG specific antibody Z2 (100 ng/ml) and rabbit complement (100ng/ml). Cultures were treated on DIV 25 with either LS-mHep7, rHS02, rHS09 or rHS10 at 1, 10 or 100 ng/ml. Cultures were allowed to recover until DIV 30, following which they were fixed with 4% PFA, and immunolabelled with SMI-31 (red, neurites) and anti-MBP (green, myelin). (a) Quantification of re/myelination shows significantly enhanced re/myelination with cultures treated with either rHS02 at 10ng/ ml or rHS10 at 1ng/ ml. The level of re/myelination produced by LS-mHep7 is illustrated by the dashed line. (b) Quantification of axon density showed no significant effects of any of the compounds tested. (c-h) Representative images of, (c) control naïve cultures DIV 30, (d) cultures 24 hr post-demyelination (DeMy 24 hr), (e) untreated DeMy cultures DIV 30, (f) rHS02 (10 ng/ ml) DIV 30, (g) rHS09 (10 ng/ ml) DIV 30, and (h) rHS10 (10 ng/ ml) DIV 30. (i) The table details the average fold change (FC) in re/myelination compared to Day 5 in DeMy cultures. (one-way ANOVA with Dunnett's multiple comparison, * = $P \leq 0.05$), ** = $P \leq 0.005$). Scale bars 50 μm , error bars SEM (n number represented by individual data points on the graph; technical replicates = 3)

6.4 Effect of rHS02, rHS09 and rHS10 and LS-mHep7 on neurite outgrowth and lesion width after injury in MC-Inj

To assess the effect of rHS02, rHS09 and rHS10 on neurite outgrowth in the CNS injury model (MC-Inj) myelinating cultures set up and described (section 2.4.5.1) (**Boomkamp *et al.*, 2012**). After cutting, cultures were treated with either 1 ng/ml or 10 ng/ml rHS02, rHS09 or rHS10. At DIV 30 (5 days post injury) assessment of neurite outgrowth across the injury site was made – neurite outgrowth was assessed by the amount of pixel immunoreactivity in the region of interest (lesion site) using thresholding. As previously shown in **Chapter 4**, LS-mHep7 at 10 ng/ml was found to significantly promote neurite extension into the injury lesion gap compared to the non-treated control MC-Inj cultures. Additionally, rHS09 at 10 ng/ml (similarly to LS-mHep7) significantly promoted neurite outgrowth compared to control injured cultures. To assess the size of the gap in MC-Inj, the resulting width was analysed in ImageJ to determine the average gap size of each treatment at DIV 30. The measurements of injury gap width revealed that LS-mHep7 and rHS09 at 10 ng/ml had correspondingly reduced gap width suggesting both these compounds had beneficial effects on neurite extension and prevention of injury site expansion (**Figure 6.4 (b)**). Additionally, rHS10 at 1 ng/ml significantly reduced the injury area width compared to control non-treated injured cultures. Treated cultures were compared to control cut cultures, which received no treatment. rHS09 promoted neurite outgrowth by 14.56-fold which was comparable to LS-mHep7 at 12.40-fold. Both rHS09 and LS-mHep7 had similar reductions in average injury gap width reductions compared to controls of 60.29% and 61.47%, respectively (**Figure 6.4 (l)**). Re/myelination adjacent to the lesion after treatment with rHS02, rHS09, rHS10 or LS-mHep7 was quantified (**Figure 6.4 (c)**). There were no differences in the level of re/myelination in any of the treatments tested, although LS-mHep7 had the highest levels in general. Overall, this data suggests that highly sulphated rHS09 is the most efficacious in promoting neurite outgrowth.



1

Compound	H7	rHS02	rHS09	rHS10
FC neurite outgrowth	12.40	7.98	14.56	6.55
Av % Injury Gap width reduction	61.47	83.32	60.29	74.77

Figure 6.4 |Effect of LS-mHep7, rHS02, rHS09 and rHS10 on neurite outgrowth and myelination after injury (MC-Inj). Myelinating cultures were allowed to develop until DIV 24 where they were cut using an 11 mm single edge razor blade. Cultures were immediately treated with LS-mHep7, rHS02, rHS09 or rHS10 (1 or 10 ng/ml). Cultures were allowed to recover until 30 DIV, following which they were fixed with 4%PFA, and immunolabelled with SMI-31 (red, neurites) and anti-MBP (green, myelin). (a) Quantification of neurite outgrowth is represented as % SMI-31 positive threshold pixels per injury region of interest. Both LS-mHep7 and rHS09 at 10 ng/ml significantly promoted neurite outgrowth into the lesion compared to control cultures. (b) Quantification of injury gap width revealed that LS-mHep7 and rHS09 at 10 ng/ml also significantly reduced the width of the area compared to control cultures. In addition, rHS10 at 1 ng/ml significantly reduced the size of the gap injury area. (c) Quantification of % myelination adjacent to the lesion showed no significant effects of any of the compounds tested. (d-g) Representative images of (d) control untreated cut cultures, (e) cut cultures treated with LS-mHep7(10 ng/ml), (f) cut cultures treated with rHS09 (10 ng/ml), and (g) cut cultures treated with rHS10 (10 ng/ml), all at DIV 30. (h-k) Representative images of % myelination adjacent to the lesion of cultures treated with (i) LS-mHep7, (j) rHS09 (k) rHS10, all at 10 ng/ml. (l) Table detailing the average fold change (FC) in neurite outgrowth and the average % reduction in injury gap width compared to compared to tied cut control cultures. (one-way ANOVA with Dunnett's multiple comparison, * = $P \leq 0.05$), ** = $P \leq 0.005$, *** = $P \leq 0.001$). Scale bars 50 μm , error bars SEM (n number represented by individual data points on the graph; technical replicates = 3)

6.5 Effect of rHS10 on *ex vivo* slice culture re/myelination

In *Chapter 5* we investigated the effects of LS-mHep7 and LS-mHep7L on their ability to enhance re/myelination in an *ex vivo* spinal cord demyelination model (SC-DeMy). We observed that LS-mHep7L significantly increased re/myelination 14 days post demyelination treatment. Therefore, to assess the abilities of these rHS in a cellularly more complex model of CNS injury, spinal cord slice cultures were set up and maintained for 14 DIV and demyelinated over-night with lysolecithin. The following day, slices were treated with LS-mHep7 or rHS10 at 100 ng/ml. These cultures were then maintained for an additional 14 days, then fixed with 4% PFA and immunolabelled with MBP (myelin) and SMI-31 (axons). After demyelination there was a loss of MBP wrapped axons, however there was no change in axon density across any of the treatments following demyelination (**Figure 6.5 (b)**). Treatment with rHS10 significantly promoted re/myelination to a similar extent as LS-mHep7 when compared to untreated slices (**Figure 6.5(a)**). There was no difference between the myelination levels between LS-mHep7 and rHS10 when compared to controlled (no demyelination) slices, suggesting that these treatments do not enhance past control levels seen in this model. This data confirms that rHS10 promotes re/myelination like LS-mHep7 and suggests that N-sulphation is an important facet for promoting CNS myelination following injury.

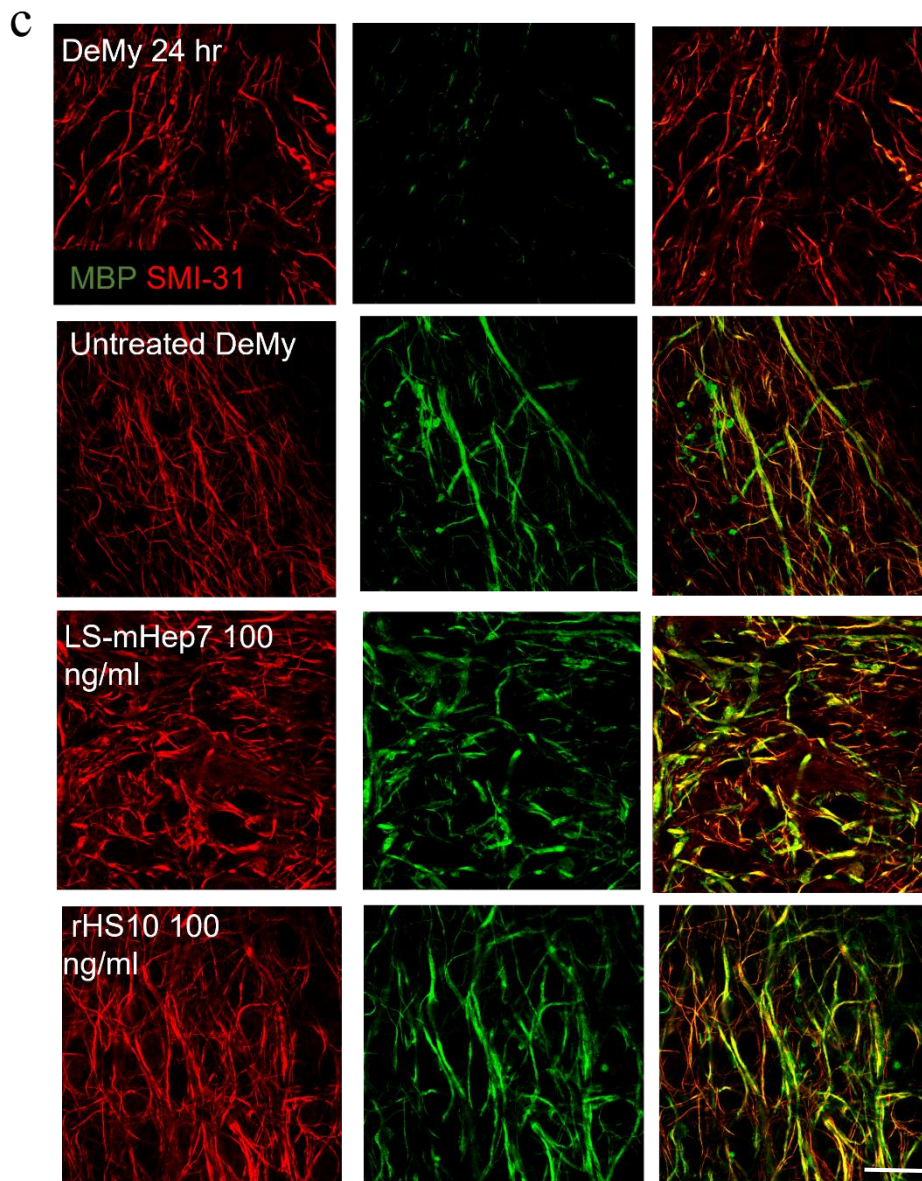
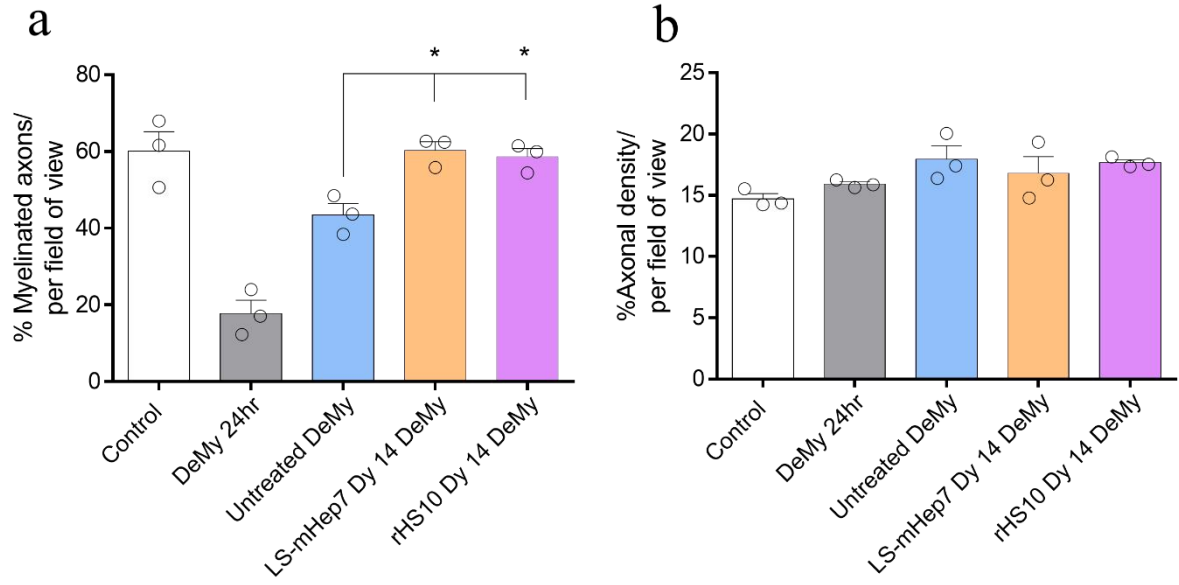


Figure 6.5 | rHS10 and LS-mHep7 enhances re/myelination after lysolecithin induced demyelination of *ex vivo* spinal cord slice cultures. P1 mouse spinal cord slice cultures were maintained for 14 DIV, then chemically demyelinated with 0.5 mg/ml lysolecithin for 24 hours. Slices were treated with either LS-mHep7 or rHS10 at 100 ng/ml for 14 days and fixed with 4% PFA. Cultures were immunolabelled with anti-MBP (green, myelin), antibody clone SMI-31 (red, axons). Quantification of myelination was established using CellProfiler. (a) Both LS-mHep7 and rHS10 enhance re/myelination compared to untreated controls. (b) Axon density per field of view remained unchanged across the treatments. (c) Representative images of cultures at DIV 30. (one-way ANOVA with Dunnett's multiple comparison, ** = $P \leq 0.01$, Scale bars 200 μm , error bars SEM $n=4$)

6.6 Effect of rHS02, rHS09 and rHS10 and LS-mHep7 on astrocytes – gap closure

Previously in *Chapter 4* we investigated the effects of LS-mHep7/LS-mHep7L on astrocyte reactivity. One of the hallmarks of CNS injury is that astrocytes move into a reactive phenotype, defined by their upregulation of the intermediate filaments GFAP and nestin, as well as morphological changes, becoming hypertrophic and extending their processes. The poor regenerative capability of CNS axons is also thought to be related to the limited ability of astrocytes to migrate and repopulate the injury site. Indeed, the slow repopulation of the injury site by astrocytes correlates with the failure of injured axons to cross the injury site (**Rhodes 2003, Silver 2004**). Therefore, determining the effect of potential therapeutics on the ability of astrocyte migration and reactivity may help overcome this failure and contribute to CNS regeneration. To investigate if rHS02, rHS09 or rHS10 has any effect on the astrocyte migration of the transition to a reactive astrocytic phenotype, we investigated using an astrocytic scratch injury model.

Neurosphere derived astrocytes were allowed to mature until a confluent monolayer was achieved. A cell free area was created by scratching the center of each cover slip with a pipette tip. Immediately after injury, cells were treated with rHS02, rHS09, rHS10 or LS-mHep7 at 10 ng/ml. Cultures were imaged at 0, 1, 2, 4 and 24 hrs. It was found that like LS-mHep7, rHS10 promoted a faster recovery of astrocyte gap closure at 4 hr compared to untreated astrocytes (**Figure 6.6(a, c)**). Additionally, LS-mHep7 promoted faster gap closure compared to control untreated cultures at 24 hr (**Figure 6.6 (b, c)**). Treatment with rHS09 prevented astrocyte scratch closure with a significantly wider gap width compared to control at both 4 hr and 24 hr (**Figure 6.6 (a, b, c)**).

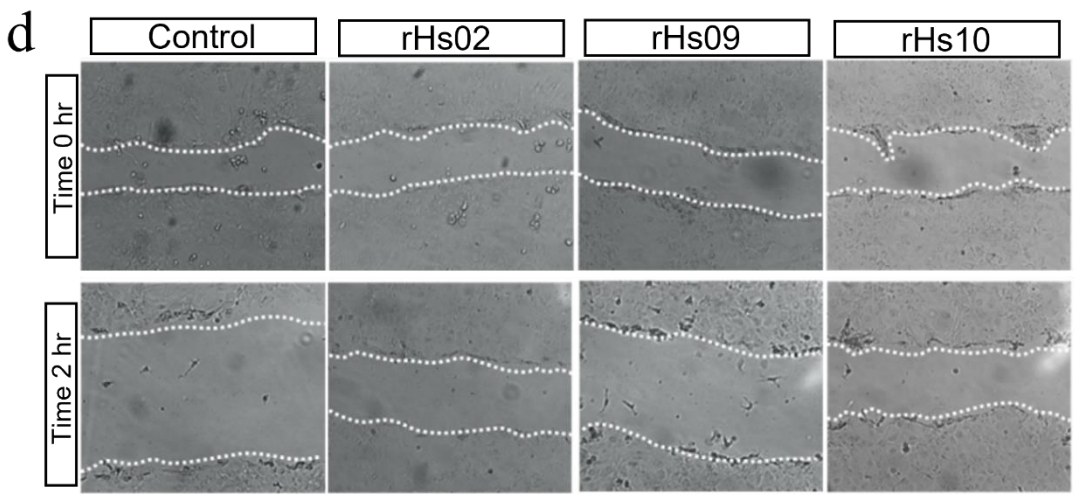
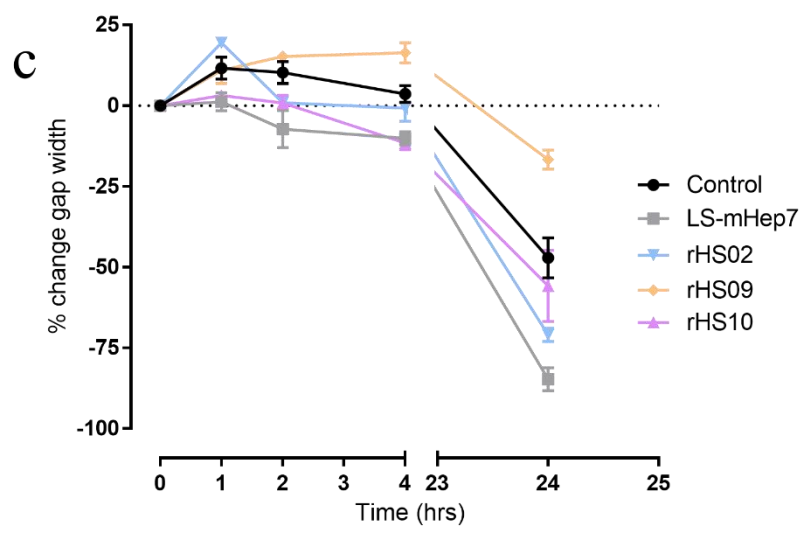
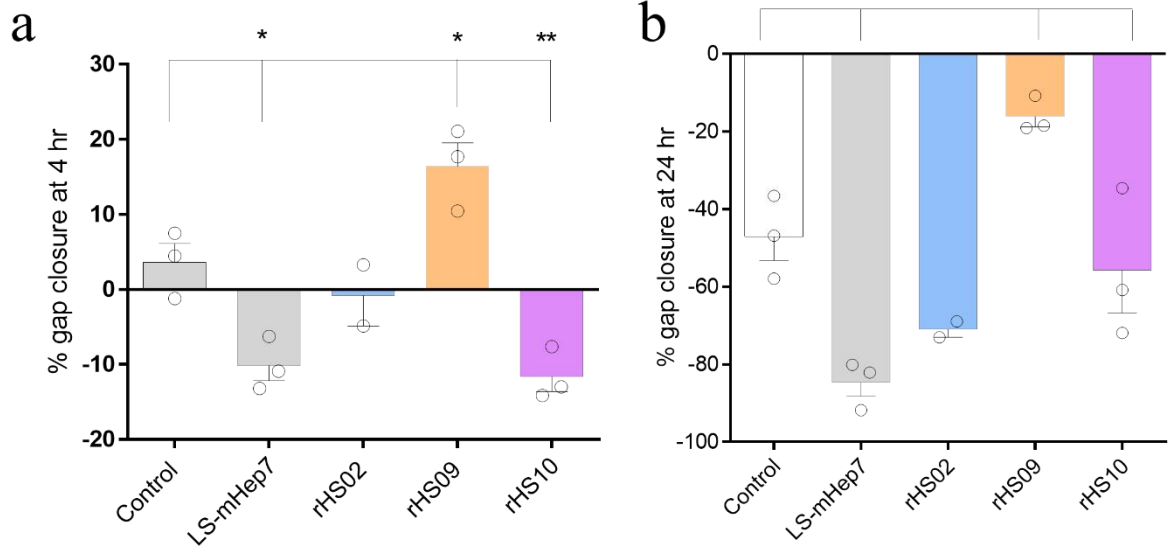


Figure 6.6 |Effect of LS-mHep7, rHS02, rHS09 and rHS10 on astrocyte reactivity after injury. Neurosphere derived astrocytes were allowed to mature until a confluent monolayer was achieved. Once confluent a cell free area was created by scratching the centre of each cover slip. Immediately after injury cells were treated with rHS02, rHS09, rHS10 or LS-mHep7 (10 ng/ml). Measurements of scratch width were made on phase images at 1, 2, 4 and 24 hr following the same injury site over time and gap width is presented as a % of the original width at time 0hr (c). (a) LS-mHep7 and rHS10 promoted a faster closure of gap width at the 4 hr timepoint compared to control cultures, whereas rHS09 caused the gap to become wider. (b) LS-mHep7 promoted a faster recovery of astrocyte gap closure at 24 hr compared to untreated astrocytes, whereas rHS09 significantly prevented closure. (d) Representative phase images of scratch astrocytes immediately after injury (Time 0 hr) or 2 hr after injury (Time 2 hr) in control, rHS02, rHS09 or rHS10 treatment. (two-way ANOVA with Dunnett's multiple comparison, * = $P \leq 0.1$, ** = $P \leq 0.01$ (n = 3; technical replicates = 3)

6.6 Effect of rHS02, rHS09 and rHS10 and LS-mHep7 on astrocyte reactivity – GFAP expression

GFAP expression was investigated to determine astrocyte reactivity after monolayers of astrocytes were scratched. Astrocyte monolayers were injured using a pipette tip and immediately treated with rHS02, rHS09, rHS10 or LS-mHep7 at 100 ng/ml, or left untreated. At each time point 0, 1, 2, 4 and 24 hr, coverslips were either fixed with 4% PFA (and immunolabelled with GFAP/astrocytes, DAPI/ nuclei) or protein lysates were taken for western blot analysis. Quantification of GFAP immunoreactivity immediately adjacent to the lesion edge using global thresholding revealed an increase in GFAP expression 1 and 2 hr after injury in untreated injured cultures (**Figure 6.7a-b**). Additionally cells treated with rHS09 revealed an increase in GFAP immunoreactivity at both 1 and 2 hr post cut compared to uninjured control cultures at 0hr. This increased expression post scratch was not found in LS-mHep7, rHS02 or rHS10 treated cultures with a significant reduction in GFAP staining compared to control 1 hr post-injury in LS-mHep7 and rHS10 treated cultures. This suggests that both LS-mHep7 and rHS10 are reducing astrocyte reactivity in these cells after induced injury immediately at the lesion edge. Quantification of global GFAP expression by western blot showed that after injury there was a significant increase in GFAP expression at 1 and 2 hr after injury compared to uninjured cultures (**Figure 6.7 d-e**). However, there were no significant changes in any of the treatments compared to either uninjured or cut astrocytes, suggesting the changes in GFAP expression are more localised to the lesion edge rather than the entire astrocyte population (**Figure 6.7 c**)

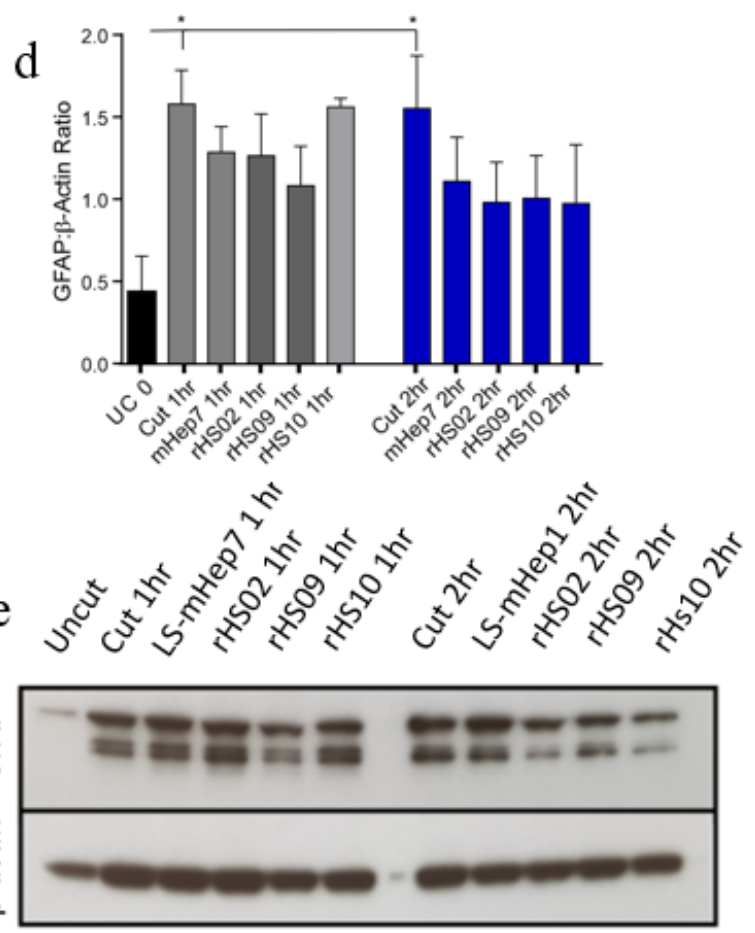
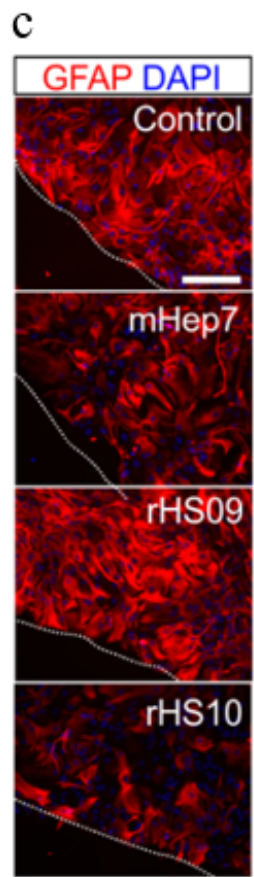
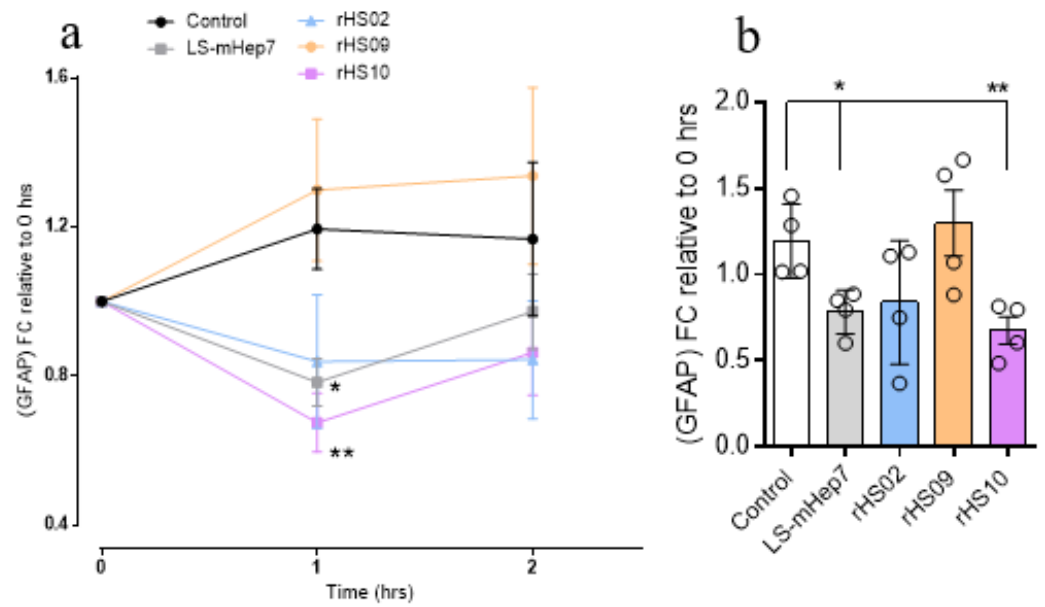


Figure 6.7 |Effect of LS-mHep7, rHS02, rHS09 and rHS10 on astrocyte reactivity after injury (GFAP expression). Neurosphere derived astrocytes were allowed to mature until a confluent monolayer was achieved. Once confluent a cell free area was created by scratching the centre of each cover slip. Immediately after injury cells were treated with rHS02, rHS09, rHS10 or LS-mHep7 (10 ng/ml). At each time point cell lysates were collected and analysed for levels of β -actin and GFAP via western blot. Lysates were collected at 1 and 2 hrs.(a) Quantification of GFAP immunohistochemistry using Image J thresholding of images captured at the lesion edge at 1 and 2 hr post injury, showed an increased in GFAP immunoreactivity in control astrocytes at the lesion edge which was not found in LS-mHep7, rHS02 and rHS10 treated astrocytes. (b) There was a significant reduction in GFAP staining in LS-mHep7 and rHS10 treated astrocytes at 1 hr post injury. rHS09 showed a similar increase in GFAP at 1 and 2 hr to that found in untreated injured astrocytes. (n number represented by individual data points on the graph, ANOVA with Dunnett’s post-test, * $p < 0.05$, ** $p < 0.01$). (c) Representative immunohistochemical images of GFAP immunoreactivity immediately adjacent to the lesion in untreated, LS-mHep7, rHS09 or rHS10 treated cut cultures 1 hr post-injury. GFAP (astrocytes, red), DAPI (nuclei, blue). (d) Quantification of GFAP from protein lysates showed a significant upregulation of GFAP 1 and 2 hr post injury in cut cultures compared to uncut controls. There was no difference in the level of GFAP expression in any treatment of the time points analysed when compared to untreated cut cultures. (n=4, Two-way ANOVA, Dunnett’s post-test, * $p < 0.05$.) (e) Western blot analysis of global GFAP levels in cut astrocytes treated with rHS02, rHS09, rHS10 or LS-mHep7 lysed at 1 and 2 hr post injury. β -actin was used as a loading control. (Dashed line indicates injury edge) (Scale bar represents 50 μ m)

6.8 Discussion

The aim of this chapter was to assess the abilities of rHS to enhance repair in several CNS injury models *in vitro* and *ex vivo* – and to compare this ability to our ‘gold standard’ repair seen with the well-established LS-mHep7. This was to determine if rHS have similar bioactivity in CNS injury models as animal derived heparin mimetics for future therapeutic investigations. Previously in **Chapter 4** and **Chapter 5** we showed that LS-mHep7/LS-mHep7L could enhance repair in *in vitro* CNS injury models. This included enhanced re/myelination after antibody and complement mediated demyelination (MC-DeMy), neurite outgrowth in MC-Inj, and reduced astrocytosis in our astrocyte injury model.

As previously discussed, heparin is currently sourced (80% of global production) from China from porcine intestines (McCarthy *et al.*, 2020). Such reliance on a specific animal source of heparin comes with risk of shortage; in 2007, massive out-breaks of porcine reproductive and respiratory syndrome resulted in a worldwide heparin shortage. Concern and risk for alternative animal heparin sources exists. Before the use of porcine intestines, heparin was sourced from bovine, but in the late 1980s, bovine spongiform encephalopathy (BSE, or

“mad cow disease”) was reported first in the United Kingdom and later in several other countries, raising concerns about the use of bovine-sourced heparin products in humans. Soon after bovine sourced heparin was banned. Production of Administration in the United States continues to address concerns about foreign heparin production and its quality control (Committee on Energy and Commerce, 2016). In 2008, non-naturally occurring over-sulphated chondroitin sulphate (OSCS) in heparin led to over 200 deaths worldwide and more than 800 reports of serious hypertension and adverse allergic reactions (**Kishimoto *et al.*, 2008**). An alternative to animal derived heparin is to source heparin from cell lines, creating recombinant heparins. TEGA pharmaceuticals (San Diego) through mammalian cell multiplex genome engineering, can direct cellular synthesis of heparin and HS (**Thacker *et al.*, 2022**) and has a library of HS compositions available commercially. Thus, these cells provide an important alternative for commercial human clinical use, as they can be grown in serum-free medium, and under GMP control. The production of these recombinant heparins by TEGA pharmaceuticals observes high batch-to-batch consistency alongside laboratory confirmed sulphate content, chain length and purity. This therefore has the potential to be a clinically relevant source of HS mimetics, which would allow an easier transition to the clinic. We were provided a panel of rHS from TEGA pharmaceuticals to determine their effects in models of CNS injury (see **Figure 6-1** for composition comparison).

In the MC-DeMy cultures we observed that rHS10 significantly promoted re/myelination. Interestingly, rHS10 (~90 *N*-sulphate groups per 100 disaccharides) which has similar disaccharide composition and sulphate composition to the well-established LS-mHep7 (~ 95 *N*-sulphate groups per 100 disaccharides) suggests that *N*-sulphation could be important for promoting re/myelination after injury. *N*-sulphation is already known to be essential in mediating specific protein interactions (**Roy *et al.*, 2014**)

Additionally, rHS02 was found to significantly promote re/myelination, but was less efficacious than rHS10 as shown by fold change analysis. When comparing the two rHS we can see that rHS02 also receives most of its sulphate groups via *N*-sulphation, however, has ~55 *N*-sulphate groups per 100 disaccharides compared to rHS10 and LS-mHep7 which have ~90 and ~95 *N*-sulphated groups per 100 disaccharides, respectfully. In SC-DeMy, we again observed that rHS10 enhanced re/myelination alongside LS-mHep7, to very similar levels. This further supports that *N*-sulphation is important for promoting re/myelination after injury since both these reagents enhance repair in a similar manner.

In MC-Inj rHS09 promoted neurite outgrowth alongside LS-mHep7. In **Chapter 4** we observed that LS-mHep7 strongly promoted neurite outgrowth across the cell free area

created by the blade. Interestingly however, rHS09 has the highest sulphation across the rHS panel, and previously we hypothesised that only LS-mHeps promoted neurite outgrowth. This contradicts previous work with mHeps where LS-mHeps enhance neurite outgrowth and HS-mHeps did not. It has been postulated that there is a sulphation code that regulates axon guidance as other HSs with varying sulphation modifications disrupts axons guidance (**Holt and Dickson, 2005**). Previously the Barnett lab shown that heparins bearing one sulphate substitution per repeating disaccharide unit at either the 2-*O*- or *N*-sulphated positions promote neurite outgrowth (**McCanney et al., 2019**) The alteration of sulphation on the uronic acid in various ways may contribute to the HS to either promote or negate neurite outgrowth by modifying various factors that play a role in the biological process. For example, *Caenorhabditis elegans* mutants which lack the enzymatic activity of 2-*O*-sulphation, display axonal patterning defects, confirming the importance of 2-*O* sulphation in neurite outgrowth and pathfinding (**Kinnunen et al., 2005**). Additionally, other HS have shown that different sulphation modifications disrupt axons guidance in the *Xenopus* visual system, with 2-*O*- and 6-*O*-sulphated HS showing marked effects (**Irie et al., 2002**).

The poor regenerative capability of CNS axons is thought to be related to the limited ability of astrocytes to migrate and repopulate the injury site. Indeed, the slow repopulation of the injury site by astrocytes correlates with the failure of injured axons to cross the injury site (**Rhodes et al., 2003; Silver and Miller, 2004**). Therefore, determining the effect of potential therapeutics on the ability of astrocyte migration and reactivity may help overcome this failure and contribute to CNS regeneration. While investigating rHSs effect on astrocyte reactivity in our injury models, we examined gap closure within our scratch assay. Astrocytes become reactive and secrete inflammatory molecules that modify the environment after CNS injury or disease (**Choi et al., 2014; Mizee et al., 2014; Jo et al., 2014; Yi et al., 2014**). Our analysis revealed that LS-mHep7 and rHS10 promoted gap closure at early time points. A proposed mechanism is the relationship between HSPGs, FGFs, and astrocytic outgrowth. FGFs are known heparin-binding growth factor (such as FGF-2) and bind to HSPGs on the cell surface and within the extracellular matrix (**Chua et al 2004; Fortsen-Williams, 2005**). FGFs are known to modulate many glial activity including astrocytic outgrowth and scar formation (**Santos-Silva et al., 2007**), OPC proliferation (**Chandran et al., 2003**) and differentially regulate maturation and proliferation of stem cell-derived astrocytes (**Savchenko et al., 2019**). Here, LS-mHep7 and rHS10 could be interacting with FGF-1/FGF-2, inducing astrocytic outgrowth and proliferation. Additionally, we observed rHS09 (the most highly sulphated compound in the panel) reducing gap closure, creating a larger cell free area compared to the initial control lesion.

Previously it has been demonstrated that highly sulphated heparan sulphates negatively repair injury in the CNS (McCanney *et al.*, 2019) and induce strong boundaries between olfactory ensheathing cells (OECs) and astrocytes (Higginson *et al.*, 2012; Santos-Silva, 2008), which was not observed with low sulphated forms. With these observations, boundary formation was dependent on *O*-sulphation, since *N*-acetylated heparin (in which *N*-sulphates are replaced with *N*-acetyl groups) also induced boundary formation. We can hypothesize that *O*-sulphation sulphation level is a major contributor to the astrogliosis modulation observed by LS-mHep7 and rHS10 as these molecules have similar *O*-sulphation levels compared to the other heparan sulphate molecules.

Astrocyte reactivity was determined via GFAP expression in our cultures. After severe activation, astrocytes secrete various neurotoxic substances and express an enhanced level of GFAP which is considered a marker protein for astrogliosis (Eng and Ghirnikar, 1994). Previously, we have found little evidence of GFAP modulation following LS-mHep7 treatment in astrocyte scratch assays assessed by western blots (McCanney *et al.*, 2019). Global GFAP saw no significant changes in any of the treatments compared to either uninjured or cut astrocytes, however, thresholding analysis of GFAP staining intensity immediately at the lesion edge showed that the low-sulphated compounds (LS-mHep7 and rHS10) reduced GFAP immunoreactivity at early time points. This suggests that changes in GFAP expression are more localised to the lesion edge rather than the entire astrocyte population. Non-stimulated astrocytes in culture expressed eight cytokines, including G-CSF, GM-CSF, GRO α (CXCL1), IL-6, IL-8 (CXCL8), MCP-1 (CCL2), MIF and Serpin E1. Following stimulation, activated astrocytes newly produced IL-1 β , IL-1ra, TNF- α , IP-10 (CXCL10), MIP-1 α (CCL3) and RANTES (CCL5) (Choi *et al.*, 2014). As discussed in previous chapters, LS-mHeps modulate CCL5 activity in MC-DeMy and SC-DeMy and has high affinity binding to LS-mHep7/L. CXCL10, was identified as LS-mHep7 binding in *Chapter 5* and could be sequestered and modulated in the astrocyte injury model leading to reduced communications and molecular pathways that lead to astrocyte reactivity.

An important consideration to make while comparing the rHS to LS-mHeps is the molecular weight and size of the recombinant molecules – especially for the use in therapeutics. As discussed in previous chapters, molecular weight is important for novel molecules in CNS, to cross the BBB, and for better bioavailability (Merli *et al.*, 2010). The approximate molecular weight of rHS02 (~40kDa) and rHS10 (~40kDa) being almost four times, and rHS09 (~20kDa) being twice as large as LS-mHep7 (~12kDa) could potentially explain why LS-mHep7 appears the most efficacious for repair across the myelinating culture screens.

Studies into the use of heparin as a cancer therapeutic demonstrated improved survival in patients treated with low molecular weight heparin (~6kDa) compared to standard heparin (~15kDa) (**Khorana *et al.*, 2004**). Heparin inhibited endothelial cell proliferation but had no effect on endothelial tube formation, whereas LMWH with a mean molecular weight of ~6 kDa had greater inhibitory effects on proliferation and reduced tube formation. Therefore, the importance of molecular weight of the rHSs in terms of the repair potential requires further investigation.

In conclusion, this chapter has shown that recombinant HS derived mimetics have the potential to be beneficial for CNS repair. In particular, the low-sulphated compound, rHS10, promoted re/myelination and modulated astrocyte reactivity like LS-mHep7, while the highly sulphated, rHS09, promoted neurite outgrowth. This confirms the importance of HS sulphation for CNS repair and provides excellent preliminary evidence of the *in vitro* repair benefits of rHS compounds.

Chapter 7

Discussion

7.0 General Discussion

The overall aim of this PhD was to validate a low molecular weight version of our lead compound LS-mHep7, to enhance repair in the CNS. To validate this low molecular weight compound – LS-mHep7 – we investigated its ability to enhance repair in several *in vitro* CNS models including MC-DeMy, MC-Inj and an astrocyte scratch assay. Additionally, we optimised a method for culturing *ex vivo* slice cultures for remyelination studies, to validate LS-mHep7L in a cellularly more complex model of CNS demyelination (SC-DeMy).

There are three principal findings of this thesis: 1) spinal cord slice cultures from P0-2 mice can produce successful cultures for the study of remyelination and screening of novel therapeutics for CNS disease. 2) LS-mHep7L can enhance repair in both *in vitro* and *ex vivo* models of CNS injury. 3) recombinant heparan sulphate mimetics are able enhance repair in both *in vitro* and *ex vivo* models of CNS injury – providing an additional source for heparin derived therapeutics.

7.1 Limitations of the study

There are several limitations to this study that need to be considered and discussed. Firstly, all *in vitro* studies in this thesis (including MC-DeMy, MC-Inj, MC-Dev and astrocytic scratch assays), do not replicate the *in vivo* environment. Although most glial cells are found to be present in all the myelinating cultures (**Boomkamp *et al.*, 2012**), their numbers are unlikely to be comparable to those found *in vivo*. This could have heavy implications for remyelination studies, as plenty of literature links other glial cells e.g. microglia to influence remyelination and intercellular communications could differ.

Although some of these limitations were overcome in **Chapter 5** with the addition of the *ex vivo* spinal cord slice cultures, many key features to a degenerating/ injured CNS microenvironment were still missing. For example, while culturing these spinal cord slices, the media was changed every 2-3 days to allow fresh nutrients to be delivered for successful cell survival, however, when this is performed, old media containing cytokines and chemokines that are released during injury (are therefore maintained *in vivo*) are taken away. *In vivo* at the site of injury however, the chemokine microenvironment is likely to be different with the contained influx of cytokines and chemokines that are released (**Garcia *et al.*, 2016; Lock *et al.*, 2002; Morganti-Kossmann *et al.*, 1997**)

These important factors could change the effectiveness of novel therapeutics *in vivo* and so this must be taken into consideration while validating the effectiveness of mHeps and rHSs to remyelinate and repair the CNS.

We must consider that the tissue used within **Chapter 5** was taken from young mice (P0-2), as we struggled to effectively maintain slice cultures from older animals. It is known that remyelination is more efficient in younger animals than older ones, and therefore this can make improvements in remyelination difficult to detect. This should be acknowledged when screening pro-remyelination therapeutics (such as the LS-mHeps and rHSs) as these are being sought mostly for translation into therapies for adult human patients where remyelinating abilities may be reduced due to age. Additionally, when setting up these *ex vivo* cultures, chopping spinal cord slices damages the tissue at these surfaces, which can affect both axons and myelin. This variability must be considered while studying the influence of therapeutics that induce or accelerate myelination. Furthermore, variability within the slice must also be considered as sagittal slices of the spinal cord will have differing amounts of white and grey, matter.

7.1.1 Effective models of CNS injury?

Another limitation for using animal models to screen compounds for CNS repair is that there is no one models that can replicate the intricacy of the molecular pathways involved in the CNS. For example, there is no single animal model that can capture the entire spectrum of heterogeneity of human MS, and its variety in clinical and radiological presentation. Here we have used two pathways to induce demyelination in our cultures – lysolecithin and antibody mediated demyelination. However, when it comes to injury of the human CNS system, are either approaches relevant to disease pathology? In the case of MS – the presence of PNS immune cells is a critical highlight in MS biology along with inflammation, immune surveillance, and immune-mediated tissue injury. None of the *in vitro* or *ex vivo* models described in this thesis incorporate the cellular complexity seen human MS pathology. However, toxin induced demyelination models (such as our *ex vivo* spinal cord slice cultures) do not attempt to mimic MS as a disease but are mainly established as systems to study the process of focal demyelination and remyelination (**Blakemore et al., 2008**). Additionally, it be argued that MC-Inj does not replicate spinal cord injury, and is not an effective model of SCI. This injury model lacks many cellular pathways seen *in vivo*, lacks the contained release of chemokine and cytokine release from cellular injury observed in SCI (due to continuous changing of media) and again lacks any PNS cells, such as lymphocytes, that have access lesions of SCI (**Beck et al., 2010**). Like with many *in vitro* models of disease, we are merely attempting to model aspects of SCI, including demyelination, reduced neurite

density adjacent to the lesion, infiltration of microglia and reactive astrocytes into the lesioned area – which are all seen in this model (**Boomkamp *et al.*, 2012**). With this, MC-Inj does provide an excellent *in vitro* model to screen potential candidates for CNS repair to later be used in animal *in vivo* models that can better replicate SCI.

7.2 Reparative compounds for CNS injury

7.2.1 Multiple sclerosis

Nine classes of DMTs with varying mechanisms of action and routes of administration, are available for RRMS, and only one for PPMS - called ocrelizumab (Ocrevus). Current therapies only reduce CNS inflammation, decreasing the frequency of attacks and preventing further damage but do not tackle disabling symptoms that are currently irreversible. The key promise to a remyelination therapeutic would be to repair the myelin sheaths damaged by MS and therefore restore some of the patients' key functions, such as mobility, cognition, or vision. There are currently no DMT's for MS that focus on remyelination – however recently there have been novel compounds/molecules going through clinical trials that focus on different strategies for remyelination. These include the Lingo-1 antibody (Opicinumab (Biogen)) (**Cadavid *et al.*, 2019**)– which focuses on OPC maturation; a myelin protein stimulant (BIIB061 (Biogen)) and highly concentrated biotin (MD1003) (MedDay Pharmaceuticals) (**Cree *et al.*, 2020**) which focuses on increasing activation of cellular processes in oligodendrocytes to produce myelin. However, in October 2020 Biogen halted the development of opicinumab, as in the Phase 2 affinity trial, the trial drug did not promote significant functional improvements or delay disability progression, when compared with placebo. This really highlights the need for the development of novel compounds for remyelination – such as the potential future use of LS-mHep7. Many novel therapeutics do not successfully progress through clinical trials, due to many reasons, but often due to the negative side effects and cost of the drugs (**Fogel, 2018**). LS-mHep7 is derived from heparin, which is already an FDA approved pharmaceutical, with relatively low cost. This makes heparin an exciting candidate for a novel remyelinating therapeutic -if successful in future work.

Remyelination is typically incomplete in patients with MS (**Prineas *et al.*, 1979**). An analysis of MS patient's shadow plaques displayed that extensive remyelination occurs in a subset of patients (**Patrikios *et al.*, 2006**). From patients investigated, 20% of them had extensive remyelination with 60-96% of the global lesion area being remyelinated. This extensive remyelination was associated with older age at death. This data suggests that patients that have better remyelination have better outcomes. Therefore, a remyelinating

therapeutic would be beneficial for patients that have a lower extent of spontaneous remyelination and could increase life duration reduce disease progression. A novel remyelinating therapeutic could work as successful combination therapy alongside current DMT's for MS, to help repair damage that has occurred during a relapse during RRMS and as a continuous therapy for PPMS.

7.2.2 Spinal cord injury

After SCI, long tracts of the injured spinal cord may survive, but become demyelinated. The ultimate objective of SCI is the regeneration of spinal cord axons to restore movement and mobility. In many patients with non-penetrating SCI a population of surviving axons remains at the injury site but do not conduct impulse due to demyelination. Spontaneous remyelination is well known to occur after SCI (**Bartus *et al.*, 2019**), but the efficiency of that process remains a matter of debate and therapeutics to enhance this repair would be hugely beneficial for patient's locomotor recovery. In terms of SCI, new therapeutics must include cell survival, axonal growth, remyelination and synapse formation. Over the last decade, researchers have been investigating molecules and compounds for regenerative therapies in SCI. However, despite this active research and clinical studies, there is no effective and globally accepted standard treatment for SCI. A major impediment to recovery after an SCI is the absence of meaningful axonal regeneration, hence, the mechanisms that govern axonal regeneration have been intensively investigated. Clinical trials have evaluated agents that can neutralize axonal growth inhibitors, such as the Rho-ROCK inhibitor (**Fehlings *et al.*, 2021**), Cethrin/VX-210 (**Fehlings *et al.*, 2018**), and anti-NOGO monoclonal antibody (**Kucher *et al.*, 2019**). However, none of these agents have become successful in terms of an approved therapeutic for SCI. Additionally, investigations into stem cell therapies have recently gone through human trials (**Curtis *et al.*, 2018**). Currently, strategies to promote remyelination after SCI are largely limited to cellular transplantation (**Assinck *et al.*, 2017**), which has additional risks. These risks include migration of cells to other areas of the CNS (**Steward *et al.*, 2014;Tuszynski *et al.*, 2014**), administration of trophic factors that are necessary for graft survival which can instigate sensory dysfunction (**Gold *et al.*, 2010**), poor survival of transplanted cells (**Anderson *et al.*, 2017**) and differentiation into unwanted, nonregenerative cell types (**Nguyen *et al.*, 2017**). Additionally, stem cell therapies are incredibly invasive and often expensive on health services. This highlights the importance of novel therapeutics such as heparin mimetics that are already FDA approved, non-invasive and generally low cost in comparison to stem cell therapies. These LS-mHeps could prove promising for neural regeneration as seen in *in vitro* studies, as they work on

the many failings of SCI including neuronal outgrowth and remyelination and reduce astrogliosis and potential reduction in the glial scar. Because SCI impacts nearly every aspect of daily activities, even partial restoration of motor function may improve patients' autonomy and enhance quality of life.

7.3 Low molecular weight heparin mimetics

One of the main aims of this thesis was to determine the abilities of a low molecular weight version of our lead compound LS-mHep7 to enhance repair in the CNS. This was performed with the understanding that low molecular weight molecules have a higher probability of crossing the BBB – a limiting factor for novel therapeutics of the CNS. The BBB prevents the uptake of most pharmaceuticals, which arises from the epithelial-like tight junctions within the brain capillary endothelium. Even in the case of LMW molecules it is thought that ~98% of all small molecules are still prevented from crossing the BBB (**Pardridge, 2005**). Although in this thesis we provide evidence of LMW heparin mimetics enhancing CNS repair – these molecules may still be too big to cross an undisturbed BBB. LS-mHep7L is approximately ~7kDa in size, however reports suggest that for molecules to cross the BBB (mainly via lipid-mediated free diffusion) the molecules must be ~400Da and only form ~8 hydrogen bonds (**Pardridge, 2012**). However, in a rodent pharmacodynamic model, which used CSF concentration and brain deposition as a read-out, it was demonstrated that following intravenous and subcutaneous delivery, ultralow-MW heparin - average MW of 2 kDa (6- 8mers) - crossed the BBB (**Ma et al., 2002**). In the case of demyelinating diseases such as MS, however, there is breakdown of the BBB during MS pathology (which is often a criterion for disease progression) (**Polman et al., 2011**), which suggest that our LMW heparin mimetics could have the potential to access the CNS. If able to cross the BBB, continual administration of HS mimetics would most likely need to occur and would most likely only result in the compounds accessing the CNS in areas of inflammation and damage. Of course, the efficacy of this strategy would depend on the absence of adverse off-target effects from prolonged treatment.

7.4 Clinical use of heparin mimetics

A main challenge to overcome for heparin to be re-purposed as a therapeutic for CNS injury is the source from which the compounds are generated. We have previously discussed that most of the world heparin is sourced from pigs, and that world shortages occur. However, the purification of heparin is also of concern. Heparin being sourced from animal tissue,

requires HS purification, and purification and separation of GAGs is notoriously difficult. The extraction and purification processes of heparin from porcine tissue consist of 1) tissue autolysis 2) tissue digestion 3) precipitation of impurities 4) removal of molecules weight of less than 3,000 daltons by ultrafiltration 5) fractional precipitation of contaminating glycosaminoglycans and 6) further purification of the obtained heparin by anion exchange chromatography (**van der Meer et al., 2017**). Contaminating GAGs have been related with adverse complications following heparin treatment, with the US Food and Drug Administration reporting 149 deaths associated with heparin contamination between 2007-2008 (**Pan et al., 2010**). Over sulphated chondroitin sulphates have been identified as one of these contaminants (**Kishimoto et al., 2008**). CSPGs are known to be inhibitory to axon growth *in vitro* (**McKeon et al., 1991; Smith-Thomas et al., 1994; Niederos et al., 1999**), and chondroitinase have been found to promotes functional recovery after spinal cord injury (**Bradbury et al., 2002**). Introduction of these contaminants into SCI patients could be incredibly detrimental to their recovery. The time and effort required to remove all these contaminants - which have safety implications for patients - from naturally derived heparin, prompts the need to develop an alternative source of heparin. This highlights the importance for investigating recombinant heparin mimetics-with incredibly high purity- for the use of heparin mimetics for CNS repair. TEGA therapeutics have demonstrated that production of rHS using optimised bioreactors can substantially improve GAG production. rHS have high batch-to-batch consistency alongside laboratory confirmed sulphate content, chain length and purity. Cellular production also offers an animal free source and allows the entire supply chain to be under GMP control (**Glass et al., 2018**).

7.5 Future work

The data established in this thesis has provided exiting results in terms of pre-liminary data for a novel therapeutic for remyelination and repair in CNS injury. There is currently a huge demand for novel therapeutics of the CNS, and the screening of these glycoproteins has created a new insight into re-purposing FDA approved drugs (such as heparin) to be multi-functional in human disease. However, the mechanisms to how these heparan sulphate mimetics are eliciting their reparative effects is still relatively unknown. We have established that one mechanisms of use could be via the sequestering of negative regulators of myelination such as CCL5, however this doesn't explain the mechanisms behind re/myelination observed in our *ex vivo* cultures, as CCL5 appeared to only affect developmental myelination.

7.5.1 Oligodendroglia populations: Flow cytometry

To better understand the mechanisms behind repair observed in SC-DeMy, it will be important to investigate oligodendroglia populations during this re/myelination process. LS-mHeps could be involved in the increase of OPC proliferation, resulting in more mature myelin producing cells available for remyelination. Additionally, they could be involved in OPC differentiation into myelin producing cells, or they could be helping resident mature oligodendrocytes to remyelinate. Currently we are unable to make a sound hypothesis without further investigations. Flow cytometry is a powerful technique for analysing and sorting cell populations based on their physical and molecular characteristics. By using specific antibodies or fluorescent dyes, we can identify and quantify oligodendrocytes within a heterogeneous cell population. Flow cytometry could provide information about oligodendrocyte subtypes, cell surface markers, and cellular properties. This will allow us to identify changes in oligodendrocyte population with the treatment of LS-mHeps during the remyelination process. Additionally primary oligodendrocyte cultures can also be prepared from brain tissue, which allows for the isolation and maintenance of oligodendrocytes *in vitro*, providing a controlled system for this study.

7.5.2 Movement across the BBB: Cuprizone model

Additionally, it is important for us to establish if LS-mHep7L can cross the BBB *in vivo*. Our lab is currently investigating the use of LS-mHeps in an EAE model, however in this experimental model of demyelination the BBB is disrupted and is 'leaky', compromising the close off CNS system from the periphery. Therefore, we are not able to say with certainty that the LS-mHeps are crossing the BBB due to their LMW and instead could be passing through via disruption. One way that we can investigate this is by using the Cuprizone model of demyelination instead of EAE, alongside the production of a fluorescently tagged LS-mHep7L that we can visualise crossing the BBB in histology samples. The BBB in the cuprizone model is not compromised, meaning that any LS-mHep7 that crosses has occurred via transport of some sort. With a fluorescently tagged version of our mHeps we can then determine through histology if and where these mHeps are in the CNS tissue. However, it must be noted that tagging a molecule with a fluorescent label could increase its molecular weight and therefore make it difficult for LS-mHep7L to cross the BBB. The confirmation of LS-mHep7L to cross into the BBB is an important factor to establish before moving into any expensive *in vivo* research, and further clinical investigations.

7.5.3 LS-mHeps and microglia

This thesis investigated the effects of LS-mHeps and glial cells such as astrocytes and their reactivity, however little was investigated in other glial cells such as microglia. As stated previously in this thesis, microglia play an important role in the CNS and are involved in the clearance of myelin debris, detect and respond to demyelination cues and transition between phenotypic states (pro-inflammatory to pro-regenerative). The different phenotypes are observed to secrete different cytokines and chemokines that are essential for these roles; pro-inflammatory secretions include iNOS⁺ TNF α ⁺ CCL2⁺, while pro-regenerative microglia secretions include Arg-1⁺ CD206⁺ IGF-1⁺. To investigate if LS-mHeps have a role in reducing or increasing microglia activity, microglia can be cultured and then exposed to Granulocyte-macrophage colony-stimulating factor (GM-CSF), which stimulates microglia into a reactive state. With the addition of LS-mHeps at this time we can then collect supernatant from these cultures and perform ELISAs for specific chemokines and cytokines levels such as IL-23, IL-6 and IL- β . Additionally we can label these microglia for analysis via FCAS to determine a change in populations between those treated with GM-CSF and LS-mHeps or GM-CSF alone. This could help us determine if LS-mHeps help reduce leucocyte recruitment *in vivo* and determine if LS-mHeps are involved in microglia reactivity.

7.5.4 Zebrafish and SCI

Although preliminary data is currently being produced by the Barnett group to investigate both LS-mHep7 and LS-mHep7L in an established EAE model (**Lindsay *et al.*, 2022**), it will be important to test these mimetics in other *in vivo* models of the CNS injury, such as dorsal incisions of larvae zebrafish as a model for SCI (**Keatinge *et al.*, 2021; El-Daher & Becker 2020**), to demonstrate that LS-mHeps can repair a variety of CNS injury. In this thesis we have investigated neurite outgrowth *in vitro*, however as stated above, although it does mimic some aspects of SCI (such as focal demyelination and astrocyte reactivity), it does not reflect SCI *in vivo*. Zebrafish possess a remarkable ability to regenerate their spinal cord after injury. Unlike mammals, zebrafish can regenerate functional neurons and restore motor function following a spinal cord injury. This regenerative capacity makes zebrafish an excellent model to study the cellular and molecular mechanisms underlying spinal cord regeneration. Zebrafish embryos are small and optically transparent, making them amenable to advanced imaging techniques. Future research could combine live imaging approaches, such as confocal microscopy or two-photon microscopy, to study the dynamics of spinal cord neurons, axonal growth cones, and synapse formation which would provide valuable

insights into the cellular behaviours and interactions occurring during spinal cord development and regeneration in the presence of LS-mHeps.

7.6 Concluding remarks

The results of this thesis demonstrated that low sulphated heparin mimetics have the potential to become novel therapeutics for remyelination and neurite outgrowth for diseases and injury of the CNS. Heparin is currently an FDA approved drug with few side effects on patients making them a relatively safe drug for use. Although LS-mHeps themselves are unlikely to be primary therapeutic drug for demyelinating disease such as MS, they could provide an excellent combination drug along side a drug that reduced relapses, allowing the mHeps to help in remyelination of demyelinated lesions in the brain and spinal cord. This could have a huge impact on patients with MS, especially for those with PPMS, where there is currently only one (very recently approved) DMT that has limited success and aims to reduce leukocyte recruitment instead of improving remyelination. Additionally, this thesis optimised an *ex vivo* slice culture system using mouse spinal cords that can be an excellent screening technique for new drugs in remyelination studies, as well as help study glial development, proliferation, and differentiation without the cost that *in vivo* work requires. *Ex vivo* screening allows for the rapid and cost-effective evaluation of many compounds in the early stages of drug discovery. This initial screening helps identify promising candidates that have the potential to be further developed into effective drugs. Additionally, a good screening system helps reduce the reliance on animal models for initial drug testing. By providing valuable data on drug efficacy, toxicity, and pharmacokinetics, *ex vivo* systems can aid in the selection and prioritization of compounds for further testing in animals, minimizing the number of animals used in preclinical research.

References

- Abbott, N. J., Rönnbäck, L. and Hansson, E. (2006)** ‘Astrocyte-endothelial interactions at the blood-brain barrier’, *Nature Reviews Neuroscience*, 7(1), pp. 41–53. doi: 10.1038/nrn1824.
- Abreu SL. (1982)** Suppression of experimental allergic encephalomyelitis by interferon. *Immunol Commun.* 1982;11(1):1-7. doi: 10.3109/08820138209050718. PMID: 6178681
- Ahmed, S. M. U. et al. (2017)** ‘Nrf2 signalling pathway: Pivotal roles in inflammation’, *Biochimica et Biophysica Acta - Molecular Basis of Disease*. Elsevier B.V., 1863(2), pp. 585–597. doi: 10.1016/j.bbadis.2016.11.005.
- Aikawa, J. I. et al. (2001)** ‘Multiple isozymes of heparan sulfate/heparin GlcNAc N-deacetylase/GlcN N-sulfotransferase. Structure and activity of the fourth member, NDST4’, *Journal of Biological Chemistry*. © 2001 ASBMB. Currently published by Elsevier Inc; originally published by American Society for Biochemistry and Molecular Biology., 276(8), pp. 5876–5882. doi: 10.1074/jbc.M009606200.
- Al-Bachari, S. et al. (2020)** ‘Blood–Brain Barrier Leakage Is Increased in Parkinson’s Disease’, *Frontiers in Physiology*, 11(December), pp. 1–12. doi: 10.3389/fphys.2020.593026.
- Albert, M. et al. (2007)** ‘Extensive cortical remyelination in patients with chronic multiple sclerosis’, *Brain Pathology*, 17(2), pp. 129–138. doi: 10.1111/j.1750-3639.2006.00043.x.
- Allen, N. J. et al. (2012)** ‘Astrocyte glypicans 4 and 6 promote formation of excitatory synapses via GluA1 AMPA receptors’, *Nature*. Nature Publishing Group, 486(7403), pp. 410–414. doi: 10.1038/nature11059.
- Alturkustani, M. et al., (2016).** Acute hypoxic-ischemia in cardiac arrest encephalopathy causes only minimal demyelination. *Neuropathology*. 2016 Oct;36(5):413-420. doi: 10.1111/neup.12287. Epub 2016 Mar 2. PMID: 26932424.
- Anderson, K. D., Sharp, K. G. and Steward, O. (2009)** ‘Bilateral cervical contusion spinal cord injury in rats’, *Experimental Neurology*, 220(1), pp. 9–22. doi: 10.1016/j.expneurol.2009.06.012.
- Andersson, A. and Karlsson, J. (2004)** ‘Genetics of experimental autoimmune encephalomyelitis in the mouse’, *Archivum Immunologiae et Therapiae Experimentalis*, 52(5), pp. 316–325. doi: 10.1002/0471142735.im1501s77.Experimental.
- Anderson A.J., et al (2017)** Preclinical efficacy failure of human CNS-derived stem cells for use in the pathway study of cervical spinal cord injury. *Stem Cell Reports* 8, 249, 2017
- Arababadi, M.K., Hassanshahi, G., Azin, H., Salehabad, V.A., Araste, M., Pourali, R. and Nekhei, Z., 2010.** No association between CCR5-Δ32 mutation and multiple sclerosis in patients of southeastern Iran. *Laboratory Medicine*, 41(1), pp.31-33
- Aricescu, A. R. et al. (2002)** ‘Heparan Sulfate Proteoglycans Are Ligands for Receptor Protein Tyrosine Phosphatase σ ’, *Molecular and Cellular Biology*, 22(6), pp. 1881–1892. doi: 10.1128/mcb.22.6.1881-1892.2002.

- Arieff**, A. I. (1981) ‘Rapid correction of hyponatremia: Cause of pontine myelinolysis?’, *The American Journal of Medicine*, 71(5), pp. 846–847. doi: 10.1016/0002-9343(81)90379-X.
- Ashammakhi**, N. et al. (2019) ‘Regenerative Therapies for Spinal Cord Injury’, *Tissue Engineering - Part B: Reviews*, 25(6), pp. 471–491. doi: 10.1089/ten.teb.2019.0182.
- Assinck**, P., et al. (2017). Cell transplantation therapy for spinal cord injury. *Nat Neurosci* 20, 637–647 <https://doi.org/10.1038/nn.4541>
- Barnett**, M. H. and Prineas, J. W. (2004) ‘Relapsing and Remitting Multiple Sclerosis: Pathology of the Newly Forming Lesion’, *Annals of Neurology*, 55(4), pp. 458–468. doi: 10.1002/ana.20016.
- Barnett**, S. C. and Linington, C. (2013) ‘Myelination: Do astrocytes play a role?’, *Neuroscientist*, 19(5), pp. 442–450. doi: 10.1177/1073858412465655.
- Batoulis**, H. et al. (2011) ‘Experimental autoimmune encephalomyelitis - achievements and prospective advances’, *Apmis*, 119(12), pp. 819–830. doi: 10.1111/j.1600-0463.2011.02794.x.
- Barber** PC (1982). Neurogenesis and regeneration in the primary olfactory pathway of mammals. *Bibliotheca Anatomica*. 1982 (23):12-25. PMID: 7138487.
- Bartus**, et al.(2019) ErbB receptor signaling directly controls oligodendrocyte progenitor cell transformation and spontaneous remyelination after spinal cord injury. *Glia*. 2019; 67: 1036– 1046. <https://doi.org/10.1002/glia.23586>
- Beattie**, M. S., Li, Q. and Bresnahan, J. C. (2000) ‘Cell death and plasticity after experimental spinal cord injury’, *Progress in Brain Research*, 128, pp. 9–21. doi: 10.1016/S0079-6123(00)28003-5.
- Beck**, J. et al. (1988) ‘Increased production of interferon gamma and tumor necrosis factor precedes clinical manifestation in multiple sclerosis: Do cytokines trigger off exacerbations?’, *Acta Neurologica Scandinavica*, 78(4), pp. 318–323. doi: 10.1111/j.1600-0404.1988.tb03663.x
- Beirowski**, B. et al. (2004) ‘Quantitative and qualitative analysis of Wallerian degeneration using restricted axonal labelling in YFP-H mice’, *Journal of Neuroscience Methods*, 134(1), pp. 23–35. doi: 10.1016/j.jneumeth.2003.10.016.
- Belting**, M. (2003) ‘Heparan sulfate proteoglycan as a plasma membrane carrier’, *Trends in Biochemical Sciences*, 28(3), pp. 145–151. doi: 10.1016/S0968-0004(03)00031-8.
- Ben Haim**, L. and Rowitch, D. H. (2016) ‘Functional diversity of astrocytes in neural circuit regulation’, *Nature Reviews Neuroscience*. Nature Publishing Group, 18(1), pp. 31–41. doi: 10.1038/nrn.2016.159.
- Bergamaschini**, L. et al. (2004) ‘Peripheral Treatment with Enoxaparin, a Low Molecular Weight Heparin, Reduces Plaques and β -Amyloid Accumulation in a Mouse Model of Alzheimer’s Disease’, *The Journal of Neuroscience*, 24(17), pp. 4181 LP – 4186. doi: 10.1523/JNEUROSCI.0550-04.2004.
- Birgbauer**, E., Rao, T. S. and Webb, M. (2004) ‘Lysolecithin induces demyelination in vitro in a cerebellar slice culture system’, *Journal of Neuroscience Research*, 78(2), pp. 157–166. doi: 10.1002/jnr.20248.

- Bjornevik, K.** et al. (2022) ‘Longitudinal analysis reveals high prevalence of Epstein-Barr virus associated with multiple sclerosis’, *Science*, 375(6578), pp. 296–301. doi: 10.1126/science.abj8222.
- Blackmore, M. G.** et al. (2012) ‘Krüppel-like Factor 7 engineered for transcriptional activation promotes axon regeneration in the adult corticospinal tract’, *Proceedings of the National Academy of Sciences of the United States of America*, 109(19), pp. 7517–7522. doi: 10.1073/pnas.1120684109.
- Blakemore, W. F.** and Franklin, R. J. M. (2008) ‘Remyelination in experimental models of toxin-induced demyelination’, *Current Topics in Microbiology and Immunology*, 318, pp. 193–212. doi: 10.1007/978-3-540-73677-6_8.
- Boggs JM.** (2006) Myelin basic protein: a multifunctional protein. *Cell Mol Life Sci. Sep*;63(17):1945-61. doi: 10.1007/s00018-006-6094-7. PMID: 16794783.
- Bögler, O.** et al. (1990) ‘Cooperation between two growth factors promotes extended self-renewal and inhibits differentiation of oligodendrocyte-type-2 astrocyte (O-2A) progenitor cells’, *Proceedings of the National Academy of Sciences of the United States of America*, 87(16), pp. 6368–6372. doi: 10.1073/pnas.87.16.6368.
- Boomkamp, S. D.** et al. (2012) ‘The development of a rat in vitro model of spinal cord injury demonstrating the additive effects of rho and ROCK inhibitors on neurite outgrowth and myelination’, *Glia*, 60(3), pp. 441–456. doi: 10.1002/glia.22278.
- Boven, L. A.** et al. (2000) ‘Macrophage inflammatory protein-1 α (MIP-1 α), MIP-1 β , and RANTES mRNA semiquantification and protein expression in active demyelinating multiple sclerosis (MS) lesions’, *Clinical and Experimental Immunology*, 122(2), pp. 257–263. doi: 10.1046/j.1365-2249.2000.01334.x.
- Bracken, M. B.** et al. (1997) ‘Administration of methylprednisolone for 24 or 48 hours or tirilazad mesylate for 48 hours in the treatment of acute spinal cord injury: Results of the Third National Acute Spinal Cord Injury randomized controlled trial’, *Jama*, 277(20), pp. 1597–1604. doi: 10.1001/jama.277.20.1597
- Bramlett, H. M.** and Dietrich, W. D. (2015) ‘Long-Term Consequences of Traumatic Brain Injury: Current Status of Potential Mechanisms of Injury and Neurological Outcomes’, *Journal of Neurotrauma*, 32(23), pp. 1834–1848. doi: 10.1089/neu.2014.3352.
- Brosnan, C. F.** and Raine, C. S. (2013) ‘The astrocyte in multiple sclerosis revisited’, *Glia*, 61(4), pp. 453–465. doi: 10.1002/glia.22443.
- Brook, Gary A., Pérez-Bouza, A., Noth, Johannes; Nacimiento, W.** (1999). Astrocytes re-express nestin in deafferented target territories of the adult rat hippocampus. *NeuroReport* 10(5):p 1007-1011,
- Buchser, W. J.** et al. (2010) ‘Kinase/phosphatase overexpression reveals pathways regulating hippocampal neuron morphology’, *Molecular Systems Biology*. Nature Publishing Group, 6(391), pp. 1–16. doi: 10.1038/msb.2010.52.
- Buckley, C. E., Goldsmith, P.** and Franklin, R. J. M. (2008) ‘Zebrafish myelination: A transparent model for remyelination?’, *DMM Disease Models and Mechanisms*, 1(4–5), pp. 221–228. doi: 10.1242/dmm.001248.

- Buckley, C. E. et al.** (2010) 'Drug reprofiling using zebrafish identifies novel compounds with potential pro-myelination effects', *Neuropharmacology*, 59(3), pp. 149–159. doi: 10.1016/j.neuropharm.2010.04.014.
- Burgos-Bravo, F. et al.** (2020) 'Application of Force to a Syndecan-4 Containing Complex With Thy-1- α V β 3 Integrin Accelerates Neurite Retraction', *Frontiers in Molecular Biosciences*, 7(September), pp. 1–16. doi: 10.3389/fmolb.2020.582257.
- Buss, A. and Schwab, M. E.** (2003) 'Sequential loss of myelin proteins during Wallerian degeneration in the rat spinal cord', *Glia*, 42(4), pp. 424–432. doi: 10.1002/glia.10220.
- Butt, A. M. and Dinsdale, J.** (2005) 'Fibroblast growth factor 2 induces loss of adult oligodendrocytes and myelin in vivo', *Experimental Neurology*, 192(1), pp. 125–133. doi: 10.1016/j.expneurol.2004.11.007.
- Cadavid D et al.,** (2019) SI; SYNERGY study investigators. Safety and efficacy of opicinumab in patients with relapsing multiple sclerosis (SYNERGY): a randomised, placebo-controlled, phase 2 trial. *Lancet Neurol.* 2019 Sep;18(9):845-856. doi: 10.1016/S1474-4422(19)30137-1. Epub 2019 Jul 5. PMID: 31285147.
- Cai, J. et al.** (2005) 'Generation of oligodendrocyte precursor cells from mouse dorsal spinal cord independent of Nkx6 regulation and Shh signaling', *Neuron*, 45(1), pp. 41–53. doi: 10.1016/j.neuron.2004.12.028.
- Canty, A. J. et al.** (2020) 'In vivo imaging of injured cortical axons reveals a rapid onset form of Wallerian degeneration', *BMC Biology*. *BMC Biology*, 18(1), pp. 1–17. doi: 10.1186/s12915-020-00869-2.
- Cardin AD, et al** (1989). Molecular modelling of protein-glycosaminoglycan interactions. *Arteriosclerosis*. 1989 Jan-Feb;9(1):21-32. doi: 10.1161/01.atv.9.1.21. PMID: 2463827.
- Carecho, R., Carregosa, D. and dos Santos, C. N.** (2020) 'Low Molecular Weight (poly)Phenol Metabolites Across the Blood-Brain Barrier: The Underexplored Journey', *Brain Plasticity*, 6(2), pp. 193–214. doi: 10.3233/bpl-200099.
- Cerpa, W. et al.** (2008) 'Wnt-7a modulates the synaptic vesicle cycle and synaptic transmission in hippocampal neurons', *Journal of Biological Chemistry*, 283(9), pp. 5918–5927. doi: 10.1074/jbc.M705943200.
- Chan, L. L. H. et al.** (2011) 'Both electrical stimulation thresholds and SMI-32-immunoreactive retinal ganglion cell density correlate with age in s334ter line 3 rat retina', *Journal of Neurophysiology*, 105(6), pp. 2687–2697. doi: 10.1152/jn.00619.2010.
- Chandra, G. et al.** (2016) 'Neutralization of RANTES and eotaxin prevents the loss of dopaminergic neurons in a mouse model of Parkinson disease', *Journal of Biological Chemistry*. © 2016 ASBMB. Currently published by Elsevier Inc; originally published by American Society for Biochemistry and Molecular Biology., 291(29), pp. 15267–15281. doi: 10.1074/jbc.M116.714824.
- Chandran, S. et al.** (2003) 'FGF-dependent generation of oligodendrocytes by a hedgehog-independent pathway', *Development*, 130(26), pp. 6599–6609. doi: 10.1242/dev.00871.

- Chen, V. S. et al.** (2017) 'Histology Atlas of the Developing Prenatal and Postnatal Mouse Central Nervous System, with Emphasis on Prenatal Days E7.5 to E18.5', *Toxicologic Pathology*, 45(6), pp. 705–744. doi: 10.1177/0192623317728134.
- Chen, Z. et al.** (2011) 'References and Notes 1.', 332(April), pp. 484–489. **Cheriyian, T. et al.** (2014) 'Spinal cord injury models: A review', *Spinal Cord*. Nature Publishing Group, 52(8), pp. 588–595. doi: 10.1038/sc.2014.91.
- Choay, J. et al** (1980). Anti-Xa active heparin oligosaccharides. *Thrombosis Research* 18, 573–578. [https://doi.org/10.1016/0049-3848\(80\)90356-4](https://doi.org/10.1016/0049-3848(80)90356-4) Choay,
- Choi, S. S. et al.** (2014) 'Human astrocytes: Secretome profiles of cytokines and chemokines', *PLoS ONE*, 9(4). doi: 10.1371/journal.pone.0092325. **Chretien, M. et al.** (1981) '1-S2.0-0006899381907162-Main', 205, pp. 15–28.
- Colin, S. et al** (1999). In Vivo Involvement of Heparan Sulfate Proteoglycan in the Bioavailability, Internalization, and Catabolism of Exogenous Basic Fibroblast Growth Factor. *Mol Pharmacol* 55, 74. <https://doi.org/10.1124/mol.55.1.74>
- Choo et al.** (2007). Contusion, dislocation, and distraction: primary hemorrhage and membrane permeability in distinct mechanisms of spinal cord injury. *J Neurosurg Spine*. 2007 Mar;6(3):255-66. doi: 10.3171/spi.2007.6.3.255. PMID: 17355025.
- Chua, C. C. et al.** (2004) 'Heparan Sulfate Proteoglycans Function as Receptors for Fibroblast Growth Factor-2 Activation of Extracellular Signal-Regulated Kinases 1 and 2', *Circulation Research*, 94(3), pp. 316–323. doi: 10.1161/01.RES.0000112965.70691.AC.
- Church, T. W. and Gold, M. G.** (2021) 'Preparation of Rat Organotypic Hippocampal Slice Cultures Using the Membrane-Interface Method', *Methods in Molecular Biology*, 2188, pp. 243–257. doi: 10.1007/978-1-0716-0818-0_12.
- Ciani, L. and Salinas, P. C.** (2005) 'WNTs in the vertebrate nervous system: From patterning to neuronal connectivity', *Nature Reviews Neuroscience*, 6(5), pp. 351–362. doi: 10.1038/nrn1665.
- Clarke, Scott R.; Shetty, Ashok K.; Bradley, Jennifer L.; Turner, Dennis A.** Reactive astrocytes express the embryonic intermediate neurofilament nestin. *NeuroReport* 5(15):p 1885-1888, October 1994.
- Coleman, M.** (2005) 'Axon degeneration mechanisms: Commonality amid diversity', *Nature Reviews Neuroscience*, 6(11), pp. 889–898. doi: 10.1038/nrn1788.
- Colombres, M. et al.** (2008) 'Heparin activates Wnt signaling for neuronal morphogenesis', *Journal of Cellular Physiology*, 216(3), pp. 805–815. doi: 10.1002/jcp.21465.
- Colombres, M. et al.** (2008) 'Heparin activates Wnt signaling for neuronal morphogenesis', *Journal of Cellular Physiology*, 216(3), pp. 805–815. doi: 10.1002/jcp.21465.
- Compston A, et al.** (2002). Multiple sclerosis. *Lancet*. 2002 Apr 6;359(9313):1221-31. doi: 10.1016/S0140-6736(02)08220-X.
- Condomitti, G. and De Wit, J.** (2018) 'Heparan sulfate proteoglycans as emerging players in synaptic specificity', *Frontiers in Molecular Neuroscience*, 11(January), pp. 1–14. doi: 10.3389/fnmol.2018.00014.

- Condomitti, G.** et al. (2018) ‘An Input-Specific Orphan Receptor GPR158-HSPG Interaction Organizes Hippocampal Mossy Fiber-CA3 Synapses’, *Neuron*. Elsevier Inc., 100(1), pp. 201–215.e9. doi: 10.1016/j.neuron.2018.08.038.
- Confavreux, C.** and Vukusic, S. (2006) ‘Natural history of multiple sclerosis: A unifying concept’, *Brain*, 129(3), pp. 606–616. doi: 10.1093/brain/awl007.
- Craner, M. J.** et al. (2004) ‘Molecular changes in neurons in multiple sclerosis: Altered axonal expression of Nav1.2 and Nav1.6 sodium channels and Na⁺/Ca²⁺ exchanger’, *Proceedings of the National Academy of Sciences of the United States of America*, 101(21), pp. 8168–8173. doi: 10.1073/pnas.0402765101.
- Crawford, A. H.** et al. (2016) ‘Developmental Origin of Oligodendrocyte Lineage Cells Determines Response to Demyelination and Susceptibility to Age-Associated Functional Decline’, *Cell Reports*. ElsevierCompany., 15(4), pp. 761–773. doi: 10.1016/j.celrep.2016.03.069.
- Crawford, C. L.** et al. (2022) ‘SARM1 Depletion Slows Axon Degeneration in a CNS Model of Neurotropic Viral Infection’, *Frontiers in Molecular Neuroscience*, 15(April), pp. 1–11. doi: 10.3389/fnmol.2022.860410.
- Cree BAC,** et al (2020); SPI2 investigative teams. Safety and efficacy of MD1003 (high-dose biotin) in patients with progressive multiple sclerosis (SPI2): a randomised, double-blind, placebo-controlled, phase 3 trial. *Lancet Neurol*. 2020 Dec;19(12):988-997. doi: 10.1016/S1474-4422(20)30347-1. Epub 2020 Oct 23. PMID: 33222767.
- Creeley, C. E.** et al. (2014) ‘Isoflurane-induced apoptosis of neurons and oligodendrocytes in the fetal rhesus macaque brain’, *Anesthesiology*, 120(3), pp. 626–638. doi: 10.1097/ALN.0000000000000037.
- Crijns H,** Vanheule V, Proost P. Targeting Chemokine-Glycosaminoglycan Interactions to Inhibit Inflammation. *Front Immunol*. 2020 Mar 31;11:483. doi: 10.3389/fimmu.2020.00483. PMID: 32296423; PMCID: PMC7138053
- Croft, C. L.** et al. (2019) ‘Organotypic brain slice cultures to model neurodegenerative proteinopathies’, *Molecular Neurodegeneration*. *Molecular Neurodegeneration*, 14(1), pp. 1–11. doi: 10.1186/s13024-019-0346-0.
- Cui, Y.** et al. (2020) ‘Axonal degeneration in an in vitro model of ischemic white matter injury’, *Neurobiology of Disease*. Elsevier, 134(November 2019), p. 104672. doi: 10.1016/j.nbd.2019.104672.
- Cummings, J.** (2018) ‘Lessons Learned from Alzheimer Disease: Clinical Trials with Negative Outcomes’, *Clinical and Translational Science*, 11(2), pp. 147–152. doi: 10.1111/cts.12491.
- Curtis E,** et al (2018) A First-in-Human, Phase I Study of Neural Stem Cell Transplantation for Chronic Spinal Cord Injury. *Cell Stem Cell*. 2018 Jun 1;22(6):941-950.e6. doi: 10.1016/j.stem.2018.05.014. PMID: 29859175.
- Cuyvers, E.** et al. (2014) ‘Investigating the role of rare heterozygous TREM2 variants in Alzheimer’s disease and frontotemporal dementia’, *Neurobiology of Aging*. Elsevier Ltd, 35(3), pp. 726.e11–726.e19. doi: 10.1016/j.neurobiolaging.2013.09.009.

- D'Angelo R**, Crisafulli C, Rinaldi C, Ruggeri A, Amato A, Sidoti A. CCR5 Δ 32 Polymorphism Associated with a Slower Rate Disease Progression in a Cohort of RR-MS Sicilian Patients. *Mult Scler Int*. 2011;2011:153282. doi: 10.1155/2011/153282. Epub 2011 Jun 23. PMID: 22096627; PMCID: PMC3195283.
- Dawson**, M. R. L. et al. (2003) 'NG2-expressing glial progenitor cells: An abundant and widespread population of cycling cells in the adult rat CNS', *Molecular and Cellular Neuroscience*, 24(2), pp. 476–488. doi: 10.1016/S1044-7431(03)00210-0.
- De Castro**, F., Bribián, A. and Ortega, M. C. (2013) 'Regulation of oligodendrocyte precursor migration during development, in adulthood and in pathology', *Cellular and Molecular Life Sciences*, 70(22), pp. 4355–4368. doi: 10.1007/s00018-013-1365-6.
- Dickson**, D. W. (1999) 'Microglia in Alzheimer's disease and transgenic models: How close the fit?', *American Journal of Pathology*. American Society for Investigative Pathology, 154(6), pp. 1627–1631. doi: 10.1016/S0002-9440(10)65416-8
- Diego De Stefani**, Maria Patron, and R. R. (2015) '乳鼠心肌提取 HHS Public Access', *Physiology & behavior*, 176(3), pp. 139 – 148. doi: 10.1146/annurev-neuro-060909-153248.Wallerian.
- Dimar**, J. R. et al. (1999) 'The influence of spinal canal narrowing and timing of decompression on neurologic recovery after spinal cord contusion in a rat model', *Spine*, 24(16), pp. 1623–1633. doi: 10.1097/00007632-199908150-00002.
- Dombrowski**, Y. et al. (2017) 'Regulatory T cells promote myelin regeneration in the central nervous system', *Nature Neuroscience*, 20(5), pp. 674–680. doi: 10.1038/nn.4528.
- Dudas**, B. et al. (2002) 'Oral and subcutaneous administration of the glycosaminoglycan C3 attenuates A β (25-35)-induced abnormal tau protein immunoreactivity in rat brain', *Neurobiology of Aging*, 23(1), pp. 97–104. doi: 10.1016/S0197-4580(01)00255-X.
- Dumont**, R. J. et al. (2001) 'Acute spinal cord injury, part I: Pathophysiologic mechanisms', *Clinical Neuropharmacology*, 24(5), pp. 254–264. doi: 10.1097/00002826-200109000-00002.
- Duncan**, I. D. et al. (2018) 'The adult oligodendrocyte can participate in remyelination', *Proceedings of the National Academy of Sciences of the United States of America*, 115(50), pp. E11807–E11816. doi: 10.1073/pnas.1808064115.
- Dunham**, K. A. et al. (2010) 'Characterization of a graded cervical hemicontusion spinal cord injury model in adult male rats', *Journal of Neurotrauma*, 27(11), pp. 2091–2106. doi: 10.1089/neu.2010.1424.
- Duprat**, F. et al. (2000) 'The neuroprotective agent riluzole activates the two P domain K⁺ channels TREK-1 and TRAAK', *Molecular Pharmacology*, 57(5), pp. 906–912.
- Durst**, F. and Tropea, C. (2016) 'The amyloid hypothesis of Alzheimer's disease at 25 years', *EMBO Molecular Medicine*, 8(6), pp. 595–608. Available at:
- Dyhrfort**, P. et al. (2019) 'Monitoring of protein biomarkers of inflammation in human traumatic brain injury using microdialysis and proximity extension assay technology in neurointensive care', *Journal of Neurotrauma*, 36(20), pp. 2872–2885. doi: 10.1089/neu.2018.6320.

- Dziedzic**, T. et al. (2010) ‘Wallerian degeneration: A major component of early axonal pathology in multiple sclerosis’, *Brain Pathology*, 20(5), pp. 976–985. doi: 10.1111/j.1750-3639.2010.00401.x.
- Edye**, M. E. et al. (2013) ‘Acidosis drives damage-associated molecular pattern (DAMP)-induced interleukin-1 secretion via a caspase-1-independent pathway’, *Journal of Biological Chemistry*. © 2013 ASBMB. Currently published by Elsevier Inc; originally published by American Society for Biochemistry and Molecular Biology., 288(42), pp. 30485–30494. doi: 10.1074/jbc.M113.478941.
- El-Daher** F, et al (2020). Neural circuit reorganisation after spinal cord injury in zebrafish. *Curr Opin Genet Dev*. 2020 Oct;64:44-51. doi: 10.1016/j.gde.2020.05.017. Epub 2020 Jun 27. PMID: 32604009.
- Elkin**, M. et al. (2001) ‘Heparanase as mediator of angiogenesis: mode of action’, *The FASEB Journal*, 15(9), pp. 1661–1663. doi: 10.1096/fj.00-0895fje.
- Elliott**, C. et al. (2012) ‘Functional identification of pathogenic autoantibody responses in patients with multiple sclerosis’, *Brain*, 135(6), pp. 1819–1833. doi: 10.1093/brain/aws105.
- Eng**, L. F. and Ghirnikar, R. S. (1994) ‘GFAP and Astrogliosis’, *Brain Pathology*, 4(3), pp. 229–237. doi: 10.1111/j.1750-3639.1994.tb00838.x.
- Ertürk**, A. et al. (2007) ‘Disorganized microtubules underlie the formation of retraction bulbs and the failure of axonal regeneration’, *Journal of Neuroscience*, 27(34), pp. 9169–9180. doi: 10.1523/JNEUROSCI.0612-07.2007.
- Fawcett**, J. W. and Asher, R. A. (1999) ‘The glial scar and central nervous system repair’, *Brain Research Bulletin*, 49(6), pp. 377–391. doi: 10.1016/S0361-9230(99)00072-6.
- Fehlings**, M. G. (2001) ‘Summary statement: the use of methylprednisolone in acute spinal cord injury.’, *Spine*, 26(24 Suppl), p. 2001. doi: 10.1097/00007632-200112151-00011.
- Fehlings** R. G. Perrin (2005). The role and timing of early decompression for cervical spinal cord injury: update with a review of recent clinical evidence. *Injury*, 36(2):S13–S26, 2005.
- Fehlings** MG, et al (2018). Rho Inhibitor VX-210 in Acute Traumatic Subaxial Cervical Spinal Cord Injury: Design of the SPinal Cord Injury Rho INhibition InvestiGation (SPRING) Clinical Trial. *J Neurotrauma*. 2018 May 1;35(9):1049-1056. doi: 10.1089/neu.2017.5434. Epub 2018 Mar 1. PMID: 29316845; PMCID: PMC5908415
- Fehlings** MG., et al. (2021). A Randomized Controlled Trial of Local Delivery of a Rho Inhibitor (VX-210) in Patients with Acute Traumatic Cervical Spinal Cord Injury. *Journal of Neurotrauma* 2021 38:15, 2065-2072
- Feng**, J. et al. (2014) ‘Curcumin inhibits mitochondrial injury and apoptosis from the early stage in EAE mice’, *Oxidative Medicine and Cellular Longevity*, 2014, pp. 1–11. doi: 10.1155/2014/728751.
- Ferenczy**, et al., (2012) Molecular biology, epidemiology, and pathogenesis of progressive multifocal leukoencephalopathy, the JC virus-induced demyelinating disease of the human brain. *Clin Microbiol Rev*. 2012 Jul;25(3):471-506. doi: 10.1128/CMR.05031-11. PMID: 22763635; PMCID: PMC3416490.

- Ferguson, B.** et al. (1997) 'Axonal damage in acute multiple sclerosis lesions', *Brain*, 120(3), pp. 393–399. doi: 10.1093/brain/120.3.393.
- Ferreirinha, F.** et al. (2004) 'Axonal degeneration in paraplegin-deficient mice is associated with abnormal mitochondria and impairment of axonal transport', *Journal of Clinical Investigation*, 113(2), pp. 231–242. doi: 10.1172/JCI200420138.
- Fersini, F., Govi, A. and Tsokos, M.** (2015) 'Central pontine myelinolysis', *Forensic Science, Medicine, and Pathology*, 11(1), pp. 130–132. doi: 10.1007/s12024-014-9628-6.
- Feyerabend, T. B.** et al. (2006) 'Heparan sulfate C5-epimerase is essential for heparin biosynthesis in mast cells', *Nature Chemical Biology*, 2(4), pp. 195–196. doi: 10.1038/nchembio777.
- Floriddia, E. M.** et al. (2020) 'Distinct oligodendrocyte populations have spatial preference and different responses to spinal cord injury', *Nature Communications*, 11(1), pp. 1–15. doi: 10.1038/s41467-020-19453-x.
- Flügel, T.** et al. (2001) 'Migratory activity and functional changes of green fluorescent effector cells before and during experimental autoimmune encephalomyelitis', *Immunity*, 14(5), pp. 547–560. doi: 10.1016/S1074-7613(01)00143-1.
- Foerster, S., Hill, M. F. E. and Franklin, R. J. M.** (2019) 'Diversity in the oligodendrocyte lineage: Plasticity or heterogeneity?', *Glia*, 67(10), pp. 1797–1805. doi: 10.1002/glia.23607.
- Fogel DB.** Factors associated with clinical trials that fail and opportunities for improving the likelihood of success: A review. *Contemp Clin Trials Commun.* 2018 Aug 7;11:156-164. doi: 10.1016/j.conctc.2018.08.001. PMID: 30112460; PMCID: PMC6092479.
- Fong, C. W.** (2015) 'Permeability of the Blood–Brain Barrier: Molecular Mechanism of Transport of Drugs and Physiologically Important Compounds', *Journal of Membrane Biology*. Springer US, 248(4), pp. 651–669. doi: 10.1007/s00232-015-9778-9.
- Forsten-Williams, K., Chua, C. C. and Nugent, M. A.** (2005) 'The kinetics of FGF-2 binding to heparan sulfate proteoglycans and MAP kinase signaling', *Journal of Theoretical Biology*, 233(4), pp. 483–499. doi: 10.1016/j.jtbi.2004.10.020.
- Frakes, A. E.** et al. (2014) 'Microglia induce motor neuron death via the classical NF- κ B pathway in amyotrophic lateral sclerosis', *Neuron*, 81(5), pp. 1009–1023. doi: 10.1016/j.neuron.2014.01.013.
- Frank, S.** et al. (2008) 'TREM2 is upregulated in amyloid plaque-associated microglia in aged APP23 transgenic mice', *Glia*, 56(13), pp. 1438–1447. doi: 10.1002/glia.20710.
- Franklin, R. J. M.** et al. (1996) 'Schwann cell-like myelination following transplantation of an olfactory bulb-ensheathing cell line into areas of demyelination in the adult CNS', *Glia*, 17(3), pp. 217–224. doi: 10.1002/(SICI)1098-1136
- Franklin, R. J. M. and Ffrench-Constant, C.** (2017) 'Regenerating CNS myelin - From mechanisms to experimental medicines', *Nature Reviews Neuroscience*, 18(12), pp. 753–769. doi: 10.1038/nrn.2017.136.
- Frese, M. A.** et al. (2009) 'Characterization of the human sulfatase Sulfl and its high affinity heparin/heparan sulfate interaction domain', *Journal of Biological Chemistry*, 284(41), pp. 28033–28044. doi: 10.1074/jbc.M109.035808.

- Friede, R. L.** (1972) 'Control of myelin formation by axon caliber. (With a model of the control mechanism)', *Journal of Comparative Neurology*, 144(2), pp. 233–252. doi: 10.1002/cne.901440207.
- Fu R, Shen Q, Xu P, Luo JJ, Tang Y** (2014). Phagocytosis of microglia in the central nervous system diseases. *Mol Neurobiol.* 2014 Jun;49(3):1422-34. doi: 10.1007/s12035-013-8620-6. Epub 2014 Jan 7. PMID: 24395130; PMCID: PMC4012154.
- Fujimoto** (2008) '基因的改变 NIH Public Access', *Bone*, 23(1), pp. 1–7. Fukushima, N. (2004) 'LPA in neural cell development', *Journal of Cellular Biochemistry*, 92(5), pp. 993–1003. doi: 10.1002/jcb.20093
- Furusho, M. et al.** (2012) 'Fibroblast growth factor receptor signaling in oligodendrocytes regulates myelin sheath thickness', *Journal of Neuroscience*, 32(19), pp. 6631–6641. doi: 10.1523/JNEUROSCI.6005-11.2012
- Gabel, B. C. et al.** (2017) 'A Review of Stem Cell Therapy for Spinal Cord Injury: Large Animal Models and the Frontier in Humans', *World Neurosurgery*. Elsevier Inc, 98, pp. 438–443. doi: 10.1016/j.wneu.2016.11.053.
- Gankam-Kengne, F. et al.** (2017) 'Osmotic stress-induced defective glial proteostasis contributes to brain demyelination after hyponatremia treatment', *Journal of the American Society of Nephrology*, 28(6), pp. 1802–1813. doi: 10.1681/ASN.2016050509.
- Gao, T. L. et al.** (2012) 'Expression of HMGB1 and RAGE in rat and human brains after traumatic brain injury', *Journal of Trauma and Acute Care Surgery*, 72(3), pp. 643–649. doi: 10.1097/TA.0b013e31823c54a6.
- Garcia, E., et al.** (2016). Cytokine and Growth Factor Activation In Vivo and In Vitro after Spinal Cord Injury." *Mediators of Inflammation* 2016: 9476020.
- Gary, P. H. . J. B. M. . S. C. T. et al** (1990) 'The New England Journal of Medicine Downloaded from nejm.org on April 1, 2015. For personal use only. No other uses without permission. Copyright © 1990 Massachusetts Medical Society. All rights reserved.', *The New English Journal of medicine*, 323(16), pp. 1120–1123.
- Gentleman, S. M. et al.** (1993) 'β-Amyloid precursor protein (βAPP) as a marker for axonal injury after head injury', *Neuroscience Letters*, 160(2), pp. 139–144. doi: 10.1016/0304-3940(93)90398-5.
- Geremia, N. M. et al.** (2017) 'The effectiveness of the anti-CD11d treatment is reduced in rat models of spinal cord injury that produce significant levels of intraspinal hemorrhage', *Experimental Neurology*. Elsevier Inc., 295, pp. 125–134. doi: 10.1016/j.expneurol.2017.06.002.
- Giammalva, G. R. et al.** (2018) 'Clinical and radiological features of Forestier's disease presenting with dysphagia', *Surgical Neurology International*, 9(1). doi: 10.4103/sni.sni.
- Ginhoux, F. et al.** (2010) 'Primitive Macrophages', *Science*, 701(November), pp. 841–845.
- Glass et al** (2018), Recombinant Heparin—New Opportunities, *Frontiers in Medicine* 5 (2018).

- Goebbels, S.** et al. (2017) ‘A neuronal PI(3,4,5)P₃ -dependent program of oligodendrocyte precursor recruitment and myelination’, *Nature Neuroscience*, 20(1), pp. 10–15. doi: 10.1038/nn.4425.
- Gold, et al** (2010). Nociceptor sensitization in pain pathogenesis. *Nat. Med.* 16, 1248–1257
- Gold, R.** et al. (2012) Placebo-controlled phase 3 study of oral BG-12 for relapsing multiple sclerosis. *N Engl J Med* 367: 1098–1107
- Gold, R.** et al. (2014) Efficacy and safety of delayed-release dimethyl fumarate in patients newly diagnosed with relapsing-remitting multiple sclerosis (RRMS). *Mult Scler* 2 July 2014. pii: 1352458514537013.
- Gordon DL,** et al (1990). Low-molecular-weight heparins and heparinoids and their use in acute or progressing ischemic stroke. *Clin Neuropharmacol.* 1990 Dec;13(6):522-43. doi: 10.1097/00002826-199012000-00005. PMID: 1703455.
- Green, A. J.** et al. (2017).Clemastine fumarate as a remyelinating therapy for multiple sclerosis (ReBUILD): a randomised, controlled, double-blind, crossover trial. *Lancet* 390, 2481–2489
- Griffin, J. W.** et al. (2009) ‘Axonal degeneration and disorders of the axonal cytoskeleton’, *The Axon: Structure, Function and Pathophysiology.* doi: 10.1093/acprof:oso/9780195082937.003.0020.
- Grundke-Iqbal, I., Iqbal, K. and Tung, Y. C.** (1986) ‘Abnormal phosphorylation of the microtubule-associated protein τ (tau) in Alzheimer cytoskeletal pathology’, *Proceedings of the National Academy of Sciences of the United States of America*, 83(13), pp. 44913–44917. doi: 10.1097/00002093-198701030-00020.
- Guerrero, R. M., Giza, C. C. and Rotenberg, A.** (2015) ‘Glutamate and GABA Imbalance Following Traumatic Brain Injury’, *Current Neurology and Neuroscience Reports*, 15(5), pp. 1–11. doi: 10.1007/s11910-015-0545-1.
- Guo, Y. E.** et al. (2018) ‘Vitamin C promotes oligodendrocytes generation and remyelination’, *Glia*, 66(7), pp. 1302–1316. doi: 10.1002/glia.23306.
- Haarmann, A.** et al. (2019) ‘Human brain endothelial CXCR2 is inflammation-inducible and mediates CXCL5-and CXCL8-triggered paraendothelial barrier breakdown’, *International Journal of Molecular Sciences*, 20(3), pp. 1–14. doi: 10.3390/ijms20030602.
- Hard, Anna-Lena; Smith, Lois; Hellstrom, A.** (2018) ‘乳鼠心肌提取 HHS Public Access’, *Physiology & behavior*, 176(1), pp. 139–148. doi: 10.1021/jacs.7b01399.Full.
- Hartline, D. K. and Colman, D. R.** (2007) ‘Rapid Conduction and the Evolution of Giant Axons and Myelinated Fibers ’ , *Current Biology*, 17(1), pp. 29–35. doi: 10.1016/j.cub.2006.11.042.
- Hauser, S. L.** et al. (2017) ‘Ocrelizumab versus Interferon Beta-1a in Relapsing Multiple Sclerosis’, *New England Journal of Medicine*, 376(3), pp. 221–234. doi: 10.1056/nejmoa1601277.

- Hedström, A. K.** et al. (2011) ‘Smoking and two human leukocyte antigen genes interact to increase the risk for multiple sclerosis’, *Brain*, 134(3), pp. 653–664. doi: 10.1093/brain/awq371.
- Herzog, C.** et al. (2019) ‘Rapid clearance of cellular debris by microglia limits secondary neuronal cell death after brain injury in vivo’, *Development (Cambridge)*, 146(9). doi: 10.1242/dev.174698.
- Hickman, S. E.** et al. (2013) ‘The microglial sensome revealed by direct RNA sequencing’, *Nature Neuroscience*. Nature Publishing Group, 16(12), pp. 1896–1905. doi: 10.1038/nn.3554.
- Hill, R. A.** et al. (2013) ‘NG2 cells in white matter but not gray matter proliferate in response to PDGF’, *Journal of Neuroscience*, 33(36), pp. 14558–14566. doi: 10.1523/JNEUROSCI.2001-12.2013.
- Hinzman, J. M.** et al. (2014) ‘Inverse neurovascular coupling to cortical spreading depolarizations in severe brain trauma’, *Brain*, 137(11), pp. 2960–2972. doi: 10.1093/brain/awu241.
- Holmes, B. B.** et al. (2013) ‘Heparan sulfate proteoglycans mediate internalization and propagation of specific proteopathic seeds’, *Proceedings of the National Academy of Sciences of the United States of America*, 110(33). doi: 10.1073/pnas.1301440110.
- Holt, C. E.** and Dickson, B. J. (2005) ‘Sugar codes for axons?’, *Neuron*, 46(2), pp. 169–172. doi: 10.1016/j.neuron.2005.03.021.
- Hughes, A. N.** and Appel, B. (2020) ‘Microglia phagocytose myelin sheaths to modify developmental myelination’, *Nature Neuroscience*. Springer US, 23(9), pp. 1055–1066. doi: 10.1038/s41593-020-0654-2.
- Humpel, C.** (2015) ‘Neuroscience forefront review organotypic brain slice cultures: A review’, *Neuroscience*. IBRO, 305, pp. 86–98. doi: 10.1016/j.neuroscience.2015.07.086.
- Hurlbert, R. J.** (2007) ‘Methylprednisolone for the treatment of acute spinal cord injury: Point’, *Neurosurgery*, 61(1), pp. 32–35. doi: 10.1227/NEU.0000000000000393.
- Hurlbert, R. J.** et al. (2013) ‘Pharmacological therapy for acute spinal cord injury’, *Neurosurgery*, 72(SUPPL.2), pp. 93–105. doi: 10.1227/NEU.0b013e31827765c6.
- Hütter, G., Neumann, M., Nowak, D., Klein, S., Klüter, H., and Hofmann, W.-K.** (2011). The Effect of the CCR5-delta32 Deletion on Global Gene Expression Considering Immune Response and Inflammation. *J. Inflamm.* 8, 29. doi:10.1186/1476-9255-8-29
- Iglesias, J., Morales, L. and Barreto, G. E.** (2017) ‘Metabolic and Inflammatory Adaptation of Reactive Astrocytes: Role of PPARs’, *Molecular Neurobiology*. *Molecular Neurobiology*, 54(4), pp. 2518–2538. doi: 10.1007/s12035-016-9833-2.
- IMSGC 2013.** International Multiple Sclerosis Genetics Consortium. Analysis of immune-related loci identifies 48 new susceptibility variants for multiple sclerosis. *Nat. Genet.* (2013) 45:1353–60. doi: 10.1038/ng.2770
- IMSGC 2018.** International Multiple Sclerosis Genetics Consortium. Low-frequency and rare-coding variation contributes to multiple sclerosis risk. *Cell* (2018) 175:1679–87.e7. doi: 10.1016/j.cell.2018.09.049

- Irie, A.** et al. (2002) ‘Specific heparan sulfate structures involved in retinal axon targeting’, *Development*, 129(1), pp. 61–70. doi: 10.1242/dev.129.1.61.
- Ito, S.** et al. (2021) ‘Enoxaparin promotes functional recovery after spinal cord injury by antagonizing PTPR σ ’, *Experimental Neurology*. Elsevier Inc., 340(March), p. 113679. doi: 10.1016/j.expneurol.2021.113679.
- Jin, W.**, Botchway, B. O. A. and Liu, X. (2021) ‘Curcumin Can Activate the Nrf2/HO-1 Signaling Pathway and Scavenge Free Radicals in Spinal Cord Injury Treatment’, *Neurorehabilitation and Neural Repair*, 35(7), pp. 576–584. doi: 10.1177/15459683211011232.
- Jo, S.** et al. (2014) ‘GABA from reactive astrocytes impairs memory in mouse models of Alzheimer’s disease’, *Nature Medicine*, 20(8), pp. 886–896. doi: 10.1038/nm.3639.
- Johnson** et al. (1995). Copolymer 1 reduces relapse rate and improves disability in relapsing-remitting multiple sclerosis: results of a phase III multicenter, double-blind placebo-controlled trial. The Copolymer 1 Multiple Sclerosis Study Group. *Neurology*. 1995 Jul;45(7):1268-76. doi: 10.1212/wnl.45.7.1268. PMID: 7617181.
- Jung, Y.** et al. (2014) ‘Comprehensive evaluation of peripheral nerve regeneration in the acute healing phase using tissue clearing and optical microscopy in a rodent model’, *PLoS ONE*, 9(4). doi: 10.1371/journal.pone.0094054.
- Kallakatta, R. N.** et al. (2011) ‘Clinical and functional outcome and factors predicting prognosis in osmotic demyelination syndrome (central pontine and/or extrapontine myelinolysis) in 25 patients’, *Journal of Neurology, Neurosurgery and Psychiatry*, 82(3), pp. 326–331. doi: 10.1136/jnnp.2009.201764.
- Keatinge M.**, et al. (2021) CRISPR gRNA phenotypic screening in zebrafish reveals pro-regenerative genes in spinal cord injury. *PLoS Genet* 17(4): e1009515. <https://doi.org/10.1371/journal.pgen.1009515>
- Kessaris, N.** et al. (2006) ‘Competing waves of oligodendrocytes in the forebrain and postnatal elimination of an embryonic lineage’, *Nature Neuroscience*, 9(2), pp. 173–179. doi: 10.1038/nn1620.
- Khandker, L.** et al. (2022) ‘Cholesterol biosynthesis defines oligodendrocyte precursor heterogeneity between brain and spinal cord’, *Cell Reports*. The Author(s), 38(9), p. 110423. doi: 10.1016/j.celrep.2022.110423.
- Khorana, A. A.** and Fine, R. L. (2004) ‘Pancreatic cancer and thromboembolic disease’, *Lancet Oncology*, 5(11), pp. 655–663. doi: 10.1016/S1470-2045(04)01606-7.
- Khorasanizadeh M.**, et al. (2019) . Neurological recovery following traumatic spinal cord injury: A systematic review and meta-analysis. *J. Neurosurg.* 2019;30:683–699. doi: 10.3171/2018.10.SPINE18802.
- Kierdorf, K.** et al. (2013) ‘Microglia emerge from erythromyeloid precursors via Pu.1- and Irf8-dependent pathways’, *Nature Neuroscience*. Nature Publishing Group, 16(3), pp. 273–280. doi: 10.1038/nn.3318.
- Kieseier, B. C.** (2011) ‘The mechanism of action of interferon- β in relapsing multiple sclerosis’, *CNS Drugs*, 25(6), pp. 491–502. doi: 10.2165/11591110-000000000-00000.

- Kigerl, K. A.** et al. (2009) ‘Identification of two distinct macrophage subsets with divergent effects causing either neurotoxicity or regeneration in the injured mouse spinal cord’, *Journal of Neuroscience*, 29(43), pp. 13435–13444. doi: 10.1523/JNEUROSCI.3257-09.2009.
- Kinnunen, T.** et al. (2005) ‘Heparan 2-O-sulfotransferase, hst-2, is essential for normal cell migration in *Caenorhabditis elegans*’, *Proceedings of the National Academy of Sciences of the United States of America*, 102(5), pp. 1507–1512. doi: 10.1073/pnas.0401591102.
- Kiray, H.** et al. (2016) ‘The multifaceted role of astrocytes in regulating myelination’, *Experimental Neurology*, 283, pp. 541–549. doi: 10.1016/j.expneurol.2016.03.009.
- Kirshblum, et al.** (2004). Late neurologic recovery after traumatic spinal cord injury1. *Archives of physical medicine and rehabilitation*, 85 (11):1811–1817, 2004.
- Kishimoto, T. K.** et al. (2008) ‘Contaminated Heparin Associated with Adverse Clinical Events and Activation of the Contact System’, *New England Journal of Medicine*, 358(23), pp. 2457–2467. doi: 10.1056/nejmoa0803200.
- Klouwer, F. C. C.** et al. (2015) ‘Zellweger spectrum disorders: Clinical overview and management approach Inherited metabolic diseases’, *Orphanet Journal of Rare Diseases*. *Orphanet Journal of Rare Diseases*, 10(1), pp. 1–11. doi: 10.1186/s13023-015-0368-9.
- Koliatsos, V. E.** and Alexandris, A. S. (2019) ‘Wallerian degeneration as a therapeutic target in traumatic brain injury’, *Current Opinion in Neurology*, 32(6), pp. 786–795. doi: 10.1097/WCO.0000000000000763.
- Konaka, K.** et al. (2017) ‘Kamishoyosan and Shakuyakukanzoto promote recovery from paclitaxel-induced neurite retraction in PC12 cells’, *Journal of Pharmaceutical Health Care and Sciences*. *Journal of Pharmaceutical Health Care and Sciences*, 3(1), pp. 1–8. doi: 10.1186/s40780-017-0090-y.
- Kornreich BG.** The patch clamp technique: principles and technical considerations. *J Vet Cardiol*. 2007 May;9(1):25-37. doi: 10.1016/j.jvc.2007.02.001. Epub 2007 May 16. PMID: 17689466.
- Kotter, M. R.** et al. (2006) ‘Myelin impairs CNS remyelination by inhibiting oligodendrocyte precursor cell differentiation’, *Journal of Neuroscience*, 26(1), pp. 328–332. doi: 10.1523/JNEUROSCI.2615-05.2006.
- Kotter, M. R., Stadelmann, C.** and Hartung, H. P. (2011) ‘Enhancing remyelination in disease - Can we wrap it up?’, *Brain*, 134(7), pp. 1882–1900. doi: 10.1093/brain/awr014.
- Kucher K,** et al. (2018) First-in-Man Intrathecal Application of Neurite Growth-Promoting Anti-Nogo-A Antibodies in Acute Spinal Cord Injury. *Neurorehabilitation and Neural Repair*. 2018;32(6-7):578-589. doi:10.1177/1545968318776371
- Kühl NM, De Keyser J, De Vries H, Hoekstra D.** Insulin-like growth factor binding proteins-1 and -2 differentially inhibit rat oligodendrocyte precursor cell survival and differentiation in vitro. *J Neurosci Res*. 2002 Jul 15;69(2):207-16. doi: 10.1002/jnr.10293. PMID: 12111802.
- Lakatos, A., Franklin, R. J. M.** and Barnett, S. C. (2000) ‘Olfactory ensheathing cells and Schwann cells differ in their in vitro interactions with astrocytes’, *Glia*, 32(3), pp. 214–225. doi: 10.1002/1098-1136(200012)32:3<214::AID-GLIA20>3.0.CO;2-7.

Lang-Lazdunski, L. et al. (2000) ‘Prevention of ischemic spinal cord injury: Comparative effects of magnesium sulfate and riluzole’, *Journal of Vascular Surgery*, 32(1), pp. 179–189. doi: 10.1067/mva.2000.105960.

LaPlaca, M. C. et al. (2007) ‘CNS injury biomechanics and experimental models’, *Progress in Brain Research*, 161, pp. 13–26. doi: 10.1016/S0079-6123(06)61002-9.

Lassmann, H., Brück, W. and Lucchinetti, C. F. (2007) ‘The immunopathology of multiple sclerosis: An overview’, *Brain Pathology*, 17(2), pp. 210–218. doi: 10.1111/j.1750-3639.2007.00064.x.

Lehmann-Horn, K., Kinzel, S. and Weber, M. S. (2017) ‘Deciphering the role of B cells in multiple sclerosis—towards specific targeting of pathogenic function’, *International Journal of Molecular Sciences*, 18(10), pp. 1–18. doi: 10.3390/ijms18102048.

Lemmon, V. P. and Goldberg, J. L. (2009) ‘Intrinsic Axon Regeneration Ability’, *Science*, 1007(2004), pp. 2007–2010.

Lendahl U, Zimmerman LB, McKay RD (1990) CNS stem cells express a new class of intermediate filament protein. *Cell* 60:585–595

Li J, Erisir A, Cline H. In vivo time-lapse imaging and serial section electron microscopy reveal developmental synaptic rearrangements. *Neuron*. 2011 Jan 27;69(2):273-86. doi: 10.1016/j.neuron.2010.12.022. PMID: 21262466; PMCID: PMC3052740.

Li, J. J., Holsworth, D. D. and Hu, L. Y. (2003) ‘Molecular properties that influence the oral bioavailability of drug candidates’, *Chemtracts*, 16(7), pp. 439–442.

Libbey, J. E. and Fujinami, R. S. (2011) ‘Experimental autoimmune encephalomyelitis as a testing paradigm for adjuvants and vaccines’, *Vaccine*, 29(17), pp. 3356–3362. doi: 10.1016/j.vaccine.2010.08.103.

Liddelow, S. A. and Barres, B. A. (2017) ‘Reactive Astrocytes: Production, Function, and Therapeutic Potential’, *Immunity*. Elsevier Inc., 46(6), pp. 957–967. doi: 10.1016/j.immuni.2017.06.006.

Lindahl, U., (1989) Biosynthesis of heparin and related polysaccharides, In: “Heparin: Chemical and Biological Properties, Clinical Applications”, Lane, D.A., and Lindahl, U., eds., Edward Arnold, London, pp. 159–189.

Lindahl, U. and Li, J. ping (2009) Chapter 3 Interactions Between Heparan Sulfate and Proteins-Design and Functional Implications. 1st edn, *International Review of Cell and Molecular Biology*. 1st edn. Elsevier Inc. doi: 10.1016/S1937-6448(09)76003-4.

Lindsay, S. L. and Barnett, S. C. (2021) ‘Therapeutic potential of niche - specific mesenchymal stromal cells for spinal cord injury repair ’, *Cells*, 10(4). doi: 10.3390/cells10040901.

Lindsay, S.L., et al. (2022) Human olfactory mesenchymal stromal cell transplantation ameliorates experimental autoimmune encephalomyelitis revealing an inhibitory role for IL16 on myelination. *acta neuropathol commun* 10, 12 (2022). <https://doi.org/10.1186/s40478-022-01316-9>

Lindsay SL, McCanney GA, Zhan J, Scheld M, Smith RS, Goodyear CS, Yates EA, Kipp M, Turnbull JE, Barnett SC (2023). Low sulfated heparan sulfate mimetic differentially

affects repair in immune-mediated and toxin-induced experimental models of demyelination. *Glia*. 2023 Jul;71(7):1683-1698. doi: 10.1002/glia.24363. Epub 2023 Mar 21. PMID: 36945189.

Liu, C. et al. (2018) 'APP upregulation contributes to retinal ganglion cell degeneration via JNK3', *Cell Death and Differentiation*. Springer US, 25(4), pp. 661–676. doi: 10.1038/s41418-017-0005-3.

Liu, D. et al. (1999) 'Neurotoxicity of glutamate at the concentration released upon spinal cord injury', *Neuroscience*, 93(4), pp. 1383–1389. doi: 10.1016/S0306-4522(99)00278-X.

Liu, K. et al. (2007) 'Anti-high mobility group box 1 monoclonal antibody ameliorates brain infarction induced by transient ischemia in rats', *The FASEB Journal*, 21(14), pp. 3904–3916. doi: 10.1096/fj.07-8770com.

Liu, Y. F. et al. (2021) 'CXCL5/CXCR2 modulates inflammation-mediated neural repair after optic nerve injury', *Experimental Neurology*. Elsevier Inc., 341(March), p. 113711. doi: 10.1016/j.expneurol.2021.113711.

Lin RC, Matesic DF, Marvin M, McKay RD, Brüstle O. Re-expression of the intermediate filament nestin in reactive astrocytes. *Neurobiol Dis*. 1995 Apr;2(2):79-85. doi: 10.1006/nbdi.1995.0008. PMID: 8980011.

Lloyd et al (2019). Central nervous system regeneration is driven by microglia necroptosis and repopulation. *Nat Neurosci*. 2019 Jul;22(7):1046-1052. doi: 10.1038/s41593-019-0418-z. Epub 2019 Jun 10. PMID: 31182869; PMCID: PMC6597360.

Lock, C. et al. (2002) Gene-microarray analysis of multiple sclerosis lesions yields new targets validated in autoimmune encephalomyelitis. *Nat Med* 8, 500–508 (2002).

Loh, S. H. Y. et al. (2008) 'Identification of new kinase clusters required for neurite outgrowth and retraction by a loss-of-function RNA interference screen', *Cell Death and Differentiation*, 15(2), pp. 283–298. doi: 10.1038/sj.cdd.4402258.

Love, S (2006) Demyelinating diseases *Journal of Clinical Pathology* 2006;**59**:1151-1159.

Lu, D. et al. (2004) 'Activation of the Wnt signaling pathway in chronic lymphocytic leukemia', *Proceedings of the National Academy of Sciences of the United States of America*, 101(9), pp. 3118–3123. doi: 10.1073/pnas.0308648100

Lu, Q. R. et al. (2002) 'Common developmental requirement for Olig function indicates a motor neuron/oligodendrocyte connection', *Cell*, 109(1), pp. 75–86. doi: 10.1016/S0092-8674(02)00678-5.

Lublin, F. D. et al. (2014) 'Defining the clinical course of multiple sclerosis: The 2013 revisions', *Neurology*, 83(3), pp. 278–286. doi: 10.1212/WNL.0000000000000560.

Ludwin, S. K. and Maitland, M. (1984) 'Long-term remyelination fails to reconstitute normal thickness of central myelin sheaths', *Journal of the Neurological Sciences*, 64(2), pp. 193–198. doi: 10.1016/0022-510X(84)90037-6.

Luster, A. D., Greenberg, S. M. and Leder, P. (1995) 'The IP-10 chemokine binds to a specific cell surface heparan sulfate site shared with platelet factor 4 and inhibits endothelial

- cell proliferation', *Journal of Experimental Medicine*, 182(1), pp. 219–231. doi: 10.1084/jem.182.1.219.
- Lv Y**, et al (2021). Brain stem and spinal cord demyelination due to acute carbon monoxide poisoning. *Undersea Hyperb Med. 2021 Third Quarter*;48(3):247-253. PMID: 34390629.
- Ma, Q.** et al. (2002) 'The blood-brain barrier accessibility of a heparin-derived oligosaccharides C3', *Thrombosis Research*, 105(5), pp. 447–453. doi: 10.1016/S0049-3848(02)00050-6.
- Maas, A. I. R.** et al. (2017) 'Traumatic brain injury: Integrated approaches to improve prevention, clinical care, and research', *The Lancet Neurology*, 16(12), pp. 987–1048. doi: 10.1016/S1474-4422(20)
- Manzella-Lapeira J**, Brzostowski J, Serra-Vinardell J. Studying Neuronal Biology Using Spinning Disc Confocal Microscopy. *Methods Mol Biol.* 2021;2304:265-283. doi: 10.1007/978-1-0716-1402-0_14. PMID: 34028722.17)30371-X
- Maroso, M.** et al. (2010) 'Toll-like receptor 4 and high-mobility group box-1 are involved in iktogenesis and can be targeted to reduce seizures', *Nature Medicine*. Nature Publishing Group, 16(4), pp. 413–419. doi: 10.1038/nm.2127.
- Massena, S.** et al (2010). A chemotactic gradient sequestered on endothelial heparan sulfate induces directional intraluminal crawling of neutrophils. *Blood* 116, 1924. <https://doi.org/10.1182/blood-2010-01-266072>
- Matsuda, R.** et al. (2009) 'Cotransplantation of mouse embryonic stem cells and bone marrow stromal cells following spinal cord injury suppresses tumor development', *Cell Transplantation*, 18(1), pp. 39–54. doi: 10.3727/096368909788237122.
- Matsushima, G. K.** and Morell, P. (2001) 'The neurotoxicant, cuprizone, as a model to study demyelination and remyelination in the central nervous system', *Brain Pathology*, 11(1), pp. 107–116. doi: 10.1111/j.1750-3639.2001.tb00385.x.
- Mayoral, S. R.** et al. (2018) 'Initiation of CNS Myelination in the Optic Nerve Is Dependent on Axon Caliber', *Cell Reports*. ElsevierCompany., 25(3), pp. 544-550.e3. doi: 10.1016/j.celrep.2018.09.052.
- McCarthy, C. P.** et al. (2020) 'Running thin: implications of a heparin shortage', *The Lancet*. Elsevier Ltd, 395(10223), pp. 534–536. doi: 10.1016/S0140-6736(19)33135-6.
- McGeer, P. L.** et al. (1987) 'Reactive microglia in patients with senile dementia of the Alzheimer type are positive for the histocompatibility glycoprotein HLA-DR', *Neuroscience Letters*, 79(1–2), pp. 195–200. doi: 10.1016/0304-3940(87)90696-3.
- McRae, B. L.** et al. (1992) 'Induction of active and adoptive relapsing experimental autoimmune encephalomyelitis (EAE) using an encephalitogenic epitope of proteolipid protein', *Journal of Neuroimmunology*, 38(3), pp. 229–240. doi: 10.1016/0165-5728(92)90016-E.
- Menon D.K.** (2010) On behalf of The Demographics and Clinical Assessment Working Group of the International and Interagency Initiative toward Common Data Elements for Research on Traumatic Brain Injury and Psychological Health (2010) Position statement: definition of traumatic brain injury. *Arch Phys Med Rehabil* 91:1637–1640

- Merli, G. J. and Groce, J. B. (2010)** ‘Pharmacological and clinical differences between low-molecular-weight heparins implications for prescribing practice and therapeutic interchange’, *P and T*, 35(2), pp. 95–105.
- Meshkini, A. et al. (2018)** ‘Riluzole can improve sensory and motor function in patients with acute spinal cord injury’, *Asian Journal of Neurosurgery*, 13(03), pp. 656–659. doi: 10.4103/ajns.ajns_259_16.
- Millecamps, S. and Julien, J. P. (2013)** ‘Axonal transport deficits and neurodegenerative diseases’, *Nature Reviews Neuroscience*. Nature Publishing Group, 14(3), pp. 161–176. doi: 10.1038/nrn3380.
- Miller, D. H. and Leary, S. M. (2007)** ‘Primary-progressive multiple sclerosis’, *Lancet Neurology*, 6(10), pp. 903–912. doi: 10.1016/S1474-4422(07)70243-0.
- Miron, V. E. et al. (2013)** ‘M2 microglia and macrophages drive oligodendrocyte differentiation during CNS remyelination’, *Nature Neuroscience*, 16(9), pp. 1211–1218. doi: 10.1038/nn.3469.
- Miron, V. E. et al. (2010)** ‘Fingolimod (FTY720) enhances remyelination following demyelination of organotypic cerebellar slices’, *American Journal of Pathology*. American Society for Investigative Pathology, 176(6), pp. 2682–2694. doi: 10.2353/ajpath.2010.091234.
- Mittal, P. et al. (2016)** ‘MRI findings in a case of spinal cord wallerian degeneration following trauma’, *Neurosciences*, 21(4), pp. 372–373. doi: 10.17712/nsj.2016.4.20160278.
- Miyatake, T. and Suzuki, K. (1972)** ‘Globoid cell leukodystrophy: Additional deficiency of psychosine galactosidase’, *Biochemical and Biophysical Research Communications*, 48(3), pp. 538–543. doi: 10.1016/0006-291X(72)90381-6.
- Mizee, M. R. et al. (2014)** ‘Astrocyte-derived retinoic acid: a novel regulator of blood–brain barrier function in multiple sclerosis’, *Acta Neuropathologica*, 128(5), pp. 691–703. doi: 10.1007/s00401-014-1335-6.
- Morimoto-Tomita, M. et al. (2002)** ‘Cloning and characterization of two extracellular heparin-degrading endosulfatases in mice and humans’, *Journal of Biological Chemistry*. © 2002 ASBMB. Currently published by Elsevier Inc; originally published by American Society for Biochemistry and Molecular Biology., 277(51), pp. 49175–49185. doi: 10.1074/jbc.M205131200.
- Morganti-Kossmann MC et al (1997)**. Production of cytokines following brain injury: beneficial and deleterious for the damaged tissue. *Mol Psychiatry*. 1997 Mar;2(2):133-6. doi: 10.1038/sj.mp.4000227. PMID: 9106236.
- Morrill, J. B. and Doty, S. D. (1986)** ‘Mechanical and cellular aspects of gastrulation in the sea urchin *Lytechinus variegatus*.’, *Progress in clinical and biological research*, 217 A(2), pp. 97–100. doi: 10.1038/nrn3156.Mitochondrial.
- Morris, R. L. and Hollenbeck, P. J. (1993)** ‘The regulation of bidirectional mitochondrial transport is coordinated with axonal outgrowth’, *Journal of Cell Science*, 104(3), pp. 917–927. doi: 10.1242/jcs.104.3.917.

- Mueller, B. P.** (1958) '(From The Rockefeller Institute)', 42(1). Neill, B. P. O. and Moser, H. W. (1982) 'Subject Review : Adrenoleukodystrophy', Canadian Journal of Neurological Sciences / Journal Canadien des Sciences Neurologiques, 9(4), pp. 449–452.
- New, P. W., Cripps, R. A. and Bonne Lee, B.** (2014) 'Global maps of non-traumatic spinal cord injury epidemiology: Towards a living data repository', Spinal Cord. Nature Publishing Group, 52(2), pp. 97–109. doi: 10.1038/sc.2012.165.
- New, P. W. and Marshall, R.** (2014) 'International Spinal Cord Injury Data Sets for non-traumatic spinal cord injury', Spinal Cord. Nature Publishing Group, 52(2), pp. 123–132. doi: 10.1038/sc.2012.160.
- Nicaise, C. et al.** (2012) 'Degeneration of phrenic motor neurons induces long-term diaphragm deficits following mid-cervical spinal contusion in mice', Journal of Neurotrauma, 29(18), pp. 2748–2760. doi: 10.1089/neu.2012.2467.
- Niederost, et al** (1999) CNS myelin contains neurite growth-inhibitory activity associated with chondroitin sulfate proteoglycans. J. Neurosci. 19, 8979–8989 (1999).
- Nimmerjahn, A., Kirchhoff, F. and Helmchen, F.** (2005) 'Resting Microglial Cells Are Highly Dynamic Surveillants of Brain Parenchyma in Vivo — Resting Microglial Cells Are Highly Dynamic Surveillants of Brain Parenchyma in Vivo — SuppoNimmerjahn, Axel, Frank Kirchhoff, and Fritjof Helmchen. 2005. "Resting Micr', Science, 308(May), pp. 1314–1319.
- Norton, W. T. and Cammer, W.** (1984) 'Isolation and Characterization of Myelin', Myelin, (1967), pp. 147–195. doi: 10.1007/978-1-4757-1830-0_5.
- Nugent, M. A. and Edelmant, E. R.** (1992) 'Kinetics of Basic Fibroblast Growth Factor Binding to Its Receptor and Heparan Sulfate Proteoglycan: A Mechanism for Cooperativity', Biochemistry, 31(37), pp. 8876–8883. doi: 10.1021/bi00152a026.
- Nguyen H et al** (2017). Systemic neutrophil depletion modulates the migration and fate of transplanted human neural stem cells to rescue functional repair. J Neurosci 37, 9269, 2017.
- Orentas, D. M. and Miller, R. H.** (1998) 'Regulation of oligodendrocyte development', Molecular Neurobiology, 18(3), pp. 247–259. doi: 10.1007/BF02741302.
- Ornitz, D. M.** (2000) 'FGFs, heparan sulfate and FGFRs: Complex interactions essential for development', BioEssays, 22(2), pp. 108–112. doi: 10.1002/(SICI)1521-1878(200002)22:2<108::AID-BIES2>3.0.CO;2-M.
- Oudega et al** (1991). Long-term effects of methylprednisolone following transection of adult rat spinal cord. Eur J Neurosci. 1999 Jul;11(7):2453-64. doi: 10.1046/j.1460-9568.1999.00666.x. PMID: 10383635
- Pan et al.,** (2010). Oversulfated chondroitin sulfate is not the sole contaminant in heparin. Nature Biotechnology 28, 203.
- Pang,
- Panter, S. S. et al.**(1990) Alteration in extracellular amino acids after traumatic spinal cord injury. Ann Neurol 27:96–99

- Paolicelli, R. C. et al.** (2011) ‘Synaptic pruning by microglia is necessary for normal brain development’, *Science*, 333(6048), pp. 1456–1458. doi: 10.1126/science.1202529.
- Paolicelli, R. C. et al.** (2022). Microglia states and nomenclature: A field at its crossroads. *Neuron*. 2022 Nov 2;110(21):3458-3483. doi: 10.1016/j.neuron.2022.10.020. PMID: 36327895.
- Pardridge, W. M.** (2007) ‘Blood-brain barrier delivery’, *Drug Discovery Today*, 12(1–2), pp. 54–61. doi: 10.1016/j.drudis.2006.10.013.
- Pardridge, W. M. and Mietus, L. J.** (1980) ‘Transport of thyroid and steroid hormones through the blood-brain barrier of the newborn rabbit: Primary role of protein-bound hormone’, *Endocrinology*, 107(6), pp. 1705–1710. doi: 10.1210/endo-107-6-1705.
- Pekny, M. and Nilsson, M.** (2005) ‘Astrocyte activation and reactive gliosis’, *Glia*, 50(4), pp. 427–434. doi: 10.1002/glia.20207.
- Pellegrini, L.** (2001) ‘Role of heparan sulfate in fibroblast growth factor signalling: A structural view’, *Current Opinion in Structural Biology*, 11(5), pp. 629–634. doi: 10.1016/S0959-440X(00)00258-X.
- Pelvig, D. P. et al.** (2008) ‘Neocortical glial cell numbers in human brains’, *Neurobiology of Aging*, 29(11), pp. 1754–1762. doi: 10.1016/j.neurobiolaging.2007.04.013.
- Pérez, Y. et al.** (2021) ‘Semaphorin 3a—glycosaminoglycans interaction as therapeutic target for axonal regeneration’, *Pharmaceuticals*, 14(9). doi: 10.3390/ph14090906.
- Périer, O. and Grégoire, A.** (1965) ‘Electron microscopic features of multiple sclerosis lesions’, *Brain*, 88(5), pp. 937–952. doi: 10.1093/brain/88.5.937.
- Peterson, J. W. et al.** (2001) ‘Transected neurites, apoptotic neurons, and reduced inflammation in cortical multiple sclerosis lesions’, *Annals of Neurology*, 50(3), pp. 389–400. doi: 10.1002/ana.1123.
- Prineas, J. W. & Connell, F.**(1979).. Remyelination in multiple sclerosis. *Ann. Neurol.* 5, 22–31
- Qian, X. et al.** (1997) ‘FGF2 concentration regulates the generation of neurons and glia from multipotent cortical stem cells’, *Neuron*, 18(1), pp. 81–93. doi: 10.1016/S0896-6273(01)80048-9.
- Rajendran, R.; Böttiger, G.; Stadelmann, C.; Karnati, S.; Berghoff, M.** FGF/FGFR Pathways in Multiple Sclerosis and in Its Disease Models. *Cells* 2021, 10, 884. <https://doi.org/10.3390/cells10040884>
- Rangachari, M. et al.** (2012) ‘Bat3 promotes T cell responses and autoimmunity by repressing Tim-3-mediated cell death and exhaustion’, *Nature Medicine*. Nature Publishing Group, 18(9), pp. 1394–1400. doi: 10.1038/nm.2871. Raviola, E. (1977) ‘266068a0’, pp. 1–2.
- Ranvier, L.**, 1871. Contributions à l’histologie et à la physiologie des nerfs périphériques. *Comptes Rendus de l’Académie des Sciences*, 73, pp.1168-1171
- Reale, M. et al.** (2009) ‘Peripheral cytokines profile in Parkinson’s disease’, *Brain, Behavior, and Immunity*. Elsevier Inc., 23(1), pp. 55–63. doi: 10.1016/j.bbi.2008.07.003.

- Redmond SA, Mei F, Eshed-Eisenbach Y, Osso LA, Leshkowitz D, Shen YA, Kay JN, Aurrand-Lions M, Lyons DA, Peles E, Chan JR.** (2016) Somatodendritic Expression of JAM2 Inhibits Oligodendrocyte Myelination. *Neuron*. Aug 17;91(4):824-836. doi: 10.1016/j.neuron.2016.07.021. Epub 2016 Aug 4. PMID: 27499083; PMCID: PMC4990461.
- Rhodes et al.** (2003). Inhibiting cell proliferation during formation of the glial scar: effects on axon regeneration in the CNS. *Neuroscience*. 2003;120(1):41-56. doi: 10.1016/s0306-4522(03)00285-9. PMID: 12849739.
- Rhodes, S. and Bond, S.** (2008) ‘A review of the practical advantages of low molecular weight heparin in the treatment of cancer-related venous thromboembolism’, *European Journal of Oncology Nursing*. Elsevier Ltd, 12(5), pp. 425–429. doi: 10.1016/j.ejon.2008.08.001.
- Riederer, F.** (2017) ‘Ocrelizumab versus placebo in primary progressive multiple sclerosis’, *Journal fur Neurologie, Neurochirurgie und Psychiatrie*, 18(1), pp. 30–31. doi: 10.1056/nejmoa1606468.
- Rock, R. B. et al.** (2004) ‘Role of microglia in central nervous system infections’, *Clinical Microbiology Reviews*, 17(4), pp. 942–964. doi: 10.1128/CMR.17.4.942-964.2004.
- Rodrigues, T. B. and Ballesteros, P.** (2007) ‘Journal of Neuroscience Research 85:3244–3253 (2007)’, *Journal of Neuroscience Research*, 3253(April), pp. 3244–3253. doi: 10.1002/jnr.
- Roloff, F. et al.** (2015) ‘Enhanced neurite outgrowth of human model (NT2) neurons by small-molecule inhibitors of Rho/ROCK signaling’, *PLoS ONE*, 10(2), pp. 1–14. doi: 10.1371/journal.pone.0118536.
- Rosso, S. B. et al.** (2005) ‘Wnt signaling through Dishevelled, Rac and JNK regulates dendritic development’, *Nature Neuroscience*, 8(1), pp. 34–42. doi: 10.1038/nn1374.
- Roy, S. et al.** (2014) ‘Synthesis and biological evaluation of a unique heparin mimetic hexasaccharide for structure-activity relationship studies’, *Journal of Medicinal Chemistry*, 57(11), pp. 4511–4520. doi: 10.1021/jm4016069.
- Rubin, G. M. and Spradling, A. C.** (1985) ‘trpcM/ryso6trpc’), 807(1983), pp. 1983–1986.
- Ruiz-Perera, L. M. et al.** (2021) ‘Neuroprotection mediated by human blood plasma in mouse Hippocampal slice cultures and in oxidatively stressed human neurons’, *International Journal of Molecular Sciences*, 22(17), pp. 1–15. doi: 10.3390/ijms22179567.
- Rumble, J. M. et al.** (2015) ‘Neutrophil-related factors as biomarkers in EAE and MS’, *Journal of Experimental Medicine*, 212(1), pp. 23–35. doi: 10.1084/jem.20141015.
- Salzer J et al.** (2012).. Vitamin D as a protective factor in multiple sclerosis. *Neurology*. 2012 Nov 20;79(21):2140-5. doi: 10.1212/WNL.0b013e3182752ea8. PMID: 23170011.
- Sanderson, N. S. R. et al.** (2017) ‘Cocapture of cognate and bystander antigens can activate autoreactive B cells’, *Proceedings of the National Academy of Sciences of the United States of America*, 114(4), pp. 734–739. doi: 10.1073/pnas.1614472114.

Santos-Silva, A. et al. (2007) ‘FGF/Heparin Differentially Regulates Schwann Cell and Olfactory Ensheathing Cell Interactions with Astrocytes: A Role in Astrocytosis’, *Journal of Neuroscience*, 27(27), pp. 7154–7167. doi: 10.1523/jneurosci.1184-07.2007.

Saraswat, D. et al. (2021) ‘Overcoming the inhibitory microenvironment surrounding oligodendrocyte progenitor cells following experimental demyelination’, *Nature Communications*. Springer US, 12(1), pp. 1–18. doi: 10.1038/s41467-021-22263-4.

Saraswat, D. et al. (2021) ‘Heparanome-mediated rescue of oligodendrocyte progenitor quiescence following inflammatory demyelination’, *Journal of Neuroscience*, 41(10), pp. 2245–2263. doi: 10.1523/JNEUROSCI.0580-20.2021.

Savchenko, E. et al. (2019) ‘FGF family members differentially regulate maturation and proliferation of stem cell-derived astrocytes’, *Scientific Reports*, 9(1), pp. 1–13. doi: 10.1038/s41598-019-46110-1.

Schultz, V. et al. (2021) ‘Zika virus infection leads to demyelination and axonal injury in mature CNS cultures’, *Viruses*, 13(1). doi: 10.3390/v13010091.

Sekizar, S. and Williams, A. (2019) ‘Ex vivo slice cultures to study myelination, demyelination, and remyelination in mouse brain and spinal cord’, *Methods in Molecular Biology*, 1936, pp. 169–183. doi: 10.1007/978-1-4939-9072-6_10.

Sempere, A. P. et al. (2021) ‘Ocrelizumab in Multiple Sclerosis: A Real-World Study From Spain’, *Frontiers in Neurology*

Sharif-Alhoseini M, et al. (2017) Animal models of spinal cord injury: a systematic review. *Spinal Cord*. 2017 Aug;55(8):714-721. doi: 10.1038/sc.2016.187. Epub 2017 Jan 24. PMID: 28117332.

Sheng, Z. H. and Cai, Q. (2012) ‘Mitochondrial transport in neurons: Impact on synaptic homeostasis and neurodegeneration’, *Nature Reviews Neuroscience*, 13(2), pp. 77–93. doi: 10.1038/nrn3156.

Sherafat, A., Hill, R. A. and Nishiyama, A. (2018) ‘Organotypic slice cultures to study oligodendrocyte proliferation, fate, and myelination’, *Methods in Molecular Biology*, 1791, pp. 145–156. doi: 10.1007/978-1-4939-7862-5_11.

Sherriff FE, et al (1994). Markers of axonal injury in postmortem human brain. *Acta Neuropathol*. 1994;88(5):433-9. doi: 10.1007/BF00389495. PMID: 7847072.

Silver, J et al (1991). Reduction of neurite outgrowth in a model of glial scarring following CNS injury is correlated with the expression of inhibitory molecules on reactive astrocytes. *J. Neurosci*. 11, 3398–3411 (1991). 4.

Silver J, Miller JH (2004) Regeneration beyond the glial scar. *Nat Rev Neurosci* 5:146–156.

Singh, T. D., Fugate, J. E. and Rabinstein, A. A. (2014) ‘Central pontine and extrapontine myelinolysis: A systematic review’, *European Journal of Neurology*, 21(12), pp. 1443–1450. doi: 10.1111/ene.12571.

Smith-Thomas, L. C. et al. (1994). An inhibitor of neurite outgrowth produced by astrocytes. *J. Cell Sci*. 107, 1687–1695 5.

- Sofroniew, M. V.** and Vinters, H. V. (2010) ‘Astrocytes: Biology and pathology’, *Acta Neuropathologica*, 119(1), pp. 7–35. doi: 10.1007/s00401-009-0619-8.
- Song, W.** et al. (2017) ‘Alzheimer’s disease-associated TREM2 variants exhibit either decreased or increased ligand-dependent activation’, *Alzheimer’s and Dementia*, 13(4), pp. 381–387. doi: 10.1016/j.jalz.2016.07.004.
- Sorensen, A.** et al. (2008) ‘Astrocytes, but not olfactory ensheathing cells or Schwann cells, promote myelination of CNS axons in vitro’, *Glia*, 56(7), pp. 750–763. doi: 10.1002/glia.20650.
- St-Amour, I.** et al. (2013) ‘Brain bioavailability of human intravenous immunoglobulin and its transport through the murine blood-brain barrier’, *Journal of Cerebral Blood Flow and Metabolism*, 33(12), pp. 1983–1992. doi: 10.1038/jcbfm.2013.160.
- Steward, O.** et al (2014). Characterization of ectopic colonies that form in widespread areas of the nervous system with neural stem cell transplants into the site of a severe spinal cord injury. *J. Neurosci.* 34, 14013–14021
- Stokin, G. B.** et al. (2005) ‘Axonopathy and transport deficits early in the pathogenesis of Alzheimer’s diseases’, *Science*, 307(5713), pp. 1282–1288. doi: 10.1126/science.1105681.
- Stopschinski, B. E.** et al. (2020) ‘A synthetic heparinoid blocks Tau aggregate cell uptake and amplification’, *Journal of Biological Chemistry*. © 2009 ASBMB. Currently published by Elsevier Inc; originally published by American Society for Biochemistry and Molecular Biology., 295(10), pp. 2974–2983. doi: 10.1074/jbc.RA119.010353.
- Sun, Q.** et al. (2014) ‘Early release of high-mobility group box 1 (HMGB1) from neurons in experimental subarachnoid hemorrhage in vivo and in vitro’, *Journal of Neuroinflammation*, 11. doi: 10.1186/1742-2094-11-106.
- Szczuciński, A.** and Losy, J. (2007) ‘Chemokines and chemokine receptors in multiple sclerosis. Potential targets for new therapies’, *Acta Neurologica Scandinavica*, 115(3), pp. 137–146. doi: 10.1111/j.1600-0404.2006.00749.x.
- Szczuciński, A.** and Losy, J. (2010) ‘CCL5, CXCL10 and CXCL11 chemokines in patients with active and stable relapsing-remitting multiple sclerosis’, *NeuroImmunoModulation*, 18(1), pp. 67–72. doi: 10.1159/000317394.
- Szuchet, S.,** Watanabe, K. and Yamaguchi, Y. (2000) ‘Differentiation/regeneration of oligodendrocytes entails the assembly of a cell-associated matrix’, *International Journal of Developmental Neuroscience*, 18(7), pp. 705–720. doi: 10.1016/S0736-5748(00)00034-4.
- Tang, G.** et al. (2020) ‘Deferoxamine Ameliorates Compressed Spinal Cord Injury by Promoting Neovascularization in Rats’, *Journal of Molecular Neuroscience*. *Journal of Molecular Neuroscience*, 70(9), pp. 1437–1444. doi: 10.1007/s12031-020-01564-1.
- Tao, Y.,** Black, I. B. and DiCicco-Bloom, E. (1996) ‘Neurogenesis in neonatal rat brain is regulated by peripheral injection of basic fibroblast growth factor (bFGF)’, *Journal of Comparative Neurology*, 376(4), pp. 653–663. doi: 10.1002/(SICI)1096-9861(19961223)376:4<653::AID-CNE11>3.0.CO;2-N.

- Teitelbaum, D.** et al. (1971) ‘Suppression of experimental allergic encephalomyelitis by a synthetic polypeptide’, *European Journal of Immunology*, 1(4), pp. 242–248. doi: 10.1002/eji.1830010406.
- Thacker, B. E.** et al. (2022) ‘Multiplex genome editing of mammalian cells for producing recombinant heparin’, *Metabolic Engineering*. Elsevier Inc., 70(January), pp. 155–165. doi: 10.1016/j.ymben.2022.01.002
- Thetiot, M.** et al. (2019) ‘Preparation and Immunostaining of Myelinating Organotypic Cerebellar Slice Cultures’, *Journal of Visualized Experiments*, 2019(145), pp. 1–7. doi: 10.3791/59163.
- Thompson, S. M.** et al. (2012) ‘Differential Sulfation Remodelling of Heparan Sulfate by Extracellular 6-O-Sulfatases Regulates Fibroblast Growth Factor-Induced Boundary Formation by Glial Cells: Implications for Glial Cell Transplantation’, *Journal of Neuroscience*, 32(45), pp. 15902–15912. doi: 10.1523/jneurosci.6340-11.2012.
- Thorlakur Jonsson, Ph.D., Hreinn Stefansson, Ph.D., Stacy Steinberg, Ph.D., Ingileif Jonsdottir, Ph.D., Palmi V. Jonsson, M.D., Jon Snaedal, M.D., Sigurbjorn Bjornsson, M.D., Johanna Huttenlocher, B.S., Allan I. Levey, M.D., Ph.D., James J. Lah, M.D., Ph., P. D. and From (2013)** ‘Variant of TREM2 associated with the risk of AD’, *New England Journal of Medicine*, 368(2), pp. 107–116. doi: 10.1056/NEJMoa1211103.Variant.
- Timmer, N. M.** et al. (2010) ‘Enoxaparin treatment administered at both early and late stages of amyloid β deposition improves cognition of APP^{swe}/PS1^{dE9} mice with differential effects on brain A β levels’, *Neurobiology of Disease*. Elsevier Inc., 40(1), pp. 340–347. doi: 10.1016/j.nbd.2010.06.008.
- Tirotta, E., Ransohoff, R. M. and Lane, T. E.** (2011) ‘CXCR2 signaling protects oligodendrocyte progenitor cells from IFN- γ /CXCL10-mediated apoptosis’, *Glia*, 59(10), pp. 1518–1528. doi: 10.1002/glia.21195.
- Titus, H. E.** et al. (2020) ‘Pre-clinical and Clinical Implications of “Inside-Out” vs. “Outside-In” Paradigms in Multiple Sclerosis Etiopathogenesis’, *Frontiers in Cellular Neuroscience*, 14(October). doi: 10.3389/fncel.2020.599717.
- Tobinick, E. and Davoodifar, S.** (2004) ‘Efficacy of etanercept delivered by perispinal administration for chronic back and/or neck disc-related pain: A study of clinical observations in 143 patients’, *Current Medical Research and Opinion*, 20(7), pp. 1075–1085. doi: 10.1185/030079903125004286.
- Tobinick, E.** et al. (2014) ‘Immediate neurological recovery following perispinal etanercept years after brain injury’, *Clinical Drug Investigation*, 34(5), pp. 361–366. doi: 10.1007/s40261-014-0186-1.
- Traiffort, E.** et al. (2020) ‘Astrocytes and Microglia as Major Players of Myelin Production in Normal and Pathological Conditions’, *Frontiers in Cellular Neuroscience*, 14(April), pp. 1–21. doi: 10.3389/fncel.2020.00079.
- Turnbull J, et al (2001).** Heparan sulfate: decoding a dynamic multifunctional cell regulator. *Trends Cell Biol.* 2001 Feb;11(2):75-82. doi: 10.1016/s0962-8924(00)01897-3. PMID: 11166215.

- Tuszynski M.H.**, et al. (2014) Neural stem cell dissemination after grafting to CNS injury sites *Cell* 156, 388,
- Ullian** et al (2001). Control of synapse number by glia. *Science*. 2001 Jan 26;291(5504):657-61. doi: 10.1126/science.291.5504.657. PMID: 11158678.
- Uzawa, A.** et al. (2013) ‘Anti-high mobility group box 1 monoclonal antibody ameliorates experimental autoimmune encephalomyelitis’, *Clinical and Experimental Immunology*, 172(1), pp. 37–43. doi: 10.1111/cei.12036.
- Van der Meer** et al (2017) J. From Farm to Pharma: An Overview of Industrial Heparin Manufacturing Methods. *Molecules*. 2017 Jun 21;22(6):1025. doi: 10.3390/molecules22061025. PMID: 28635655; PMCID: PMC6152658.
- Van De Waterbeemd, H.** et al. (1998) ‘Estimation of blood-brain barrier crossing of drugs using molecular size and shape, and H-bonding descriptors’, *Journal of Drug Targeting*, 6(2), pp. 151–165. doi: 10.3109/10611869808997889.
- Van Rappard, D. F.**, Boelens, J. J. and Wolf, N. I. (2015) ‘Metachromatic leukodystrophy: Disease spectrum and approaches for treatment’, *Best Practice and Research: Clinical Endocrinology and Metabolism*. Elsevier, 29(2), pp. 261–273. doi: 10.1016/j.beem.2014.10.001.
- van Veen, T.** et al. (2007) ‘CCL5 and CCR5 genotypes modify clinical, radiological and pathological features of multiple sclerosis’, *Journal of Neuroimmunology*, 190(1–2), pp. 157–164. doi: 10.1016/j.jneuroim.2007.08.005.
- Vanický, I.** et al. (2001) ‘A simple and reproducible model of spinal cord injury induced by epidural balloon inflation in the rat’, *Journal of Neurotrauma*, 18(12), pp. 1399–1407. doi: 10.1089/08977150152725687.
- Van't Veer A, Du Y, Fischer TZ, Boetig DR, Wood MR, Dreyfus CF.** Brain-derived neurotrophic factor effects on oligodendrocyte progenitors of the basal forebrain are mediated through trkB and the MAP kinase pathway. *J Neurosci Res*. 2009 Jan;87(1):69-78. doi: 10.1002/jnr.21841. PMID: 18752299; PMCID: PMC4912000.
- Venero Galanternik, M., Kramer, K. L. and Piotrowski, T.** (2015) ‘Heparan Sulfate Proteoglycans Regulate Fgf Signaling and Cell Polarity during Collective Cell Migration’, *Cell Reports*. The Authors, 10(3), pp. 414–428. doi: 10.1016/j.celrep.2014.12.043.
- Voet, S., Prinz, M. and van Loo, G.** (2019) ‘Microglia in Central Nervous System Inflammation and Multiple Sclerosis Pathology’, *Trends in Molecular Medicine*, 25(2), pp. 112–123. doi: 10.1016/j.molmed.2018.11.005.
- Vlodavsky, I.** et al. (1991). Extracellular sequestration and release of fibroblast growth factor: a regulatory mechanism? *Trends in Biochemical Sciences* 16, 268–271. [https://doi.org/10.1016/0968-0004\(91\)90102-2](https://doi.org/10.1016/0968-0004(91)90102-2)
- Voet S,** et al (2019) Microglia in Central Nervous System Inflammation and Multiple Sclerosis Pathology. *Trends Mol Med*. 2019 Feb;25(2):112-123. doi: 10.1016/j.molmed.2018.11.005. Epub 2018 Dec 18. PMID: 30578090.

- Wake, H.** et al. (2009) ‘Resting microglia directly monitor the functional state of synapses in vivo and determine the fate of ischemic terminals’, *Journal of Neuroscience*, 29(13), pp. 3974–3980. doi: 10.1523/JNEUROSCI.4363-08.2009.
- Wallis, N.** et al. (2012) ‘Combined excitotoxic-oxidative stress and the concept of non-cell autonomous pathology of ALS: Insights into motoneuron axonopathy and astrogliosis’, *Neurochemistry International*. Elsevier Ltd, 61(4), pp. 523–530. doi: 10.1016/j.neuint.2012.02.026.
- Waly, B.** et al. (2020) ‘Longitudinal Intravital Microscopy Reveals Axon Degeneration Concomitant With Inflammatory Cell Infiltration in an LPC Model of Demyelination’, *Frontiers in Cellular Neuroscience*.
- Walz, A.** et al. (1997) ‘Essential role of heparan sulfates in axon navigation and targeting in the developing visual system’, *Development*, 124(12), pp. 2421–2430. doi: 10.1242/dev.124.12.2421.
- Wang, J. T., Medress, Z. A. and Barres, B. A.** (2012) ‘Axon degeneration: Molecular mechanisms of a self-destruction pathway’, *Journal of Cell Biology*, 196(1), pp. 7–18. doi: 10.1083/jcb.201108111.
- Wang, P.** et al. (2018) ‘Binding and neurotoxicity mitigation of toxic tau oligomers by synthetic heparin like oligosaccharides’, *Chemical Communications*. Royal Society of Chemistry, 54(72), pp. 10120–10123. doi: 10.1039/c8cc05072d.
- Werner, S., Unsicker, K. and von Bohlen und Halbach, O.** (2011) ‘Fibroblast growth factor-2 deficiency causes defects in adult hippocampal neurogenesis, which are not rescued by exogenous fibroblast growth factor-2’, *Journal of Neuroscience Research*, 89(10), pp. 1605–1617. doi: 10.1002/jnr.22680.
- Williams, A.** et al. (2007) ‘Semaphorin 3A and 3F: Key players in myelin repair in multiple sclerosis?’, *Brain*, 130(10), pp. 2554–2565. doi: 10.1093/brain/awm202.
- Winkler, S.** et al. (2002) ‘Syndecan-3 and perlecan are differentially expressed by progenitors and mature oligodendrocytes and accumulate in the extracellular matrix’, *Journal of Neuroscience Research*, 69(4), pp. 477–487. doi: 10.1002/jnr.10311.
- Wu, Z. L.** et al. (2003) ‘The involvement of heparan sulfate (HS) in FGF1/HS/FGFR1 signaling complex’, *Journal of Biological Chemistry*. © 2003 ASBMB. Currently published by Elsevier Inc; originally published by American Society for Biochemistry and Molecular Biology., 278(19), pp. 17121–17129. doi: 10.1074/jbc.M212590200.
- Xu, G. Y.** et al. (2004) ‘Concentrations of glutamate released following spinal cord injury kill oligodendrocytes in the spinal cord’, *Experimental Neurology*, 187(2), pp. 329–336. doi: 10.1016/j.expneurol.2004.01.029.
- Yang, Locomotor.S.** et al. (2022) ‘Development of the Blood-Brain Barrier in Ducks’, *Microscopy and Microanalysis*, 28(2), pp. 504–514. doi: 10.1017/S143192762200006X.
- Yates, E. A.** et al. (1996) ‘¹H and ¹³C NMR spectral assignments of the major sequences of twelve systematically modified heparin derivatives’, *Carbohydrate Research*, 294, pp. 15–27. doi: 10.1016/s0008-6215(96)90611-4.

- Yates, E. A.** et al. (2018) 'Low sulfated heparins target multiple proteins for central nervous system repair', *Glia*, (August 2018), pp. 668–687. doi: 10.1002/glia.23562.
- Yayon, A.** et al. (1991) 'Cell surface, heparin-like molecules are required for binding of basic fibroblast growth factor to its high affinity receptor', *Cell*, 64(4), pp. 841–848. doi: 10.1016/0092-8674(91)90512-W.
- Yednock, T. A.** et al. (1992) 'Prevention of experimental autoimmune encephalomyelitis by antibodies against $\alpha 4\beta 1$ integrin', *Nature*, 356(6364), pp. 63–66. doi: 10.1038/356063a0.
- Yi, H.** et al. (2014) 'IL-17A Induces MIP-1 α Expression in Primary Astrocytes via Src/MAPK/PI3K/NF-kB Pathways: Implications for Multiple Sclerosis', *Journal of Neuroimmune Pharmacology*, 9(5), pp. 629–641. doi: 10.1007/s11481-014-9553-1.
- Yuen, T. J.** et al. (2013) 'Identification of endothelin 2 as an inflammatory factor that promotes central nervous system remyelination', *Brain*, 136(4), pp. 1035–1047. doi: 10.1093/brain/awt024.
- Yuzaki, M.** (2018) 'Two Classes of Secreted Synaptic Organizers in the Central Nervous System', *Annual Review of Physiology*, 80, pp. 243–262. doi: 10.1146/annurev-physiol-021317-121322.
- Zalc B.** et al. (2000). Origins of vertebrate success. *Science*. Apr 14;288(5464):271-2. doi: 10.1126/science.288.5464.271c. PMID: 10777405.
- Zeng Z, Lan T, Wei Y, Wei X.** CCL5/CCR5 axis in human diseases and related treatments. *Genes Dis.* 2022 Jan;9(1):12-27. doi: 10.1016/j.gendis.2021.08.004. Epub 2021 Aug 26. PMID: 34514075; PMCID: PMC8423937.
- Zhang, C.** et al. (2021) 'Effects of the combination therapy of electric field stimulation and polyethylene glycol in the ex vivo spinal cord of female rats after compression', *Journal of Neuroscience Research*, 99(7), pp. 1850–1863. doi: 10.1002/jnr.24839.
- Zhang, H.** et al. (2011) 'Central nervous system remyelination in culture - A tool for multiple sclerosis research', *Experimental Neurology*. Elsevier Inc., 230(1), pp. 138–148. doi: 10.1016/j.expneurol.2011.04.009.
- Zhou, X.** et al. (2021) 'The hspg syndecan is a core organizer of cholinergic synapses', *Journal of Cell Biology*, 220(9). doi: 10.1083/jcb.202011144.
- Zlokovic, B. V.** (2011) 'Neurovascular pathways to neurodegeneration in Alzheimer's disease and other disorders', *Nature Reviews Neuroscience*. Nature Publishing Group, 12(12), pp. 723–738. doi: 10.1038/nrn3114.